A Finite Element Model of the Pregnant Female Occupant: Analysis of Injury Mechanisms and Restraint Systems

David M. Moorcroft

Thesis submitted to the Faculty of the
Virginia Polytechnic Institute and State University
in partial fulfillment of the requirements for the degree of

Master of Science
in
Engineering Mechanics

Stefan M. Duma, Chair
Harry Dankowicz
Michael L. Madigan
Greg G. Duma

July 26, 2002
Blacksburg, Virginia

Keywords: Pregnant, Restraint, Model, Madymo

A Finite Element Model of the Pregnant Female Occupant: Analysis of Injury Mechanisms and Restraint Systems

David M. Moorcroft

(ABSTRACT)

For women of reproductive age, automobile crashes are the leading cause of death worldwide. It has been estimated that 40,000 women in the second half of pregnancy are involved in motor-vehicle crashes each year. It has been estimated that between 300 to 3800 will experience a fetal loss. Placental abruption has been shown to account for 50% to 70% of fetal losses in motor vehicle crashes. While there is a growing database of medical case studies and retrospective studies describing the outcome of motor vehicle accidents involving pregnant occupants, as well as the effect of seatbelts on fetal survival, previous research has not produced a tool for engineers to use to improve the safety of a pregnant occupant in a motor vehicle. The goal of this project was to develop a model that can quantify the stresses and strains on the uterus of a pregnant woman in order to predict the risk of injury. A finite element uterine model of a 7-month pregnant female was created and integrated into a multi-body human model. Unrestrained, 3-pt belt, and 3-pt belt plus airbag tests were simulated at speeds ranging from 13 kph to 55 kph.

Peak uterine strain was found to be a good predictor of fetal outcome. The uterine strain sufficient to cause placental abruption was seen in simulations known to have greater than 75% risk of adverse fetal outcome. Head injury criteria (HIC) and viscous criterion (V*C) were examined as a check of overall occupant protection. The 3-pt belt plus airbag restraint provided the greatest amount of protection to the mother.

The model proved successful at predicting risk of fetal demise from placental abruption and verified experimental findings noting the importance of proper restraint use for the pregnant occupant.

Disclaimer

Mention of company names or products does not constitute endorsement in any way by the Virginia Polytechnic Institute and State University.

Acknowledgements

This research would not have been possible without the support and encouragement of the people in my life. Primarily, I would like to thank my advisor, Dr. Stefan M. Duma, for providing support, advice, guidance, and encouragement. I also thank Dr. Michael L. Madigan, Dr. Harry Dankowicz, and Dr. Greg G. Duma for sitting on my committee and reviewing my thesis. Additionally, I appreciate all the Madymo technical support provided by Ronald de Lange.

A special thanks goes to the IBL. From coffee breaks and Google searches to just venting, I would never have completed my project without Ginny, Joe, Joel, or Will. I also need to thank my roommate for technical knowledge, nights on the town and our good friend Ms. Olga Phactor.

Above all, thanks to my family for their prayers, words of encouragement and cash.

Table of Contents

Abstract ..... **ii**

Acknowledgements ..... **iv**

Table of Contents ..... **v**

List of Figures ..... **vii**

List of Tables ..... **ix**

List of Equations ..... **x**

Chapter 1 Background **1**

1.1 Anatomy 1
1.1.1 Pregnant Abdomen 1
1.1.2 Placental positioning 5
1.2 Background 6
1.2.1 Injury Types 7
1.2.2 Injury Incidence 9
1.3 Previous Laboratory Studies 11
1.3.1 Pregnant Animal Testing 11
1.3.2 Abdominal Response 13
1.3.2 Modeling Pregnant Occupants 16
1.3.2 Pregnant Crash Test Dummies 17
1.4 Injury Mechanisms 29
1.5 Injury Criteria 33
1.5.1 Crash Severity and Restraint Use 33
1.5.2 Peak Dummy Uterine Pressure 35
1.5.3 Tissue Failure 36
1.6 Research Objectives 36

Chapter 2 Computational Model of the Pregnant Occupant: Predicting the Risk of Injury in Automobile crashes **38**

Abstract 38
2.1 Introduction 38

2.2 Materials and Methods 39
2.3 Results 42
2.4 Comment 46
References 47

Chapter 3 a finite Element Model of the Pregnant Occupant for the Analysis of Injury Risk and Restraint Effectiveness 49

Abstract 49
3.1 Introduction 49
3.2 Methodology 54
3.3 Results and Discussion 59
3.4 Conclusions 67
References 68

References 71

Appendix A Methodology, Validation, and Limitations 76

A.1 Introduction 76
A.2 Formulation of the FE Uterine Model 77
A.2.1 Geometry 77
A.2.2 Material Properties 80
A.2.3 Meshing Technique 83
A.3 Madymo 86
A.3.1 Human Body Model 86
A.3.2 Contacts and Constraints 89
A.3.3 Vehicle Interior 90
A.3.4 Restraints 93
A.4 Model Validation 94
A.4.1 Belt Loading 94
A.4.2 Rigid Bar Impact 95
A.5 Test Matrix 96
A.6 Limitations 97

Appendix B Truncated Madymo Code 99

Vita 149

List of Figures

Chapter 1

Figure 1 Pregnant uterus 2
Figure 2 Anatomy of the pregnant uterus 3
Figure 3 Structure of the placenta 4
Figure 4 Uterosacral and round ligaments 5
Figure 5 Placenta position; a) fundal, b) anterior, c) posterior 6
Figure 6 Steering wheel and belt loading on a pregnant occupant (Pearlman, 1997) 8
Figure 7 Pregnant monkey in the 4-pt netting system (van Kirk, 1969) 12
Figure 8 Schematic of pregnant baboon sled test (King, 1971) 13
Figure 9 Rigid bar impactor corridor (Hardy, 2001; scaled by Rupp, 2001) 15
Figure 10 Belt loading corridor (Hardy, 2001; scaled by Rupp, 2001) 15
Figure 11 Surrogate airbag loading corridor (Hardy, 2001; scaled by Rupp, 2001) 16
Figure 12 1st generation pregnant dummy (Pearlman, 1996) 18
Figure 13 Fetus, "amniotic fluid", and uterus of the 1st generation pregnant dummy 18
Figure 14 1st generation pregnant dummy test results: Abdominal force (Viano, 1998) 20
Figure 15 1st generation pregnant dummy test results: Fetal head acceleration (Viano, 1998) 21
Figure 16 MAMA-2b, 2nd generation pregnant dummy (Rupp, 2001) 22
Figure 17 Abdominal contour: MAMA-2b vs. 1st pregnant dummy (Rupp, 2001) 23
Figure 18 Thorax calibration test results for the MAMA-2b (Rupp, 2001) 24
Figure 19 Airbag deployment during sled test with MAMA-2b (Rupp, 2001) 25
Figure 20 MAMA-2b abdominal response to rigid bad impact (Rupp, 2001) 26
Figure 21 MAMA-2b abdominal response to 3 m/s belt loading (Rupp, 2001) 27
Figure 22 MAMA-2b abdominal response to airbag loading (Rupp, 2001) 27
Figure 23 MAMA-2b test results: Pressure vs. crash speed (Rupp, 2001) 28
Figure 24 Typical anterior pressure-time history (Rupp, 2001) 29
Figure 25 Cross-section of uterus with fetus during drop test (Rupp, 2001) 30
Figure 26 Pressure gradient in uterus after 35 g deceleration (Rupp, 2001) 32
Figure 27 Direct loading of uterus by hemispherical impactor (Rupp, 2001) 33
Figure 28 Adverse fetal outcome risk curve (Klinich, 1999b) 35
Figure 29 Risk curve developed from the MAMA-2b (Rupp, 2001) 36

Chapter 2

Figure 30 Pregnant occupant in vehicle interior 40
Figure 31 Pregnant occupant in a 35 kph crash at peak uterine strain; a) no restraint at 101 ms, b) 3-pt belt at 75 ms, c) 3-pt belt and airbag at 82 ms 44

Figure 32 Peak strain in the uterus as a predictor of adverse fetal outcome..... 45

Chapter 3
Figure 33 Anatomy of a 40-week pregnant woman (ligaments not shown)..... 51
Figure 34 Risk of adverse fetal outcome as a function of crash speed and restraint (Klinich, 1999b) 53
Figure 35 Side view of the FE uterus model 55
Figure 36 Pregnant occupant in vehicle interior..... 58
Figure 37 Abdominal response of the pregnant model compared to the scaled corridor..... 60
Figure 38 Pregnant occupant in a 35 kph crash at peak uterine strain; a) no restraint at 101 ms, b) 3-pt belt at 75 ms, c) 3-pt belt and airbag at 82 ms 63
Figure 39 Steering wheel contact with the uterine model at 60 ms..... 64
Figure 40 Belt loading of the uterine model at 60 ms 64
Figure 41 Peak strain in the uterus as a predictor of adverse fetal outcome..... 65
Figure 42 Von Mises stress in the uterus during steering wheel loading 66

Appendix
Figure 43 Dimensioned drawing of the pregnant uterus and placenta (in gray)... 78
Figure 44 Pregnant uterine model..... 79
Figure 45 Side view of the fat that surrounds the uterus 80
Figure 46 Test setup for grid independence test..... 85
Figure 47 Results of grid independence test..... 85
Figure 48 5^{th} percentile human model and spine..... 87
Figure 49 Flexible bodies of the human model 87
Figure 50 Human model skin stretched around the uterus 89
Figure 51 Vehicle interior showing uterus clearance and overlap..... 91
Figure 52 Comparison of abdominal contours 92
Figure 53 Comparison of defined sled pulse to actual sled pulse..... 93
Figure 54 Driver side airbag used in Madymo simulations..... 94
Figure 55 Abdominal response of the pregnant model to 3 m/s belt loading..... 95
Figure 56 Abdominal response of the pregnant model to 6 m/ rigid bar impact.. 96

List of Tables

Chapter 1

Table 1	Estimates of annual incidence	10
Table 2	Test matrix for MAMA-2b (Rupp, 2001)	25

Chapter 2

Table 3	Effect of restraint use and crash speed on risk of injury and peak uterine strain	42

Chapter 3

Table 4	Material properties used for the pregnant uterus model	55
Table 5	Element types used for the pregnant uterus	57
Table 6	Pregnant model test parameters and results	61

Appendix A

Table 7	Dimensions of the uterus	79
Table 8	Material properties of the uterine model	81
Table 9	Tissue properties of the uterus and placenta	82
Table 10	Summary of finite elements	84
Table 11	Test matrix for the pregnant model simulations	96

List of Equations

Chapter 1
Equation 1 Risk of adverse fetal outcome as a function of pressure...……. 35

Chapter 3
Equation 2 Risk of adverse fetal outcome for improper restraint…...…… 53
Equation 3 Risk of adverse fetal outcome for proper restraint……...…… 53

Chapter 1
Background

This chapter contains an overview of pregnant women in motor vehicle crashes. The basic anatomy of a pregnant woman is given, along with background on pregnant women in motor vehicle crashes, including types of injury and incidence of crashes. The relevant research is summarized, highlighting animal testing, abdominal response, testing of pregnant dummies and previous modeling. The injury mechanisms and injury criteria related to the project undertaken are also included.

The next two chapters are stand alone papers describing the basic model creation and detailing the results of this study as it applies to the medical community (Chapter 2) and the automotive community (Chapter 3). A detailed description of the procedures undertaken to create the model, along with validation results and limitations, are contained in Appendix A. A truncated Madymo code is included in Appendix B.

1.1 Anatomy

An introduction to the pregnant abdomen is given to understand terminology and design decisions. The general anatomy of a pregnant uterus and the position of the placenta in the uterus help to shed light on the difficulties a pregnant woman has in a motor vehicle crash.

1.1.1 Pregnant Abdomen

The uterus is a muscular organ the size of a lemon located within the abdominal cavity. As the fetus grows during pregnancy, the abdomen stretches to the size of a watermelon (Figure 1). The internal volume increases from 0.005 L to 5 L and as much as 10 L. The target weight gain for a pregnant female is 0.23 kg (0.5 lb) per week for the first 20 weeks and 0.45 kg (1.0 lb) for the second 20 weeks (Institute of Medicine, 1990). At thirty weeks, weight gain is about 9.1 kg (20 lbs). The uterine wall is uniform prior to

delivery, with a thickness of about 1 cm prior to delivery. The uterus is freely mobile in the abdominal cavity, however the pelvis, spine, other abdominal organs, and the abdominal wall limit its movements. The uterosacral and round ligaments extend from the uterus to the pelvis and act to support the uterus.

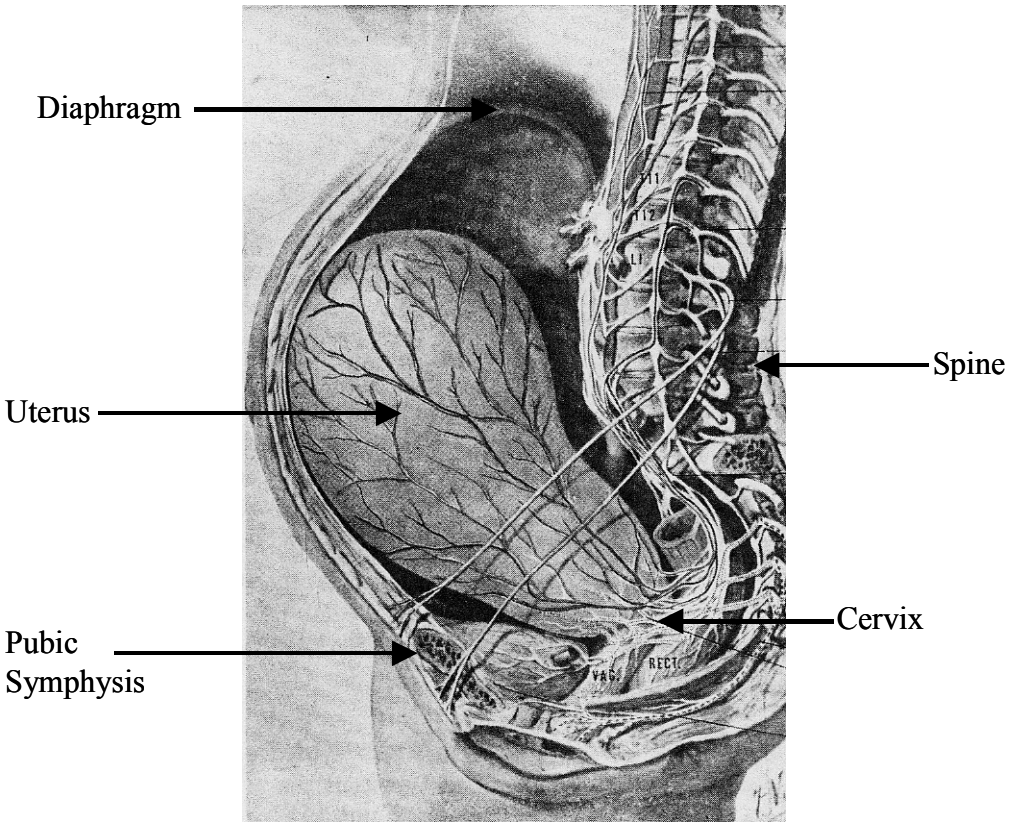

Figure 1: Pregnant uterus [Netter, 1997]

The interior of the uterus contains the fetus, which is surrounded by amniotic fluid and the placenta (Figure 2). The amniotic fluid acts as a shock absorber, allows the fetus to move freely, and stabilizes the intrauterine pressure. It is 99% water and 1% solid. The placenta is a vascular organ that acts as a permeable membrane that exchanges oxygen, nutrients, and waste products between the mother and fetus via the umbilical cord (Figure 3). The placenta is comprised of muscular tissue that is engorged with blood. It is a flat, roughly circular structure approximately 22 cm in diameter and 2 cm thick in the center. The placenta attaches to the uterus at the uteroplacental interface

(UPI) via microvilli. The microvilli grow into the superficial covering of the uterine wall, called the decidual layer.

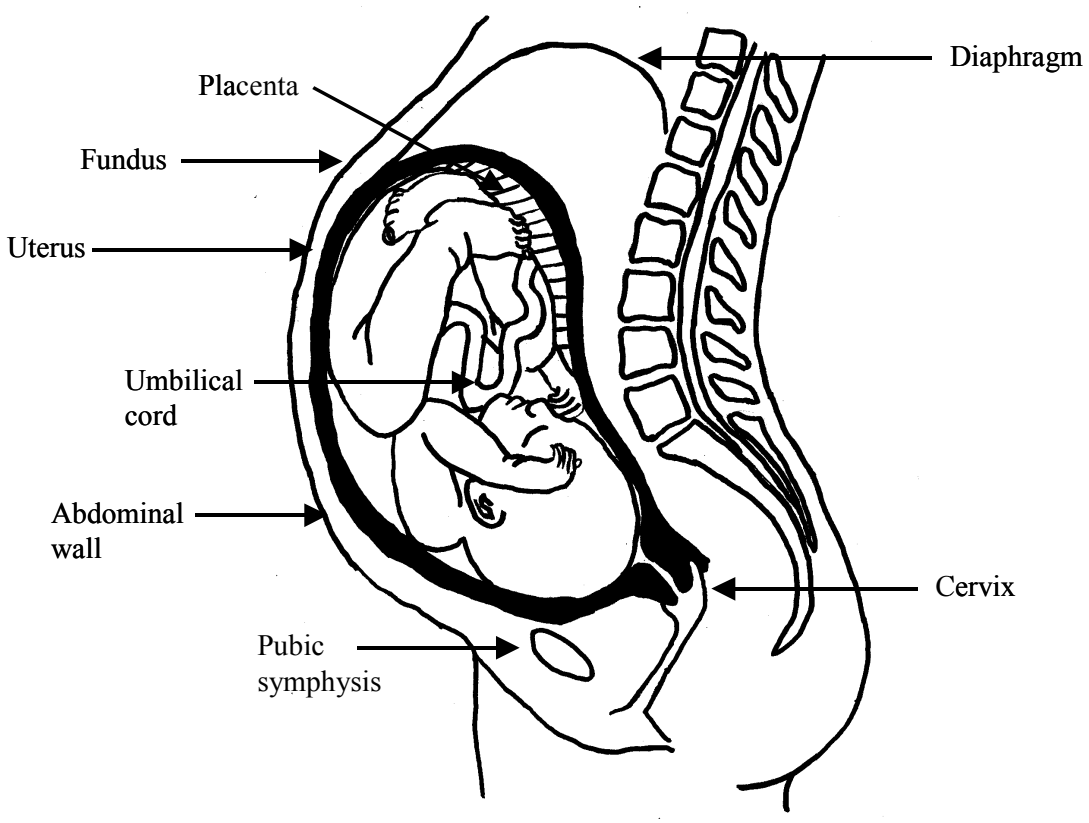

Figure 2: Anatomy of the pregnant uterus

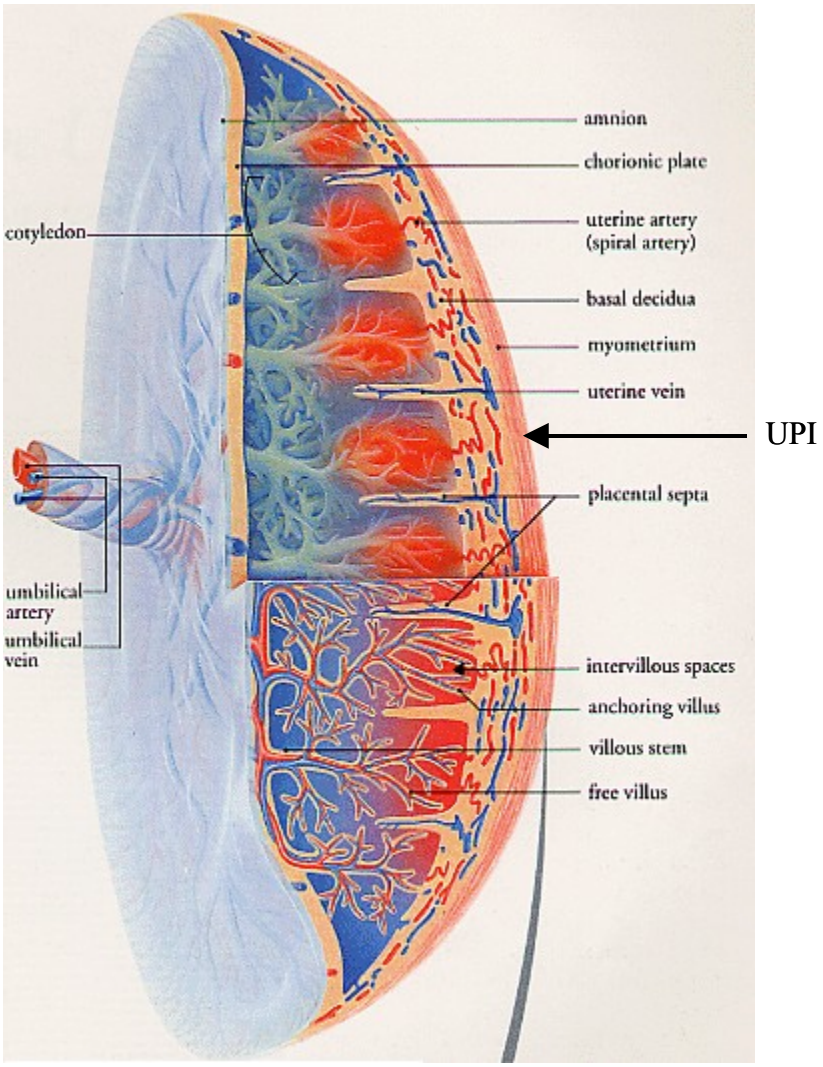

Figure 3: Structure of the placenta [Takahashi, 1994]

The uterus in mainly supported by two pairs of ligaments, the uterosacral and round ligaments (Figure 4). During pregnancy, the ligaments stretch to accommodate the growing uterus. The uterosacral ligaments connect the distal, posterior region of the uterus to the sacrum. These ligaments are approximately 3 mm in diameter and 10 cm long. The round ligaments connect the lateral region of the uterus to the sidewalls of the pelvis. They are 4 mm to 5 mm thick and 30 cm long. The ligaments are surrounded by peritoneum and are difficult to differentiate in vivo.

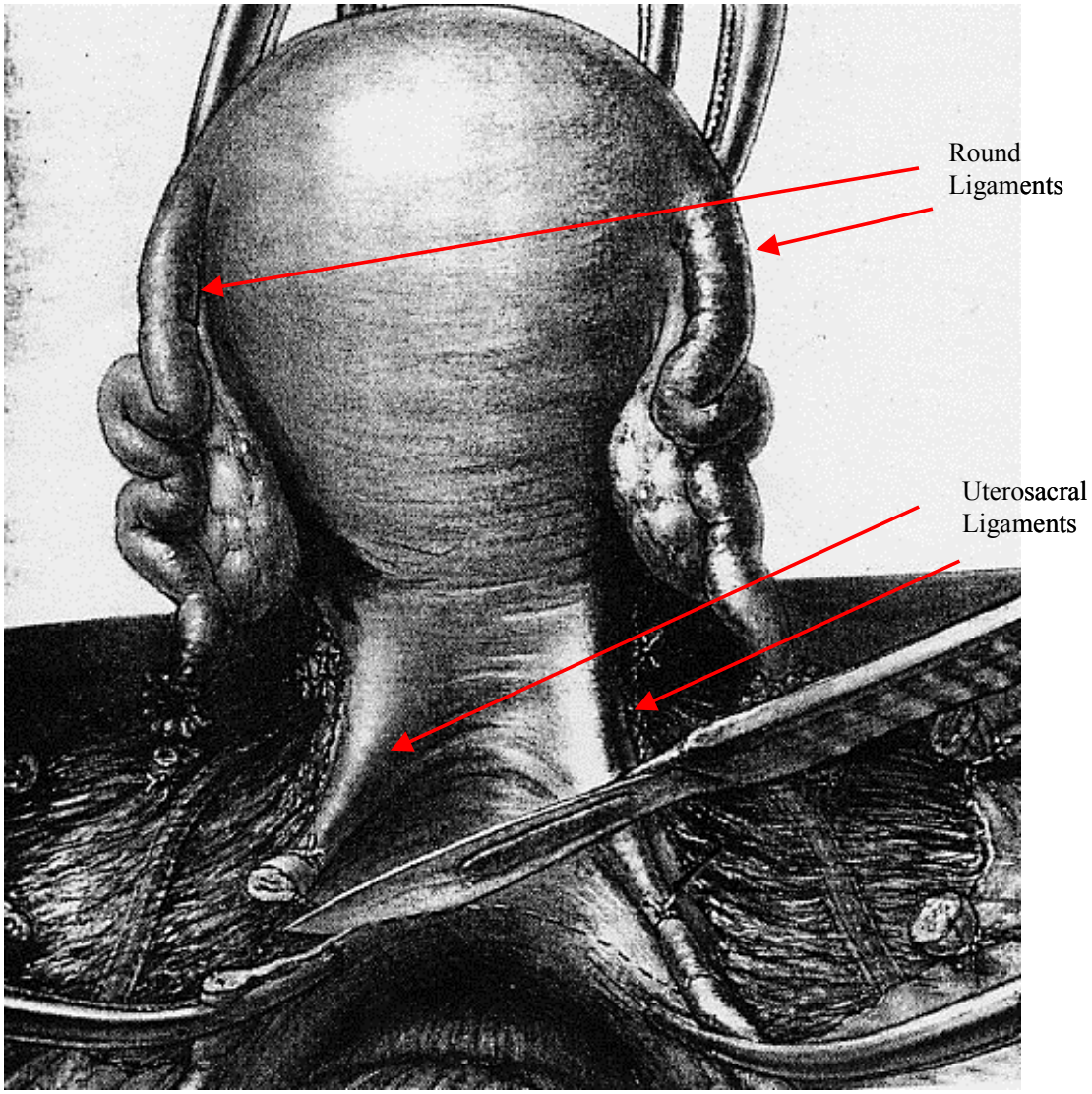

Figure 4: Uterosacral and round ligaments [Thompson, 1996]

1.1.2 Placental positioning:

A review of 800 ultrasonographic placentographies by Fried (1978) showed a wide and relatively even distribution of placental bulk. This precluded any meaningful conclusion as to the most likely site for the placenta. However, 95% of placentas were in the upper half of uterus. Of those, 31% of the placentas were wholly or partly fundal (at the top of the uterus) and by the 3rd trimester, 40% of placentas were fundal (Figure 5). In the cephalic presentation, in which the fetus is in a head down position, anterior placentas out number posterior placentas 1.63 to 1 and anterior plus anterior-fundal

placentas out number posterior plus posterior-fundal placentas 1.2 to 1. Similar patterns emerged for breech and transverse presentations.

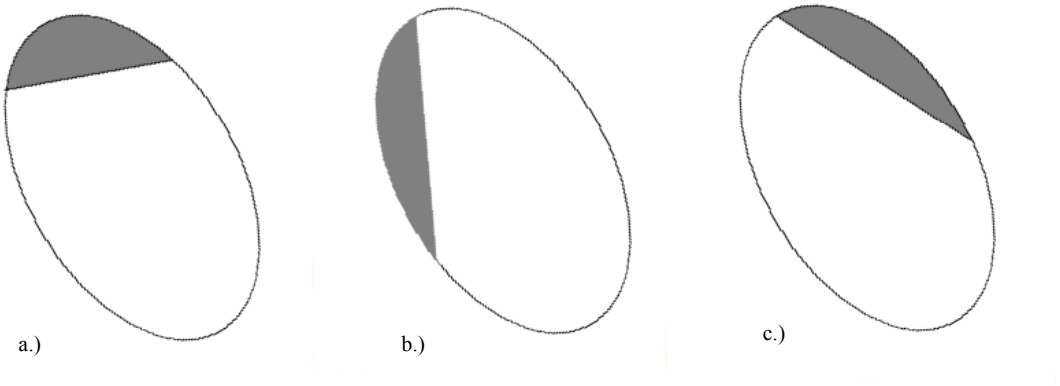

Figure 5: Placenta position; a) fundal, b) anterior, c) posterior

The cephalic presentation was seen in about 75% of the cases reviewed. In breech presentation, the fetus is in a head up position. Breech presentation was seen in about 20% of the cases. The transverse presentation is when the fetus lays across the women's abdomen. Transverse presentation was only seen in about 5% of the cases.

From modeling completed at the University of Michigan Transportation Research Institute (UMTRI), it was determined that an anterior placental location would be the worst case for direct loading, such as contact with the steering wheel. A posterior placental location would be the worst case for a posterior pressure build up due to fluid inertia. From the Fried data and the UMTRI modeling, it can be determined that the placental should be located in the upper half of the uterus and that a fundal location, with the placenta extending to the anterior and posterior regions of the uterus, would allow for measurement of both direct and inertial loading on the placenta.

1.2 Background

For women of reproductive age, accidents and homicide are the leading cause of death worldwide (Pearlman 1997). It has been estimated that trauma affects between 6% and 7% of all pregnancies and that two-thirds of all trauma during pregnancy is the result of motor vehicle crashes (Pearlman, 1997). In a 1953 study, it was found that travel did

not produce traumatic effects to the mother or the fetus (Guilbeau, 1953). From a sample of 1917 patients traveling at least 300 miles during pregnancy, there was a 4.2% incidence of abortion, which is below the generally accepted incidence of 10% for spontaneous abortion.

Crosby and Costiloe reported in 1971, “the leading single cause of fetal death in unrestrained mothers was death of the mother.” Maternal death has a near 100 percent fetal mortality rate. Therefore, the main method of protecting the fetus is to protect the mother. It is a basic principle, according to Rothenberger (1978), “the mother will do better inside the car, strapped in; and if the mother does better, the fetus will do better." Since 1971, several researchers have found that the majority of fetal losses have resulted from minor maternal injuries, primarily because most motor vehicle crashes (MVCs), greater than 90% according to Pearlman, result in minor maternal injuries (Pearlman, 1997; Williams, 1990; Goodwin, 1990; Dahmus, 1993). Up to 70% of fetal losses with maternal survival are due to placental abruption (Pearlman, 1990).

1.2.1 Injury Types

Injuries unique to a pregnant occupant are a result of the change in abdominal geometry and anatomy. A common non-fatal complication from motor vehicle crashes is premature delivery. Of greater concern are fetal losses resulting from a motor vehicle crash. Loading of the uterus by the steering wheel, seatbelt, airbag, or inertia can cause placental abruption, uterine rupture, direct fetal injury, and maternal death (Figure 6). Placental abruption is the premature separation of the placenta from the wall of the uterus, disrupting the supply of nutrients and oxygen to the fetus. Placental abruption may account for 50% to 70% of fetal losses in motor vehicle crashes (Pearlman, 1990). Uterine rupture and direct fetal injury account for less then 10% of fetal losses and the remaining 20% to 40% of fetal losses are the result of severe maternal injuries, including maternal death (Pearlman, 1990). It has been noted that uterine or direct fetal injury is typically accompanied by placental abruption, while placental abruption occurs without uterine or direct fetal injury (Klinich, 1999b). This implies that the UPI is weaker then either the uterus or placenta and usually fails before either the uterus or placenta (Klinich, 1999b). Placental abruption is believed to occur when the strain in the UPI exceeds 60%

based on postpartum tests conducted by Ashton-Miller (reported in Rupp, 2001). Ultrasound measurements conducted by Pearlman et al. (1999) confirmed the findings of Ashton-Miller. Pearlman measured the thickness of the uterine wall immediately following delivery. It was found that the placenta separated from the uterus when uterine strain exceeded 60% in the radial direction and 450% in the circumferential direction.

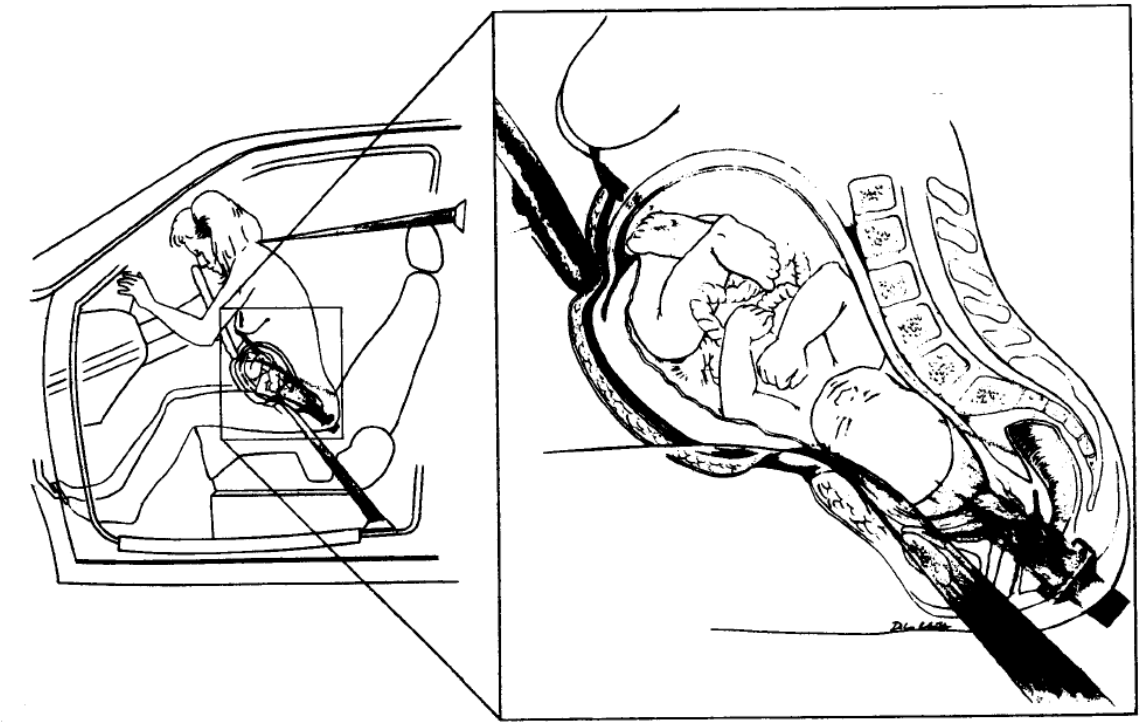

Figure 6: Steering wheel and belt loading on a pregnant occupant (Pearlman, 1997)

Klinich et al. (1999b) reviewed studies on the frequency of trauma in pregnant women in motor vehicle crashes. There were two main types of studies, clinical and epidemiological. Clinical studies typically focus on injuries from a medical standpoint (Dahmus, 1993; Elliot, 1966; Esposito, 1991; Fort, 1970; Goodwin, 1990; Hoff, 1991; Kissinger, 1991; Pearlman, 1990; Rothenberger, 1978; Timberlake, 1989; Williams, 1990). The studies are reviews of hospital medical records. Epidemiological studies focus on the automotive side (Agran, 1986; Aitokallio-Tallberg, 1997; Crosby, 1971; Fildes, 1992; Herbert, 1977; Lane P, 1989; Pepperell, 1977; Wolf, 1993). The studies are typically based off police accident reports. These studies are based on local or statewide records, and include no statistical analysis to estimate national trends in injury incidence,

type, or severity for pregnant occupants in MVCs. In order to estimate national trends, the National Automotive Sampling System (NASS) could be used. However, the NASS is not an accurate method of estimating fetal loss in MVCs, as there is no specific injury coding that details fetal outcome (Klinich, 1999b).

Klinich et al. (1999b) summarized 100 cases from the literature that involved pregnant occupants in motor vehicle crashes, excluding occupants below 20 weeks gestation. Two additional case studies were found for the year 2000 (Bunai, 2000; Gimovsky, 2000). For the combined 102 cases, most occupants were drivers (55%), only 24% were properly belted, and 62% were in frontal crashes. Maternal injuries were minor or none in 73 cases. There were 7 maternal deaths, all accompanied by fetal death. There were a staggering 81 fetal deaths out of 102 pregnant women (79%). Direct fetal injury was found in 28 fetal deaths, but 20 of those fetal deaths included placental injury. 53 fetal deaths occurred with no direct fetal injury, including 39 deaths with placental injuries. Overall, placental injury was involved in 73% of fetal deaths. Klinich et al. (1999b) noted that cases in medical journals are typically reported because they involve unusual or serious injuries. Therefore, these cases are not considered representative of the experience of pregnant occupants in general.

1.2.2 Injury Incidence

From a search of the National Automotive Sampling System (NASS), it was found that approximately 230,000 pregnant women were involved in motor vehicle crashes (MVCs) from 1995 to 2000 (Jernigan, 2002). Of these pregnant occupants, 78% were drivers, 49% were in frontal impacts, and 83.6% were belted. The occupants were broken down by trimester with 42.5% in the first trimester of pregnancy, 28.4% in the second trimester, and 29.1% in the third trimester. Belt use was also broken down by trimester with 60.4% belt use in the first trimester occupants, 92.5% in the second trimester, and 85.4% in the third trimester. Of the 38,000 pregnant women involved in motor vehicle crashes (MVCs) each year, nearly 70% were injured (Table 1).

Table 1: Estimates of annual incidence

Author	Pregnant Women in Crashes	Pregnant Women Injured	Pregnant Women Killed	Estimates of Fetal Losses
Jernigan (2002)	38412	24903	85	943
Pearlman (1996a)	N/A	130000	N/A	1300-3900
Klinich (1999b)	128255	29923	163	1283-3848
Klinich (1999b)	128255	29923	163	462-1061
Klinich (1999b)	128255	29923	163	333
Klinich (1999b)	128255	29923	163	1490-3724

Due to injuries sustained in the crash, a total of 509 pregnant occupants died. In addition, 434 severe placental and uterogenital injuries resulted in an assumed fetal loss. In total, there were 943 known fetal losses as a result of the trauma sustained to pregnant women in motor vehicle crashes. For the six year period from 1995-2000, this is an average of 157 each year. However, because NASS has no specific injury coding for fetal outcome, these estimates are low, and only reflect those cases with such severe injury as to be confident of fetal fatality as an outcome. None of the occupants who had fetal loss were exposed to an airbag deployment, and all of the injuries were induced by either the seatbelt, the instrument panel, or the steering wheel.

Several estimates of fetal loss due to motor vehicle crashes (MVCs) can be found in the literature. Pearlman (1996a) estimated 1300 to 3900 annual fetal losses based on the number of births in the U.S. (4 million annually). The 4 million births was multiplied by the reported 6% to 7% of women who experience trauma during pregnancy (6.5% was used in the calculation), multiplied by 50% for those traumas that are attributed to MVCs, and multiplied by a 1% to 3% fetal loss rate (FLR) for placental abruption.

Klinich et al. (1999b) reported four alternative methods to estimate the number of fetal losses per year. The 1998 U.S. Census female population was compared to the number of births in one year based on 1996 Center for Disease Control (CDC) data, to yield the percentage of the population that is pregnant. The 1996 Traffic Safety Facts was used to determine the number of women in MVCs, separated into injured, killed, and

uninjured. The number of pregnant women in MVCs was derived from the previous two values and then multiplied by 20/52 to represent the number of women of greater than 20 weeks gestation in one year (52 weeks). This total number of pregnant women, greater then 20 weeks gestation, in motor vehicle crashes was then filtered through different fetal loss rates to determine the annual number of fetal losses due to MVCs. The first method used 1% and 3% to predict 1283 to 3848 fetal losses. The second method divided the total number of women in MVCs into women killed and women injured, excluding the uninjured women. A 100% FLR was applied to the killed women, while 1% and 3% was used for the injured women. The result was an estimated 462 to 1061 fetal losses.

From the 1996 NASS database, 99.4% of women in MVCs had an Injury Severity Score (ISS) of less than 20. Using the ISS, a fetal lose rate of 1% was associated with ISS < 20 and a 20% FLR was associated with ISS ≥ 20. Thus, the third method produced an estimated 333 annual fetal losses. For the fourth method, the 1996 NASS database was analyzed for crash severity. Crashes were divided by crash change in velocity (ΔV) into minor (< 24 kph), moderate (24 – 48 kph), and severe (> 48 kph). Klinich reported that 72% of women were involved in minor crashes, 26% in moderate crashes, and 1% in severe crashes. Fetal loss rates based on crash severity were taken from the injury risk curves developed by the second-generation pregnant dummy (see Section 2.4.1.2). This method estimated 1490 to 3724 fetal losses. Overall, Klinich's estimates ranged from 333 to 3848 fetal losses.

1.3 Previous Laboratory Studies

The relevant research is broken down into pregnant animal tests, human abdominal response, modeling of the pregnant uterus, and development of pregnant crash test dummies.

1.3.1 Pregnant Animal Testing

Conducted in the late 60's and early 70's, several researchers investigated seatbelt effectiveness on pregnant baboons and monkeys. Snyder et al. (1966) tested six female baboons during seven lap belt-only sled tests. Peak sled deceleration was 20 g's in six tests and 40 g's in the other. Three of the female baboons were pregnant and three were

implanted with an artificial uterus. Maternal injuries ranged from uninjured to death, with maternal death occurring in two of the 20 g's tests and in the single 40 g's test. All three fetuses died.

Crosby et al. (1968) conducted 12 sled tests on eleven pregnant baboons. In eight tests, the baboon wore a lap belt only and in the other four tests, the baboon wore a 3-point belt. Peak sled deceleration was 20 g's in 10 cases, 40 g's in one case, and 33 g's in the last case. Severe maternal injuries occurred in three baboons and none of the fetuses survived. Due to the low number of tests, no conclusions were drawn comparing the use of a 3-point belt to a lap belt. However, because of the predominance of ejection as a cause of occupant death, the use of a lap belt was recommended for pregnant women.

Van Kirk et al. (1969) conducted eleven sled tests on 3 monkeys using a lap belt (1 test), a 4-point netting system (3 tests), and a 5-point net (7 tests). Peak sled deceleration ranged from 12 g's to 61 g's. The netting systems were designed to cover the entire thorax (Figure 7). Although each monkey was tested several times, none of the monkeys received significant injuries from the sled tests. As impressive as these results are, the use of a netting system in motor vehicles seems unlikely based on maternal comfort and appearance.

Figure 7: Pregnant monkey in the 4-pt netting system (van Kirk, 1969)

Because the previous studies looking at lap belt and 3-point belts did not include a significant number of survivable impacts, additional sled tests were conducted by King et al. (1971). The testing included lap belt and 3-pt belt restraint, with all tests run at approximately 42 kph. Data from 22 sled tests (Figure 8) showed a fetal death rate of 8.33% (1/12) for baboons subjected to a 3-point belt and a fetal death rate of 50% (5/10) for baboons subjected to a lap belt only. It was concluded that the shoulder harness provided superior protection to both mother and fetus as compared to the lap belt only.

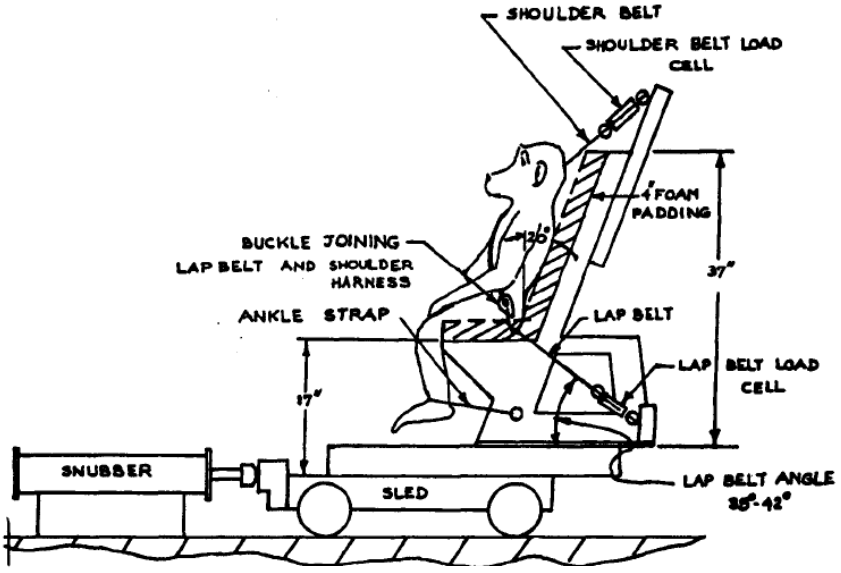

Figure 8: Schematic of pregnant baboon sled test (King, 1971)

1.3.2 Abdominal Response

Proper response of the abdomen is fundamental in providing a biofidelic model of a pregnant occupant in a motor vehicle crash. Typically, cadavers would be used to determine appropriate dynamic response of the abdomen, however pregnant cadavers are not available. Rupp et al. (2001) examined the differences between pregnant and non-pregnant abdomens. The resting pressure of a non-pregnant abdomen is approximately 1 kPa (8 mm Hg), while the resting pressure of a pregnant abdomen is 2 kPa (15 mm Hg). Computer simulations conducted by Rupp et al. suggest that the resting abdominal

pressure difference between pregnant and non-pregnant abdomens does not significantly influence the pressure response during dynamic loading. The pressure induced by loading was large compared to the initial pressure in both cases. Quasi-static testing of volunteers showed that the stiffness of the abdomen is not significantly different between pregnant and non-pregnant abdomens (Rupp, 2001). Tests were performed using a 2.54 cm diameter rigid bar impactor, the force was limited to 45 N and penetration was limited to 5 cm. It was concluded that non-pregnant abdominal response is valid for pregnant abdomens.

The 50th percentile male abdominal response for rigid bar impact, belt loading, and surrogate airbag loading was reported by Hardy et al. (2001), Rupp et al scaled the corridors to the mass of a 5th percentile pregnant female. Rigid bar impacts used a 2.54 cm diameter rigid bar impactor attached to a 48 kg ballistic pendulum. Both the 6 m/s corridor and the 3 m/s average are linear (Figure 9). Belt loading was accomplished by wrapping a belt around the abdomen at mid-abdomen (umbilicus) level and pneumatically retracting the yoke at 3 m/s. The belt corridor has an initial slope of about 1000 N per 1 cm of abdominal deflection (Figure 10). The slope of the final corridor begins to level off at about 3 cm of deflection and becomes negative around 7 cm deflection. The surrogate airbag loading tests simulate airbag deployment with the uterus in contact with the airbag. The impactor is a 7.6 cm diameter, 20.3 cm long hollow cylinder that is pneumatically accelerated to 13 m/s (Figure 11).

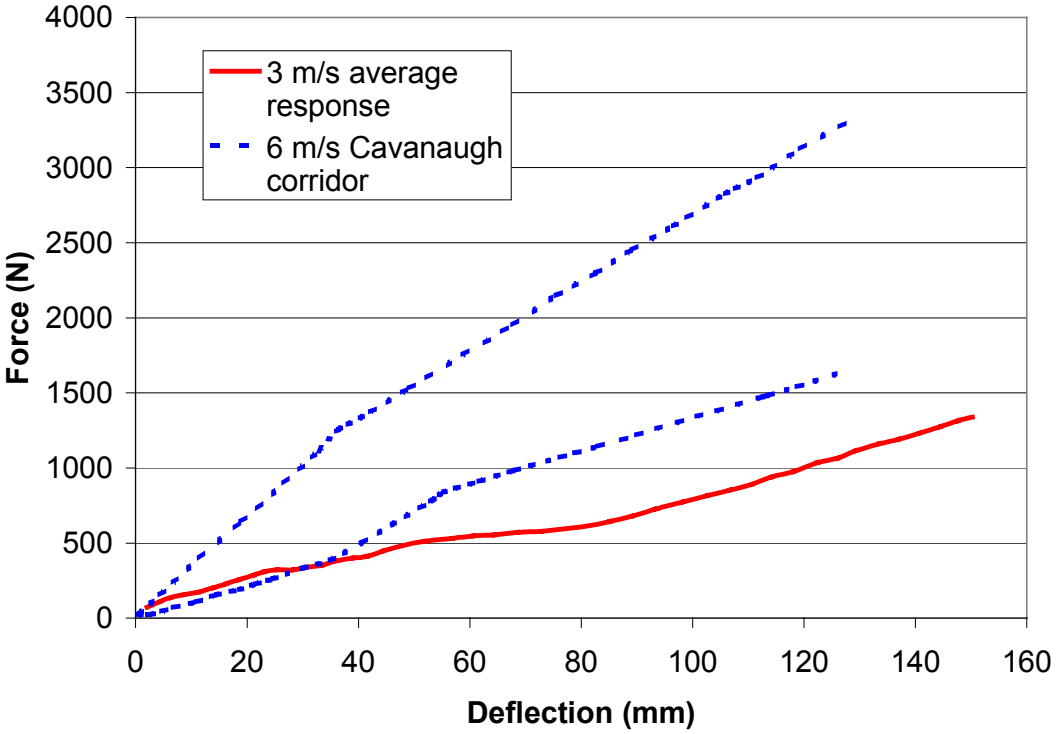

Figure 9: Rigid bar impactor corridors (Hardy, 2001; scaled by Rupp, 2001)

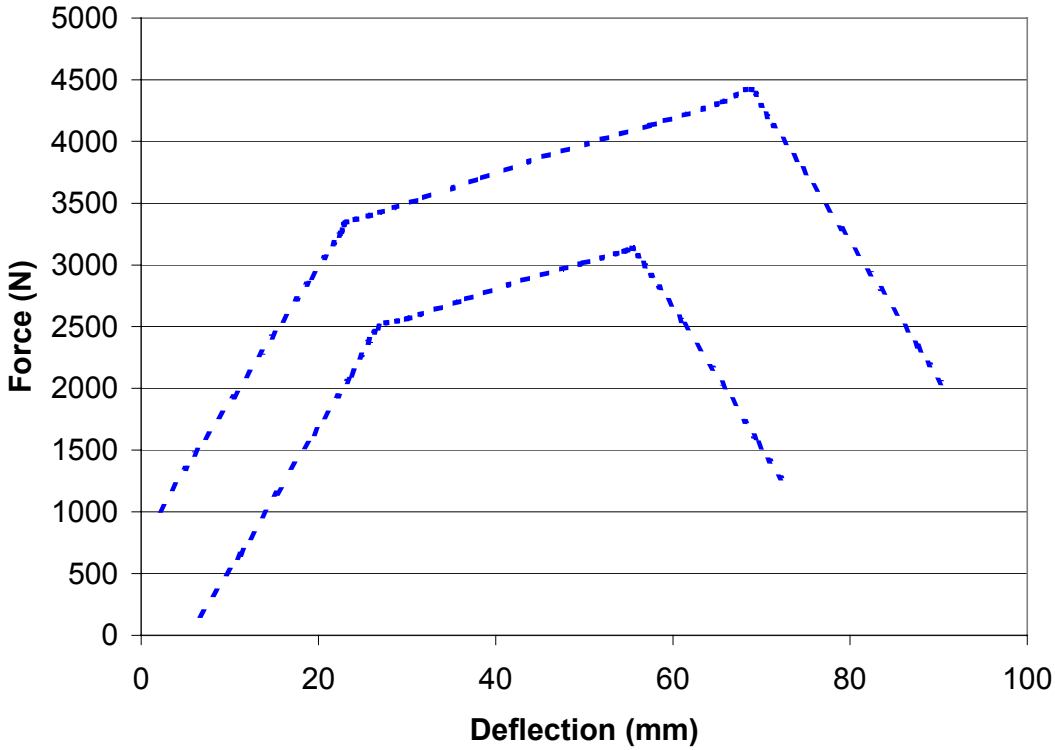

Figure 10: Belt loading corridor (Hardy, 2001; scaled by Rupp, 2001)

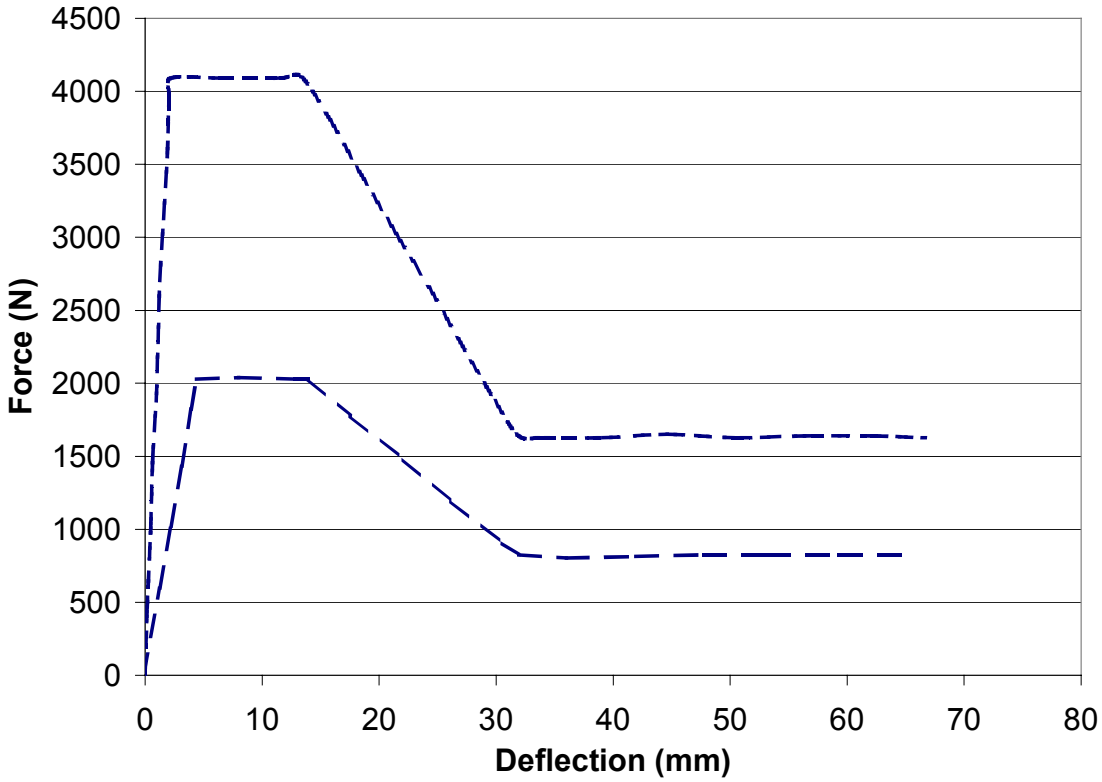

Figure 11: Surrogate airbag loading corridor (Hardy, 2001; scaled by Rupp, 2001)

1.3.3 Modeling Pregnant Occupants

A search of the literature found several modeling efforts for the pregnant uterus during labor and delivery (Mizrahi 1975, Rice 1976). The only research on the pregnant abdomen in motor vehicle crashes was conducted at UMTRI. Rupp et al. investigated placental abruption using a finite element model of the uterus.

The primary goal of the UMTRI modeling was to determine the most probable mechanisms of placental abruption. The five hypothesized causes of placental abruption were tested using a dynamic finite element solver. Because the hypothesized causes focus on different aspects of the interactions in the pregnant abdomen, the model was modified for each mechanism. The main model represented a seven-month pregnant uterus using simplified shapes to represent the uterine bodies. The basic model was a spherical uterus with a placenta and amniotic fluid. The fetus was only included in one series of tests, for which it was represented by two ellipsoids. The uterus, placenta, and amniotic fluid were modeled with solid elements and the material properties were taken

from the literature. The solid elements used for the amniotic fluid were given a zero shear modulus and a sliding contact was set between the fluid and the uterus. To evaluate the different mechanisms, boundary and loading conditions were varied to focus the model on the relevant injury mechanism. The results of the simulations will be presented with the relevant injury mechanism.

The simplified model of Rupp et al. (2001) provided valuable information regarding the injury mechanisms of placental abruption. The model however, is not functional as a tool to determine fetal loss for actual crashes. The dynamics of an occupant in a motor vehicle crash cannot be simplified to just an applied acceleration or a simple rigid bar impact. The motion of the occupant in the vehicle and the uterus in the abdomen is complex and leads to combined loading on the fetus. The spherical shape of the model used by Rupp, while convenient, is not representative of the uterus. A sphere has three axes of symmetry, while the uterus only has one. In addition, Rupp et al. did not include the material properties or dimensions of the uterus; therefore, this model cannot be used as a building block for future researchers.

1.3.4 Pregnant Crash Test Dummies

The First-Generation Pregnant Dummy (Figure 12):

Developed in 1996, the first-generation pregnant dummy was a 5th percentile female Hybrid III anthropometric testing devices (ATD) that was retrofitted with an abdominal insert (Pearlman, 1996b; Viano, 1998). The pregnant abdomen was represented by a fetus surrounded by "amniotic fluid" gel, and encased in a "uterus" lining (Figure 13). No placenta was included in the ATD. The uterus and amniotic fluid were molded using Skinflex III urethane. The fetus was 17.4 cm long, 11.8 cm deep, 7.6 cm wide, and weighed 1.68 kg. This corresponds to the size and weight of a 50th percentile fetus at 7 months based on data from Culver and Viano (1990).

Figure 12: 1st generation pregnant dummy (Pearlman, 1996b)

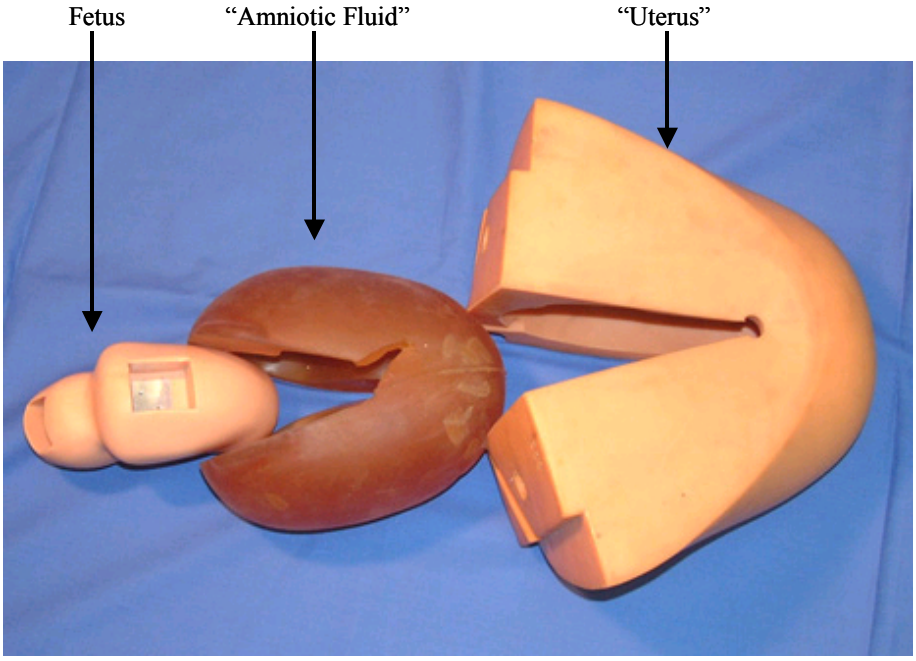

Figure 13: Fetus, "amniotic fluid", and uterus of the 1st generation pregnant dummy

Triaxial accelerometers were inserted into the head and torso of the fetus to measure head and chest acceleration. To estimate the force transmission through the uterus, four load bolts were attached to a reaction plate anterior to the spine.

The production Hybrid III female dummy was modified to accommodate the pregnancy insert. The top and front surface of the pelvis was machined with a 9.50 cm radius. Total dummy weight was 132 lb, which was a 22.0 lb increase over the non-pregnant dummy. This weight was consistent with the average weight gain at 28-32 weeks gestation as reported by Culver and Viano (1990).

Test Conditions: Using a Hyge sled, two series of tests were conducted at various speeds to evaluate fetal response as a function of restraint. The first series consisted of 31 tests at speeds of 16 kph, 24 kph, 32 kph, and 40 kph. Four restraint conditions were examined, proper placement of the lap-shoulder belt, lap belt only, placement of the lap belt over the uterus with and without the shoulder belt, and unbelted. The second series examined the effects of airbags; eight tests were conducted with airbag deployment at speeds of 0 kph, 24 kph, 32 kph, and 40 kph. Airbag deployments were performed on both lap-shoulder belt and unbelted cases. Additionally, "out of position" airbag deployment was examined. For these tests, the dummy was positioned against the airbag without the lap-shoulder belt.

Results/Conclusions: Initially, static belt compression tests were performed to determine the stiffness of the pregnant insert. An anterior-posterior deflection of 70 mm to 95 mm was applied to the abdomen and normal loads of 780 N to 1350 N were measured. This resulted in a stiffness of 12.7 N/mm ± 1.6 N/mm.

From the first test series, an increase in speed resulted in larger head and chest acceleration and greater force transmission through the uterus. The authors found a threefold to fourfold increase in the measured abdominal force for tests with improper lap belt placement compared to the recommended belt placement (Figure 14). Tests without a shoulder belt, in which the lap belt was placed over the abdomen, produced the largest abdominal force. These results are consistent with results from animal experiments (Crosby, 1972).

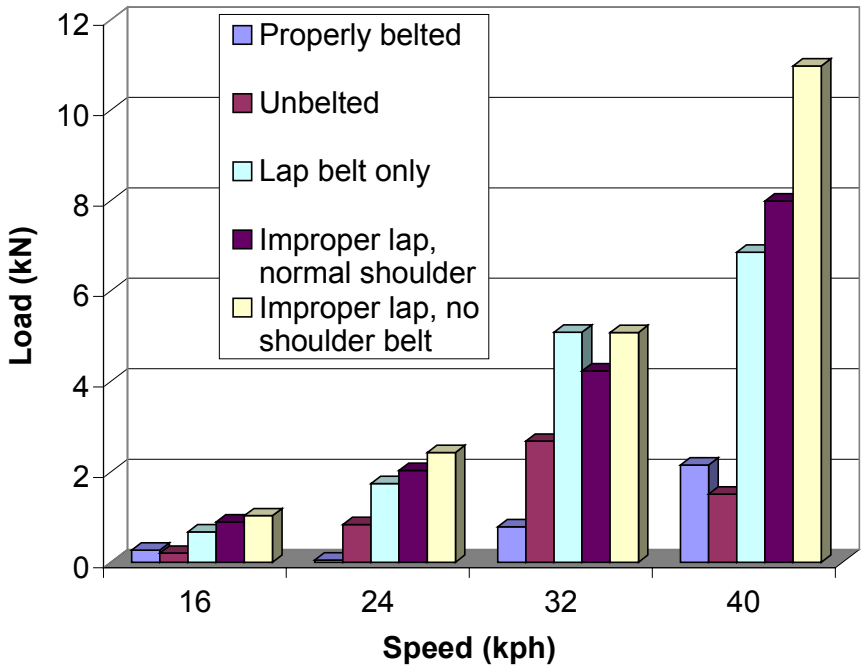

Figure 14: 1st generation pregnant dummy test results: Abdominal force (Viano, 1998)

In the second series of tests, a decrease in the abdominal force through the uterus was seen with airbag deployment compared to the non-airbag cases regardless of seatbelt use. Out-of-position tests produced the highest levels of fetal head and torso acceleration and force transmission (Figure 15). The high levels of acceleration could increase the risk of placental abruption or direct fetal injury. It was noted that these out-of-position tests were artificial, but considering the protrusion of the abdomen, there is an anatomical rationale for these tests.

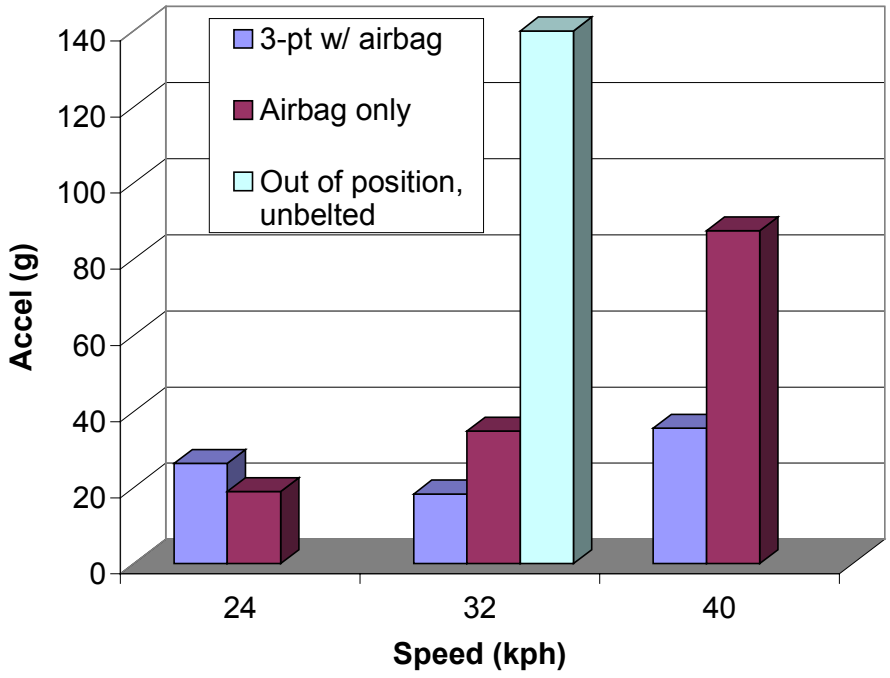

Figure 15: 1st generation pregnant dummy results: Fetal head acceleration (Viano, 1998)

As in the production dummy, the pregnant dummy showed increased safety, as measured by head and chest acceleration, with the proper placement of the lap-shoulder belt. For both the mother and fetus, 3-pt belts reduced the likelihood of injury. The authors suggested that future pregnant dummies include an uteroplacental interface to measure the forces required to cause placental abruption.

The Second-Generation Pregnant Dummy:

Rupp et al., (2001) at the University of Michigan Transportation Institute (UMTRI) developed the Maternal Anthropometric Measurement Apparatus, version 2b (MAMA-2b) as a second-generation pregnant test dummy. The primary objectives for the MAMA-2b were to develop an ATD with a more realistic abdominal size and shape, a more biofidelic force-deflection response and to instrument the dummy to assess the risk of fetal loss from placental abruption. The last objective, instrumentation aimed at a specific injury, is a departure from traditional ATD design, which is instrumented to assess injury criteria for a body region.

The MAMA-2b is a retrofitted Hybrid III small-female dummy (Figure 16). The 5th percentile dummy is thought to show the worse case scenario because small females tend to sit closer to the steering wheel compared to larger females. The abdominal insert represents a pregnant abdomen of thirty weeks gestation. The size was chosen because it was the largest component that can fit inside the small female dummy without redesign of the ribs. The external contour of the pregnant abdomen is based on anthropomorphic data collected by Klinich et al. (1999a). The MAMA-2b's abdomen does not protrude as far forward as the original pregnant dummy (Figure 17).

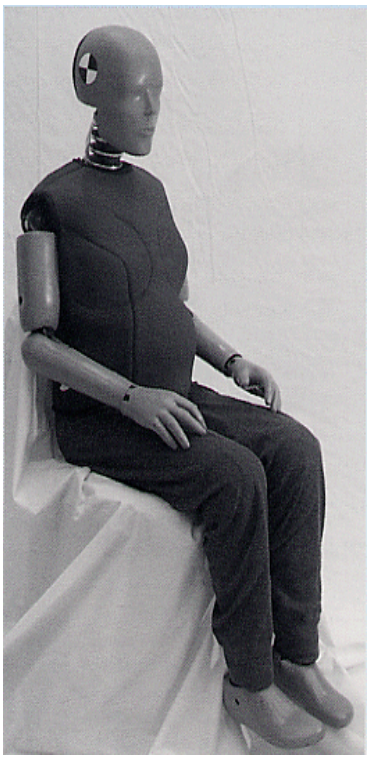

Figure 16: MAMA-2b, 2nd generation pregnant dummy (Rupp, 2001)

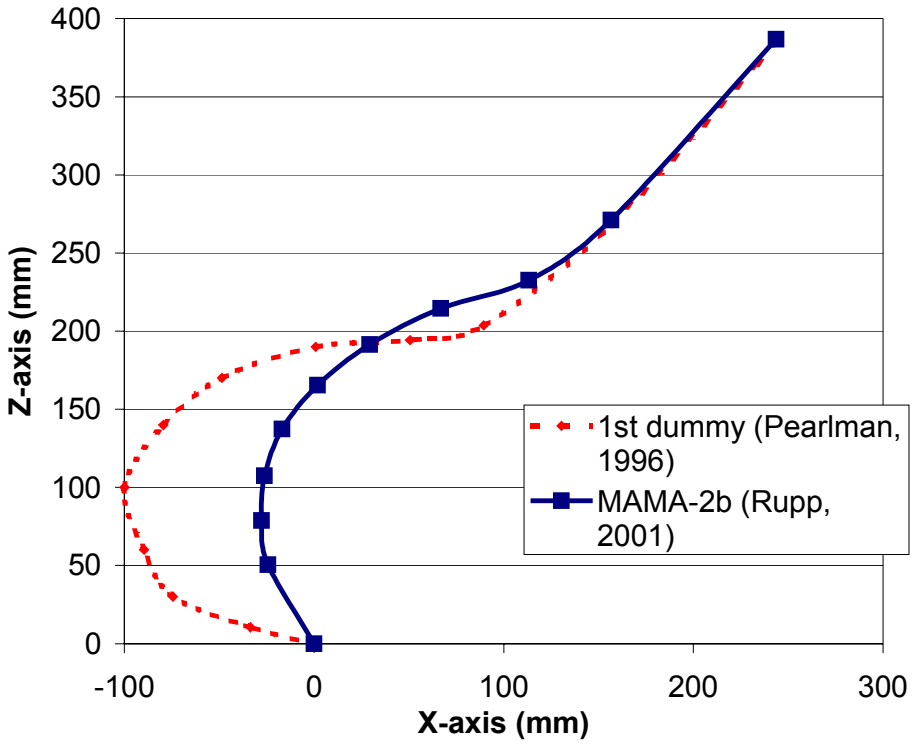

Figure 17: Abdominal contour: MAMA-2b vs. 1st pregnant dummy (Rupp, 2001)

A fluid filled bladder was chosen for the abdominal insert because it offered greater rate sensitivity to impact loading versus a solid insert like the one used on the first-generation pregnant dummy, and a fluid filled bladder would allow for direct measurement of pressure in the abdomen. Water was chosen as the fluid for the bladder because amniotic fluid is 99% water. The abdominal insert does not contain a fetus or placenta because the proposed injury mechanisms of placental abruption are independent of the fetus. In addition, there was anticipated difficulty in the repeatability of measured responses. The bladder was molded from 50-durameter-silicone rubber, with a thickness of 6 mm a major axis of 196 mm, and a minor axis of 172 mm.

The fluid filled bladder was glued to two cradles, one on the superior posterior, and the other on the inferior posterior. These cradles were used to attach the abdominal insert to the small-female dummy. The lower cradle represents the interaction of the uterus with the pelvis. The upper cradle simulates the viscous resistance to forward motion thought to occur.

A standard Hybrid III small female has a mass of 49 kg (108 lb). At 30 weeks gestation, a pregnant female gains a mass of 9 kg (Jensen, 1996). The MAMA-2B has a mass of 58 kg (128 lb), with a mass of 5.3 kg added to the pelvis, 2.5 kg distributed along the spine box and the remaining added mass due to the abdominal insert. The seated center of gravity for the dummy was 227 mm above and 169 mm forward of the H-point (the center of the femoral head), and is 8 mm forward and 10 mm down from the standard small female dummy.

To insure proper fit of the abdominal insert, half of the sternum plate was removed and the 4th, 5th, and 6th ribs were altered to create an inverted "V" shaped opening. Spring-steel stiffeners were added to stabilize the altered ribs. A standard 6.7 m/s thorax calibration test was conducted to determine if the altered thorax would meet specifications for the standard small female dummy (Figure 18). In the final dummy prototype, the bladder was instrumented with an anterior pressure transducer.

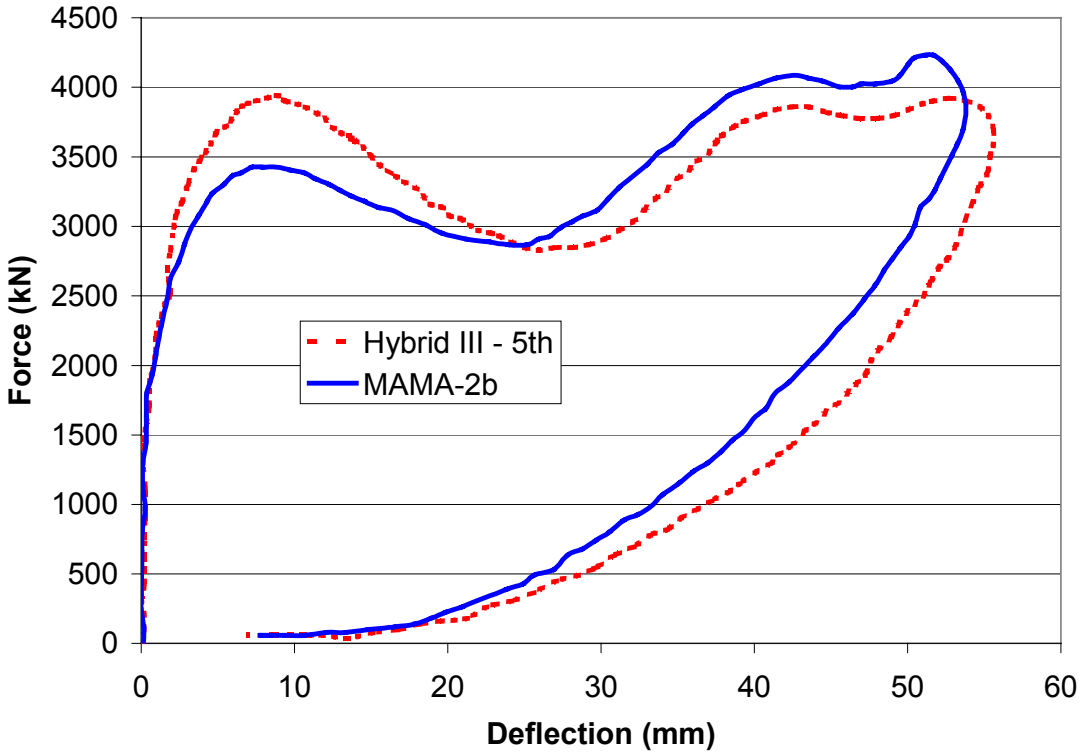

Figure 18: Thorax calibration test results for the MAMA-2b (Rupp, 2001)

Test Conditions: A series of 15 sled tests were performed utilizing both driver and frontal passenger configurations (Table 2). The restraint type was varied from no restraint to 3-point belt plus airbag (Figure 19). The change in velocity (delta V) ranged from 13 kph to 55 kph.

Table 2: Test Matrix for MAMA-2b (Rupp, 2001)

Test	Position	Restraint	Delta V (kph)	Risk (%)
1	Driver	None	13	36
2	Driver	None	20	54
3	Driver	None	35	86
4	Driver	3-pt belt	13	9
5	Driver	3-pt belt	25	26
6	Driver	3-pt belt	35	51
7	Driver	3-pt belt	35	51
8	Driver	3-pt belt	45	76
9	Driver	3-pt belt	55	90
10	Driver	3-pt belt + airbag	25	26
11	Driver	3-pt belt + airbag	25	26
12	Driver	3-pt belt + airbag	45	76
13	Passenger	3-pt belt	13	9
14	Passenger	3-pt belt	35	51
15	Passenger	3-pt belt	55	90

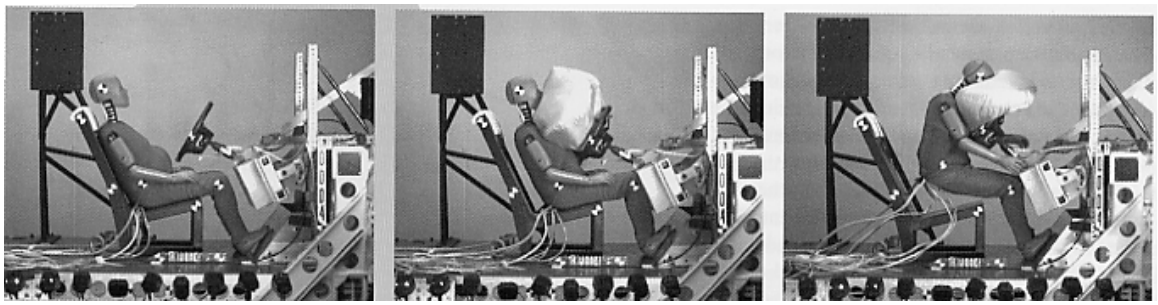

Figure 19: Airbag deployment during sled test with MAMA-2b (Rupp, 2001)

Results/Conclusions: The MAMA-2b abdomen was validated using 6 m/s and 3 m/s rigid bar impacts, 3 m/s belt loading, and surrogate airbag loading. The dummy abdomen lacks the rate sensitivity of the human abdomen, as witnessed in the rigid bar

tests (Figure 20). The dummy abdomen force deflection response falls near the lower bound of the 6 m/s corridor and was slightly stiffer than the 3 m/s average response. The belt loading response was within the corridor, except between 20 mm and 40 mm, where the response was less stiff then the corridor (Figure 21). In surrogate airbag loading tests, the pregnant dummy abdomen was initially less stiff then the corridor, but falls within the corridor after 5 mm of penetration (Figure 22). Based on these results, Rupp et al. deemed the abdominal response acceptable.

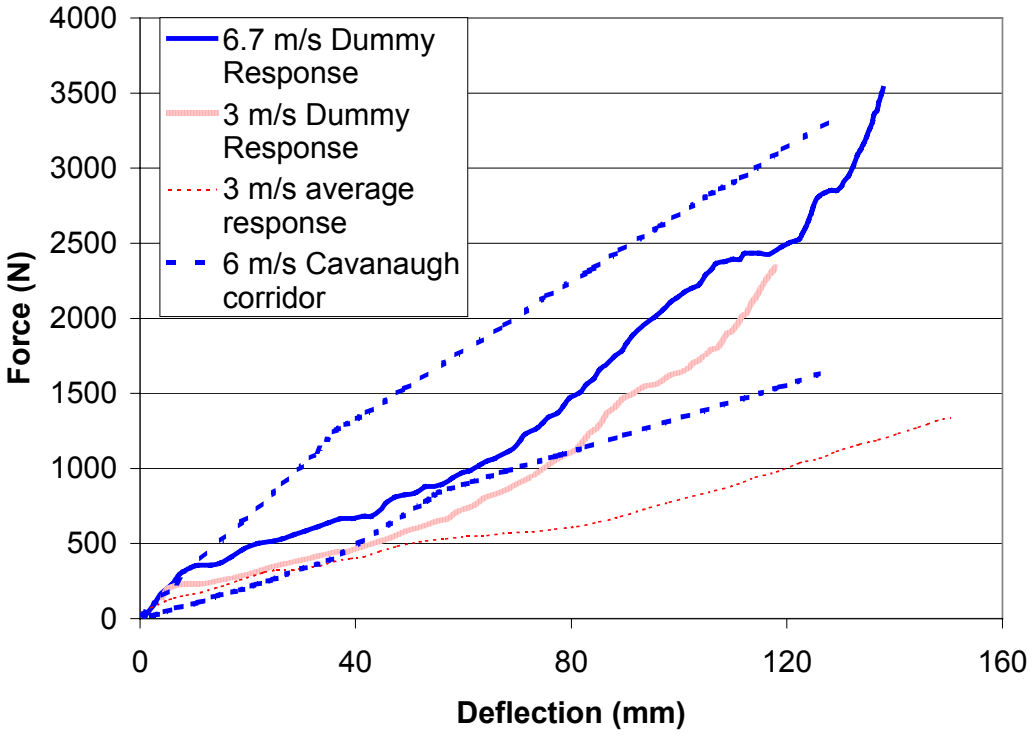

Figure 20: MAMA-2b abdominal response to rigid bar impact (Rupp, 2001)

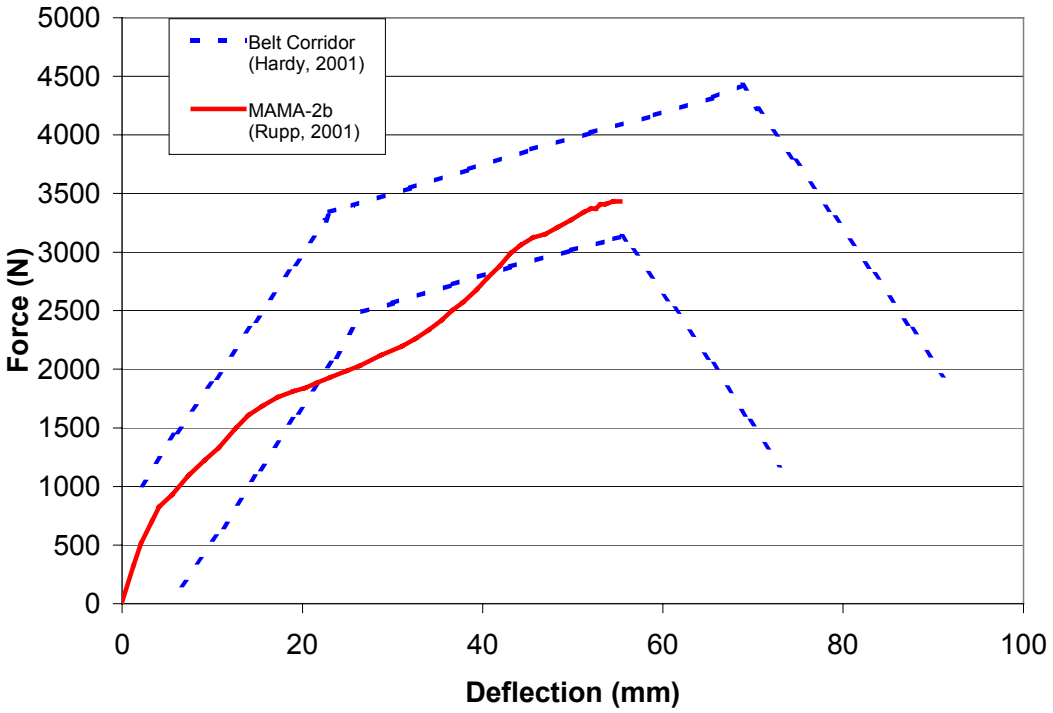

Figure 21: MAMA-2b abdominal response to 3 m/s belt loading (Rupp, 2001)

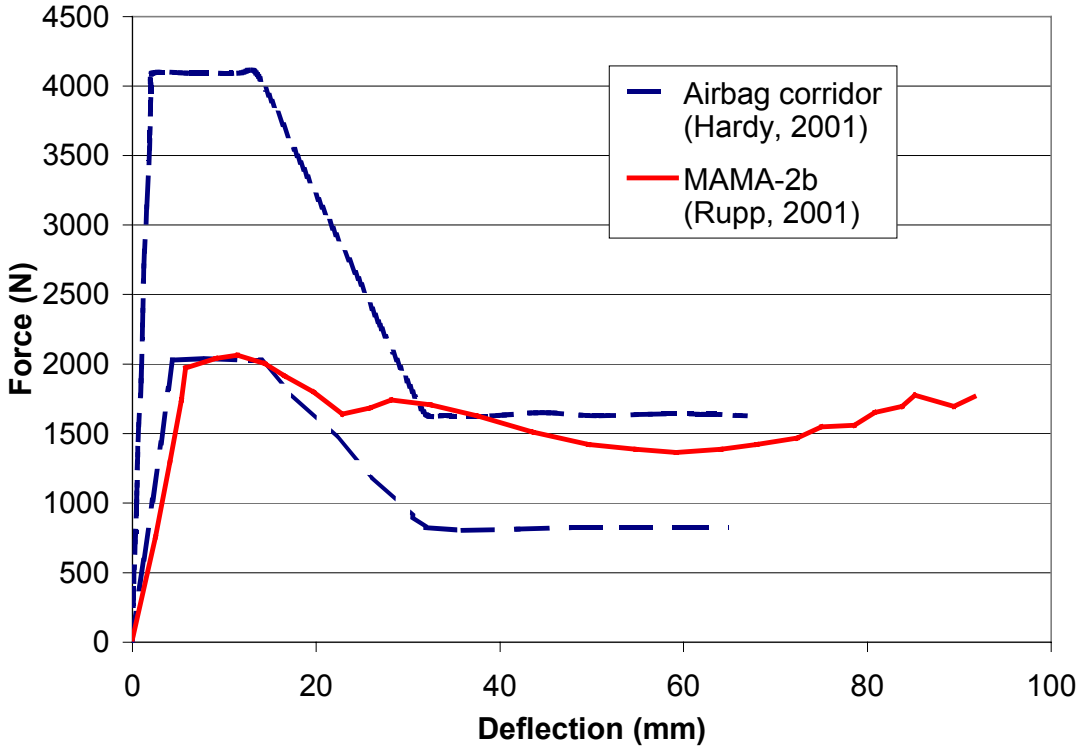

Figure 22: MAMA-2b abdominal response to airbag loading (Rupp, 2001)

For the full dummy sled tests, head, chest, and pelvis acceleration, as well as abdomen pressure were recorded. As mentioned before, the posterior pressure was erratic and deemed faulty. The primary result was therefore the peak anterior pressure, which was used to develop an injury criteria (Figure 23). As was expected, the peak anterior pressure increased as the crash speed increased and was greatest for unrestrained drivers.

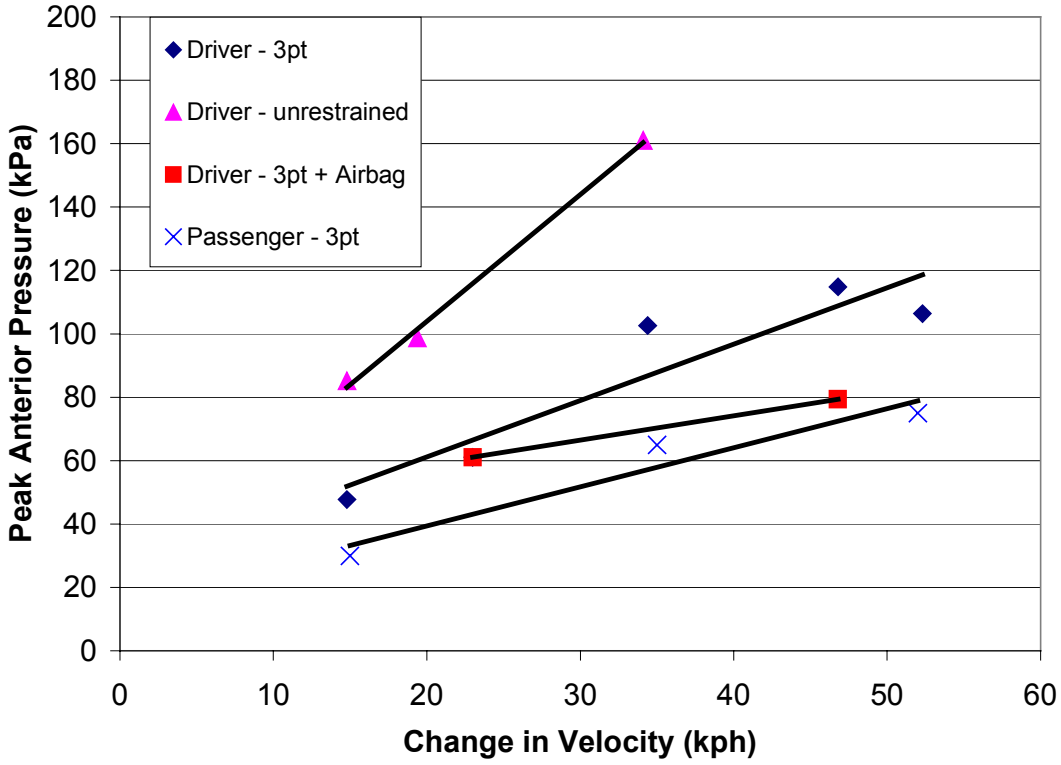

Figure 23: MAMA-2b test results: Pressure vs. crash speed (Rupp, 2001)

For the typical pressure time history, anterior pressure was positive throughout the tests (Figure 24). Anterior pressure was positive because of the compressive loading and fluid inertia. Bladder pressure peaked when the belt loading and chest deceleration peaked. These peaks reflect loading by the lap belt, shoulder belt, and steering wheel.

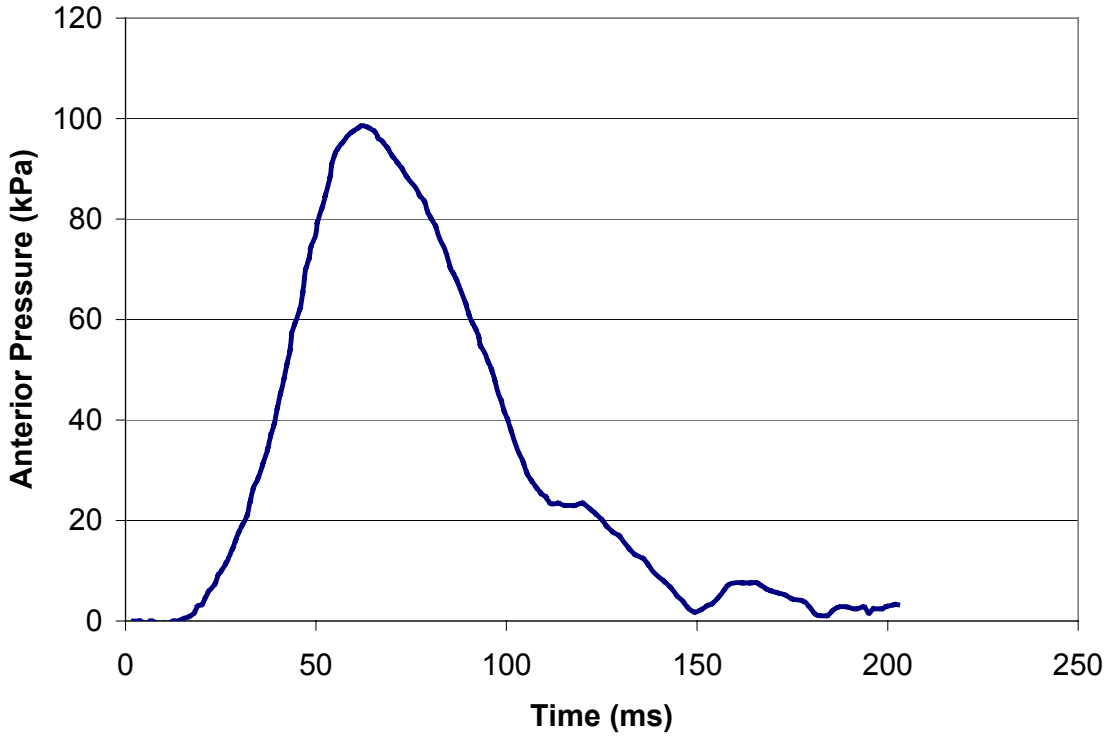

Figure 24: Typical anterior pressure-time history (Rupp, 2001)

Rupp at al. noted a limitation to using only peak anterior pressure; because the pressure is a function of fluid displacement, a small object penetrating deep into the abdomen could produce the same peak pressure as a large object with minimal penetration. Although the injury function would predict the same risk of adverse fetal outcome, this may not be realistic, specifically if a small object impacts away from the placenta. It was concluded that the prototype dummy was durable, repeatable, and that future work should focus on instrumentation and tissue testing.

1.4 Injury Mechanisms

As mentioned previously, up to 70% of fetal losses with maternal survival are due to placental abruption (Pearlman, 1990). The actual mechanisms of placental abruption

are not known. Rupp et al. (2001) hypothesized five mechanisms of UPI failure. Based on computer modeling discussed previously, two of the mechanisms were regarded as most likely to cause placental abruption. The other three mechanisms were discounted as unlikely to be the main cause of placental abruption. Rupp et al. (2001) believe that more than one mechanism could be responsible for placental abruption.

Discounted Mechanisms of Placental Abruption

1) Fetus-placenta interaction

To test this hypothesis, a fetus made up of two ellipsoids was added to the uterus model previously discussed. The uterine model was dropped onto a rigid plate at several angles (Figure 25). The stress in the UPI peaked at two occasions, both coincident with large uterine deformation. From these simulations, it was concluded that stresses and strains generated in the UPI due to the contribution of the fetus is small relative to the strain caused by deformation of the uterine wall. Additionally, because the placenta is typically in the upper portion of the uterus, the fetus is unlikely to load the placenta during anterior-posterior (A-P) compression from a MVC.

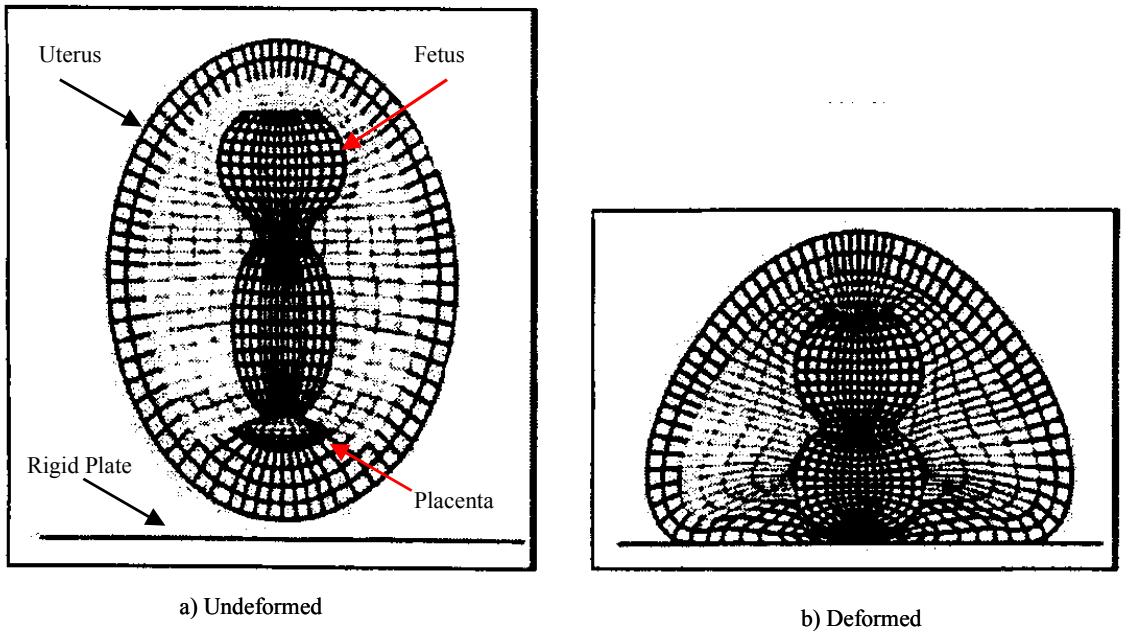

Figure 25: Cross-section of uterus with fetus during drop test (Rupp, 2001)

2) Inertial loading of the UPI by the placenta

The uterine model, without a fetus, was fixed to a rigid boundary to simulate viscous resistance to motion that is expected to occur in the posterior uterus due to dynamic loading. This model was impacted 180° from the rigid boundary to simulate the A-P compression found in MVCs. It was found that UPI shear stresses produced by placental inertia were small compared to shear stresses due to deformation of the uterine wall.

3) Shear strains at the UPI due to pressure-induced circumferential strains in the uterus

Circumferential strain was evaluated by a simple mathematical model of a spherical uterus. Compression of the bottom half of the uterus, causing all the amniotic fluid to be displaced into the upper half of the uterus, resulted in 26% circumferential strain. It is thought that 60% strain is required for placental abruption; therefore, pressure-induced circumferential strain was discounted as a cause of placental abruption.

Likely Mechanisms of Placental Abruption

1) Tensile loading at the UPI due to pressure gradients generated by the inertia of the amniotic fluid

During impact loading, the negative pressure in the posterior uterus may cause tensile strains in the UPI. In the uterus model, the UPI was modeled using beam elements. The constrained uterine model was decelerated at 35 g to simulate a 48 kph barrier impact. At 3 ms, with minimal uterine deformation, a pressure gradient develops across the uterus with a posterior pressure of –34 kPa (Figure 26). At 10 ms, the pressure is –40 kPa in the posterior uterus. Based on the lower bound UPI failure tension of 15.6 kPa (Pearlman, 1999), negative pressure in the posterior uterus is a likely cause of placental abruption. This pressure gradient can develop in the absence of, or prior to, direct loading of the uterus.

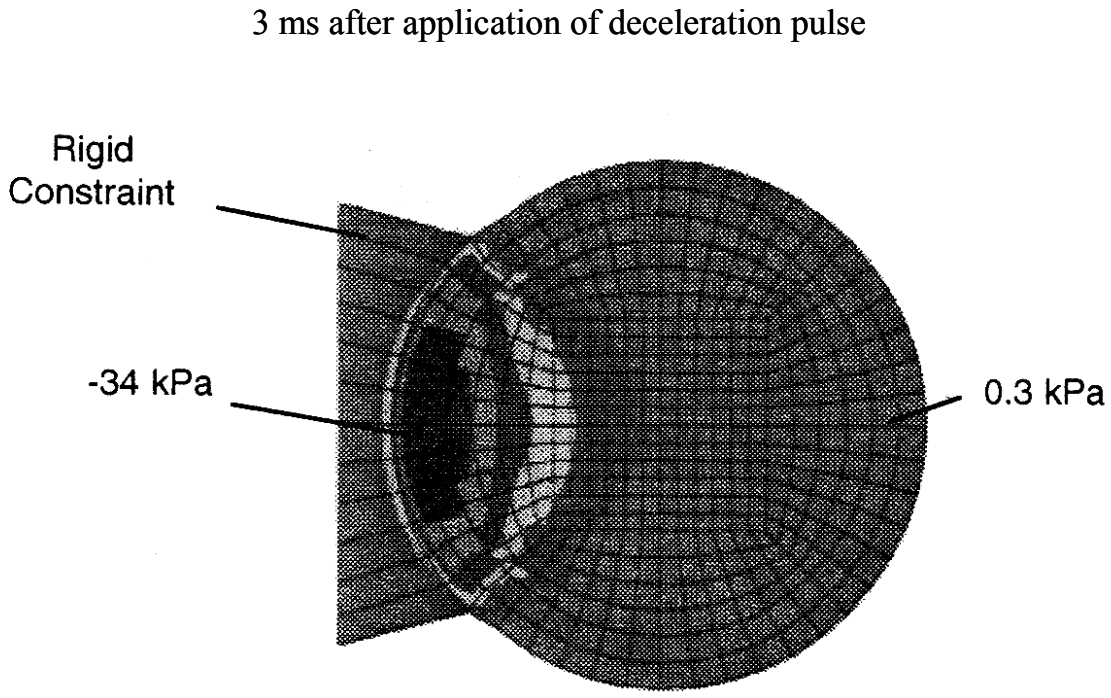

Figure 26: Pressure gradient in uterus after 35 g deceleration (Rupp, 2001)

2) Shear strains in the UPI from local curvature changes in the uterus due to direct loading of the abdomen.

The uterine model was constrained by a hemi-spherical rigid boundary and impacted with a 2.5 cm diameter hemispherical impactor (Figure 27). Peak uterine strains exceeded 60%, resulting in predicted placental abruption. Stress and strain decreased rapidly away from the impact site, suggesting that placental abruption will only occur if the impact location is close to the UPI.

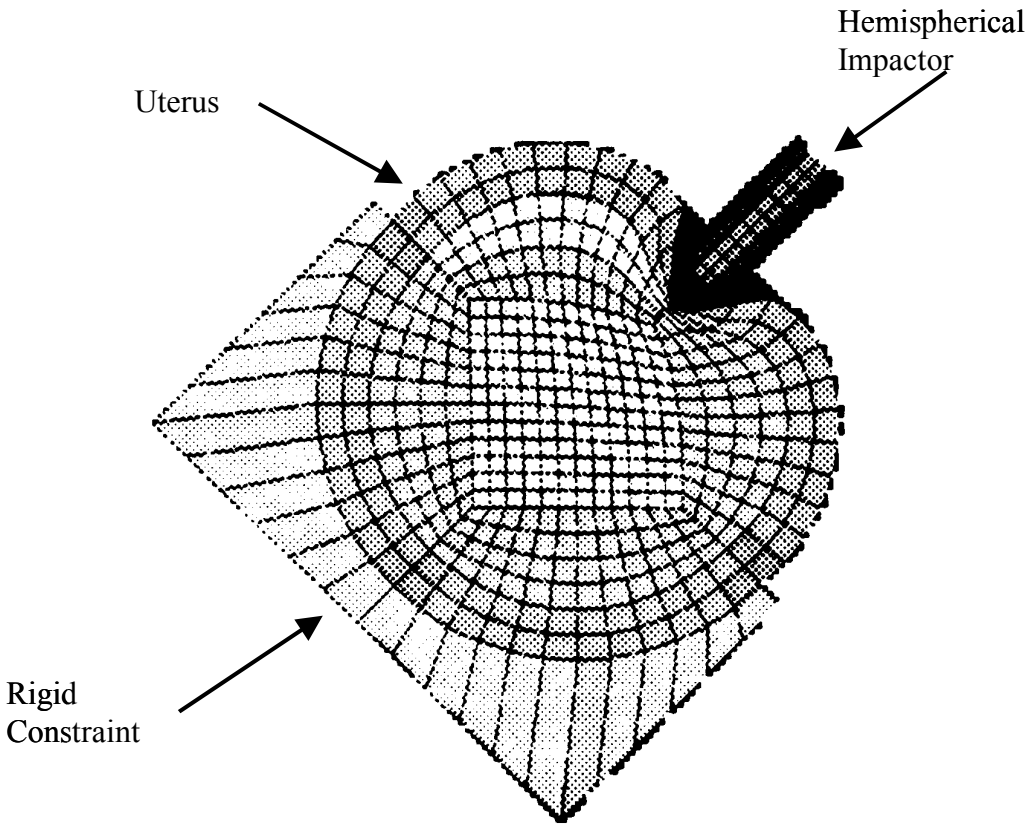

Figure 27: Direct loading of uterus by hemispherical impactor (Rupp, 2001)

1.5 Injury Criteria

Fetal injury from a motor vehicle crash can be inferred by three methods. The risk of adverse fetal outcome was correlated to both crash speed and restraint use by Klinich et al. (1999b). Rupp et al. (2001) combined that risk curve with the peak anterior pressure measured in the second generation pregnant dummy, resulting in a injury criteria that can be utilized in sled tests. Finally, placental abruption can be inferred from tissue failure in the uterine wall or uteroplacental interface.

1.5.1 Crash Severity and Restraint Use

In order to investigate the circumstances surrounding the incidence of pregnant women in MVCs and to determine an injury risk function, Klinich et al. (1999b) conducted 42 detailed investigations of crashes involving pregnant occupants. Crashes

involving occupant less than 20 weeks pregnant, rollovers or multiple impacts, and participants who did not agree to participate were excluded from this study. The 42 investigations comprised of 43 pregnant occupants where 60% were the drivers, 62% were involved in frontal crashes, and 72% were wearing a 3-pt belt or a 3-pt belt with an airbag. Of the 43 occupants, 77% suffered minor or no injuries. There was favorable fetal outcome for 27 of the 43 occupants (63%). Of the 8 major injuries and 8 fetal deaths, 7 included placental abruption. There were four maternal deaths, three were accompanied by fetal demise, and one accompanied by major fetal complications. In general, it was found that crash severity (ΔV) and maternal injury had a negative effect on fetal outcome and restraint use had a positive effect on fetal outcome. It was concluded that protection of the mother was important for protecting the fetus.

Fetal outcome was divided into two categories: good outcome or minor complications and major complications or fetal loss. Logistic regression was performed to establish risk curves for adverse fetal outcome (Figure 28). Proper restraint was defined as 3-pt belt or 3-pt belt plus an airbag. Improper restraint was defined as unrestrained, airbag only, or shoulder belt only.

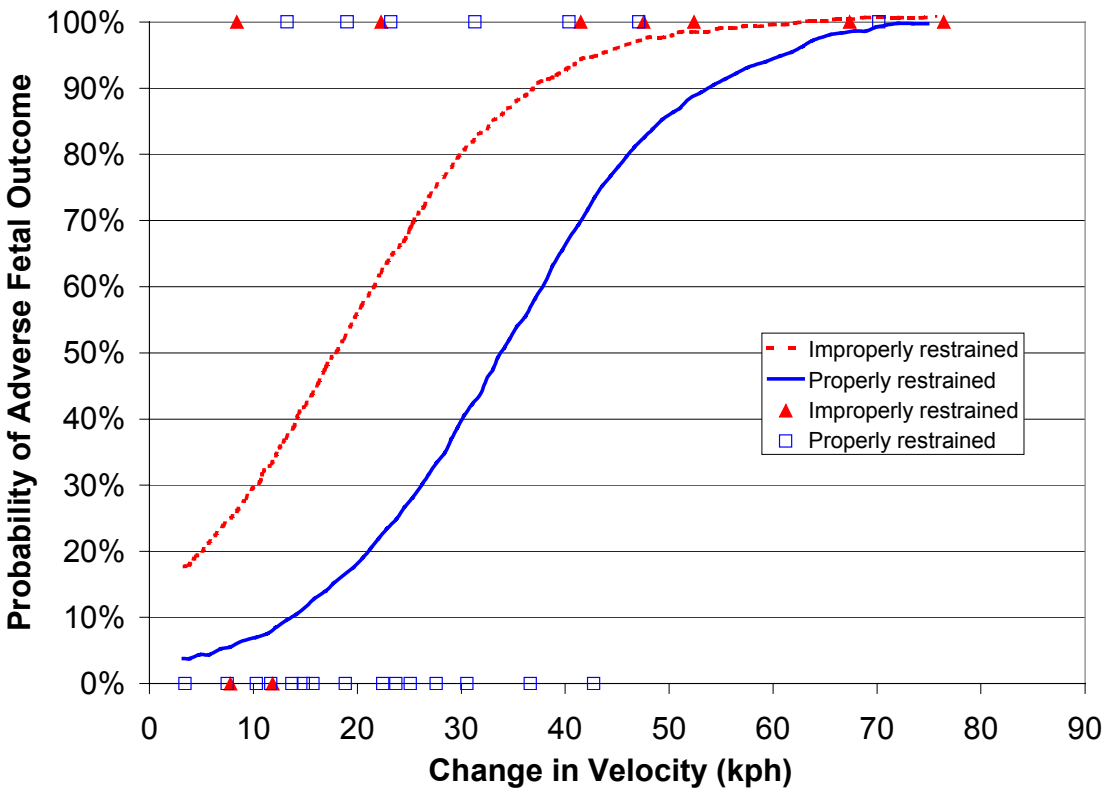

Figure 28: Adverse fetal outcome risk curve (Klinich, 1999b)

1.5.2 Peak Dummy Uterine Pressure

Rupp et al. used the relationship between crash speed, restraint, and risk of adverse fetal outcome from Klinich et al. (Figure 28), along with the results of sled tests conducted with the pregnant dummy (Figure 23), to develop a risk function based on peak anterior pressure and risk of adverse fetal outcome (Figure 29). A power law relationship was applied to the data (Equation 1).

$$\Theta = 0.0021\ P^{2.25} \qquad \text{Equation. 1}$$

where Θ is the percent risk of adverse fetal outcome and P is the peak anterior pressure (kPa). The development of injury criteria based on strain, posterior pressure, or a pressure gradient were unsuccessful due to instrumentation problems.

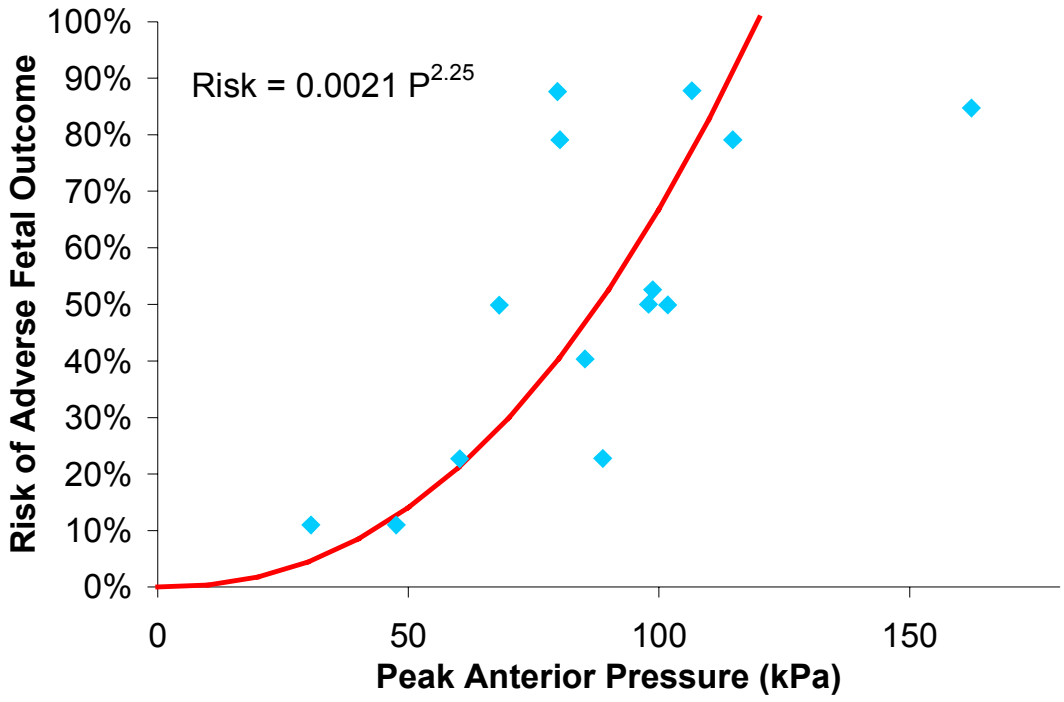

Figure 29: Risk curve developed from the MAMA-2b (Rupp, 2001)

1.5.3 Tissue Failure

Injury can also be predicted from tissue limits. Placental abruption is believed to occur when the strain in the UPI exceeds 60% or when uterine strain exceeds 60% in the circumferential direction and 450% in the radial direction (Ashton-Miller, reported in Rupp, 2001; Pearlman, 1999). In general, the uterine tensile strength ranges from 483 kPa to 2068 kPa with an average of 1034 kPa (Pearsall, 1978; Wood, 1965). The literature did not contain data on the tensile limits of the placenta. The tensile strength of the UPI is approximately 16 kPa (Rupp, 2001).

1.6 Research Objectives

The objective of this study was to create a pregnant uterine model which, once integrated into a 5th percentile female human body model, predicts fetal outcome from impact loading based on placental abruption. Secondary objectives were to evaluate the

interaction of current seatbelts and airbags with the pregnant abdomen, and to test new restraint designs.

In order to investigate pregnant women in motor vehicle crashes, a finite element model of the pregnant uterus was created. The model simulates a uterus of 30 weeks gestation without a fetus. The fetus was not included because the injury mechanisms of placental abruption were reported by Rupp et al. not to be effected by the fetus. The uterus, which contains the placenta and amniotic fluid, is surrounded by fat and supported to the pelvis by two pairs of ligaments. The uterine model was integrated into a pre-existing 5^{th} percentile female model. The abdominal response of the new pregnant model was compared to the appropriate abdominal corridors for rigid bar impacts and belt loading. Dynamic loading was accomplished by simulating frontal sled tests with the pregnant model as a driver. The sled deceleration and the restraint used were varied to investigate the role of each. The strain in the uterine wall near the placenta and the anterior-posterior pressure differential in the uterus were recorded for each test.

The next two chapters are stand alone papers describing the basic model creation and detailing the results of this study as it applies to the medical community (Chapter 2) and the automotive community (Chapter 3). A detailed description of the procedures undertaken to create the model, along with the truncated code, are contained in the appendix. Also included in the appendix are additional results, particularly time history plots of the pregnant model.

Chapter 2

Computational Model of the Pregnant Occupant: Predicting the Risk of Injury in Automobile Crashes

Abstract

OBJECTIVE: The goal of this study was to create a computational model of the pregnant occupant to predict fetal outcome in motor vehicle crashes.

STUDY DESIGN: A finite element uterine model of a 7-month pregnant female was created and integrated into a multi-body human model. Unrestrained, 3-pt belt, and 3-pt belt plus airbag tests were simulated at speeds ranging from 13 kph to 55 kph.

RESULTS: Peak uterine strain was found to be a good predictor of fetal outcome. The strain in the uterine wall exceeded the limits of the tissue in simulations of no restraint at 35 kph and 3-pt belt tests at 45 kph and 55kph. The safest restraint for the pregnant driver is the combination 3-pt belt and airbag.

CONCLUSIONS: The model proved successful at predicting risk of fetal demise and verified experimental findings noting the importance of proper restraint use for the pregnant occupant.

2.1 Introduction

For women of reproductive age, accidents and homicide are the leading cause of death worldwide (Pearlman, 1997). It has been estimated that trauma affects between 6% and 7% of all pregnancies and that two-thirds of all trauma during pregnancy is the result of motor vehicle crashes (Pearlman, 1997). Placental abruption has been shown to account for 50% to 70% of fetal losses in motor vehicle crashes (Pearlman, 1990). Uterine rupture and direct fetal injury account for less than 10% of fetal losses and the remaining 20% to 40% of fetal losses are the result of severe maternal injuries, including maternal death (Pearlman, 1990).

The medical literature contains hundreds of individual case studies on injuries sustained by pregnant occupants in motor vehicle crashes (Dahmus, 1993; Elliot, 1966; Esposito, 1991; Fort, 1970; Goodwin, 1990; Hoff, 1991; Kissinger, 1991; Pearlman, 1990; Rothenberger, 1978; Timberlake, 1989; Williams, 1990). These studies are typically reviews of hospital medical records, and although they present a good resource for incidence and types of injuries, the cases are limited in their ability to determine injury mechanisms and are inherently unable to predict the risk of injury in future crashes.

Conducted in the late 60's and early 70's, several researchers investigated seatbelt effectiveness on pregnant baboons and monkeys. It was concluded that the 3-pt belt system provided superior protection to both mother and fetus as compared to the lap belt only (Snyder, 1966; Crosby, 1968; Van Kirk, 1969; King, 1971). In the mid 90's and early 2000, two prototype pregnant dummies were developed by Pearlman and Viano (1996), and Rupp et al. (2001). Both dummies were tested utilizing several restraint conditions. Their findings agree with results from animal testing regarding the use of a 3-pt belt and preliminary data suggests that an airbag coupled with a 3-pt belt system provided further protection to both mother and fetus. Testing using crash test dummies is costly and does not show the biofidelity of a human occupant.

Rupp et al. (2001) performed simplified computer modeling to determine the most likely causes of placental abruption from impact loading. It was found that pressure gradients generated by the inertia of the amniotic fluid and strains in the uteroplacental interface (UPI) due to direct loading of the abdomen were the dominant mechanisms of placental abruption. The simplified model of Rupp et al. (2001) provided valuable information regarding the injury mechanisms of placental abruption; however, the model is not functional as a tool to determine fetal loss from motor vehicle crashes.

The purpose of this study was to create a computational model of a pregnant occupant and evaluate this occupant under a range of loading conditions.

2.2 Materials and Methods

Motor vehicle crashes were simulated in MADYMO (TNO, Netherlands), a program specifically designed for occupant safety analysis. A finite element model of a

pregnant uterus was developed and inserted into the abdomen of a multi-body human model (Figure 30). The human model is a 5th percentile human model (5 ft tall, 110 lbs) and the uterus is designed to represent an occupant in her 30th week of gestation. The multibody human model provides biofidelic response of an occupant in a motor vehicle crash, while reducing the computational time compared to a full finite element human model. The uterine model includes the uterus, placenta, and amniotic fluid and is supported within the human abdomen by the uterosacral and round ligaments, as well as the cervix. The uterine model is surrounded by fat to accurately represent the boundary between the uterus and spine, abdominal organs, and pelvis. A fetus was not included because the injury mechanisms that predominantly contribute to placental abruption, as described by Rupp et al. (2001), are independent of the fetus. The uterus is 27 cm long, 18cm wide, and 1 cm thick, while the placenta is located at the fundus of the uterus and is 2 cm thick. The remainder of the interior of the uterus is filled with the amniotic fluid. The uterus, placenta, and amniotic fluid are modeled as linear elastic isotropic solids. The uterine model, including the ligaments and fat, is made up of 11,632 elements and 16,335 nodes. The weight of the pregnant model is 135 lbs.

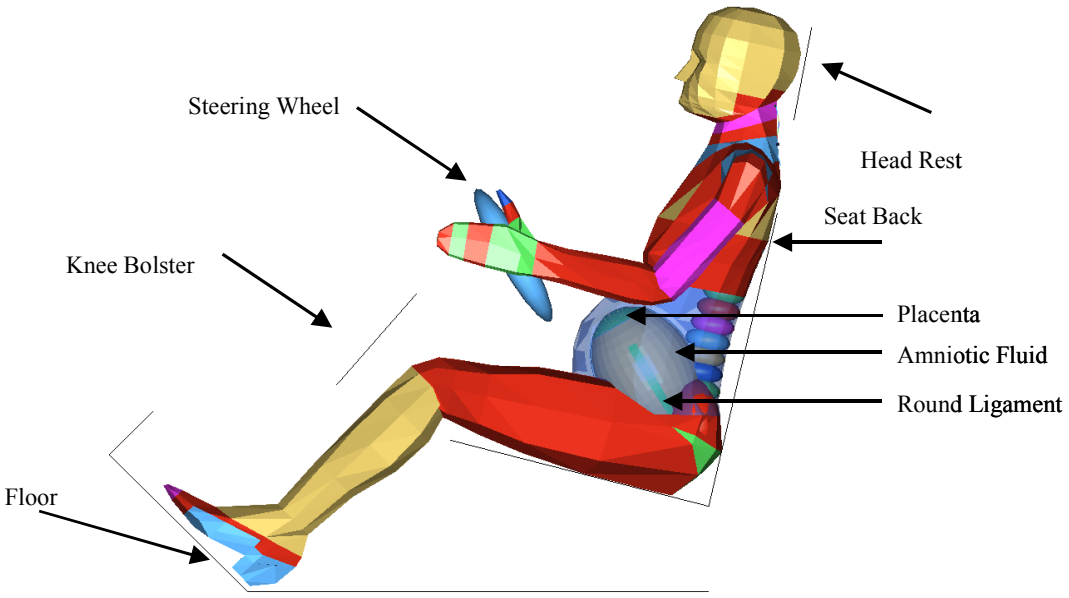

Figure 30: Pregnant occupant in vehicle interior

Injury to the fetus can be determined through an injury risk curve developed by Klinich et al. (1999b) from investigations of motor vehicle crashes involving pregnant women. The curve predicts risk adverse fetal outcome based on crash speed for improper restraint and proper restraint. Proper restraint was defined as the correct use of a 3-pt belt or 3-pt belt plus an airbag. Improper restraint included all other forms of restraint, from no restraint to shoulder belt only or airbag only. Injury can also be predicted from tissue failure. Placental abruption is believed to occur when the strain in the UPI exceeds 60%, or when uterine strain exceeds 60% (Pearlman, 1999).

The anthropometry of a pregnant woman was quantified by Klinich et al. (1999a). The abdominal contour of the pregnant model closely matches the Klinich data used for the second-generation pregnant dummy. Positioning of the pregnant occupant in the Madymo vehicle was based on the Klinich et al. (1999a) data for the small female group at 30 weeks gestation. The initial distance between the abdomen and the bottom of the steering wheel is 38 mm. The overlap of the uterus to the steering wheel is 12%. The overlap is defined as the ratio of the height of the uterus above the steering wheel to the total height of the uterus. The seatback angle, relative to vertical, is 13 degrees and the steering wheel tilt is 29 degrees from vertical.

The pregnant model was validated by simulating belt loading and rigid bar impact tests. The abdominal response of the pregnant model is within the defined upper and lower bounds developed by Hardy (1999) for the 50^{th} percentile male and scaled to a 5^{th} percentile pregnant women by Rupp et al. (2001).

The test matrix for this study included twelve sled test simulations (Table 3). The simulations included occupants with no restraint, a 3-pt belt, and a 3-pt belt plus airbag under various crash speeds ranging from 13 kph to 55 kph. The test matrix was designed to identify inertial, steering wheel, seatbelt, and airbag loading on the pregnant uterus, and to match testing of the second-generation pregnant dummy (Rupp, 2001). In each test, the pregnant occupant was a driver in a frontal crash. Simulations were run in excess of 100 ms, in order to ensure that the forward motion of the occupant had stopped. The computational model uses peak Von Mises strain in the uterus near the placenta as the measure for predicting risk of injury. This strain was compared to the risk of adverse

fetal outcome, as defined by Klinich et al. (1999b), to determine if strain could be used as a predictive tool.

2.3 Results

For all three restraint groups, the risk of adverse fetal outcome and the maximum uterus strain increased as the crash speed increased (Table 3). For tests run at the same speeds, the unrestrained pregnant female had the highest risk of adverse fetal outcome and the highest uterus strain compared to the tests with a 3-pt seatbelt or a 3-pt seatbelt and an airbag. In particular, the matched tests at 35 kph resulted in a 60.8% strain value for the unrestrained occupant to 52.6% strain for the 3-pt seatbelt and only 33.0% strain for the 3-pt seatbelt and airbag combination.

Table 3: Effect of restraint use and crash speed on risk of injury and peak uterine strain

Test Number	Restraint Configuration	Crash Speed (kph)	Risk of Adverse Fetal Outcome (%) *	Maximum Strain in the Uterus (%)
1	None	13	36	23.2
2	None	20	54	36.6
3	None	25	70	44.6
4	None	35	86	60.8
5	3-pt Belt	13	9	15.5
6	3-pt Belt	25	26	27.9
7	3-pt Belt	35	51	52.6
8	3-pt Belt	45	76	58.7
9	3-pt Belt	55	90	61.2
10	Airbag + 3-pt Belt	25	26	28.1
11	Airbag + 3-pt Belt	35	51	33.0
12	Airbag + 3-pt Belt	45	76	46.6

***** Risk based on crash investigations (Klinich, 1999).

Three sled tests at the same crash speed, 35 kph, were compared to reveal the kinematic and loading differences between the three restraint types tested (Figure 31). The first frame (a) shows an unbelted pregnant occupant contacting the steering wheel resulting in large deformation of the uterus. The peak strain is a result of substantial steering wheel loading resulting in large deformation of the uterus. The second frame (b) shows a matched belted occupant simulation in which steering wheel contact is minimal resulting in a lower strain in the uterus. However, there is considerable neck flexion, which could lead to maternal injury. The last frame (c) shows an airbag deployment combined with a 3-pt belt. As with the 3-pt belt, the abdomen has minimal contact with the steering wheel and because the airbag absorbs some of the energy of the crash, the uterine strain is reduced by approximately half compared to the no-restraint case. During the belted simulations, with or without an airbag, peak strain occurs when the forward momentum of the pregnant occupant is halted. In other words, the peak strain in the belted simulations is primarily a result of inertial loading.

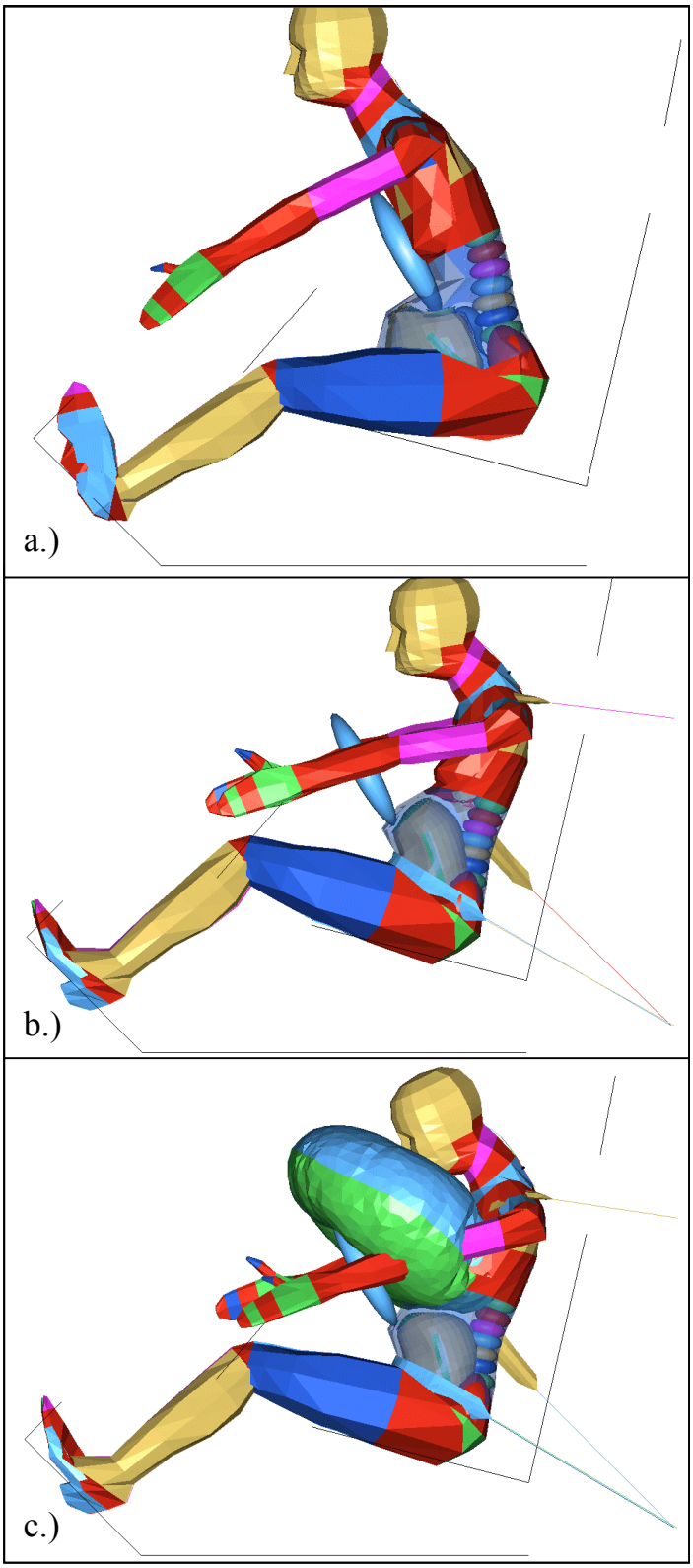

Figure 31: Pregnant occupant in a 35 kph crash at peak uterine strain; a) no restraint at 101 ms, b) 3-pt belt at 75 ms, c) 3-pt belt and airbag at 82 ms

The peak uterine strain was compared to the risk of adverse fetal outcome, as defined by Klinich et al. (1999b), to determine if strain could be used as a predictive tool (Figure 32). A two variable linear regression of the entire data shows that the uterine strain from the computational model is a good predictive measure of the risk of fetal injury ($R^2 = 0.85$).

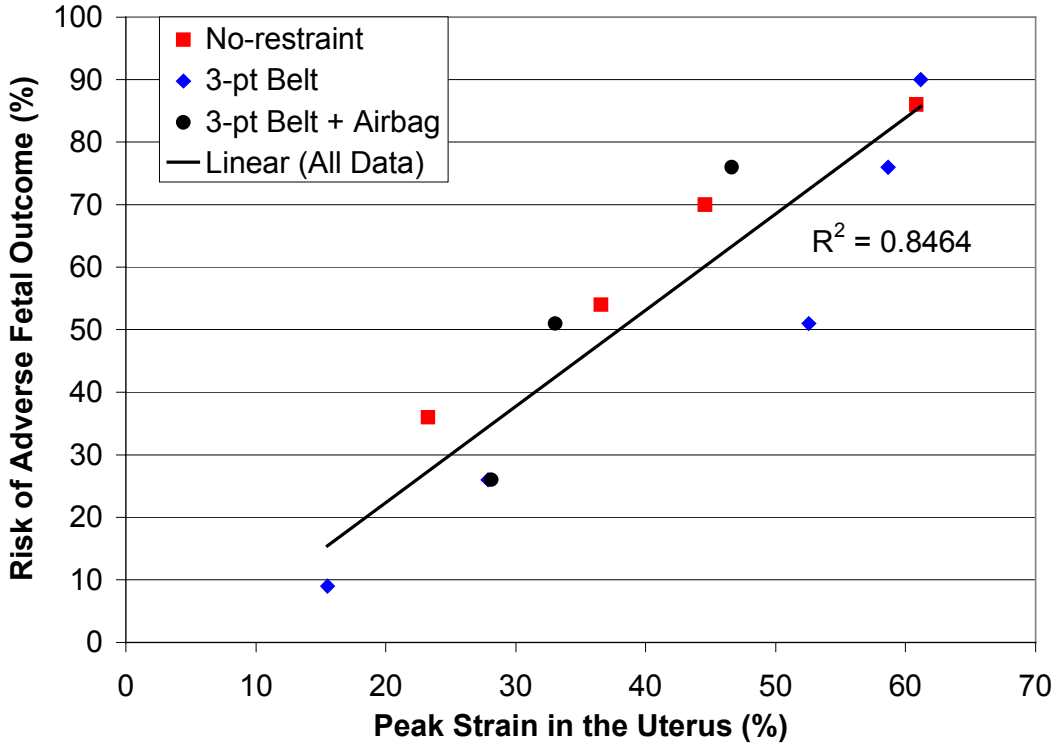

Figure 32: Peak strain in the uterus as a predictor of adverse fetal outcome

The main method of protecting the fetus is to protect the mother. Head injury criteria (HIC) and viscous criterion (V*C) were examined as a check of overall occupant protection. The small female HIC injury criterion is set at 1000 (Hutchinson, 1998). The maximum HIC in the simulations was 310 in the 55 kph, 3-pt belt test. In general, the HIC was lowest for 3-pt belt plus airbag tests and highest for no-restraint tests. The V*C limit is 1.0; the simulations recorded a high of 0.7 in the no restraint 35 kph test. The airbag tests showed a slight increase in V*C compared to the 3-pt belt only. The 3-pt belt plus airbag restraint provided the greatest amount of protection to the mother.

2.4 Comment

The peak uterine strain was found to be a good predictor of fetal outcome. The 3-pt belted tests produced the greatest variation, typically predicting uterine strain greater than the airbag tests. This result is not unexpected. The 3-pt belt plus airbag restraint is generally considered safer than a 3-pt belt restraint and the associated risk of adverse fetal outcome is based on proper restraint use, which includes 3-pt belt and 3-pt belt plus airbag restraint use. Therefore, 3-pt belt tests should report higher strains than the 3-pt belt plus airbag simulations.

The kinematic output of the model allows for a close-up view of the interior of the uterus. This reveals the motion and deformation of the uterine wall and placenta, which is an advantage over dummy testing. The location of tissue failure can be determined and used to design advanced restraint systems.

Several assumptions were made in the formulation of the finite element uterine model. The uterus, placenta, and amniotic fluid were assumed linear, elastic, isotropic solid materials. The uterus is known to be anisotropic and viscoelastic, however there is not currently enough data to apply these material properties to the model. The geometry, although an improvement over previous modeling efforts, is simplified. It is recommended that these improvements be included in future versions of the model.

Conclusion

A finite element model of the pregnant abdomen was created to predict fetal outcome following a motor vehicle crash. The model was incorporated into a human body model in a dynamic solver and validated with data from previous studies. The model can distinguish between inertial, steering wheel, seatbelt, and airbag loading.

Uterine strain was found to be good predictor of fetal injury due to placental abruption. Injury to the mother, particularly head and chest trauma, must also be considered. The model has verified previous experimental findings regarding the importance of proper restraint use for the pregnant occupant. The combination of a 3-pt seatbelt and airbag was found to be the safest restraint system for the pregnant occupant. The model can be used to quickly run numerous tests and design advanced restraint systems specifically designed for pregnant occupants.

References

Crosby WM, Snyder RG, Snow CC, Hanson PG (1968). Impact injuries in pregnancy. American Journal of Obstetrics and Gynecology, 101(1), 100

Dahmus MA, Sibai BM (1993). Blunt abdominal trauma: are there any predictive factors for abruptio placentae or maternal-fetal distress. American Journal of Obstetrics and Gynecology, 169(4), 1054-1059.

Elliott M (1966). Vehicular accidents and pregnancy. Aust NZJ Obstet Gynaec, 6(4), 279-286.

Esposito TJ, Gens DR, Smith LG, Scorpio R, Buchman T (1991). Trauma during pregnancy. a review of 79 cases. Archives of Surgery, 126, 1073-1078.

Fort AT, Harlin RS (1970). Pregnancy outcome after noncatastrophic maternal trauma during pregnancy. Obstetrics and Gynecology, 35, 912-915.

Goodwin TM, Breen MT (1990). Pregnancy outcome and fetomaternal hemorrhage after noncatastrophic trauma. American Journal of Obstetrics and Gyncology, 162, 665-667.

Hardy WN, Schneider LW, Rouhana SW (2001). Abdominal impact response to rigid-bar, seatbelt, and airbag loading. Stapp Car Crash Journal, 45, 1-32.

Hoff WS, Lucke JF, Diamond DL, et al. (1991). Maternal predictors of fetal demise in trauma during pregnancy. Surgery, Gynecology, and Obstetrics, 172 (3), 175-180.

Hutchinson J, Kaiser MJ, Lankarani HM (1998). The head injury criterion (HIC) functional. Applied Mathematics and Computation, 96, 1-16.

King AI, Crosby WM, Stout LC, Eppinger RH (1971). Effects of lap belt and three-point restraints on pregnant baboons subjected to deceleration. 15th Stapp Car Crash Conference Proceedings, 68:83.

Kissinger DP, Rozycki GS, Morris JA, Knudson MM, Copes WS, Bass SM, Yates HK, Champion HR (1991). Trauma in pregnancy - Predicting pregnancy outcome. Archives of Surgery, 126, 1079-1086.

Klinich KD, Schneider LW, Eby B, Rupp J, Pearlman MD (1999a). Seated anthropometry during pregnancy. UMTRI-99-16.

Klinich KD, Schneider LW, Moore JL, Pearlman (1999b). Investigations of crashes involving pregnant occupants. UMTRI-99-29.

Pearlman MD, Tintinalli JE, Lorenz RP (1990). A prospective controlled study of ourcome after trauma during pregnancy. American Journal of Obstetrics and Gynecology, 162, 1502-1510.

Pearlman MD, Viano D (1996). Automobile crash simulation with the first pregnant crash test dummy. American Journal of Obstetrics and Gynecology, 175 (4), 977-981.

Pearlman MD (1997). Motor vehicle crashes, pregnancy loss and preterm labor. International Journal of Gynecology and Obstetrics, 57, 127-132.

Pearlman MD, Ashton-Miller JA, Dyer T, Reis P (1999). Data acquisition for development to characterize the uteroplacental interface for the second-generation pregnant abdomen. Submitted to NHTSA.

Rothenberger D, Quattlebaum FW, Perry Jr. JF, Zabel J, Fischer RP (1978). Blunt maternal trauma: A review of 103 cases. The Journal of Trauma, 18(3), 173-179.

Rupp JD, Schneider LW, Klinich KD, Moss S, Zhou J, Pearlman MD (2001). Design, Development, and testing of a new pregnant abdomen for the Hybrid III small female crash test dummy. UMTRI-2001-07.

Snyder RG, Snow CC, Crosby WM, Hanson P, Fineg J, Chandler R (1966). Impact injury to the pregnant female and fetus in lap belt restraint. Proceedings of the 10th International Stapp Car Crash Conference, 249:259.

Timberlake GA, McSwain Jr NE (1989). Trauma in pregnancy - A 10-year perspective. The American Surgeon, 55, 151-153.

van Kirk DJ, King AI A preliminary study of an effective restraint system for pregnant women and children., 13th Stapp Car Crash Conference Proceedings, 353-364.

Williams JK, McClain L, Rosemurgy AS, Colorado NM (1990). Evaluation of blunt abdominal trauma in the third trimester of pregnancy: maternal and fetal considerations. Obstetrics and Gynecology, 75(1), 33-37.

Chapter 3

A Finite Element Model of the Pregnant Occupant for the Analysis of Injury Risk and Restraint Effectiveness

Abstract

A finite element model of a 7-month pregnant uterus was created and integrated into a multi-body human model. The uterine model contains 11,632 elements and 16,335 nodes. The pregnant occupant model was validated using known abdominal response corridors. Unrestrained, 3-pt belt, and 3-pt belt plus airbag tests were simulated at speeds ranging from 13 kph to 55 kph. Peak uterine strain was found to be a good predictor of fetal outcome (R^2= 0.85). The strain in the uterine wall exceeded 60%, sufficient to cause placental abruption, in simulations of no restraint at 35 kph and 3-pt belt tests at 45 kph and 55kph. These tests represent a greater than 75% risk of adverse fetal outcome. For matched tests at 35 kph, strains of 60.8% for the unrestrained occupant, 52.6% strain for the 3-pt seatbelt and only 33.0% strain for the 3-pt seatbelt and airbag combination were recorded. The model proved successful at predicting risk of fetal demise and verified experimental findings noting the importance of proper restraint use for the pregnant occupant.

3.1 Introduction

For women of reproductive age, accidents and homicide are the leading causes of death worldwide (Pearlman, 1997). It has been estimated that trauma affects between 6% and 7% of all pregnancies and that two-thirds of all trauma during pregnancy is the result of motor vehicle crashes (Pearlman, 1997). Placental abruption has been shown to account for 50% to 70% of fetal losses in motor vehicle crashes (Pearlman, 1990). Uterine rupture and direct fetal injury account for less then 10% of fetal losses and the remaining 20% to 40% of fetal losses are the result of severe maternal injuries, including maternal death (Pearlman, 1990).

The medical literature contains hundreds of individual case studies on injuries sustained by pregnant occupants in motor vehicle crashes (Dahmus, 1993; Elliot, 1966; Esposito, 1991; Fort, 1970; Goodwin, 1990; Hoff, 1991; Kissinger, 1991; Pearlman, 1990; Rothenberger, 1978; Timberlake, 1989; Williams, 1990). These studies are typically reviews of hospital medical records, and although they present a good resource for incidence and types of injury, the cases are limited in their ability to determine injury mechanisms and are inherently unable to predict the risk of injury in future crashes.

Anatomy Review

The uterus is a muscular organ the size of a lemon located within the abdominal cavity. As the fetus grows during pregnancy, the abdomen stretches to the size of a watermelon. The internal volume increases from 0.005 L to 5 L and as much as 10 L (Rupp, 2001). The uterine wall is uniform prior to delivery, with a thickness of about 1 cm. The uterosacral and round ligaments extend from the uterus to the pelvis and act to support the uterus. The interior of the uterus contains the fetus, which is surrounded by amniotic fluid and the placenta (Figure 33). The placenta is a vascular organ that acts as a permeable membrane that exchanges oxygen, nutrients, and waste products between the mother and fetus via the umbilical cord. It is a flat, roughly circular structure 2 cm thick in the center. Most placentas, as many as 95%, are in the upper half of the uterus (Fried, 1978). Testing by Fried (1978) showed that 31% of the placentas were wholly or partly fundal (at the top of the uterus) and by the 3rd trimester, 40% of the placentas were fundal. The cephalic presentation, in which the fetus is in a head down position, comprises about 75% of pregnancies (Fried, 1978).

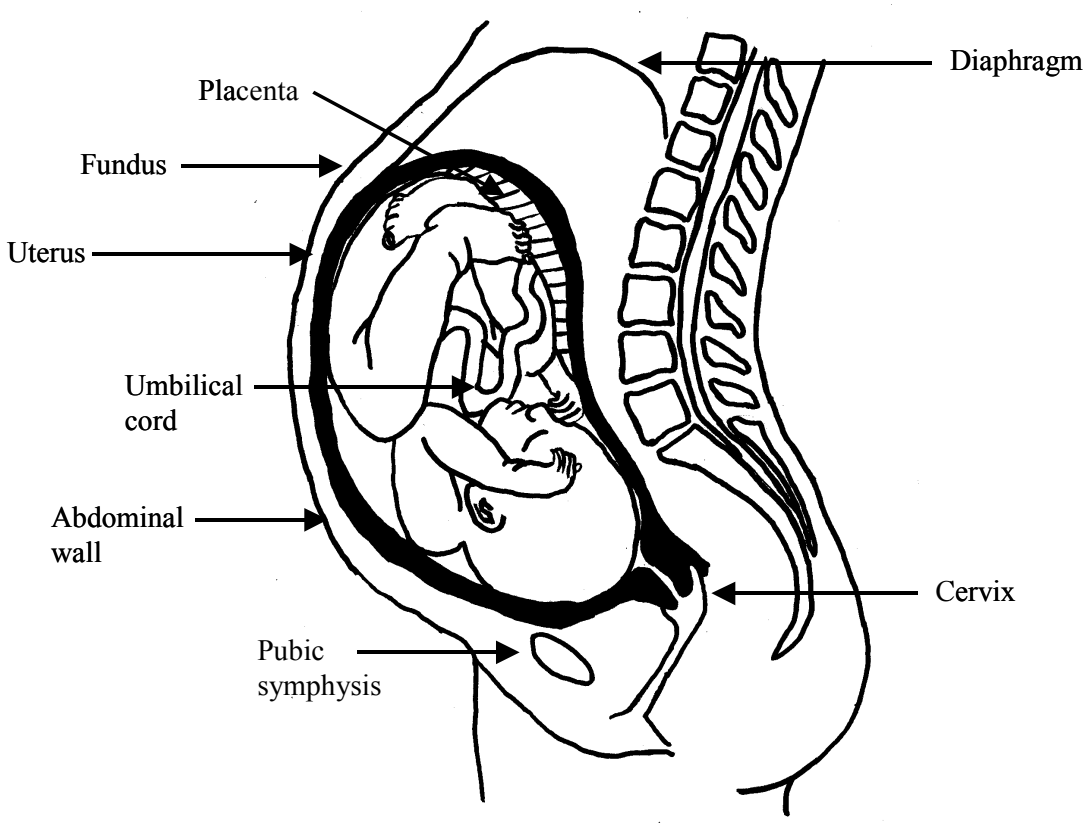

Figure 33: Anatomy of a 40-week pregnant woman (ligaments not shown)

Background

Conducted in the late 60's and early 70's, several researchers investigated seatbelt effectiveness on pregnant baboons and monkeys. It was concluded that the 3-pt belt system provided superior protection to both mother and fetus as compared to the lap belt only (Snyder, 1966; Crosby, 1968; Van Kirk, 1969; King, 1971). In the mid 90's and early 2000, two prototypes of pregnant dummies were developed by Pearlman and Viano (1996), and Rupp et al. (2001). Both dummies were tested utilizing several restraint conditions. Their findings agree with results from animal testing regarding the use of a 3-pt belt and preliminary data suggests that an airbag coupled with a 3-pt belt system provided further protection to both mother and fetus. Testing using these crash test dummies is costly and does not show the biofidelity of a human occupant.

Rupp et al. (2001) performed simplified computer modeling to determine the most likely causes of placental abruption from impact loading. It was found that pressure

gradients generated by the inertia of the amniotic fluid and strains in the uteroplacental interface (UPI) due to direct loading of the abdomen were the dominant mechanisms of placental abruption. The simplified model of Rupp et al. (2001) provided valuable information regarding the injury mechanisms of placental abruption; however, the model is not functional as a tool to determine fetal loss from motor vehicle crashes.

Injury Criteria

Injury to the fetus can be determined through injury risk curves developed by Klinich et al. (1999b) from investigations of motor vehicle crashes involving pregnant women (Figure 34). The curve predicts risk of adverse fetal outcome based on crash speed for improper restraint (Equation 2) and proper restraint (Equation 3). Proper restraint was defined as the correct use of a 3-pt belt or 3-pt belt plus an airbag. Improper restraint included all other forms of restraint, from no restraint to shoulder belt only or airbag only. The logistic regression was found to be reasonably predictive of fetal outcome ($R^2 = 0.55$).

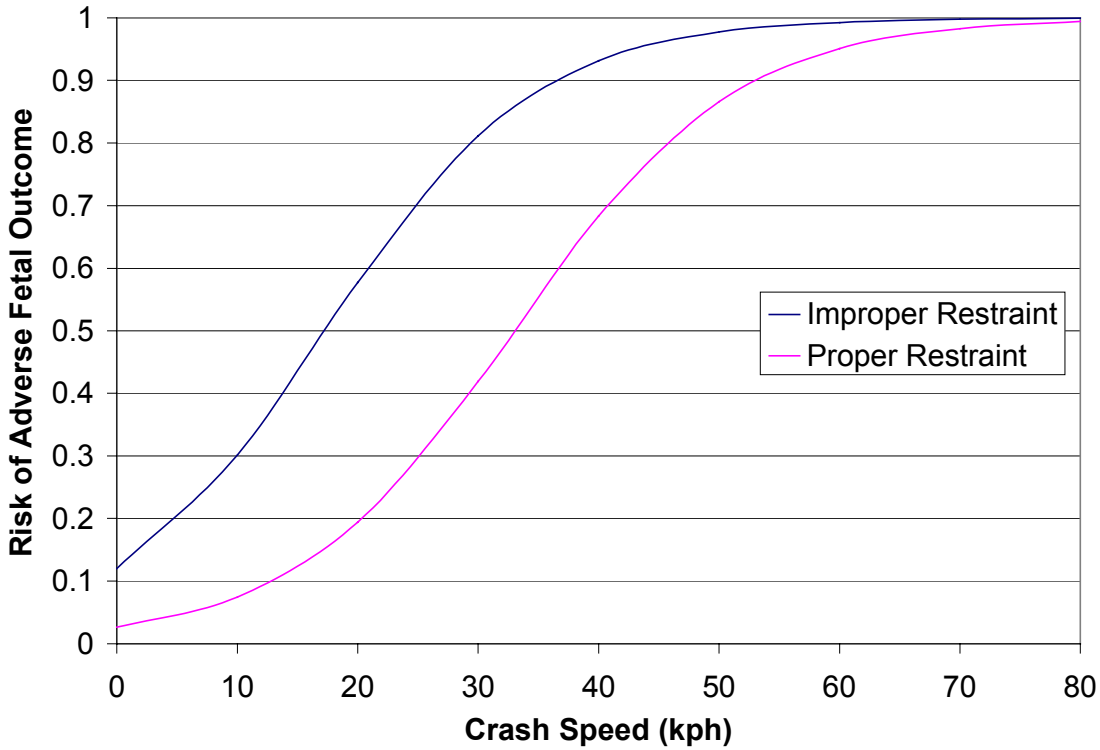

Figure 34: Risk of adverse fetal outcome as a function of crash speed and restraint (Klinich, 1999b)

$$Risk = \frac{1}{1+e^{-(0.1150x-1.9903)}} \qquad \text{[Equation 2]}$$

$$Risk = \frac{1}{1+e^{-(0.1096x-3.6154)}} \qquad \text{[Equation 3]}$$

Injury can also be predicted from tissue failure. Placental abruption is believed to occur when the strain in the UPI exceeds 60% or when uterine wall strain exceeds 60% (Pearlman, 1999). In general, the uterine tensile strength ranges from 483 kPa to 2068 kPa with an average of 1034 kPa (Pearsall, 1978; Wood, 1965). The current literature does not contain data on the tensile limits of the placenta. The tensile strength of the UPI is approximately 16 kPa (Rupp, 2001).

The purpose of this study was to create a computational model of a pregnant occupant and to evaluate the response from a range of loading conditions. In particular,

the goal of this study is to develop a model that can quantify the stresses and strains on the uterus of a pregnant woman in order to predict the risk of injury.

3.2 Methodology

In order to study a pregnant female in a motor vehicle crash, a finite element model of the pregnant uterus was developed and inserted into a multi-body model. Geometry, material property, and element type information is presented.

Geometry

The finite element uterine model is designed to represent an occupant in her 30th week of gestation. A fetus was not included because the injury mechanisms that predominantly contribute to fetal loss, as described by Rupp et al. (2001), are independent of the fetus. The uterus is 27 cm long, 18cm wide, and 1 cm thick (Figure 35). The placenta is located at the fundus of the uterus and is 2 cm thick. The remainder of the interior of the uterus is filled with the amniotic fluid.

The uterine model is supported to the human model by the uterosacral and round ligaments, as well as the cervix. The uterine model is also surrounded by fat to represent the boundary conditions involving the spine, abdominal organs, and the pelvis.

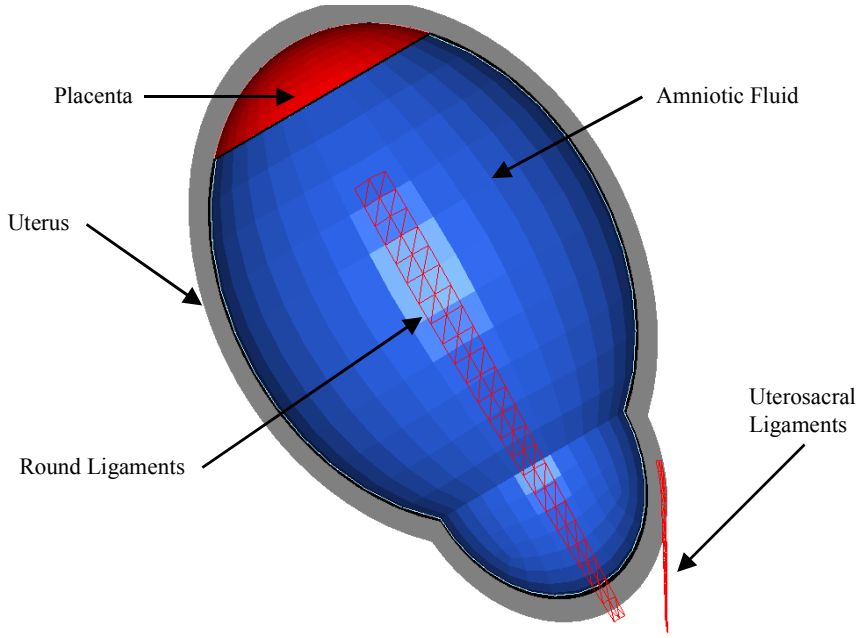

Figure 35: Side view of the FE uterus model

Material Properties

All uterine bodies were modeled as linear elastic solids (Table 4). Although the uterus and placenta are considered visco-elastic and anisotropic (Conrad, 1966; Pearsall, 1978; Mizrahi, 1975), sufficient data was not available to accurately apply these material types. The amniotic fluid was modeled as a solid because Madymo does not recognize fluid elements.

Table 4: Material properties used for the pregnant uterus model

Structure	Material Model	Density (kg/m^3)	Young's Modulus (kPa)	Poisson's Ratio
Uterus	Linear elastic	1052	566	0.40
Placenta	Linear elastic	995	63	0.45
Amniotic Fluid	Linear elastic	993	20	0.49
Ligaments	Linear elastic	1000	566000	0.40
Fat	Linear elastic	993	47	0.49

Tension tests on human uterus tissue have been reported by Pearlman (1999), Pearsall (1978), and Wood (1964). The Young's modulus ranged from 20.3 kPa to 1379 kPa, with an average of 566 kPa. The Poisson's ratio is set to 0.40 since the uterus is a muscular organ and the density is 1052 kg/m^3 (Duck, 1990). Pearlman (1999) reported the results of five tension tests on placental specimen. The average modulus was 33 kPa, with a high of 63 kPa. Testing was not taken to failure. The highest modulus is used in the pregnant model because it is expected that the placenta is stiffer than the fat. The Poisson's ratio is assumed to be 0.45 because it is muscular tissue (ν=0.40) engorged with blood (ν=0.50). The density of the placenta is 995 kg/m^3 (Duck, 1990). The amniotic fluid, which is 99% water and therefore incompressible, was assumed to have a negligible Young's modulus and a Poisson's ratio of 0.49. The Young's modulus of 20 kPa is used for the fluid because moduli of lower values produced unstable results.

Material properties of the ligaments connecting the uterus to the pelvis were not available in the literature. A brief search of general ligament properties showed that the elastic modulus of ligaments is typically two orders of magnitude greater then the uterus (Iwamoto, 1999; Zhang, 2001; Yamada, 1970). Therefore, the elastic modulus of the uterosacral and round ligaments is set to 100 times the modulus of the uterus. The density and Poisson's ratio were also taken from general ligament data (Iwamoto, 1999; Zhang, 2001).

An isotropic representation of fatty tissue has been used by Todd and Thacker (1994) in modeling of the human buttocks. The Young's modulus for a seated female is 47 kPa with a Poisson's ratio of 0.49. This Poisson's ratio represents a nearly incompressible material.

Element Types

The uterus, placenta, amniotic fluid, and fat were meshed using solid 8-noded brick elements in ANSYS (ANSYS Inc., Canonsburg, PA). Brick elements were chosen because they are more accurate then tetrahedral elements. The brick elements carry tension, compression, and shear loads. In order to utilize solid brick elements, the elliptical geometries had to be partitioned into several sections before meshing. The ligaments were modeled as 3-noded membrane elements, which are plane, constant stress

triangular elements with in-plane stiffness, and no bending stiffness. The uterine model, including the ligaments and fat, is made up of 11,632 elements and 16,335 nodes (Table 5).

Table 5: Element types used for the pregnant uterus

Structure	Element Type	# of Elements	# of Nodes
Uterus	8-noded Brick	2736	5476
Placenta	8-noded Brick	2000	2330
Amniotic Fluid	8-noded Brick	3136	3540
Ligaments	Triangular membranes	300	320
Fat	8-noded Brick	3460	4669
	Total	**11,632**	**16,335**

Human Model

Motor vehicle crashes were simulated in MADYMO (TNO, Netherlands), a program specifically designed for occupant safety analysis. In order to create the pregnant occupant, the finite element model of a pregnant uterus was inserted into the abdomen of a multibody human model (Figure 36). The human model is a 5th percentile female (5 ft tall, 110 lbs) and the weight of the pregnant occupant model is 135 lbs. The multibody human model provides biofidelic response of an occupant in a motor vehicle crash, while reducing the computational time compared to a full finite element human model. The anthropometry of a pregnant woman was quantified by Klinich et al. (1999a). The abdominal contour of the pregnant model closely matches the Klinich data used for the second-generation pregnant dummy. Positioning of the pregnant occupant in the Madymo vehicle was based on the Klinich et al. (1999a) data for the small female group at 30 weeks gestation. The initial distance between the abdomen and the bottom of the steering wheel is 38 mm. The overlap of the uterus to the steering wheel is 12%. The overlap is defined as the ratio of the height of the uterus above the steering wheel to the total height of the uterus. The seatback angle is 13 degrees relative to vertical and the steering wheel tilt is 29 degrees from vertical.

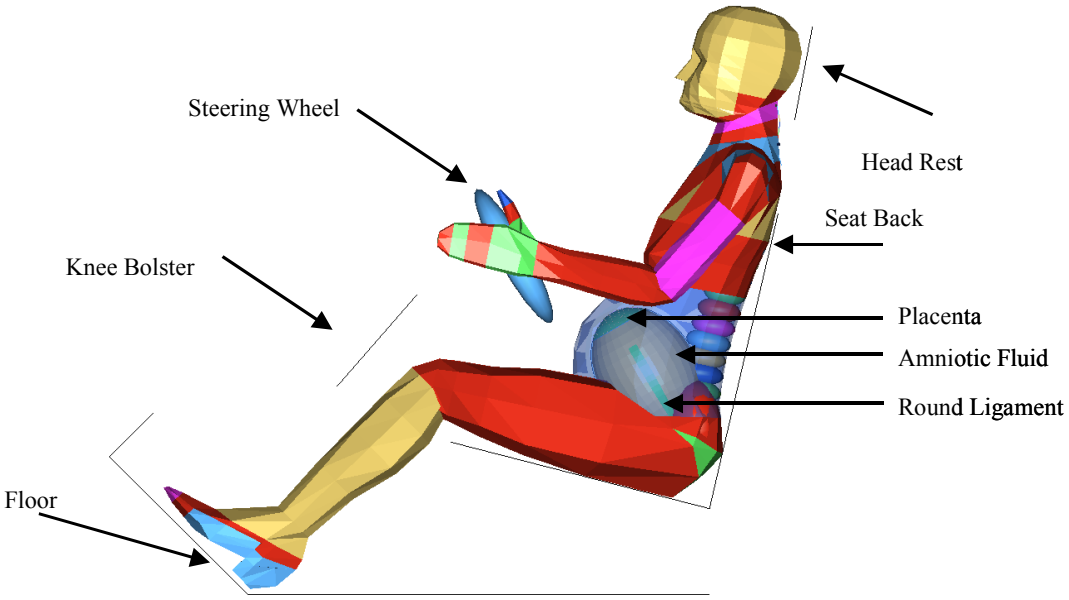

Figure 36: Pregnant occupant in vehicle interior

Validation

Proper response of the abdomen during loading is essential for an accurate model. The abdominal response of the pregnant model was compared to the appropriate abdominal corridors for belt loading and rigid bar impacts. The abdominal response corridors of a non-pregnant abdomen have been assumed valid for the pregnant abdomen based on quasi-static testing (Rupp 2001). Abdominal force deflection corridors were developed by Hardy (1999) for the 50th percentile male and scaled to a 5th percentile pregnant woman by Rupp et al. (2001).

Belt loading: Simulating the test conditions used by Hardy et al. (2001), a finite element belt was positioned at umbilicus level and an initial velocity of 3 m/s was applied to the pregnant model. The force in the belt was recorded along with the displacement of the abdomen.

Rigid Bar Impact: A 2.54 cm diameter, 48 kg cylinder was created in Madymo to represent the impactor used by Hardy et al. (2001). The cylinder was used to impact the abdomen at umbilicus level at 6 m/s. The force between the cylinder and pregnant abdomen and the abdominal displacement were recorded.

Test Matrix

The test matrix for this study included twelve sled test simulations (Table 6). The simulations included occupants with no restraint, 3-pt belt, and 3-pt belt plus airbag under various crash speeds ranging from 13 kph to 55 kph. The test matrix was designed to identify inertial, steering wheel, seatbelt, and airbag loading on the pregnant uterus, and to match testing of the second-generation pregnant dummy (Rupp, 2001). In each test, the pregnant occupant was a driver in a frontal crash. Simulations were run in excess of 100 ms in order to ensure that the forward motion of the occupant had stopped. The computational model uses peak Von Mises strain in the uterus near the placenta as the measure for predicting risk of injury. This strain was compared to the risk of adverse fetal outcome, as defined by Klinich et al. (1999b), to determine if strain could be used as a predictive tool.

3.3 Results and Discussion

Validation

The abdominal response of the pregnant model is within the defined upper and lower bounds for both belt loading and rigid bar impacts. The abdominal response for 3 m/s belt loading is approximately 90 N/mm from 0 mm to 40 mm (Figure 37). The simulation is limited to 40 mm of deflection because the motion of the pregnant model stalled after 40 mm of deflection. The 6 m/s rigid bar impact response is approximately 20 N/mm from 0 mm to 60 mm. Data for additional validation tests, in particular for the uterine components, while desirable, is unavailable.

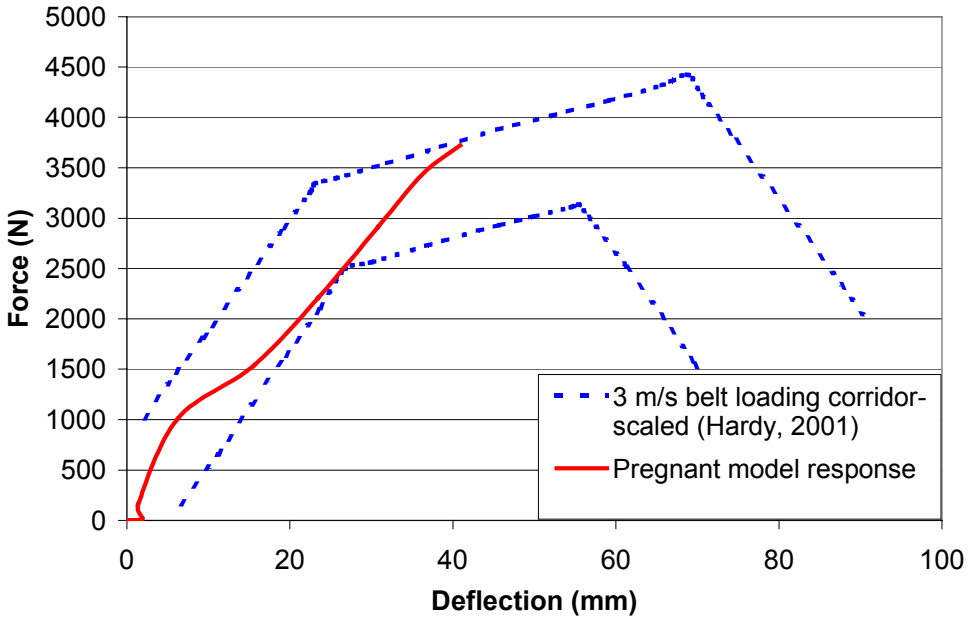

Figure 37: Abdominal response of the pregnant model compared to the scaled corridor

Simulations

For all three restraint groups, the risk of adverse fetal outcome and the maximum uterus strain increased as the crash speed increased (Table 6). For tests run at the same speeds, the unrestrained pregnant female had the highest risk of adverse fetal outcome and the highest uterus strain compared to the tests with a 3-pt seatbelt or a 3-pt seatbelt and an airbag. In particular, the matched tests at 35 kph resulted in a 60.8% strain value for the unrestrained occupant to 52.6% strain for the 3-pt seatbelt and only 33.0% strain for the 3-pt seatbelt and airbag combination. Although the 3-pt belt and 3-pt belt plus airbag tests have identical risks, the peak strain was higher in the 3-pt belt only tests for crash speeds greater then 25 kph.

Table 6: Pregnant model test parameters and results

Restraint	**Crash Speed (kph)**	**Risk (%) ***	**Maximum Strain in the Uterine Wall (%)**	**HIC**	**V*C (m/s)**	**Chest Deflection (mm)**
None	13	36	23.3	1.2	0.12	38.6
None	20	54	36.6	13.3	0.31	39.1
None	25	70	44.6	40.6	0.47	39.4
None	35	86	60.8	156	0.72	39.7
3-pt Belt	13	9	15.5	4	0.027	43.4
3-pt Belt	25	26	27.9	62.3	0.091	47.1
3-pt Belt	35	51	52.6	185	0.12	52.4
3-pt Belt	45	76	58.7	211	0.13	54.3
3-pt Belt	55	90	61.2	310	0.17	58.2
3-pt Belt + Airbag	25	26	28.1	48.5	0.22	45.1
3-pt Belt + Airbag	35	51	33.0	114	0.24	48.2
3-pt Belt + Airbag	45	76	46.6	173	0.20	49

* Developed by Klinich et al. (1999b)

Three sled tests at the same crash speed, 35 kph, were compared to reveal the kinematic and loading differences between the three restraint types tested (Figure 38). The first frame (a) shows an unbelted pregnant occupant contacting the steering wheel resulting in large deformation of the uterus. The peak strain is a result of substantial steering wheel loading resulting in large deformation of the uterus (Figure 39). The second frame (b) shows a matched belted occupant simulation in which steering wheel contact is minimal resulting in a lower strain in the uterus (Figure 40). However, there is considerable neck flexion, which could lead to maternal injury. The last frame (c) shows an airbag deployment combined with a 3-pt belt. As with the 3-pt belt, the abdomen has minimal contact with the steering wheel and because the airbag absorbs some of the energy of the crash, the uterine strain is reduced by approximately half compared to the

no-restraint case. During the belted simulations, with or without an airbag, peak strain occurs when the forward momentum of the pregnant occupant is halted. In other words, the peak strain in the belted simulations is primarily a result of inertial loading.

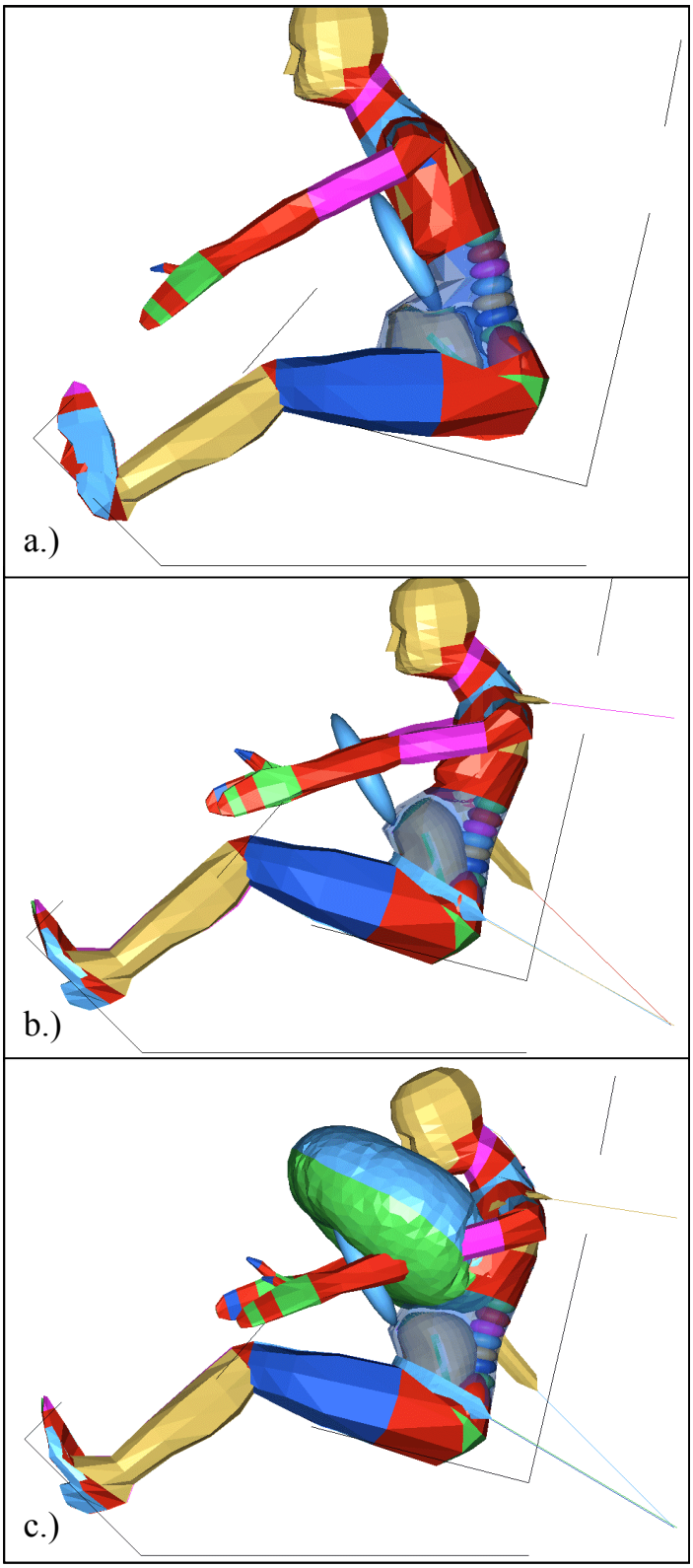

Figure 38: Pregnant occupant in a 35 kph crash at peak uterine strain; a) no restraint at 101 ms, b) 3-pt belt at 75 ms, c) 3-pt belt and airbag at 82 ms

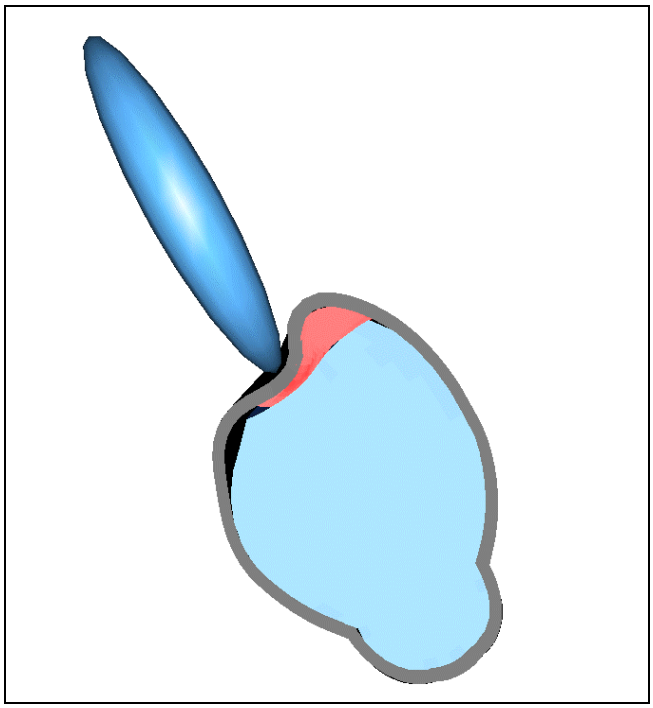

Figure 39: Steering wheel contact with the uterine model at 60 ms

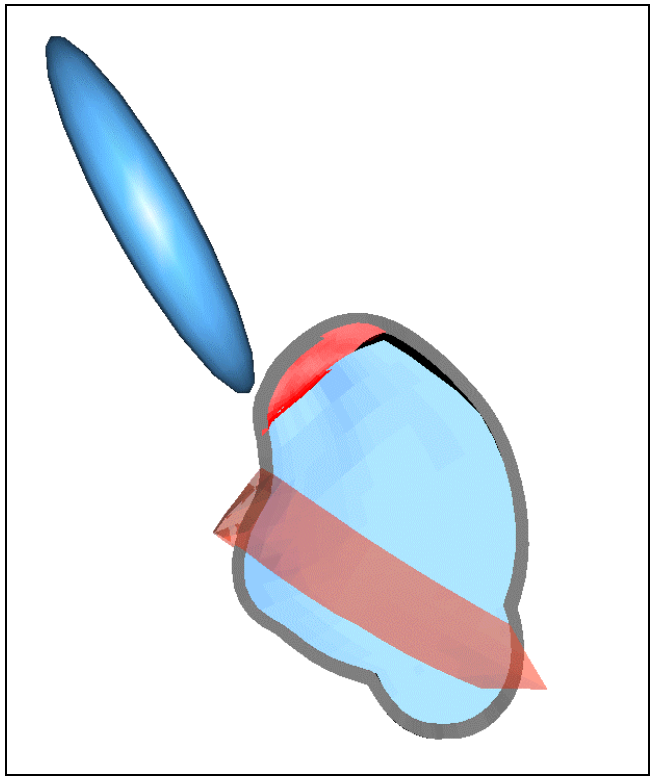

Figure 40: Belt loading of the uterine model at 60 ms

The peak uterine strain was compared to the risk of adverse fetal outcome, as defined by Klinich et al. (1999b), to determine if strain could be used as a predictive tool (Figure 41). A two variable linear regression of the entire data shows that the uterine strain from the computational model is a good predictive measure of the risk of fetal injury due to placental abruption ($R^2 = 0.85$). At 85% risk of adverse fetal outcome the strain in the uterus is predicted to be 60%, which is the failure threshold. The regression shows that uterine strain increases linearly to tissue failure as the risk approaches 100%.

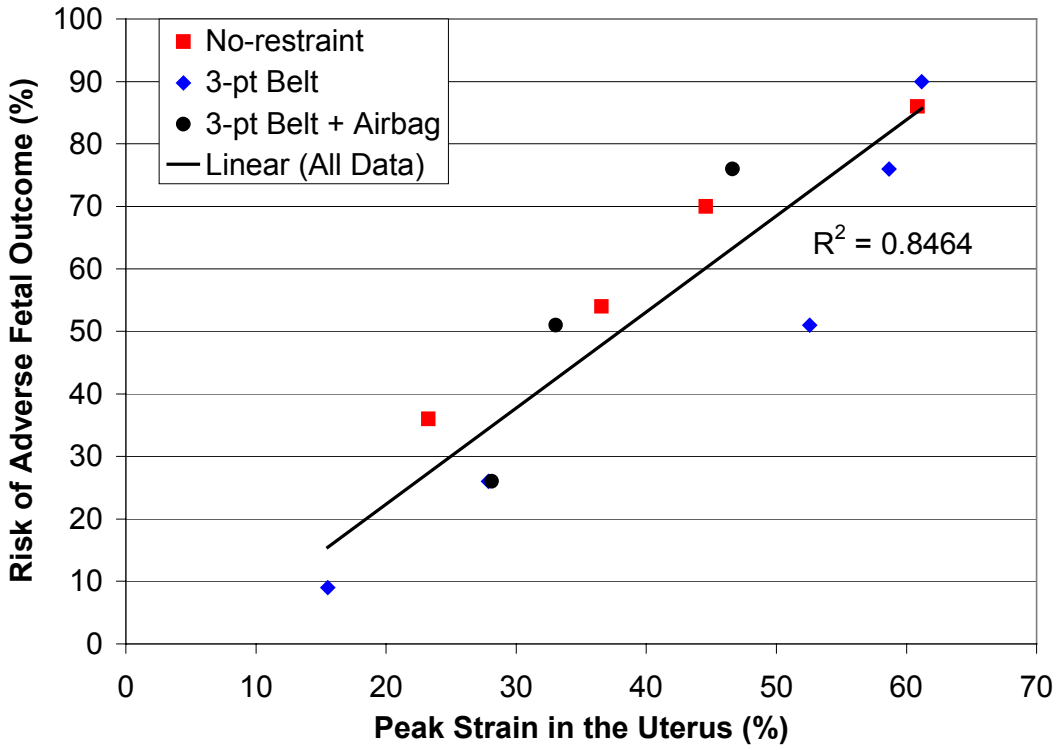

Figure 41: Peak strain in the uterus as a predictor of adverse fetal outcome

The von Mises stress in the uterus was examined for the 35 kph matched tests. In no-restraint simulations, high stresses were seen in the immediate location of contact with the steering wheel and at the cervix support (Figure 42). The peak von Mises stress in the anterior uterus was nearly twice as large in the no–restraint case (218 kPa) than the 3-pt belt plus airbag case (121 kPa). The levels of stress recorded did not approach even the lower bounds of the uterine tensile strength (483 kPa).

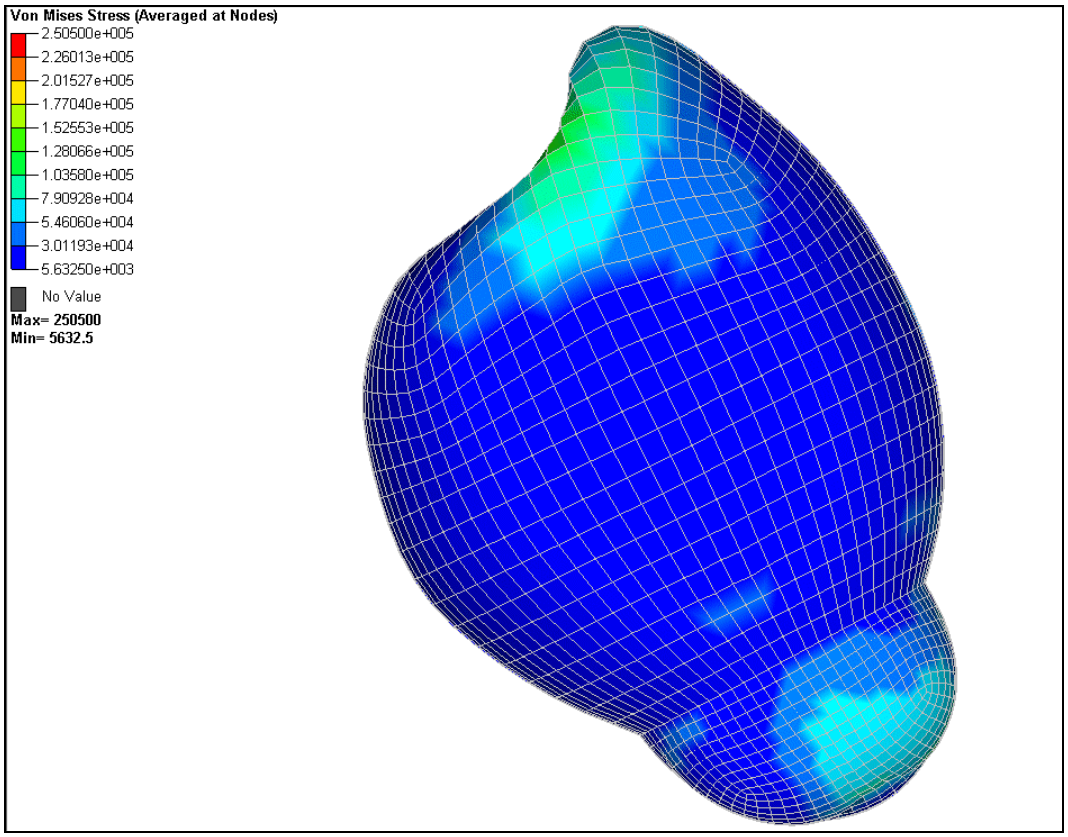

Figure 42: Von Mises stress in the uterus during steering wheel loading

The main method of protecting the fetus is to protect the mother. Head injury criteria (HIC) and viscous criterion (V*C) were examined as a check of overall occupant protection. The small female HIC injury criterion is set at 1000 (Hutchinson, 1998). The maximum HIC in the simulations was 310 in the 55 kph, 3-pt belt test. In general, the HIC was lowest for 3-pt belt plus airbag tests and highest for no-restraint tests. The V*C limit is 1.0; the simulations recorded a high of 0.7 in the no restraint 35 kph test. The airbag tests showed a slight increase in V*C compared to the 3-pt belt only, however the airbag minimized the chest deflection. The 3-pt belt plus airbag restraint provided the greatest amount of protection to the mother.

Discussion

The peak uterine strain was found to be a good predictor of fetal outcome. The 3-pt belted tests produced the greatest variation, typically predicting uterine strain greater than the airbag tests. This result is not unexpected. The 3-pt belt plus airbag restraint is generally considered safer than a 3-pt belt restraint and the risk of adverse fetal outcome is based on proper restraint use, which includes 3-pt belt and 3-pt belt plus airbag restraint use. Therefore, 3-pt belt tests should report higher strains than the 3-pt belt plus airbag simulations.

The kinematic output of the model allows for a close-up view of the interior of the uterus. This reveals the motion and deformation of the uterine wall and placenta, which is an advantage over dummy testing. The location of tissue failure can be determined and used to design advanced restraint systems.

Several assumptions were made in the formulation of the finite element uterine model. The uterus, placenta, and amniotic fluid were assumed linear, elastic, isotropic solid materials. The uterus is known to be anisotropic and viscoelastic, however there is not currently enough data to apply these material properties to the model. The amniotic fluid was defined as a solid because Madymo does not allow fluids to be defined. The geometry, although an improvement over previous modeling efforts, is simplified. Ultrasound measurements or CT data could be used to improve the geometry. The global coordinate system does not coincide with the uterine radial and circumferential directions and therefore limits the strain output. It is recommended that these improvements be included in future versions of the FE model. Further validation of the model should be conducted when the results of future experimental work is made available.

3.4 Conclusions

A finite element model of the pregnant abdomen was created to predict fetal outcome following a motor vehicle crash. The model was incorporated into a human body model in a dynamic solver and validated with data from previous studies. The model can distinguish between inertial, steering wheel, seatbelt, and airbag loading.

Uterine strain was found to be a good predictor of fetal injury (R^2 = 0.85). Uterine strain above the 60% limit was found for the crashes with a known risk of 75% or greater. Injury to the mother, particularly head and chest trauma, must also be considered. The model has verified previous experimental findings regarding the importance of proper restraint use for the pregnant occupant. The model can be used to quickly run numerous tests and design advanced restraint systems specifically designed for pregnant occupants.

References

Conrad JT, Kuhn WK, Johnson WL (1966). Stress relaxation in human uterine muscle. American Journal of Obstetrics and Gynecology, 95(2), 254-265.

Crosby WM, Snyder RG, Snow CC, Hanson PG (1968). Impact injuries in pregnancy. American Journal of Obstetrics and Gynecology, 101(1), 100

Dahmus MA, Sibai BM (1993). Blunt abdominal trauma: are there any predictive factors for abruptio placentae or maternal-fetal distress. American Journal of Obstetrics and Gynecology, 169(4), 1054-1059.

Duck (1990). Physical Properties of Tissue. London: Academic Press

Elliott M (1966). Vehicular accidents and pregnancy. Aust NZJ Obstet Gynaec, 6(4), 279-286.

Esposito TJ, Gens DR, Smith LG, Scorpio R, Buchman T (1991). Trauma during pregnancy. a review of 79 cases. Archives of Surgery, 126, 1073-1078.

Fort AT, Harlin RS (1970). Pregnancy outcome after noncatastrophic maternal trauma during pregnancy. Obstetrics and Gynecology, 35, 912-915.

Fried AM (1978). Distribution of the bulk of the normal placenta. Review and classification of 800 cases by ultrasonography. American Journal of Obstetrics and Gynecology, 132(6), 675-680.

Goodwin TM, Breen MT (1990). Pregnancy outcome and fetomaternal hemorrhage after noncatastrophic trauma. American Journal of Obstetrics and Gyncology, 162, 665-667.

Hardy WN, Schneider LW, Rouhana SW (2001). Abdominal impact response to rigid-bar, seatbelt, and airbag loading. Stapp Car Crash Journal, 45, 1-32.

Hoff WS, Lucke JF, Diamond DL, et al. (1991). Maternal predictors of fetal demise in trauma during pregnancy. Surgery, Gynecology, and Obstetrics, 172 (3), 175-180.

Hutchinson J, Kaiser MJ, Lankarani HM (1998). The head injury criterion (HIC) functional. Applied Mathematics and Computation, 96, 1-16.

Iwamoto M, Miki K, Yang KH, King AI (1999). Development of a finite element model of the human shoulder. AMERI-PAM '99.

King AI, Crosby WM, Stout LC, Eppinger RH (1971). Effects of lap belt and three-point restraints on pregnant baboons subjected to deceleration. 15th Stapp Car Crash Conference Proceedings, 68:83.

Kissinger DP, Rozycki GS, Morris JA, Knudson MM, Copes WS, Bass SM, Yates HK, Champion HR (1991). Trauma in pregnancy - Predicting pregnancy outcome. Archives of Surgery, 126, 1079-1086.

Klinich KD, Schneider LW, Eby B, Rupp J, Pearlman MD (1999a). Seated anthropometry during pregnancy. UMTRI-99-16.

Klinich KD, Schneider LW, Moore JL, Pearlman (1999b). Investigations of crashes involving pregnant occupants. UMTRI-99-29.

Mizrahi J, Karni Z (1975). A mechanical model for uterine muscle activity during labor and delivery. Israel Journal of Technology, 13, 185-191.

Pearlman MD, Tintinalli JE, Lorenz RP (1990). A prospective controlled study of ourcome after trauma during pregnancy. American Journal of Obstetrics and Gynecology, 162, 1502-1510.

Pearlman MD, Viano D (1996). Automobile crash simulation with the first pregnant crash test dummy. American Journal of Obstetrics and Gynecology, 175 (4), 977-981.

Pearlman MD (1997). Motor vehicle crashes, pregnancy loss and preterm labor. International Journal of Gynecology and Obstetrics, 57, 127-132.

Pearlman MD, Ashton-Miller JA, Dyer T, Reis P (1999). Data acquisition for development to characterize the uteroplacental interface for the second-generation pregnant abdomen. Submitted to NHTSA.

Pearsall GW, Roberts VL (1978). Passive mechanical properties of uterine muscle (myometrium) tested in vitro. Journal of Biomechanics, 11, 167-176.

Rothenberger D, Quattlebaum FW, Perry Jr. JF, Zabel J, Fischer RP (1978). Blunt maternal trauma: A review of 103 cases. The Journal of Trauma, 18(3), 173-179.

Rupp JD, Schneider LW, Klinich KD, Moss S, Zhou J, Pearlman MD (2001). Design, Development, and testing of a new pregnant abdomen for the Hybrid III small female crash test dummy. UMTRI-2001-07.

Snyder RG, Snow CC, Crosby WM, Hanson P, Fineg J, Chandler R (1966). Impact injury to the pregnant female and fetus in lap belt restraint. Proceedings of the 10th International Stapp Car Crash Conference, 249:259.

Timberlake GA, McSwain Jr NE (1989). Trauma in pregnancy - A 10-year perspective. The American Surgeon, 55, 151-153.

Todd BA, Thacker JG (1994). Three-dimensional computer model of the human buttocks, in vivo. Journal of Rehabilitation Research and Development, 31(2), 111-119.

van Kirk DJ, King AI A preliminary study of an effective restraint system for pregnant women and children., 13th Stapp Car Crash Conference Proceedings, 353-364.

Williams JK, McClain L, Rosemurgy AS, Colorado NM (1990). Evaluation of blunt abdominal trauma in the third trimester of pregnancy: maternal and fetal considerations. Obstetrics and Gynecology, 75(1), 33-37.

Wood C (1964). Physiology of uterine contractions. British Journal of Obstetrics and Gynecology, 71, 360-373.

Yamada H (1970). Strength of biological materials. Baltimore: The Williams & Wilkins Company.

Zhang L, Yang KH, Dwarampudi R, Omori K, Li T, Chang K, Hardy WN, Khalil TB, King AI (2001). Recent advances in brain injury research: A new human head model development and validation. Stapp Car Crash Journal, 45, 369-394.

References

Agran PF, Dunkle DE, Winn DG, Kent D (1986). Fetal death in motor vehicle collisions. 30th Annual Proceedings, American Association for Automotive Medicine, 285:294.

Aitokallia-Tallberg A, Halmesmaki E (1997). Motor vehicle accident during the second or third trimester of pregnancy. Acta Obstet Gynecol Scand, 76, 313-317.

Am-I-Pregnant.com (1999). Week by week. http://www.am-i-pregnant.com/weeks.shtml.

Bunai Y, Nagai A, Nakamura I, Ohya I (2000). Fetal death from abruptio placentae associated with incorrect use of a seatbelt. The American Journal of Forensic Medicine and Pathology, 21(3), 207-209.

Conrad JT, Kuhn WK, Johnson WL (1966). Stress relaxation in human uterine muscle. American Journal of Obstetrics and Gynecology, 95(2), 254-265.

Crosby WM, Snyder RG, Snow CC, Hanson PG (1968). Impact injuries in pregnancy. American Journal of Obstetrics and Gynecology, 101(1), 100

Crosby WM, Costiloe JP (1971). Safety of lap-belt restraint for pregnant victims of automobile collisions. The New England Journal of Medicine, 284(12), 632-636.

Culver CC, Viano DC (1990). Anthropometry of seated women during pregnancy: defining a fetal region for crash pretection research. Human Factors, 32(6), 625-636.

Dahmus MA, Sibai BM (1993). Blunt abdominal trauma: are there any predictive factors for abruptio placentae or maternal-fetal distress. American Journal of Obstetrics and Gynecology, 169(4), 1054-1059.

Duck FA (1990). Physical Properties of Tissue. London: Academic Press

Elliott M (1966). Vehicular accidents and pregnancy. Aust NZJ Obstet Gynaec, 6(4), 279-286.

Esposito TJ, Gens DR, Smith LG, Scorpio R, Buchman T (1991). Trauma during pregnancy. a review of 79 cases. Archives of Surgery, 126, 1073-1078.

Fildes J, Reed L, Jones N, Martin M, Barrett J (1992). Trauma: the leading cause of maternal death. The Journal of Trauma, 32(5), 643-645.

Fort AT, Harlin RS (1970). Pregnancy outcome after noncatastrophic maternal trauma during pregnancy. Obstetrics and Gynecology, 35, 912-915.

Fried AM (1978). Distribution of the bulk of the normal placenta. Review and classification of 800 cases by ultrasonography. American Journal of Obstetrics and Gynecology, 132(6), 675-680.

Gillespie EC (1950). Principles of uterine growth in pregnancy. American Journal of Obstetrics and Gynecology, 59 (5), 949-956.

Gimovsky ML, Nunez G, Beck P (2000). Fetal heart rate monitoring casebook. Journal of Perinatology, 4, 270-273.

Goodwin TM, Breen MT (1990). Pregnancy outcome and fetomaternal hemorrhage after noncatastrophic trauma. American Journal of Obstetrics and Gyncology, 162, 665-667.

Guilbeau Jr JA, Turner JL (1953). The effect of travel upon the interruption of pregnancy. American Journal of Obstetrics and Gyncology, 66(6), 1224-1230.

Happee R, Ridella S, Nayef A, Morsink P, de Lange R, Bours R, van Hoof J. (2000). Mathematical human body models representing a mid size male and a small female for frontal, lateral and rearward impact loading. IRCOBI Conference, 67-81.

Hardy WN, Schneider LW, Rouhana SW (2001). Abdominal impact response to rigid-bar, seatbelt, and airbag loading. Stapp Car Crash Journal, 45, 1-32.

Herbert DC, Henderson JM (1977). Motor-car accidents during pregnancy 2. Medical Journal of Australia, 1 (18), 670-671.

Hoff WS, Lucke JF, Diamond DL, et al. (1991). Maternal predictors of fetal demise in trauma during pregnancy. Surgery, Gynecology, and Obstetrics, 172 (3), 175-180.

Hutchinson J, Kaiser MJ, Lankarani HM (1998). The head injury criterion (HIC) functional. Applied Mathematics and Computation, 96, 1-16.

Institute of Medicine (1990). Nutrition during pregnancy, weight gain and nutrient supplements. Report of the Subcommittee on Nutritional Status and Weight Gain during Pregnancy. Washington, DC, National Acadamy Press, 1:233, 333:341.

Iwamoto M, Miki K, Yang KH, King AI (1999). Development of a finite element model of the human shoulder. AMERI-PAM '99.

Jensen RK, Doucet S, Treitz T 1996. Changes in segment mass and mass distribution during pregnancy. Journal of Biomechanics, 29 (2) , 251:256.

Jernigan MV (2002). Statistical analysis and computational modeling of injuries in automobile crashes. MS Thesis, Virginia Polytechnic Institute and State University.

King AI, Crosby WM, Stout LC, Eppinger RH (1971). Effects of lap belt and three-point restraints on pregnant baboons subjected to deceleration. 15th Stapp Car Crash Conference Proceedings, 68:83.

Kissinger DP, Rozycki GS, Morris JA, Knudson MM, Copes WS, Bass SM, Yates HK, Champion HR (1991). Trauma in pregnancy - Predicting pregnancy outcome. Archives of Surgery, 126, 1079-1086.

Klinich KD, Schneider LW, Eby B, Rupp J, Pearlman MD (1999a). Seated anthropometry during pregnancy. UMTRI-99-16.

Klinich KD, Schneider LW, Moore JL, Pearlman (1999b). Investigations of crashes involving pregnant occupants. UMTRI-99-29.

Lane PL (1989). Traumatic fetal deaths. The Journal of Emergency Medicine, 7, 433-435.

Mizrahi J, Karni Z (1975). A mechanical model for uterine muscle activity during labor and delivery. Israel Journal of Technology, 13, 185-191.

Mowafi (1999) Anatomy of the Female Pelvis.
http://matweb.hcuge.ch/El_Mowafi/anatomy_of_the_female_pelvis.htm

Netter FH (1997). Atlas of human anatomy. East Hanover, NJ: Novartis.

Pearlman MD, Tintinalli JE, Lorenz RP (1990). A prospective controlled study of ourcome after trauma during pregnancy. American Journal of Obstetrics andGynecology, 162, 1502-1510.

Pearlman MD, Phillips ME (1996a). Safety belt use during pregnancy. Obstetrics and Gynecology, 88(6), 1026-1029.

Pearlman MD, Viano D (1996b). Automobile crash simulation with the first pregnant crash test dummy. American Journal of Obstetrics and Gynecology, 175 (4), 977-981.

Pearlman MD (1997). Motor vehicle crashes, pregnancy loss and preterm labor. International Journal of Gynecology and Obstetrics, 57, 127-132.

Pearlman MD, Ashton-Miller JA, Dyer T, Reis P (1999). Data acquisition for development to characterize the uteroplacental interface for the second-generation pregnant abdomen. Submitted to NHTSA.

Pearsall GW, Roberts VL (1978). Passive mechanical properties of uterine muscle (myometrium) tested in vitro. Journal of Biomechanics, 11, 167-176.

Pepperell RJ, Rubinstein E, MacIsaac IA (1977). Motor-car accidents during pregnancy. The Medical Journal of Australia, 1, 203-205.

Power ED, Stitzel JD, Duma SM, Herring IP, West RL. (2002) Investigation of ocular injuries from high velocity objects in an automobile collision. SAE Technical Paper Series Society of Automotive Engineers, Inc., 1-8.

Rice DA, Yang TY (1976). A nonlinear viscoelastic membrane model applied to the human cervix. Journal of Biomechanics, 9, 201-210.

Rothenberger D, Quattlebaum FW, Perry Jr. JF, Zabel J, Fischer RP (1978). Blunt maternal trauma: A review of 103 cases. The Journal of Trauma, 18(3), 173-179.

Rupp JD, Schneider LW, Klinich KD, Moss S, Zhou J, Pearlman MD (2001). Design, Development, and testing of a new pregnant abdomen for the Hybrid III small female crash test dummy. UMTRI-2001-07.

Snyder RG, Snow CC, Crosby WM, Hanson P, Fineg J, Chandler R (1966). Impact injury to the pregnant female and fetus in lap belt restraint. Proceedings of the 10th International Stapp Car Crash Conference, 249:259.

Takahashi T (1994). Atlas of the human body. New York: Harper.

Timberlake GA, McSwain Jr NE (1989). Trauma in pregnancy - A 10-year perspective. The American Surgeon, 55, 151-153.

Todd BA, Thacker JG (1994). Three-dimensional computer model of the human buttocks, in vivo. Journal of Rehabilitation Research and Development, 31(2), 111-119.

Thompson JD, Rock JA (1996). Te Linde's Operative Gynecology. Hagerstown, MD: Lippincott Williams & Wilkins Publishers.

van Kirk DJ, King AI A preliminary study of an effective restraint system for pregnant women and children., 13th Stapp Car Crash Conference Proceedings, 353-364.

Verrallis S (1993) Anatomy and physiology applied to obstetrics. New York: Churchill Livingstone.

Viano D, Smrcka J, Jedrzejczak E, Deng B, Kempf P, Pearlman M (1998). Belt and airbag testing with a pregnant hybrid III dummy. Journal of Traffic Medicine, 26(3-4), 125-138.

Williams JK, McClain L, Rosemurgy AS, Colorado NM (1990). Evaluation of blunt abdominal trauma in the third trimester of pregnancy: maternal and fetal considerations. Obstetrics and Gynecology, 75(1), 33-37.

Wolf ME, Alexander BH, Rivara FP, Hickok DE, Maier RV, Starzyk PM (1993). A retrospective cohort study of seatbelt use and pregnancy outcome after a motor vehicle crash. The Journal of Trauma, 34(1), 116-119.

Wood C (1964). Physiology of uterine contractions. British Journal of Obstetrics and Gynaecology, 71, 360-373.

Wood C (1965). Resting tension in the human uterus. Aust NZJ Obstet Gynaec, 5, 219-221.

Yamada H (1970). Strength of biological materials. Baltimore: The Williams & Wilkins Company.

Zhang L, Yang KH, Dwarampudi R, Omori K, Li T, Chang K, Hardy WN, Khalil TB, King AI (2001). Recent advances in brain injury research: A new human head model development and validation. Stapp Car Crash Journal, 45, 369-394.

Appendix A
Methodology, Validation, and Limitations

A.1 Introduction

The 5th percentile female is considered to be at greatest risk of injury due to contact with the vehicle interior. The small female, as well as the gestational period of 30 weeks, was also chosen to facilitate comparison to the MAMA-2b pregnant dummy. Due to the large percent of fetal deaths attributed to placental abruption, up to 70%, the pregnant model was designed to predict placental abruption. The injury mechanisms described by Rupp et al. (2001) were used to predict placental abruption. Because these mechanisms are independent of the fetus, as reported by Rupp et al. (2001), no fetus was modeled. In order to model an actual pregnant occupant, including the geometry of a pregnant uterus, it was decided to use a human model instead of a dummy model. Based on the high incidence, the pregnant model will be the driver (~75%) in frontal crashes (~50%). In summary, based on the literature, the following design choices were made for the present work:

1. 5th percentile female
2. 30 weeks gestation
3. Predict placental abruption (no fetus)
4. Human model instead of dummy
5. Driver in frontal crashes

A finite element model of the pregnant uterus was constructed using ANSYS (ANSYS Inc., Canonsburg, PA) and Hypermesh (Altair, Troy, MI). Abdominal structures included are the uterus, placenta, and amniotic fluid. The model was imported into Madymo (TNO, The Netherlands) and attached to a 5th percentile female flexible human body model to simulate sled tests with a pregnant driver. Ligaments, skin, and fat support the uterus. Material and geometric properties were gathered from the literature wherever possible and approximated whenever not available.

Madymo was chosen for its ability to dynamically model rigid bodies and deformable finite elements, as well as the pre-programmed human body models and

airbags. Good results have been found between simulations incorporating the Madymo human models and experiments with small female cadavers.

This chapter describes the formulation of the finite element model, the Madymo 5th percentile female model, and the vehicle interior used during simulations. The validation tests and test matrix undertaken are also described. A limitations section is included at the end.

A.2 Formulation of the Finite Element Uterine Model

Three main characteristics must be defined for every finite element model prior to applying boundary conditions and loads: geometry, material properties, and element type. This section describes the methods used to choose and define each of these three characteristics.

A.2.1 Geometry

The model represents a uterus at 30 weeks of gestation. A fetus was not included because the mechanisms of placental abruption are independent of fetal interactions (Rupp, 2001). The size of the fetus, and therefore the uterus, is independent of maternal size. Uterine size varies and the literature is sparse of solid data on the size of the typical uterus at 30 weeks gestation. Ideally, the pregnant model would be based on solid data of the uterus, such as from ultrasound measurements, however that information was not available at the time of model creation. Therefore, the size of the uterus was approximated from the literature (Table 7, Figure 43). To check the validity of the uterine size, the overall abdominal contour of the pregnant occupant was compared to data from the literature (Section A.3.3). The uterus is axisymetric along its long axis (Gillespie, 1950). Two ellipsoids, one to accommodate the fetal body, major axis of 12 cm, minor axis of 9 cm, and one for the fetal head, major axis of 7 cm, minor axis of 5.25 cm, comprise the pear-shaped uterus. To create this geometry in ANSYS, spheres were created and scaled by 0.75, 1.0, 0.75. The result is a non-uniform thickness of 1 cm at the top and bottom and 0.75 cm at the sides. The smaller ellipsoid is positioned 9 cm posterior to the larger ellipsoid. The interior of the uterus is separated into two sections,

the placenta and amniotic fluid (Figure 44). The placenta is 2 cm thick, roughly circular in shape, and located at the top of the uterus. The remainder of the interior is amniotic fluid. The uterus, amniotic fluid, and placenta will hereafter be referred to as the uterine model.

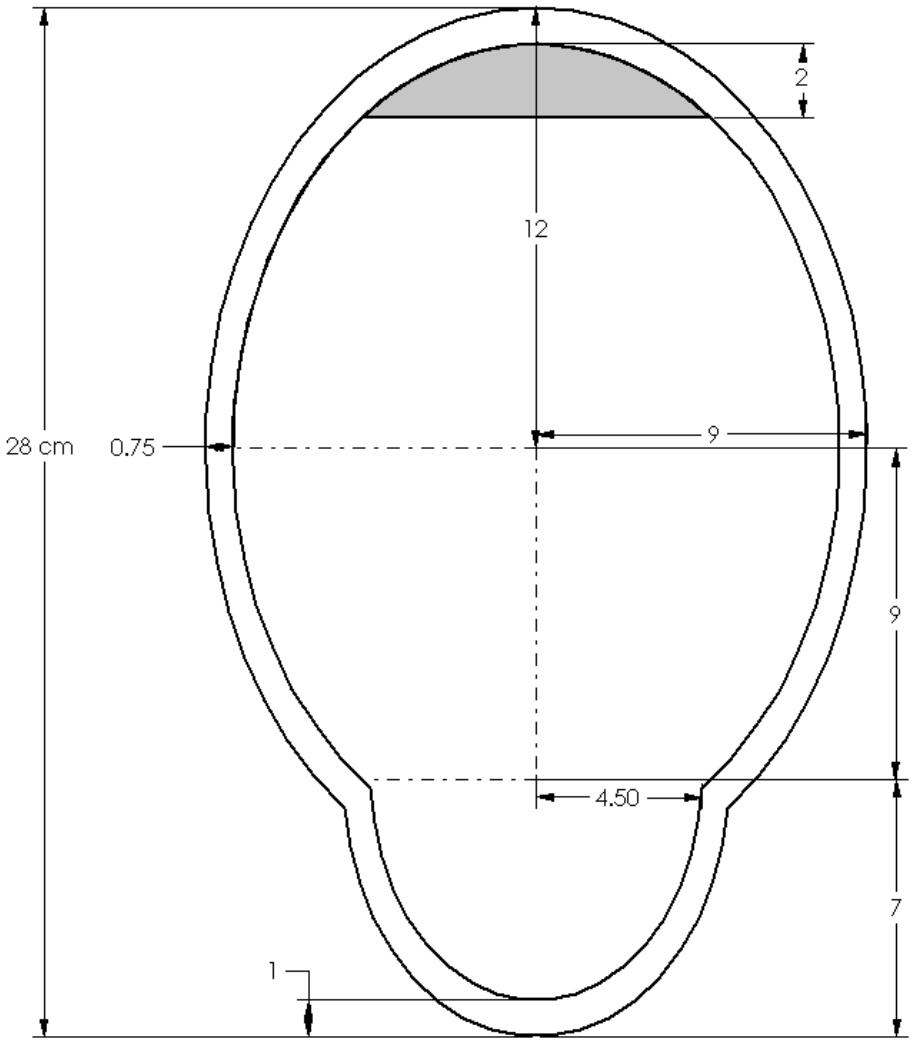

Figure 43: Dimensioned drawing of the pregnant uterus and placenta (in gray)

Table 7: Dimensions of the uterus

Author (Year)	Weeks	Uterine Dimensions
Mowafi (1999)	40	35 cm x 25 cm x 20 cm
Am-I-Pregnant.com (1999)	30	L = 27 cm
Verrallis (1993)	40	30 cm x 23 cm x 20 cm
Rice (1976)	40	7 cm x 5.3 cm (fetal head)

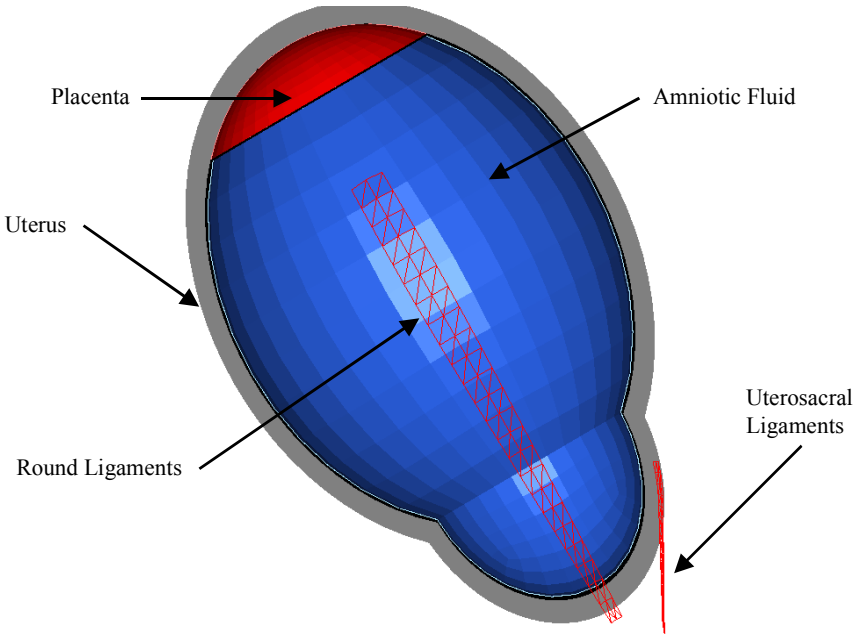

Figure 44: Pregnant Uterine Model

Two pairs of ligaments function as uterine supports. The uterosacral ligaments are connected to the inferior, posterior of the uterus and extend 10 cm to where the pelvis resides. The round ligaments connect to the lateral sides of the uterus and extend 30 cm to the pelvis. Both sets of ligaments are rectangular planes approximately 1 cm wide and 1 cm thick.

The uterus is surrounded by fat. The fat is representative of the abdominal contents above, below, and behind the uterus and is primarily used as a boundary condition. The fat is one element thick (<1cm) between the uterus and the skin in the front (Figure 45). The remainder of the fat is three elements thick (~2.5 cm). This fat

restricts the motion of the uterus posteriorly, superiorly, and inferiorly. These soft boundaries represent organs and the spine in the posterior, other organs and the rib cage superiorly, and the pelvis inferiorly. The human model does not have an anatomically correct pelvis. The use of soft fat, instead of rigid plates, to simulate the pelvic boundary was chosen for stability.

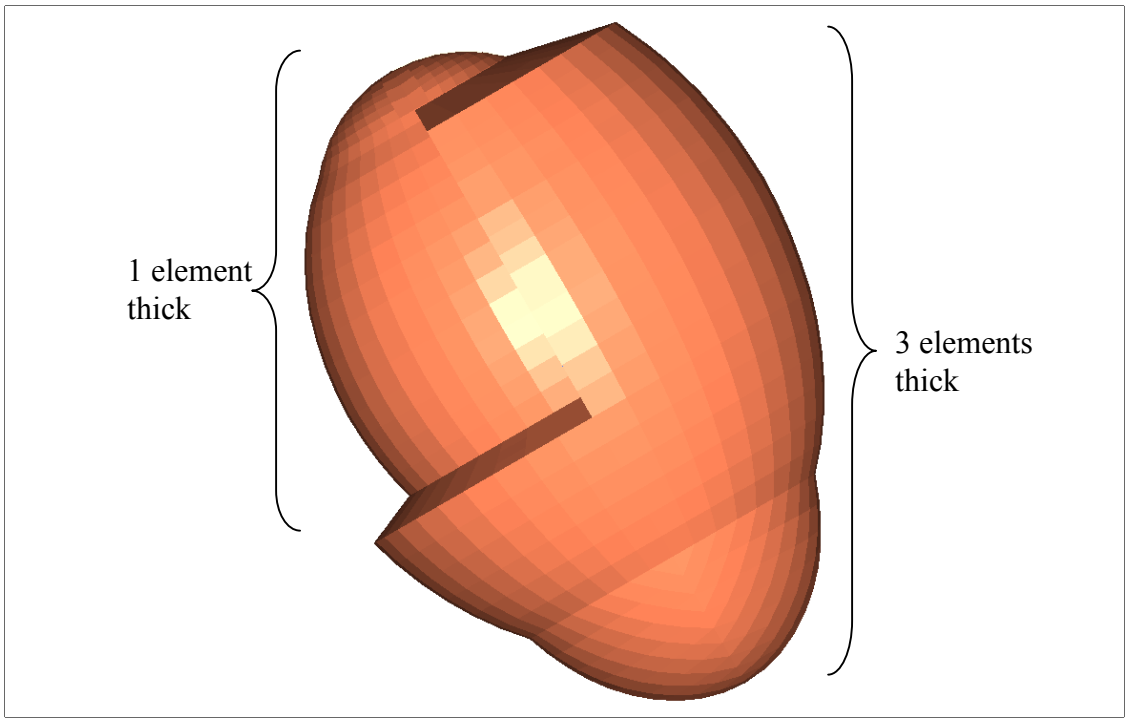

Figure 45: Side view of the fat that surrounds the uterus

A.2.2 Material Properties

The material properties of the model were determined from the literature. When material properties were unavailable, those properties were assumed based on composition. All uterine bodies were modeled as linear elastic solids (Table 8). Although the uterus and placenta are considered visco-elastic and anisotropic (Conrad, 1966; Pearsall, 1978; Mizrahi, 1975), sufficient data was not available to accurately apply these material types. Pearsall and Roberts (1978) found that changing the strain rate ten-fold, from 0.5/min, produced less then a two-fold variation in stress. The amniotic fluid was modeled as a solid because Madymo does not recognize fluid elements. Although

not ideal, many researchers have modeled fluids as solids with minimal error associated with this practice (Power, 2002).

Table 8: Material properties of the uterine model

Structure	Material Model	Density (kg/m^3)	Young's Modulus (kPa)	Poisson's Ratio
Uterus	Linear elastic	1052	566	0.40
Placenta	Linear elastic	995	63	0.45
Amniotic Fluid	Linear elastic	993	20	0.49
Ligaments	Linear elastic	1000	566000	0.40
Fat	Linear elastic	993	47	0.49

A limited amount of data is available on the material properties of the uterus and placenta (Table 9). Tension tests on human uterus tissue have been reported by Pearlman (1999), Pearsall (1978), and Wood (1964). Pearsall and Roberts (1978) tested an unspecified number of uterus tissue samples in a uniaxial tension configuration. Only one of the samples was from a pregnant woman. Specimens were taken from the upper uterine wall and fundus. The elastic moduli ranged from 483 kPa to 1379 kPa and tensile strengths from 552 kPa to 2068 kPa. Pearsall and Roberts (1978) also reported data from Conrad and Wood. The data was converted to true stress and true strain and yielded an elastic modulus of 965 kPa for a non-pregnant uterus (Conrad), 586 kPa for a pregnant uterus (Conrad), and 1207 kPa for the lower uterine segment (Wood). The specimens tested by Wood (1964) included both pregnant and non-pregnant uterus tissue. Pearlman (1999) conducted 4 uniaxial tension tests at 100 mm/min. The Young's modulus ranged from 20.3 kPA to 279.3 kPA. Tests conducted by Pearsall, Wood, and Conrad were conducted to failure of the specimen, while tests by Pearlman were not tested to failure. An average was taken for the data, with a bias towards the Pearlman data because the loading rate was similar to that of a MVC.

Table 9: Tissue properties of the uterus and placenta

Author (Year)	Tissue	Speed (mm/min)	Modulus (kPa)	Strength (kPa)
Pearsall (1978)	Uterus	12.7	483 - 1379	552 - 2068
Conrad (1966)	Non-pregnant uterus	--	965	
Conrad (1966)	Pregnant uterus	--	586	
Wood (1964)	Lower uterus	0.5	1207	
Wood (1965)	Uterus	--	--	483
Pearlman (1999)	Pregnant uterus	100	20.3	
Pearlman (1999)	Pregnant uterus	100	29.3	
Pearlman (1999)	Pregnant uterus	100	143.9	
Pearlman (1999)	Pregnant uterus	100	279.3	
Pearlman (1999)	Placenta	100	12.4	
Pearlman (1999)	Placenta	100	25.6	
Pearlman (1999)	Placenta	100	31.0	
Pearlman (1999)	Placenta	100	31.5	
Pearlman (1999)	Placenta	100	62.9	

Pearlman (1999) reported the results of five tension tests on placental specimen. Tests were conducted at 100 mm/min. The average modulus was 33 kPa, with a high of 63 kPa. Testing was not taken to failure. No other data on the material properties of the placenta was found in the literature. The Poisson's ratio was assumed to be 0.45 because it is muscular tissue (ν=0.40) engorged with blood (ν=0.50). The density of the uterus and placenta was taken from Duck (1990).

An isotropic representation of fatty tissue has been used by Todd and Thacker (1994) in modeling of the human buttocks. The Young's modulus for a supine female was 12 kPa with a Poisson's ratio of 0.49. The Poisson's ratio represents a nearly

incompressible material. The amniotic fluid, which is 99% water, was assumed to have a negligible Young's modulus (20 kPa) and a Poisson's ratio of 0.49.

Material properties of the ligaments connecting the uterus to the pelvis were not found in the literature. A search of general ligament properties showed that the elastic modulus of ligaments is typically two orders of magnitude greater then the uterus (Iwamoto, 1999; Zhang, 2001; Yamada, 1970). Therefore, the elastic modulus of the uterosacral and round ligaments was set to 100 times the modulus of the uterus. The density and Poisson's ratio were also taken from general ligament data (Iwamoto, 1999; Zhang, 2001).

A.2.3 Meshing Techniques

The uterus, placenta, amniotic fluid, and fat were meshed using solid 8-noded brick elements in ANSYS (Table 10). Brick elements were chosen because they are more accurate then tetrahedral elements (Ansys documentation). The brick elements carry tension, compression, and shear loads. The mass of the element is lumped and distributed equally over each node. In order to utilize solid brick elements, the elliptical geometries had to be partitioned into several sections before meshing. This provided ANSYS with a starting and ending surface to mesh. The mesh density of the amniotic fluid is coarser then the uterus and placenta because the focus of this study is on the interaction of the uterus and placenta. The ligaments were modeled as 3-noded membrane elements, which are plane, constant stress triangular elements with in-plane stiffness, and no bending stiffness (Madymo theory manual). Triangular elements were chosen instead of quadrilateral elements to yield better stability when solving the Madymo code, as recommended by the TNO technical support group. To connect the placenta to the uterus, 149 two-node truss elements were defined between adjacent nodes of the placenta and uterus. These truss elements mimic the constraint condition of the uteroplacental interface. The 1 cm thick truss elements were given the material properties of the placenta.

Table 10: Summary of finite elements

Structure	Element Type	# of Elements	# of Nodes
Uterus	8-noded Brick	2736	5476
Placenta	8-noded Brick	2000	2330
Amniotic Fluid	8-noded Brick	3136	3540
Ligaments	Triangular membranes	300	320
Fat	8-noded Brick	3460	4669
	Total	11,632	16,335

Grid Independence

The mesh density was varied to test for convergence. The uterus was supported in the posterior region, allowing zero displacement. Three levels of compression were applied to the fundus (Figure 46). The maximum stress in the uterine body was recorded and plotted versus the number of elements (Figure 47). Any increase in elements along the flat portion of the curve would yield little increase in accuracy compared to the associated increase in computational time. The final model contains 11,632 elements.

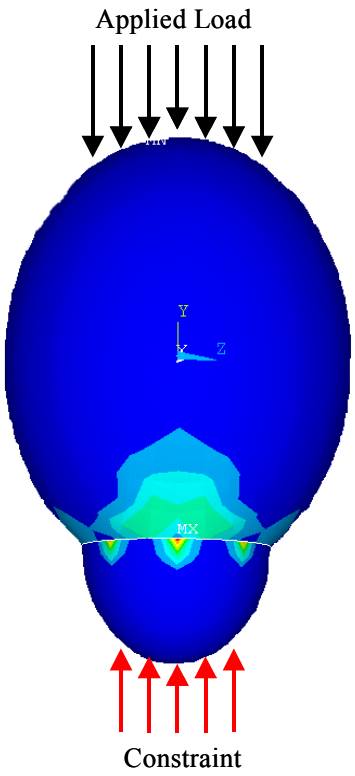

Figure 46: Test setup for Grid independence test

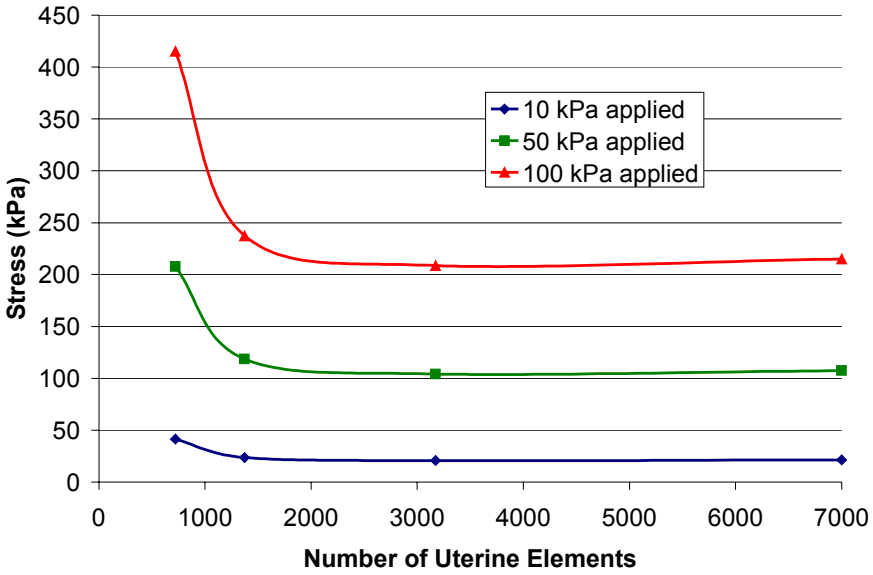

Figure 47: Result of grid independence test

A.3 Madymo

The geometry created and meshed in ANSYS was converted into the Madymo syntax utilizing the Altair Hypermesh translation software. Information such as material properties, element type, and membrane thickness defined in ANSYS cannot be inputted into the Madymo syntax file. Only the coordinates of each node and the number of nodes per element comprising a mesh are transferable.

A.3.1 Human Body Model

In order to represent an occupant in sled tests, Madymo has developed dummy models and human models. The dummy models are representations of various dummies used in crash tests (typically the Hybrid III). The dummy models are available in a rigid ellipsoid model, as well as a facet model. The human models are representations of humans and are therefore more biofidelic then the dummy models. The human models are available in a flexible body model for the 50^{th} percentile and 5^{th} percentile human, as well as a full finite element model (for 50^{th} percentile human only). One example of the difference between the human model and the dummy model is the spine. The human model spine is represented by individual vertebra that can rotate separately. The dummy model spine is comprised of a rigid thorax box and two rubber columns for the lumbar and cervical spine. It was determined that the human model would provide the best platform to create a pregnant occupant.

The 5^{th} percentile human occupant model, developed by TNO/Madymo, is multi-directional and applicable for frontal, lateral, rearward, and rollover impacts. The outer surface of the occupant model is described by facet surfaces, instead of rigid ellipsoids in the dummy models (Figure 48). Flexible bodies are used to model abdominal and thoracic deformation (Figure 49). The model was validated against small female impact corridors for the SID2s dummy and small female post mortem human subject (PMHS) tests (Happee, 2000).

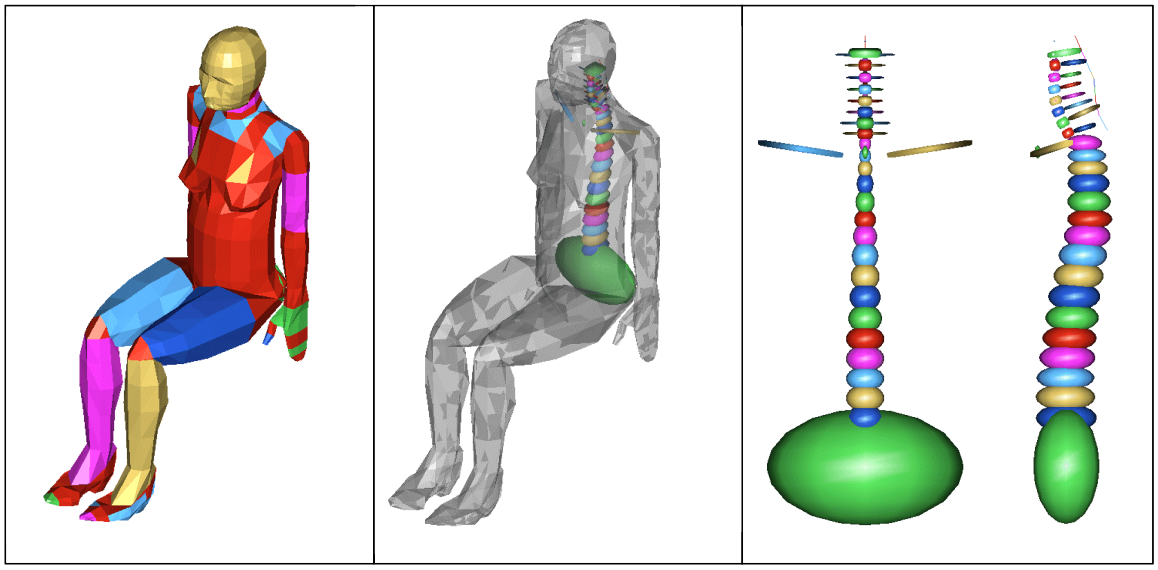

a.) 5th percentile human model b.) Transparent model showing spine c.) Close-up of spine and scapula

Figure 48: 5th percentile human model and spine

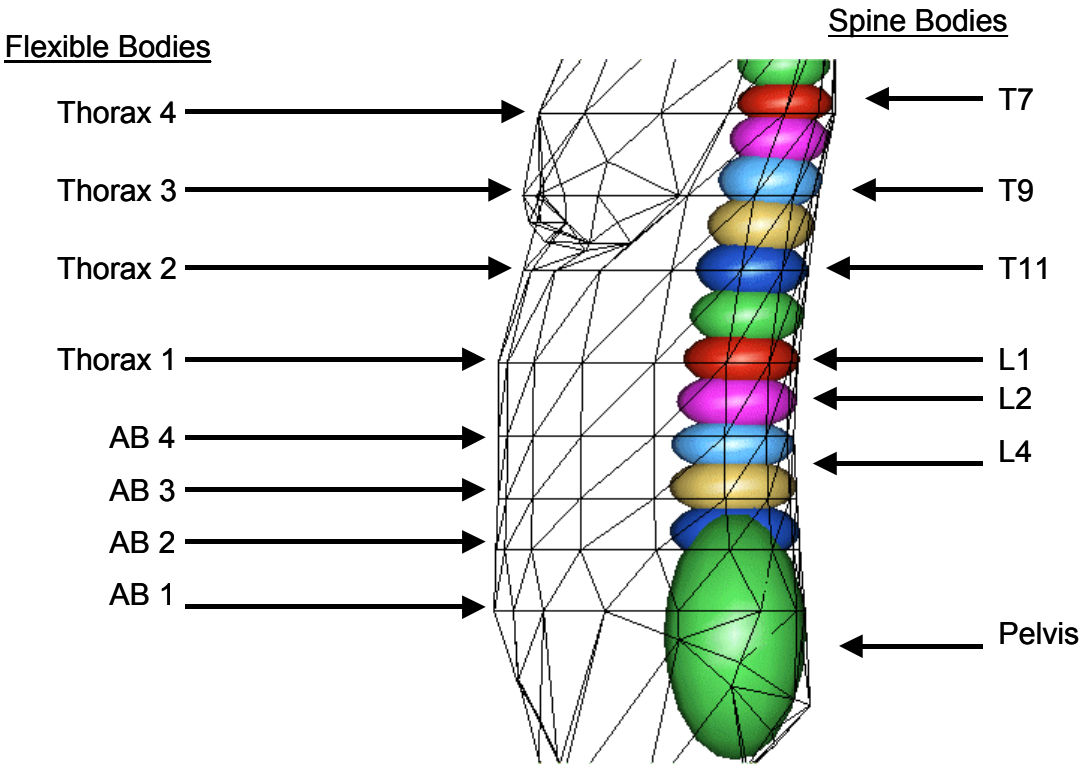

Figure 49: Flexible bodies of the human model

The anthropometry of the model was obtained from the RAMSIS software package database. The 5th percentile model is 1.52 m (~5ft) tall and weighs 49.8 kg (~110 lb). The model is composed of 92 bodies, including eight flexible bodies, four in the thorax and four in the abdomen. The geometry of the flexible bodies is defined by the nodes of the surrounding skin.

The thorax and abdomen have been modeled such that during impact they deform in a 3-D manner due to contact and spinal deformation. This torso deformation corresponds to experimental data. Overall, the small female model was validated using impact corridors for the SID2s dummy, as well as PMHS tests.

The pregnant model was inserted into the human model be defining its position with respect to the pelvis of the human model. This allows the relative position of the uterine model with respect to the human model to be fixed during setup of the model. The skin was stretched around the uterus to accommodate the uterus (Figure 50). With the uterine model in position, contacts were defined to allow for interaction between the uterine model, the human model, and the vehicle interior. The target weight gain for a pregnant female is 0.23 kg (0.5 lb) per week for the first 20 weeks and 0.45 kg (1.0 lb) for the second 20 weeks (Institute of Medicine, 1990). At thirty weeks, weight gain is about 9.1 kg (20 lbs). The weight of the pregnant model is 131 lbs.

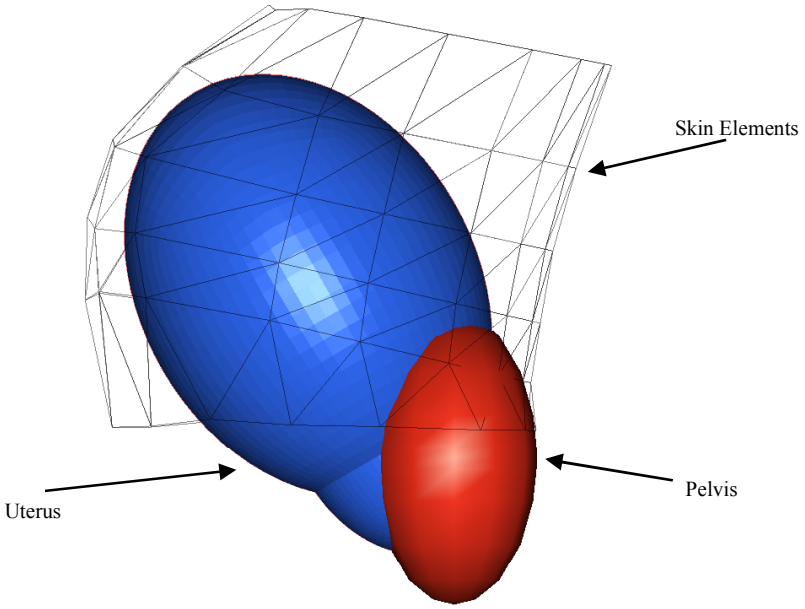

Figure 50: Human model skin stretched around the uterus

A.3.2 Contacts and Constraints

In order for objects to interact in Madymo, specific contacts must be defined between each object. Contacts can be defined between two rigid bodies (MB), between a rigid body and a finite element body (FE) and between two finite element bodies. Because both the skin of the human model and the uterus model are FE bodies, only the second two types of contact were used.

For MB-FE contact, the contact force can be based on a characteristic or kinematic type. The characteristic contact model defines the contact force using the contact properties of the slave surface. This contact model was used for contacts between the vehicle interior and the human body using the predefined contact characteristics of the human model. The kinematic contact model does not allow the FE model to penetrate the rigid body. This contact was used for contacts between the vehicle interior and the uterus model.

For FE-FE contact, the contact force can be based on the characteristic contact model or a penalty-based model. For the penalty-based model, the contact force is based

on the bulk modulus of the master surface and is designed to limit penetrations. The parameters of the penalty model are scaled to adjust the penetrations and to avoid instabilities. The coarser mesh should be chosen as the master surface because the elements of the master surface contact the nodes of the slave surface. Penalty based contacts were defined between all the uterine model components as well as between the uterus and the skin. Redundant contacts were defined between the uterus and the lap belt, steering wheel, and the airbag, as well as between the fluid and the skin, lap belt, steering wheel, and airbag. The redundant contacts reduced penetrations, especially with objects that penetrated the skin. Skin penetration, defined as an object penetrating the elements of the skin, is possible because contact is defined between objects and the nodes of the skin. The skin is made up of 16 nodes for each vertical level.

Because the penalty model of contact uses the bulk modulus of the master surface, the skin of the human model had to be altered. The skin has no material property because the deformation of the skin is defined by the deformable bodies. In order for the skin and uterus to interact, a bulk modulus was defined for the skin nodes that contacted the uterus. A value of 20 kPa was chosen because it limited penetration while remaining stable.

In addition to contacts, several constraints were defined to produce a more biofidelic model. The inferior ends of the ligaments and the fat were constrained to move with the pelvis of the human model including translation and rotation. A circular region on the inferior uterus 4 cm in diameter was also constrained to the pelvis. This region represents the cervix.

A.3.3 Vehicle Interior

The vehicle interior used in the simulations is a typical Madymo interior, however, the position of the planes was modified to correspond to the seated anthropometry of a pregnant women in her 30th week of pregnancy (Klinich, 1999a). The vehicle interior is made up of seven rigid planes and an ellipsoid. The planes are the seatback, seat cushion, head restraint, knee bolster, floor plane, foot plane and foot stop (Figure 51). The planes represent a simple model of a driver's seat. The steering wheel is modeled as an ellipsoid.

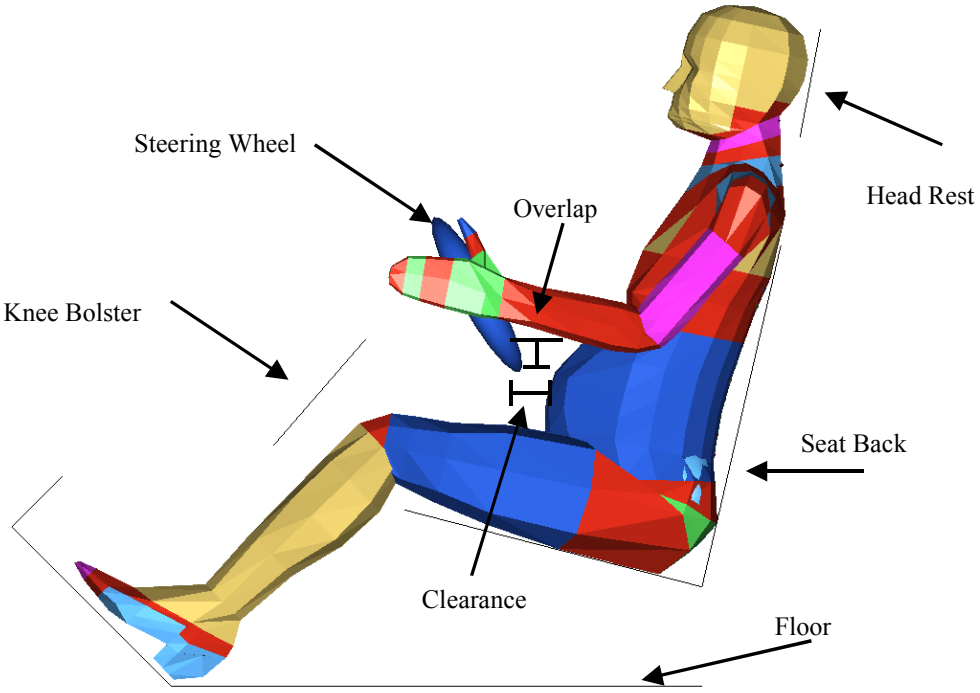

Figure 51: Vehicle interior showing uterus clearance and overlap

Seated Anthropometry

The anthropomentry of a pregnant woman was quantified by Klinich et al. (1999a). The abdominal contour was taken from the full group of volunteers and is the contour used for the MAMA-2b by Rupp et al. (2001). The abdominal contour of the pregnant model closely matches the Klinich data (Figure 52). Positioning of the pregnant occupant was based on the average of the first group at 30 weeks gestation. Group 1 was the smallest group, with a height of approximately 5 feet and weighing 134 lbs. The average distance between the abdomen and the bottom of the steering wheel was 38 mm. The mean overlap of the uterus to the steering wheel was 12%. The overlap is defined as the ratio of the height of the uterus above the steering wheel to the total height of the uterus. The seatback angle, relative to vertical, is 13 degrees and the steering wheel tilt is 29 degrees from vertical.

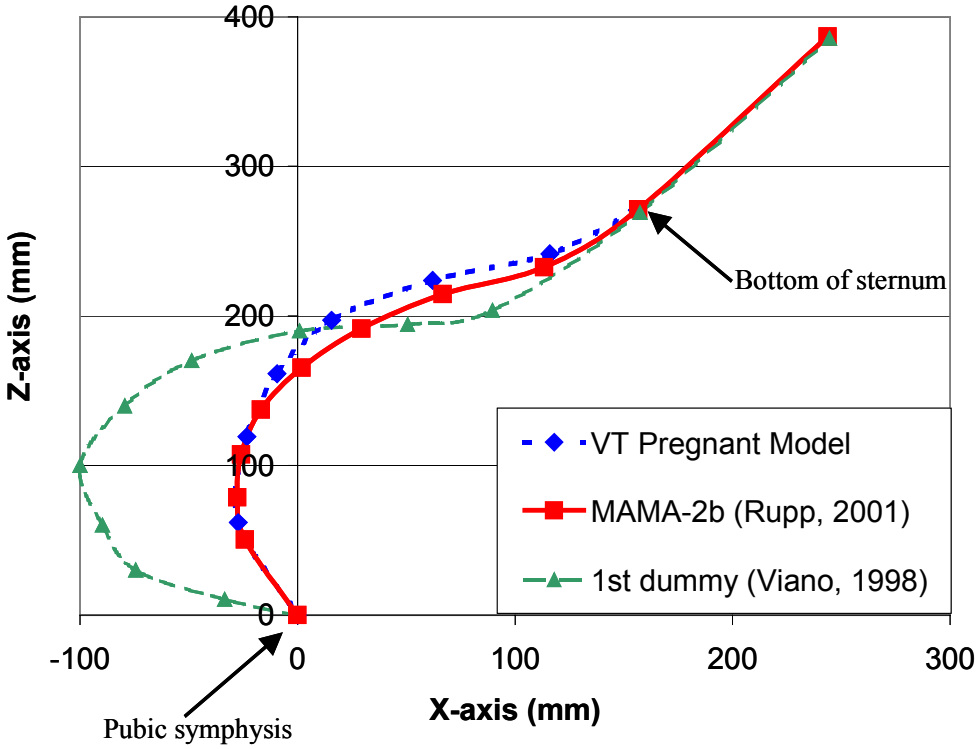

Figure 52: Comparison of abdominal contours

Sled Pulse

During physical tests, a moving sled is decelerated by impacting an object, such as a car or rigid barrier. In simulations, it is customary to accelerate the dummy relative to a stationary sled (Madymo database manual). The acceleration is defined with respect to time, thus the area under the curve is the change in velocity of the crash (Figure 53). The applied sled pulses are half-sine waves. The duration of the pulse was determined from sled pulses in the NHTSA database.

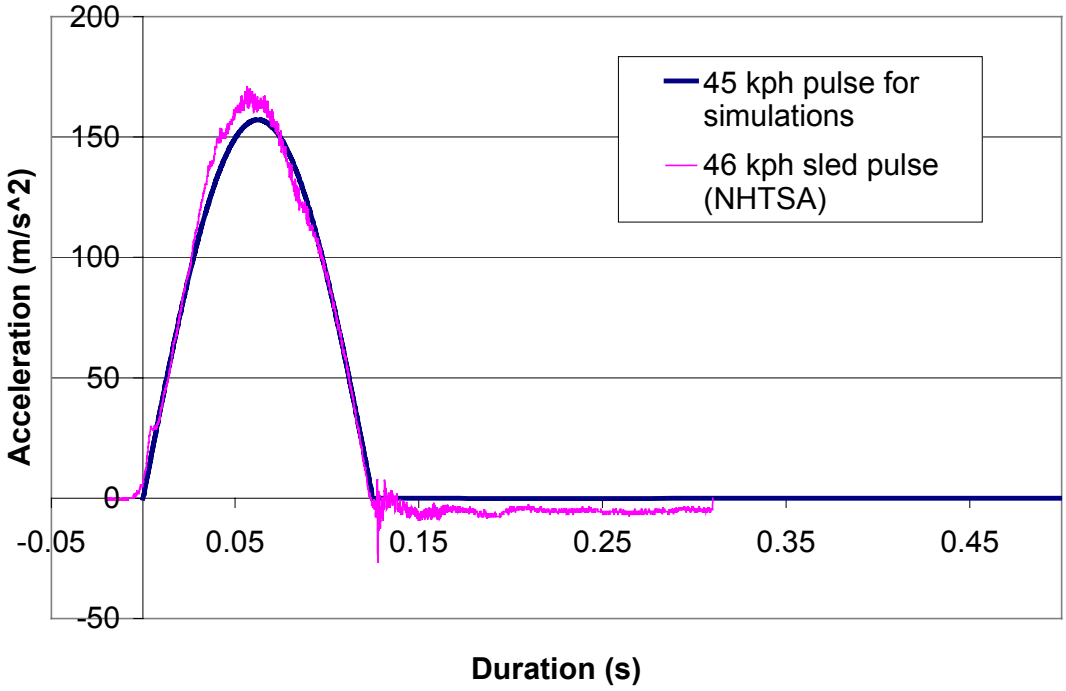

Figure 53: Comparison of defined sled pulse to actual sled pulse

A.3.4 Restraints

The American College of Obstetricians and Gynecologists (ACOG) recommends that pregnant women use the 3-pt belt system throughout pregnancy and that the airbag should not be disabled. The ACOG recommends that the lap belt should be placed under the abdomen, over both anterior superior iliac spines and the pubic symphysis. The shoulder harness should be placed between the breasts. Excessive slack should be eliminated from both the lap and shoulder belts.

A problem many pregnant women, especially small women, experience is belt slippage. During driving, the belt will ride upward onto the abdomen. This results in increased abdominal loading and has been associated with adverse fetal outcome. In order to model belt slippage, the Madymo finite element seatbelts were chosen. The conventional belts in Madymo, consisting of just springs, are attached directly to the occupant and therefore do not allow slippage. A standard Madymo 600 mm driver airbag

was used in tests with airbag deployment (Figure 54). The inflation was triggered 15 ms into the crash simulation.

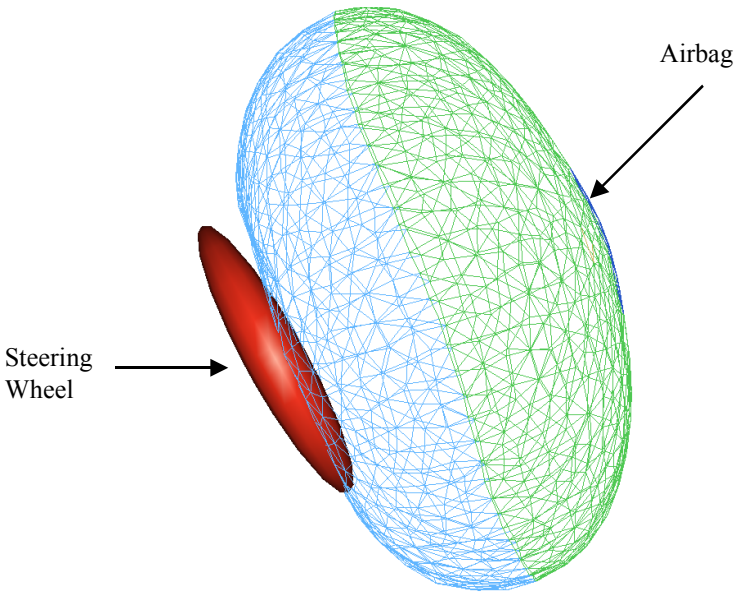

Figure 54: Driver side airbag used in Madymo simulations

A.4 Model Validation

Proper response of the abdomen during loading is essential for an accurate model. The abdominal response of the pregnant model was compared to the appropriate abdominal corridors for belt loading and rigid bar impacts. The abdominal response corridors of a non-pregnant abdomen have been assumed valid for the pregnant abdomen based on quasi-static testing (Rupp 2001). Abdominal force deflection corridors were developed by Hardy (1999) for the 50th percentile male and scaled to a 5th percentile pregnant woman by Rupp et al. (2001).

A.4.1: Belt Loading

Simulating the test conditions used by Hardy et al. (2001), a finite element belt was positioned at umbilicus level and an initial velocity of 3 m/s was applied to the pregnant model. The force in the belt was plotted versus the displacement of the abdomen (Figure 13). The abdominal response of the pregnant model is within the

defined upper and lower bounds up to 40 mm of deflection. The abdominal response for 3 m/s belt loading is approximately 90 N/mm from 0 mm to 40 mm. The simulation is limited to 40 mm of deflection because the motion of the pregnant model stalled after 40 mm of deflection.

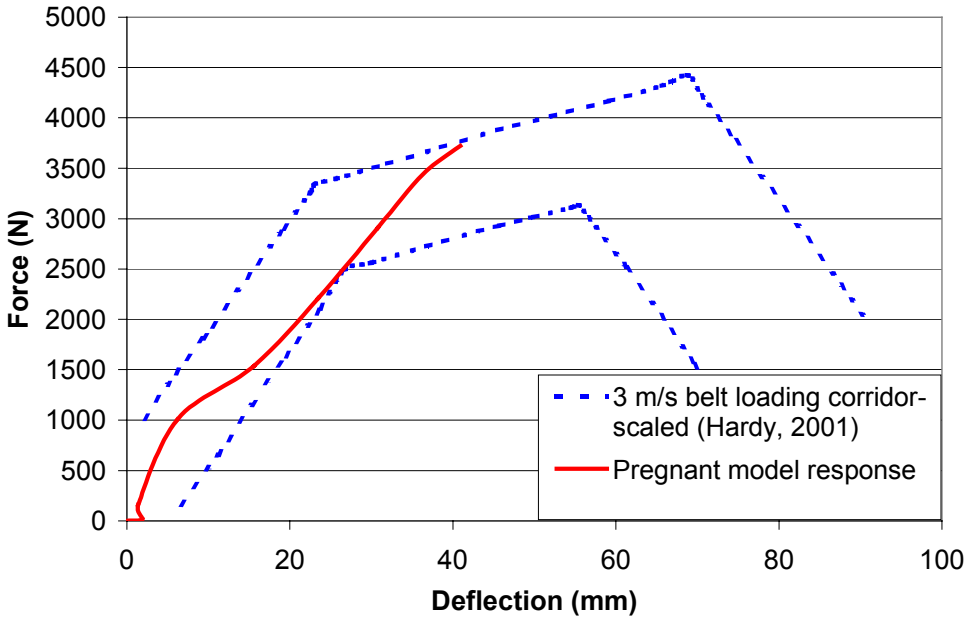

Figure 55: Abdominal response of the pregnant model to 3 m/s belt loading

A.4.2: Rigid Bar Impact

The abdominal response to impact with a rigid bar was also investigated. A 2.54 cm diameter, 48 kg cylindrical impactor was used to impact the abdomen at umbilicus level. The tests were run at 6 m/s (Figure 14). The abdominal response of the pregnant model is within the defined upper and lower bounds. The 6 m/s rigid bar impact response is approximately 20 N/mm from 0 mm to 60 mm.

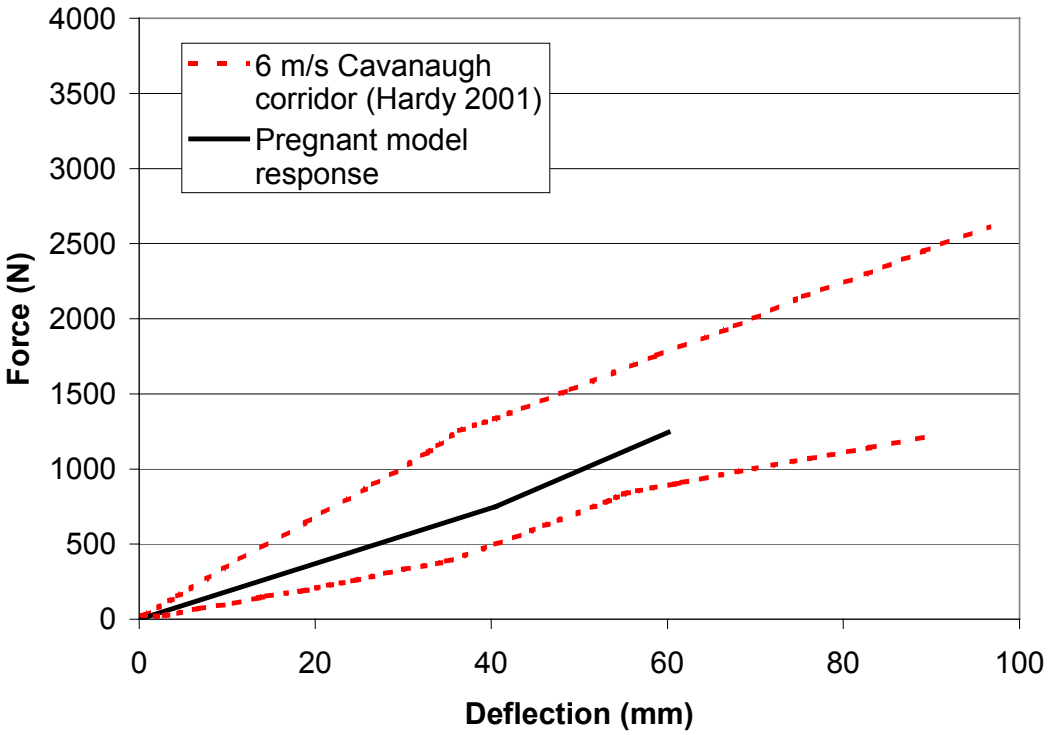

Figure 56: Abdominal response of the pregnant model to 6 m/s rigid bar impact

A.5 Test Matrix

The test matrix for this study included twelve sled test simulations (Table 5). The simulations included occupants with no restraint, 3-pt belt, and 3-pt belt plus airbag under various crash speeds ranging from 13 kph to 55 kph. The test matrix was designed to identify inertial, steering wheel, seatbelt, and airbag loading on the pregnant uterus, and to match testing of the second-generation pregnant dummy (Rupp, 2001). In each test, the pregnant occupant was a driver in a frontal crash. Simulations were run in excess of 100 ms in order to ensure that the forward motion of the occupant had stopped. The computational model uses peak Von Mises strain in the uterus near the placenta as the measure for predicting risk of injury. This strain was compared to the risk of adverse fetal outcome, as defined by Klinich et al. (1999b), to determine if strain could be used as a predictive tool.

Table 11: Test matrix for the pregnant model simulations

Test Number	Restraint Configuration	Crash Speed (kph)	Risk of Adverse Fetal Outcome (%) *
1	None	13	36
2	None	20	54
3	None	25	70
4	None	35	86
5	3-pt Belt	13	9
6	3-pt Belt	25	26
7	3-pt Belt	35	51
8	3-pt Belt	45	76
9	3-pt Belt	55	90
10	Airbag + 3-pt Belt	25	26
11	Airbag + 3-pt Belt	35	51
12	Airbag + 3-pt Belt	45	76

***** Risk based on crash investigations (Klinich, 1999).

A.6 Limitations

Several assumptions were made in the formulation of the finite element uterine model. The geometry, although an improvement over previous modeling efforts, is simplified. The human model pelvis is elliptical and does not accurately represent a female pelvis. The addition of a FE pelvis would be beneficial in terms of uterine boundary conditions, support for the ligaments, and would provide for more accurate positioning of the uterus in the abdomen. In addition to a FE pelvis, the entire spine could be made out of finite elements. This addition would increase the accuracy of the uterine boundary conditions. The uterus, although made of solid elements, is only one element thick. Either a membrane or a multi-element thick solid should be used for the uterus. The use solid elements would provide the separation of interior and exterior stress and strain.

The uterus, placenta, and amniotic fluid were assumed linear, elastic, isotropic solid materials. The uterus is known to be anisotropic and viscoelastic, however there is not currently enough data to apply these material properties to the model. The amniotic fluid was defined as a solid because Madymo does not allow fluids to be defined. The global coordinate system does not coincide with the uterine radial and circumferential directions and therefore limits the strain output.

Validation was limited to abdominal force deflection. Additional validation, such as a check of the stress and strain recorded in the uterine wall or placenta, is desirable. Data of this type is not currently available and may not become available due to the ethics of testing a pregnant abdomen.

The abdominal deformable bodies of the human model, which define the force-deflection of the abdomen, were left in the model. During validation, it was found that the lower abdominal response of the non-pregnant model did not fall within the corridors defined by Hardy (2001) and scaled by Rupp et al. (2001). It has been suggested by the Madymo tech support that the abdomen deformable bodies may produce unwanted results and should be removed in future versions.

It is recommended that these improvements be included in future versions of the FE model.

Appendix B
Truncated Madymo Code

The Madymo input is separated into three main files: a main user file and two include files that include information on the small female human model and the pregnant uterine model. For the main file, a 3-pt belt plus airbag user file is included. This file contains all the specs used for the no restraint and 3-pt belt tests. Sled pulses were interchanged to vary the crash speed. The standard include file for the human model was used, therefore the code is not included here. The include file for the uterine model is included, with the nodal coordinates and elements removed in order to save space.

Preg_belt+bag35.xml

```
<?xml version="1.0" encoding="UTF-8"?>
<!DOCTYPE MADYMO SYSTEM "mtd_3d.dtd">
<MADYMO RELEASE="R6.0">
 <TYPEDEFS>
  <INCLUDE FILE="typedefs.xml"    />
 </TYPEDEFS>
 <RUNID>
                <PRODUCT_INFORMATION DATE="$Date: 2001/05/09 08:48:37 $"
DESCRIPTION="MADYMO 5th percentile human female occupant model"
FILE="$RCSfile: h_occ05f_usr.xml,v $ (user file)" STATE="$State: Exp $"
VERSION="$Revision: 1.1 $">
    <COPYRIGHT>
(c) 2001 TNO Automotive
   P.O. Box 6033, 2600 JA Delft, The Netherlands

 All rights reserved

 MADYMO software programs and MADYMO databases are confidential
 information and proprietary products of TNO, Delft, The Netherlands.
 The terms and conditions governing the licensing of MADYMO software
 consist solely of those set forth in the written contracts between
 TNO and its customers. The software may only be used or copied in
```

accordance with the terms of these contracts.
</COPYRIGHT>
</PRODUCT_INFORMATION>
Human occupant model
Female 05%, v2.0
Madymo 6.0
</RUNID>
<!--5th percentile Pregnant Female in Klinich vehicle interior with 3pt belt + airbag and a 35 kph sled pulse-->
<CONTROL_ALLOCATION C_SIZE.RANGE="[1,)" C_SIZE.TYPE="INTEGER" C_SIZE="1000000" FLAG.RANGE="[1,)" FLAG.TYPE="INTEGER" I_SIZE.TYPE="INTEGER" I_SIZE="4000000" I_SIZE.RANGE="[1,)" NR_PROC.RANGE="[1,)" NR_PROC.TYPE="INTEGER" R_SIZE.RANGE="[1,)" R_SIZE.TYPE="INTEGER" R_SIZE="5000000" />
<CONTROL_ANALYSIS.TIME CONSTRAINT_TOL.TYPE="REAL" CONSTRAINT_TOL="1.000000E-09" INT_MTH="EULER" INT_TOL.TYPE="REAL" INT_TOL.RANGE="(0,)" MAX_STEP.RANGE="(0,)" MAX_STEP.TYPE="REAL" RACO.RANGE="[0,)" RACO="0.01 0.1" RACO.TYPE="REAL[2]" RAMP.RANGE="[0,)" RAMP.TYPE="REAL[2]" TIME_END="0.150" TIME_END.TYPE="REAL" TIME_START.TYPE="REAL" TIME_STEP.TYPE="REAL" TIME_STEP="1.78572E-06" TIME_STEP.RANGE="(0,)" />
<CONTROL_OUTPUT PADDING_TIME.RANGE="[0,)" PADDING_TIME.TYPE="REAL" TIME_STEP.RANGE="(0,)" TIME_STEP.TYPE="REAL" TIME_STEP="1.000000E-04" TIME_STEP_KIN="0.001" TIME_STEP_KIN.RANGE="(0,)" TIME_STEP_KIN.TYPE="REAL" >
<RESULT_ANIMATION_FE ANIMATION_OUTPUT_LIST.TYPE="LIST" ANIMATION_OUTPUT_LIST="uterus_out" FE_MODEL.TYPE="REF" FE_MODEL="/3/UTERUS" />
<RESULT_ANIMATION_FE ANIMATION_OUTPUT_LIST.TYPE="LIST" ANIMATION_OUTPUT_LIST="placenta_out" FE_MODEL.TYPE="REF" FE_MODEL="/3/A_FLUID" />
<RESULT_ANIMATION_FE ANIMATION_OUTPUT_LIST.TYPE="LIST" ANIMATION_OUTPUT_LIST="fat_out" FE_MODEL.TYPE="REF" FE_MODEL="/3/FAT" />
<TIME_HISTORY_MB BELT_OUTPUT_LIST.TYPE="LIST" BODY_OUTPUT_LIST="HeadCG_lds HeadOC_lds T1AO_lds HeadCG_lac HeadOC_lac T1AO_lac Sternum_CFC180_lac Sternum_lac Pelvis_lac HeadCG_aac T1_aac" BODY_OUTPUT_LIST.TYPE="LIST" BODY_REL_OUTPUT_LIST="HeadCG_T1AO_rds HeadOC_T1AO_rds Sternum_T1AO_dvl Ribs1_Spine_dvl Ribs2_Spine_dvl Ribs3_Spine_dvl Ribs4_Spine_dvl" BODY_REL_OUTPUT_LIST.TYPE="LIST" CONTROL_SYSTEM_OUTPUT_LIST.TYPE="LIST" DESCRIPTION="Output signals Pregnant Human Female 5th percentile Occupant model" JOINT_CONSTRAINT_OUTPUT_LIST="NeckLow_Torque NeckLow_Force

NeckUp_Torque NeckUp_Force NeckUp_CFC1000_Force"
JOINT_CONSTRAINT_OUTPUT_LIST.TYPE="LIST"
JOINT_DOF_OUTPUT_LIST.TYPE="LIST"
MUSCLE_OUTPUT_LIST.TYPE="LIST"
RESTRAINT_OUTPUT_LIST="AbdomenFront1 AbdomenFront2 AbdomenFront3
AbdomenFront4 ThoraxFront1 ThoraxFront2 ThoraxFront3 ThoraxFront4 AbdomenR1
AbdomenR2 AbdomenR3 AbdomenR4 ThoraxR1 ThoraxR2 ThoraxR3 ThoraxR4
AbdomenL1 AbdomenL2 AbdomenL3 AbdomenL4 ThoraxL1 ThoraxL2 ThoraxL3
ThoraxL4 Head_wrt_T1 T1_wrt_RefSpace Head_wrt_RefSpace"
RESTRAINT_OUTPUT_LIST.TYPE="LIST"
SENSOR_OUTPUT_LIST.TYPE="LIST" SYSTEM.TYPE="REF"
SYSTEM="PregHumanFemale05%" >
<COMMENT><![CDATA[
Available output signals

BODY_OUTPUT_LIST
HeadCG_lds
HeadOC_lds
T1AO_lds
HeadCG_lac
HeadOC_lac
T1AO_lac
Sternum_CFC180_lac
Sternum_lac
Pelvis_lac
HeadCG_aac
T1_aac

BODY_REL_OUTPUT_LIST
HeadCG_T1AO_rds
HeadOC_T1AO_rds
Sternum_T1AO_dvl
Ribs1_Spine_dvl
Ribs2_Spine_dvl
Ribs3_Spine_dvl
Ribs4_Spine_dvl

JOINT_CONSTRAINT_OUTPUT_LIST
NeckLow_Torque
NeckLow_Force
NeckUp_Torque
NeckUp_Force
NeckUp_CFC1000_Force

RESTRAINT_OUTPUT_LIST
AbdomenFront1

AbdomenFront2
AbdomenFront3
AbdomenFront4
ThoraxFront1
ThoraxFront2
ThoraxFront3
ThoraxFront4
AbdomenR1
AbdomenR2
AbdomenR3
AbdomenR4
ThoraxR1
ThoraxR2
ThoraxR3
ThoraxR4
AbdomenL1
AbdomenL2
AbdomenL3
AbdomenL4
ThoraxL1
ThoraxL2
ThoraxL3
ThoraxL4
Head_wrt_T1
T1_wrt_RefSpace
Head_wrt_RefSpace

MARKER_OUTPUT_LIST
HeadCG_mark
HeadOC_mark
T1AO_mark
]]></COMMENT>
</TIME_HISTORY_MB>
<TIME_HISTORY_MB BELT_OUTPUT_LIST.TYPE="LIST"
BELT_OUTPUT_LIST="belt_out_01 belt_out_02 belt_out_03 belt_out_04"
BODY_OUTPUT_LIST.TYPE="LIST" BODY_REL_OUTPUT_LIST.TYPE="LIST"
CONTROL_SYSTEM_OUTPUT_LIST.TYPE="LIST"
JOINT_CONSTRAINT_OUTPUT_LIST.TYPE="LIST"
JOINT_DOF_OUTPUT_LIST.TYPE="LIST"
MUSCLE_OUTPUT_LIST.TYPE="LIST"
RESTRAINT_OUTPUT_LIST.TYPE="LIST"
SENSOR_OUTPUT_LIST.TYPE="LIST" SYSTEM.TYPE="REF" />
<TIME_HISTORY_FE AIRBAG_OUTPUT_LIST.TYPE="LIST"
CROSS_SECTION_OUTPUT_LIST.TYPE="LIST"
ELEMENT_OUTPUT_LIST.TYPE="LIST" ELEMENT_OUTPUT_LIST="ut_out
pla_out" FE_MODEL.TYPE="REF" FE_MODEL="/3/UTERUS"

JET_OUTPUT_LIST.TYPE="LIST" NODE_OUTPUT_LIST.TYPE="LIST"
STRAP_OUTPUT_LIST.TYPE="LIST" />
  <TIME_HISTORY_FE AIRBAG_OUTPUT_LIST="1:6"
AIRBAG_OUTPUT_LIST.TYPE="LIST"
CROSS_SECTION_OUTPUT_LIST.TYPE="LIST"
ELEMENT_OUTPUT_LIST.TYPE="LIST" FE_MODEL.TYPE="REF"
FE_MODEL="/Airbag/Driver_Airbag_600mm_diameter"
JET_OUTPUT_LIST.TYPE="LIST" NODE_OUTPUT_LIST.TYPE="LIST"
STRAP_OUTPUT_LIST.TYPE="LIST" />
 </CONTROL_OUTPUT>
  <SYSTEM.REF_SPACE ID.RANGE="[1,)" ID.TYPE="INTEGER" ID="1"
NAME="VEHICLE" NAME.TYPE="NAME" >
  <SURFACE.PLANE BODY.TYPE="REF" CHAR.TYPE="REF" ID.RANGE="[1,)"
ID="1" ID.TYPE="INTEGER" NAME="Foot_Plane" NAME.TYPE="NAME"
POINT_1.TYPE="REAL[3]" POINT_1="0.817 0.1500 -0.053"
POINT_2.TYPE="REAL[3]" POINT_2="0.817 -0.1500 -0.053" POINT_3="1.042 -
.01500 0.172" POINT_3.TYPE="REAL[3]" />
  <SURFACE.PLANE BODY.TYPE="REF" CHAR.TYPE="REF" ID.RANGE="[1,)"
ID="2" ID.TYPE="INTEGER" NAME="Floor_Plane" NAME.TYPE="NAME"
POINT_1.TYPE="REAL[3]" POINT_1="0.0670 0.5000 -0.053"
POINT_2.TYPE="REAL[3]" POINT_2="0.0670 -0.5000 -0.053" POINT_3="0.8170 -
0.5000 -0.053" POINT_3.TYPE="REAL[3]" />
  <SURFACE.PLANE BODY.TYPE="REF" CHAR.TYPE="REF" ID.RANGE="[1,)"
ID="3" ID.TYPE="INTEGER" NAME="Seat_cushion" NAME.TYPE="NAME"
POINT_1.TYPE="REAL[3]" POINT_1="0.0670 0.1750 0.0870"
POINT_2.TYPE="REAL[3]" POINT_2="0.0670 -.1750 0.0870" POINT_3="0.4870 -
.1750 0.1956" POINT_3.TYPE="REAL[3]" />
  <SURFACE.PLANE BODY.TYPE="REF" CHAR.TYPE="REF" ID.RANGE="[1,)"
ID="4" ID.TYPE="INTEGER" NAME="Seat_Back" NAME.TYPE="NAME"
POINT_1.TYPE="REAL[3]" POINT_1="-.0443 0.1750 0.5690"
POINT_2.TYPE="REAL[3]" POINT_2="-.0443 -.1750 0.5690" POINT_3="0.0670 -
.1750 0.0870" POINT_3.TYPE="REAL[3]" />
  <SURFACE.PLANE BODY.TYPE="REF" CHAR.TYPE="REF" ID.RANGE="[1,)"
ID="5" ID.TYPE="INTEGER" NAME="Head_rest" NAME.TYPE="NAME"
POINT_1.TYPE="REAL[3]" POINT_1="-.1003 0.1000 0.8750"
POINT_2.TYPE="REAL[3]" POINT_2="-.1003 -0.1000 0.8750" POINT_3="-.0713 -
.1000 0.7220" POINT_3.TYPE="REAL[3]" />
  <SURFACE.PLANE BODY.TYPE="REF" CHAR.TYPE="REF" ID.RANGE="[1,)"
ID="6" ID.TYPE="INTEGER" NAME="Foot_Stop" NAME.TYPE="NAME"
POINT_1.TYPE="REAL[3]" POINT_1="0.9710 -.1500 0.2430"
POINT_2.TYPE="REAL[3]" POINT_2="0.9710 0.1500 0.2430" POINT_3="1.0420
0.1500 0.1720" POINT_3.TYPE="REAL[3]" />
  <SURFACE.PLANE BODY.TYPE="REF" CHAR="Knee_contact"
CHAR.TYPE="REF" ID.RANGE="[1,)" ID="7" ID.TYPE="INTEGER"
NAME="Knee_blocker" NAME.TYPE="NAME" POINT_1.TYPE="REAL[3]"

```
POINT_1="0.6720 0.2000 0.2870" POINT_2.TYPE="REAL[3]" POINT_2="0.6720 -
.2000 0.2870" POINT_3="0.54200 -.2000 0.4370" POINT_3.TYPE="REAL[3]"    />
   <GROUP_MB BODY_LIST.TYPE="LIST" ID.RANGE="[1, )" ID="1"
ID.TYPE="INTEGER" JOINT_LIST.TYPE="LIST" NAME="Seat_cushion"
NAME.TYPE="NAME" RESTRAINT_LIST.TYPE="LIST"
SURFACE_LIST.TYPE="LIST" SURFACE_LIST="Seat_cushion"
SYSTEM.TYPE="REF"    />
   <GROUP_MB BODY_LIST.TYPE="LIST" ID.RANGE="[1, )" ID="2"
ID.TYPE="INTEGER" JOINT_LIST.TYPE="LIST" NAME="Seat_Back"
NAME.TYPE="NAME" RESTRAINT_LIST.TYPE="LIST"
SURFACE_LIST.TYPE="LIST" SURFACE_LIST="Seat_Back"
SYSTEM.TYPE="REF"    />
   <GROUP_MB BODY_LIST.TYPE="LIST" ID.RANGE="[1, )" ID="3"
ID.TYPE="INTEGER" JOINT_LIST.TYPE="LIST" NAME="Sled_Floor"
NAME.TYPE="NAME" RESTRAINT_LIST.TYPE="LIST"
SURFACE_LIST.TYPE="LIST" SURFACE_LIST=" Foot_Plane Foot_Stop
Floor_Plane" SYSTEM.TYPE="REF"    />
   <GROUP_MB BODY_LIST.TYPE="LIST" ID.RANGE="[1, )" ID="4"
ID.TYPE="INTEGER" JOINT_LIST.TYPE="LIST" NAME="Knee"
NAME.TYPE="NAME" RESTRAINT_LIST.TYPE="LIST"
SURFACE_LIST.TYPE="LIST" SURFACE_LIST="Knee_blocker"
SYSTEM.TYPE="REF"    />
   <GROUP_MB BODY_LIST.TYPE="LIST" ID.RANGE="[1, )" ID="5"
ID.TYPE="INTEGER" JOINT_LIST.TYPE="LIST" NAME="Steering_wheel"
NAME.TYPE="NAME" RESTRAINT_LIST.TYPE="LIST"
SURFACE_LIST.TYPE="LIST" SURFACE_LIST="Steering_wheel"
SYSTEM.TYPE="REF"    />
   <CHARACTERISTIC.CONTACT AMPLIFICATION.TYPE="REF"
CONTACT_MODEL="FORCE" DAMP_AMP_FUNC.TYPE="REF"
DAMP_COEF.RANGE="[0, )" DAMP_COEF.TYPE="REAL"
DAMP_VEL_FUNC.TYPE="REF" ELAS_LIMIT.RANGE="[0, )"
ELAS_LIMIT.TYPE="REAL" HYS_MODEL="1" HYS_SLOPE="5.0E5"
HYS_SLOPE.RANGE="[0, )" HYS_SLOPE.TYPE="REAL" ID="1" ID.RANGE="[1,
)" ID.TYPE="INTEGER" LOAD_FUNC="Loading" LOAD_FUNC.TYPE="REF"
NAME.TYPE="NAME" NAME="Knee_contact" UNLOAD_FUNC.TYPE="REF"    />
   <FUNCTION.XY ID.RANGE="[1, )" ID.TYPE="INTEGER" ID="1"
NAME="Loading" NAME.TYPE="NAME"    >
     <TABLE TYPE="XY_PAIR"     >|       XI       YI       |
          0.000   0.00
          0.020   3000.00
          0.080   4000.00
          0.100   15000.00
</TABLE>
   </FUNCTION.XY>
   <SURFACE.ELLIPSOID CHAR.TYPE="REF" DEGREE.RANGE="[2, )"
DEGREE.TYPE="REAL" ID.RANGE="[1, )" ID="9" ID.TYPE="INTEGER"
```

```
NAME="Steering_wheel" NAME.TYPE="NAME" SEMI_AXIS=".025  .125  .125"
SEMI_AXIS.RANGE="(0, )" SEMI_AXIS.TYPE="REAL[3]"    >
    <CRDSYS_OBJECT_1 BODY.TYPE="REF" NODE.TYPE="INTEGER"
ORIENT.TYPE="REF" ORIENT="Steering_orientation" POS=".3850  0  .50"
POS.TYPE="REAL[3]"      />
   </SURFACE.ELLIPSOID>
   <ORIENTATION.SUCCESSIVE_ROT AXIS_1="Y" ID.RANGE="[1, )" ID="1"
ID.TYPE="INTEGER" NAME="Steering_orientation" NAME.TYPE="NAME"
R1="0.506" R1.TYPE="REAL" R2.TYPE="REAL" R3.TYPE="REAL"    />
<FE_MODEL ID.RANGE="[1, )" ID.TYPE="INTEGER" ID="1"
NAME="FE1_Shoulder_belt" NAME.TYPE="NAME"    >
    <CONTROL_FE_MODEL ALPHA_COEF="100" ALPHA_COEF.RANGE="[0, )"
ALPHA_COEF.TYPE="REAL" ALPHA_FUNC.TYPE="REF"
IMM_STRETCH_PRINT.RANGE="[0, 100]"
IMM_STRETCH_PRINT.TYPE="INTEGER"      />
    <CONTROL_FE_TIME_STEP CRITICAL_ELEMENTS.RANGE="[1, 100]"
CRITICAL_ELEMENTS.TYPE="INTEGER" MAX_STEP.RANGE="(0, )"
MAX_STEP.TYPE="REAL" MIN_STEP.RANGE="[0, )" MIN_STEP.TYPE="REAL"
NR_OF_CYCLES.TYPE="INTEGER" REDUCTION_FACTOR.TYPE="REAL"      />
    <TABLE TYPE="COORDINATE.CARTESIAN"      ><![CDATA[ |      ID      X
Y           Z      |
]]></TABLE>
    <MATERIAL.HYSISO CHAR="char_mat_1" CHAR.TYPE="REF"
DENSITY.RANGE="(0, )" DENSITY="800.0" DENSITY.TYPE="REAL"
ID.RANGE="[1, )" ID="1" ID.TYPE="INTEGER" KAPPA.RANGE="[0, )"
KAPPA.TYPE="REAL" NAME="mat_1" NAME.TYPE="NAME"      >
     <COMMENT><![CDATA[
        *NODE_ID       GLOBAL_X       GLOBAL_Y       GLOBAL_Z  REF_SYS
NODE_MASS
        *   CollectorName>> 2
        *    ID    TYPE    NODE1    NODE2    NODE3    NODE4    NODE5
NODE6    NODE7    NODE8
        ]]></COMMENT>
    </MATERIAL.HYSISO>
    <PROPERTY.MEM3NL ID.RANGE="[1, )" ID="1" ID.TYPE="INTEGER"
IMM_DAMP.RANGE="[0, )" IMM_DAMP.TYPE="REAL"
IMM_STRAIN.TYPE="REAL" IMM_TRANS.TYPE="REAL" NAME="prp_1"
NAME.TYPE="NAME" THICK.RANGE="(0, )" THICK.TYPE="REAL"
THICK="0.003"      />
    <PART ID.RANGE="[1, )" ID.TYPE="INTEGER" ID="1"
MATERIAL.TYPE="REF" MATERIAL="1" NAME.TYPE="NAME"
PROPERTY.TYPE="REF" PROPERTY="1"      />
    <TABLE TYPE="ELEMENT.TRIAD3"      ><![CDATA[
|      ID      PART       N1       N2       N3 |
       ]]></TABLE>
```

```
    <CHARACTERISTIC.MATERIAL DAMP_COEF.RANGE="[0, )"
DAMP_COEF.TYPE="REAL" DAMP_FUNC.TYPE="REF" ELAS_LIMIT="0.0"
ELAS_LIMIT.RANGE="[0, )" ELAS_LIMIT.TYPE="REAL" HYS_MODEL="1"
HYS_SLOPE="6.000000E+09" HYS_SLOPE.RANGE="[0, )"
HYS_SLOPE.TYPE="REAL" ID="13" ID.RANGE="[1, )" ID.TYPE="INTEGER"
LOAD_FUNC="fid_36" LOAD_FUNC.TYPE="REF" NAME.TYPE="NAME"
NAME="char_mat_1" UNLOAD_FUNC.TYPE="REF" UNLOAD_FUNC="fid_37"
/>
    <FUNCTION.XY ID.RANGE="[1, )" ID.TYPE="INTEGER" ID="36"
NAME="fid_36" NAME.TYPE="NAME"     >
      <COMMENT><![CDATA[
          !   1 loading curve
          ]]></COMMENT>
      <TABLE TYPE="XY_PAIR"       ><![CDATA[
|      XI               YI      |
  0.00000000E+00     0.00000000E+00
  1.10000000E-02     2.00000000E+07
  2.00000000E-02     5.90000000E+07
  1.10000000E-01     1.90000000E+08
  1.15000000E-01     2.00000000E+08
          ]]></TABLE>
    </FUNCTION.XY>
    <FUNCTION.XY ID.RANGE="[1, )" ID.TYPE="INTEGER" ID="37"
NAME="fid_37" NAME.TYPE="NAME"     >
      <COMMENT><![CDATA[
          !   2 unloading curve
          ]]></COMMENT>
      <TABLE TYPE="XY_PAIR"       ><![CDATA[
|      XI               YI      |
  0.00000000E+00     0.00000000E+00
  1.00000000E-01     2.00000000E+07
          ]]></TABLE>
    </FUNCTION.XY>
  </FE_MODEL>
  <FE_MODEL ID.RANGE="[1, )" ID.TYPE="INTEGER" ID="2"
NAME="FE2_LAPBELT" NAME.TYPE="NAME"   >
    <CONTROL_FE_MODEL ALPHA_COEF="50" ALPHA_COEF.RANGE="[0, )"
ALPHA_COEF.TYPE="REAL" ALPHA_FUNC.TYPE="REF"
IMM_STRETCH_PRINT.RANGE="[0, 100]"
IMM_STRETCH_PRINT.TYPE="INTEGER"     />
    <CONTROL_FE_TIME_STEP CRITICAL_ELEMENTS.RANGE="[1, 100]"
CRITICAL_ELEMENTS.TYPE="INTEGER" MAX_STEP.RANGE="(0, )"
MAX_STEP.TYPE="REAL" MIN_STEP.RANGE="[0, )" MIN_STEP.TYPE="REAL"
NR_OF_CYCLES.TYPE="INTEGER" REDUCTION_FACTOR.TYPE="REAL"     />
    <TABLE TYPE="COORDINATE.CARTESIAN"     ><![CDATA[ |      ID      X
Y           Z      |
```

```
]]></TABLE>
    <MATERIAL.HYSISO CHAR="char_mat_1" CHAR.TYPE="REF"
DENSITY.RANGE="(0, )" DENSITY="800.0" DENSITY.TYPE="REAL"
ID.RANGE="[1, )" ID="1" ID.TYPE="INTEGER" KAPPA.RANGE="[0, )"
KAPPA.TYPE="REAL" NAME="mat_1" NAME.TYPE="NAME"     >
      <COMMENT><![CDATA[
         *NODE_ID        GLOBAL_X        GLOBAL_Y        GLOBAL_Z  REF_SYS
NODE_MASS
         *   CollectorName>> 2
         *    ID    TYPE    NODE1    NODE2    NODE3    NODE4    NODE5
NODE6    NODE7    NODE8
         ]]></COMMENT>
    </MATERIAL.HYSISO>
    <PROPERTY.MEM3NL ID.RANGE="[1, )" ID="1" ID.TYPE="INTEGER"
IMM_DAMP.RANGE="[0, )" IMM_DAMP.TYPE="REAL"
IMM_STRAIN.TYPE="REAL" IMM_TRANS.TYPE="REAL" NAME="prp_1"
NAME.TYPE="NAME" THICK.RANGE="(0, )" THICK.TYPE="REAL"
THICK="0.003"     />
    <PART ID.RANGE="[1, )" ID.TYPE="INTEGER" ID="1"
MATERIAL.TYPE="REF" MATERIAL="1" NAME.TYPE="NAME"
PROPERTY.TYPE="REF" PROPERTY="1"     />
    <TABLE TYPE="ELEMENT.TRIAD3"     ><![CDATA[
|       ID       PART        N1        N2        N3 |
       ]]></TABLE>
    <CHARACTERISTIC.MATERIAL DAMP_COEF.RANGE="[0, )"
DAMP_COEF.TYPE="REAL" DAMP_FUNC.TYPE="REF" ELAS_LIMIT="0.0"
ELAS_LIMIT.RANGE="[0, )" ELAS_LIMIT.TYPE="REAL" HYS_MODEL="1"
HYS_SLOPE="6.000000E+09" HYS_SLOPE.RANGE="[0, )"
HYS_SLOPE.TYPE="REAL" ID="14" ID.RANGE="[1, )" ID.TYPE="INTEGER"
LOAD_FUNC="fid_40" LOAD_FUNC.TYPE="REF" NAME.TYPE="NAME"
NAME="char_mat_1" UNLOAD_FUNC.TYPE="REF" UNLOAD_FUNC="fid_41"
/>
    <FUNCTION.XY ID.RANGE="[1, )" ID.TYPE="INTEGER" ID="40"
NAME="fid_40" NAME.TYPE="NAME"     >
      <COMMENT><![CDATA[
         !   1 loading curve
         ]]></COMMENT>
      <TABLE TYPE="XY_PAIR"       ><![CDATA[
|      XI               YI      |
  0.00000000E+00     0.00000000E+00
  1.10000000E-02     2.00000000E+07
  2.00000000E-02     5.90000000E+07
  1.10000000E-01     1.90000000E+08
  1.15000000E-01     2.00000000E+08
          ]]></TABLE>
    </FUNCTION.XY>
```

```
    <FUNCTION.XY ID.RANGE="[1, )" ID.TYPE="INTEGER" ID="41"
NAME="fid_41" NAME.TYPE="NAME"     >
      <COMMENT><![CDATA[
          !   2 unloading curve
          ]]></COMMENT>
      <TABLE TYPE="XY_PAIR"       ><![CDATA[
|      XI               YI      |
  0.00000000E+00      0.00000000E+00
  1.00000000E-01      2.00000000E+07
          ]]></TABLE>
    </FUNCTION.XY>
  </FE_MODEL>
  <INITIAL.FE_MODEL BODY.TYPE="REF" FE_MODEL.TYPE="REF"
FE_MODEL="FE1_Shoulder_belt" ORIENT.TYPE="REF" ORIENT="989"
POS.TYPE="REAL[3]" POS="-0.05 0.05 0.0" REF_NODE.RANGE="[1, )"
REF_NODE.TYPE="INTEGER" VEL.TYPE="REAL[3]" VEL="0.0 0.0 0.0"    />
  <ORIENTATION.SUCCESSIVE_ROT AXIS_1="X" ID.RANGE="[1, )" ID="989"
ID.TYPE="INTEGER" NAME="belt-rotate_ori" NAME.TYPE="NAME" R1="0.11"
R1.TYPE="REAL" R2.TYPE="REAL" R3.TYPE="REAL"   />
  <INITIAL.FE_MODEL BODY.TYPE="REF" FE_MODEL.TYPE="REF"
FE_MODEL="FE2_LAPBELT" ORIENT.TYPE="REF" POS.TYPE="REAL[3]"
POS="-0.05 0.0 0.0" REF_NODE.RANGE="[1, )" REF_NODE.TYPE="INTEGER"
VEL.TYPE="REAL[3]" VEL="0.00 0.0 0.0"    />
  <GROUP_FE CONTACT_CHAR.TYPE="REF" ELEMENT_LIST="ALL"
ELEMENT_LIST.TYPE="ILIST" FE_MODEL.TYPE="REF"
FE_MODEL="FE1_Shoulder_belt" ID.RANGE="[1, )" ID="6" ID.TYPE="INTEGER"
MATERIAL_LIST.TYPE="LIST" NAME="ShoulderBelt_gfe" NAME.TYPE="NAME"
NODE_LIST.TYPE="ILIST" PART_LIST.TYPE="LIST"
PROPERTY_LIST.TYPE="LIST"    />
  <GROUP_FE CONTACT_CHAR.TYPE="REF" ELEMENT_LIST="ALL"
ELEMENT_LIST.TYPE="ILIST" FE_MODEL.TYPE="REF"
FE_MODEL="FE2_LAPBELT" ID.RANGE="[1, )" ID="7" ID.TYPE="INTEGER"
MATERIAL_LIST.TYPE="LIST" NAME="LapBelt_gfe" NAME.TYPE="NAME"
NODE_LIST.TYPE="ILIST" PART_LIST.TYPE="LIST"
PROPERTY_LIST.TYPE="LIST"    />
 </SYSTEM.REF_SPACE>
 <SYSTEM.MODEL ID.RANGE="[1, )" ID.TYPE="INTEGER" ID="2"
NAME="PregHumanFemale05%" NAME.TYPE="NAME"  >
  <INCLUDE FILE="preg_inc6-19.xml"    />
  <CRDSYS_OBJECT BODY.TYPE="REF" ID.RANGE="[1, )" ID="1"
ID.TYPE="INTEGER" NAME="Human_Attachment" NAME.TYPE="NAME"
NODE.TYPE="INTEGER" ORIENT.TYPE="REF"
ORIENT="Human_Attachment_ori" POS.TYPE="REAL[3]" POS="0.0         0.0
0.0"    />
  <ORIENTATION.SUCCESSIVE_ROT AXIS_1="X" AXIS_2="Y" AXIS_3="Z"
ID.RANGE="[1, )" ID="1" ID.TYPE="INTEGER" NAME="Human_Attachment_ori"
```

NAME.TYPE="NAME" R1="0.78" R1.TYPE="REAL" R2.TYPE="REAL" R2="0.0"
R3.TYPE="REAL" R3="0.0" />
<INITIAL.JOINT_POS D1.TYPE="REAL" D1="0.143" D2.TYPE="REAL"
D3="0.20" D3.TYPE="REAL" JOINT.TYPE="REF" JOINT="Human_jnt"
ORIENT="Human_ori" ORIENT.TYPE="REF" Q1.TYPE="REAL" Q2.TYPE="REAL"
Q3.TYPE="REAL" Q4.TYPE="REAL" Q5.TYPE="REAL" Q6.TYPE="REAL"
Q7.TYPE="REAL" R1.TYPE="REAL" R2.TYPE="REAL" R3.TYPE="REAL" />
<INITIAL.JOINT_POS D1.TYPE="REAL" D2.TYPE="REAL" D3.TYPE="REAL"
JOINT.TYPE="REF" JOINT="Sacrum-L5_jnt" ORIENT="Sacrum-L5_ori"
ORIENT.TYPE="REF" Q1.TYPE="REAL" Q2.TYPE="REAL" Q3.TYPE="REAL"
Q4.TYPE="REAL" Q5.TYPE="REAL" Q6.TYPE="REAL" Q7.TYPE="REAL"
R1.TYPE="REAL" R2.TYPE="REAL" R3.TYPE="REAL" />
<INITIAL.JOINT_POS D1.TYPE="REAL" D2.TYPE="REAL" D3.TYPE="REAL"
JOINT.TYPE="REF" JOINT="L5-L4_jnt" ORIENT="L5-L4_ori"
ORIENT.TYPE="REF" Q1.TYPE="REAL" Q2.TYPE="REAL" Q3.TYPE="REAL"
Q4.TYPE="REAL" Q5.TYPE="REAL" Q6.TYPE="REAL" Q7.TYPE="REAL"
R1.TYPE="REAL" R2.TYPE="REAL" R3.TYPE="REAL" />
<INITIAL.JOINT_POS D1.TYPE="REAL" D2.TYPE="REAL" D3.TYPE="REAL"
JOINT.TYPE="REF" JOINT="L4-L3_jnt" ORIENT="L4-L3_ori"
ORIENT.TYPE="REF" Q1.TYPE="REAL" Q2.TYPE="REAL" Q3.TYPE="REAL"
Q4.TYPE="REAL" Q5.TYPE="REAL" Q6.TYPE="REAL" Q7.TYPE="REAL"
R1.TYPE="REAL" R2.TYPE="REAL" R3.TYPE="REAL" />
<INITIAL.JOINT_POS D1.TYPE="REAL" D2.TYPE="REAL" D3.TYPE="REAL"
JOINT.TYPE="REF" JOINT="L3-L2_jnt" ORIENT="L3-L2_ori"
ORIENT.TYPE="REF" Q1.TYPE="REAL" Q2.TYPE="REAL" Q3.TYPE="REAL"
Q4.TYPE="REAL" Q5.TYPE="REAL" Q6.TYPE="REAL" Q7.TYPE="REAL"
R1.TYPE="REAL" R2.TYPE="REAL" R3.TYPE="REAL" />
<INITIAL.JOINT_POS D1.TYPE="REAL" D2.TYPE="REAL" D3.TYPE="REAL"
JOINT.TYPE="REF" JOINT="L2-L1_jnt" ORIENT="L2-L1_ori"
ORIENT.TYPE="REF" Q1.TYPE="REAL" Q2.TYPE="REAL" Q3.TYPE="REAL"
Q4.TYPE="REAL" Q5.TYPE="REAL" Q6.TYPE="REAL" Q7.TYPE="REAL"
R1.TYPE="REAL" R2.TYPE="REAL" R3.TYPE="REAL" />
<INITIAL.JOINT_POS D1.TYPE="REAL" D2.TYPE="REAL" D3.TYPE="REAL"
JOINT.TYPE="REF" JOINT="L1-T12_jnt" ORIENT="L1-T12_ori"
ORIENT.TYPE="REF" Q1.TYPE="REAL" Q2.TYPE="REAL" Q3.TYPE="REAL"
Q4.TYPE="REAL" Q5.TYPE="REAL" Q6.TYPE="REAL" Q7.TYPE="REAL"
R1.TYPE="REAL" R2.TYPE="REAL" R3.TYPE="REAL" />
<INITIAL.JOINT_POS D1.TYPE="REAL" D2.TYPE="REAL" D3.TYPE="REAL"
JOINT.TYPE="REF" JOINT="T12-T11_jnt" ORIENT="T12-T11_ori"
ORIENT.TYPE="REF" Q1.TYPE="REAL" Q2.TYPE="REAL" Q3.TYPE="REAL"
Q4.TYPE="REAL" Q5.TYPE="REAL" Q6.TYPE="REAL" Q7.TYPE="REAL"
R1.TYPE="REAL" R2.TYPE="REAL" R3.TYPE="REAL" />
<INITIAL.JOINT_POS D1.TYPE="REAL" D2.TYPE="REAL" D3.TYPE="REAL"
JOINT.TYPE="REF" JOINT="T11-T10_jnt" ORIENT="T11-T10_ori"
ORIENT.TYPE="REF" Q1.TYPE="REAL" Q2.TYPE="REAL" Q3.TYPE="REAL"

Q4.TYPE="REAL" Q5.TYPE="REAL" Q6.TYPE="REAL" Q7.TYPE="REAL"
R1.TYPE="REAL" R2.TYPE="REAL" R3.TYPE="REAL" />
<INITIAL.JOINT_POS D1.TYPE="REAL" D2.TYPE="REAL" D3.TYPE="REAL"
JOINT.TYPE="REF" JOINT="T10-T9_jnt" ORIENT="T10-T9_ori"
ORIENT.TYPE="REF" Q1.TYPE="REAL" Q2.TYPE="REAL" Q3.TYPE="REAL"
Q4.TYPE="REAL" Q5.TYPE="REAL" Q6.TYPE="REAL" Q7.TYPE="REAL"
R1.TYPE="REAL" R2.TYPE="REAL" R3.TYPE="REAL" />
<INITIAL.JOINT_POS D1.TYPE="REAL" D2.TYPE="REAL" D3.TYPE="REAL"
JOINT.TYPE="REF" JOINT="T9-T8_jnt" ORIENT="T9-T8_ori"
ORIENT.TYPE="REF" Q1.TYPE="REAL" Q2.TYPE="REAL" Q3.TYPE="REAL"
Q4.TYPE="REAL" Q5.TYPE="REAL" Q6.TYPE="REAL" Q7.TYPE="REAL"
R1.TYPE="REAL" R2.TYPE="REAL" R3.TYPE="REAL" />
<INITIAL.JOINT_POS D1.TYPE="REAL" D2.TYPE="REAL" D3.TYPE="REAL"
JOINT.TYPE="REF" JOINT="T8-T7_jnt" ORIENT="T8-T7_ori"
ORIENT.TYPE="REF" Q1.TYPE="REAL" Q2.TYPE="REAL" Q3.TYPE="REAL"
Q4.TYPE="REAL" Q5.TYPE="REAL" Q6.TYPE="REAL" Q7.TYPE="REAL"
R1.TYPE="REAL" R2.TYPE="REAL" R3.TYPE="REAL" />
<INITIAL.JOINT_POS D1.TYPE="REAL" D2.TYPE="REAL" D3.TYPE="REAL"
JOINT.TYPE="REF" JOINT="T7-T6_jnt" ORIENT="T7-T6_ori"
ORIENT.TYPE="REF" Q1.TYPE="REAL" Q2.TYPE="REAL" Q3.TYPE="REAL"
Q4.TYPE="REAL" Q5.TYPE="REAL" Q6.TYPE="REAL" Q7.TYPE="REAL"
R1.TYPE="REAL" R2.TYPE="REAL" R3.TYPE="REAL" />
<INITIAL.JOINT_POS D1.TYPE="REAL" D2.TYPE="REAL" D3.TYPE="REAL"
JOINT.TYPE="REF" JOINT="T6-T5_jnt" ORIENT="T6-T5_ori"
ORIENT.TYPE="REF" Q1.TYPE="REAL" Q2.TYPE="REAL" Q3.TYPE="REAL"
Q4.TYPE="REAL" Q5.TYPE="REAL" Q6.TYPE="REAL" Q7.TYPE="REAL"
R1.TYPE="REAL" R2.TYPE="REAL" R3.TYPE="REAL" />
<INITIAL.JOINT_POS D1.TYPE="REAL" D2.TYPE="REAL" D3.TYPE="REAL"
JOINT.TYPE="REF" JOINT="T5-T4_jnt" ORIENT="T5-T4_ori"
ORIENT.TYPE="REF" Q1.TYPE="REAL" Q2.TYPE="REAL" Q3.TYPE="REAL"
Q4.TYPE="REAL" Q5.TYPE="REAL" Q6.TYPE="REAL" Q7.TYPE="REAL"
R1.TYPE="REAL" R2.TYPE="REAL" R3.TYPE="REAL" />
<INITIAL.JOINT_POS D1.TYPE="REAL" D2.TYPE="REAL" D3.TYPE="REAL"
JOINT.TYPE="REF" JOINT="T4-T3_jnt" ORIENT="T4-T3_ori"
ORIENT.TYPE="REF" Q1.TYPE="REAL" Q2.TYPE="REAL" Q3.TYPE="REAL"
Q4.TYPE="REAL" Q5.TYPE="REAL" Q6.TYPE="REAL" Q7.TYPE="REAL"
R1.TYPE="REAL" R2.TYPE="REAL" R3.TYPE="REAL" />
<INITIAL.JOINT_POS D1.TYPE="REAL" D2.TYPE="REAL" D3.TYPE="REAL"
JOINT.TYPE="REF" JOINT="T3-T2_jnt" ORIENT="T3-T2_ori"
ORIENT.TYPE="REF" Q1.TYPE="REAL" Q2.TYPE="REAL" Q3.TYPE="REAL"
Q4.TYPE="REAL" Q5.TYPE="REAL" Q6.TYPE="REAL" Q7.TYPE="REAL"
R1.TYPE="REAL" R2.TYPE="REAL" R3.TYPE="REAL" />
<INITIAL.JOINT_POS D1.TYPE="REAL" D2.TYPE="REAL" D3.TYPE="REAL"
JOINT.TYPE="REF" JOINT="T2-T1_jnt" ORIENT="T2-T1_ori"
ORIENT.TYPE="REF" Q1.TYPE="REAL" Q2.TYPE="REAL" Q3.TYPE="REAL"

Q4.TYPE="REAL" Q5.TYPE="REAL" Q6.TYPE="REAL" Q7.TYPE="REAL"
R1.TYPE="REAL" R2.TYPE="REAL" R3.TYPE="REAL" />
<INITIAL.JOINT_POS D1.TYPE="REAL" D2.TYPE="REAL" D3.TYPE="REAL"
JOINT.TYPE="REF" JOINT="T1-C7_jnt" ORIENT="T1-C7_ori"
ORIENT.TYPE="REF" Q1.TYPE="REAL" Q2.TYPE="REAL" Q3.TYPE="REAL"
Q4.TYPE="REAL" Q5.TYPE="REAL" Q6.TYPE="REAL" Q7.TYPE="REAL"
R1.TYPE="REAL" R2.TYPE="REAL" R3.TYPE="REAL" />
<INITIAL.JOINT_POS D1.TYPE="REAL" D2.TYPE="REAL" D3.TYPE="REAL"
JOINT.TYPE="REF" JOINT="C7-C6_jnt" ORIENT="C7-C6_ori"
ORIENT.TYPE="REF" Q1.TYPE="REAL" Q2.TYPE="REAL" Q3.TYPE="REAL"
Q4.TYPE="REAL" Q5.TYPE="REAL" Q6.TYPE="REAL" Q7.TYPE="REAL"
R1.TYPE="REAL" R2.TYPE="REAL" R3.TYPE="REAL" />
<INITIAL.JOINT_POS D1.TYPE="REAL" D2.TYPE="REAL" D3.TYPE="REAL"
JOINT.TYPE="REF" JOINT="C6-C5_jnt" ORIENT="C6-C5_ori"
ORIENT.TYPE="REF" Q1.TYPE="REAL" Q2.TYPE="REAL" Q3.TYPE="REAL"
Q4.TYPE="REAL" Q5.TYPE="REAL" Q6.TYPE="REAL" Q7.TYPE="REAL"
R1.TYPE="REAL" R2.TYPE="REAL" R3.TYPE="REAL" />
<INITIAL.JOINT_POS D1.TYPE="REAL" D2.TYPE="REAL" D3.TYPE="REAL"
JOINT.TYPE="REF" JOINT="C5-C4_jnt" ORIENT="C5-C4_ori"
ORIENT.TYPE="REF" Q1.TYPE="REAL" Q2.TYPE="REAL" Q3.TYPE="REAL"
Q4.TYPE="REAL" Q5.TYPE="REAL" Q6.TYPE="REAL" Q7.TYPE="REAL"
R1.TYPE="REAL" R2.TYPE="REAL" R3.TYPE="REAL" />
<INITIAL.JOINT_POS D1.TYPE="REAL" D2.TYPE="REAL" D3.TYPE="REAL"
JOINT.TYPE="REF" JOINT="C4-C3_jnt" ORIENT="C4-C3_ori"
ORIENT.TYPE="REF" Q1.TYPE="REAL" Q2.TYPE="REAL" Q3.TYPE="REAL"
Q4.TYPE="REAL" Q5.TYPE="REAL" Q6.TYPE="REAL" Q7.TYPE="REAL"
R1.TYPE="REAL" R2.TYPE="REAL" R3.TYPE="REAL" />
<INITIAL.JOINT_POS D1.TYPE="REAL" D2.TYPE="REAL" D3.TYPE="REAL"
JOINT.TYPE="REF" JOINT="C3-C2_jnt" ORIENT="C3-C2_ori"
ORIENT.TYPE="REF" Q1.TYPE="REAL" Q2.TYPE="REAL" Q3.TYPE="REAL"
Q4.TYPE="REAL" Q5.TYPE="REAL" Q6.TYPE="REAL" Q7.TYPE="REAL"
R1.TYPE="REAL" R2.TYPE="REAL" R3.TYPE="REAL" />
<INITIAL.JOINT_POS D1.TYPE="REAL" D2.TYPE="REAL" D3.TYPE="REAL"
JOINT.TYPE="REF" JOINT="C2-C1_jnt" ORIENT="C2-C1_ori"
ORIENT.TYPE="REF" Q1.TYPE="REAL" Q2.TYPE="REAL" Q3.TYPE="REAL"
Q4.TYPE="REAL" Q5.TYPE="REAL" Q6.TYPE="REAL" Q7.TYPE="REAL"
R1.TYPE="REAL" R2.TYPE="REAL" R3.TYPE="REAL" />
<INITIAL.JOINT_POS D1.TYPE="REAL" D2.TYPE="REAL" D3.TYPE="REAL"
JOINT.TYPE="REF" JOINT="C1-Head_jnt" ORIENT="C1-Head_ori"
ORIENT.TYPE="REF" Q1.TYPE="REAL" Q2.TYPE="REAL" Q3.TYPE="REAL"
Q4.TYPE="REAL" Q5.TYPE="REAL" Q6.TYPE="REAL" Q7.TYPE="REAL"
R1.TYPE="REAL" R2.TYPE="REAL" R3.TYPE="REAL" />
<INITIAL.JOINT_POS D1.TYPE="REAL" D2.TYPE="REAL" D3.TYPE="REAL"
JOINT.TYPE="REF" JOINT="ScapulaR-ArmUpR_jnt" ORIENT="ScapulaR-
ArmUpR_ori" ORIENT.TYPE="REF" Q1.TYPE="REAL" Q2.TYPE="REAL"

Q3.TYPE="REAL" Q4.TYPE="REAL" Q5.TYPE="REAL" Q6.TYPE="REAL"
Q7.TYPE="REAL" R1.TYPE="REAL" R2.TYPE="REAL" R3.TYPE="REAL" />
<INITIAL.JOINT_POS D1.TYPE="REAL" D2.TYPE="REAL" D3.TYPE="REAL"
JOINT.TYPE="REF" JOINT="ElbowR_jnt" ORIENT.TYPE="REF"
Q1.TYPE="REAL" Q2.TYPE="REAL" Q3.TYPE="REAL" Q4.TYPE="REAL"
Q5.TYPE="REAL" Q6.TYPE="REAL" Q7.TYPE="REAL" R1.TYPE="REAL"
R2.TYPE="REAL" R2="1.1" R3.TYPE="REAL" />
<INITIAL.JOINT_POS D1.TYPE="REAL" D2.TYPE="REAL" D3.TYPE="REAL"
JOINT.TYPE="REF" JOINT="WristR_jnt" ORIENT.TYPE="REF" Q1.TYPE="REAL"
Q2.TYPE="REAL" Q3.TYPE="REAL" Q4.TYPE="REAL" Q5.TYPE="REAL"
Q6.TYPE="REAL" Q7.TYPE="REAL" R1.TYPE="REAL" R2.TYPE="REAL"
R3.TYPE="REAL" />
<INITIAL.JOINT_POS D1.TYPE="REAL" D2.TYPE="REAL" D3.TYPE="REAL"
JOINT.TYPE="REF" JOINT="ScapulaL-ArmUpL_jnt" ORIENT="ScapulaL-
ArmUpL_ori" ORIENT.TYPE="REF" Q1.TYPE="REAL" Q2.TYPE="REAL"
Q3.TYPE="REAL" Q4.TYPE="REAL" Q5.TYPE="REAL" Q6.TYPE="REAL"
Q7.TYPE="REAL" R1.TYPE="REAL" R2.TYPE="REAL" R3.TYPE="REAL" />
<INITIAL.JOINT_POS D1.TYPE="REAL" D2.TYPE="REAL" D3.TYPE="REAL"
JOINT.TYPE="REF" JOINT="ElbowL_jnt" ORIENT.TYPE="REF"
Q1.TYPE="REAL" Q2.TYPE="REAL" Q3.TYPE="REAL" Q4.TYPE="REAL"
Q5.TYPE="REAL" Q6.TYPE="REAL" Q7.TYPE="REAL" R1.TYPE="REAL"
R2.TYPE="REAL" R2="-1.1" R3.TYPE="REAL" />
<INITIAL.JOINT_POS D1.TYPE="REAL" D2.TYPE="REAL" D3.TYPE="REAL"
JOINT.TYPE="REF" JOINT="WristL_jnt" ORIENT.TYPE="REF" Q1.TYPE="REAL"
Q2.TYPE="REAL" Q3.TYPE="REAL" Q4.TYPE="REAL" Q5.TYPE="REAL"
Q6.TYPE="REAL" Q7.TYPE="REAL" R1.TYPE="REAL" R2.TYPE="REAL"
R3.TYPE="REAL" />
<INITIAL.JOINT_POS D1.TYPE="REAL" D2.TYPE="REAL" D3.TYPE="REAL"
JOINT.TYPE="REF" JOINT="HipR_jnt" ORIENT="HipR_ori" ORIENT.TYPE="REF"
Q1.TYPE="REAL" Q2.TYPE="REAL" Q3.TYPE="REAL" Q4.TYPE="REAL"
Q5.TYPE="REAL" Q6.TYPE="REAL" Q7.TYPE="REAL" R1.TYPE="REAL"
R2.TYPE="REAL" R3.TYPE="REAL" />
<INITIAL.JOINT_POS D1.TYPE="REAL" D2.TYPE="REAL" D3.TYPE="REAL"
JOINT.TYPE="REF" JOINT="KneeR_jnt" ORIENT="KneeR_ori"
ORIENT.TYPE="REF" Q1.TYPE="REAL" Q2.TYPE="REAL" Q3.TYPE="REAL"
Q4.TYPE="REAL" Q5.TYPE="REAL" Q6.TYPE="REAL" Q7.TYPE="REAL"
R1.TYPE="REAL" R2.TYPE="REAL" R3.TYPE="REAL" />
<INITIAL.JOINT_POS D1.TYPE="REAL" D2.TYPE="REAL" D3.TYPE="REAL"
JOINT.TYPE="REF" JOINT="AnkleR_jnt" ORIENT="AnkleR_ori"
ORIENT.TYPE="REF" Q1.TYPE="REAL" Q2.TYPE="REAL" Q3.TYPE="REAL"
Q4.TYPE="REAL" Q5.TYPE="REAL" Q6.TYPE="REAL" Q7.TYPE="REAL"
R1.TYPE="REAL" R2.TYPE="REAL" R3.TYPE="REAL" />
<INITIAL.JOINT_POS D1.TYPE="REAL" D2.TYPE="REAL" D3.TYPE="REAL"
JOINT.TYPE="REF" JOINT="HipL_jnt" ORIENT="HipL_ori" ORIENT.TYPE="REF"
Q1.TYPE="REAL" Q2.TYPE="REAL" Q3.TYPE="REAL" Q4.TYPE="REAL"

Q5.TYPE="REAL" Q6.TYPE="REAL" Q7.TYPE="REAL" R1.TYPE="REAL"
R2.TYPE="REAL" R3.TYPE="REAL" />
<INITIAL.JOINT_POS D1.TYPE="REAL" D2.TYPE="REAL" D3.TYPE="REAL"
JOINT.TYPE="REF" JOINT="KneeL_jnt" ORIENT="KneeL_ori"
ORIENT.TYPE="REF" Q1.TYPE="REAL" Q2.TYPE="REAL" Q3.TYPE="REAL"
Q4.TYPE="REAL" Q5.TYPE="REAL" Q6.TYPE="REAL" Q7.TYPE="REAL"
R1.TYPE="REAL" R2.TYPE="REAL" R3.TYPE="REAL" />
<INITIAL.JOINT_POS D1.TYPE="REAL" D2.TYPE="REAL" D3.TYPE="REAL"
JOINT.TYPE="REF" JOINT="AnkleL_jnt" ORIENT="AnkleL_ori"
ORIENT.TYPE="REF" Q1.TYPE="REAL" Q2.TYPE="REAL" Q3.TYPE="REAL"
Q4.TYPE="REAL" Q5.TYPE="REAL" Q6.TYPE="REAL" Q7.TYPE="REAL"
R1.TYPE="REAL" R2.TYPE="REAL" R3.TYPE="REAL" />
<ORIENTATION.SUCCESSIVE_ROT AXIS_1="X" AXIS_2="Y" AXIS_3="Z"
ID.RANGE="[1,)" ID="53" ID.TYPE="INTEGER" NAME="Human_ori"
NAME.TYPE="NAME" R1="0.0" R1.TYPE="REAL" R2.TYPE="REAL" R2="0.0"
R3.TYPE="REAL" R3="0.0" />
<ORIENTATION.SUCCESSIVE_ROT AXIS_1="X" AXIS_2="Y" AXIS_3="Z"
ID.RANGE="[1,)" ID="54" ID.TYPE="INTEGER" NAME="Sacrum-L5_ori"
NAME.TYPE="NAME" R1="-0.22" R1.TYPE="REAL" R2.TYPE="REAL" R2="0.0"
R3.TYPE="REAL" R3="0.0" />
<ORIENTATION.SUCCESSIVE_ROT AXIS_1="X" AXIS_2="Y" AXIS_3="Z"
ID.RANGE="[1,)" ID="55" ID.TYPE="INTEGER" NAME="L5-L4_ori"
NAME.TYPE="NAME" R1="0.0" R1.TYPE="REAL" R2.TYPE="REAL" R2="0.0"
R3.TYPE="REAL" R3="0.0" />
<ORIENTATION.SUCCESSIVE_ROT AXIS_1="X" AXIS_2="Y" AXIS_3="Z"
ID.RANGE="[1,)" ID="56" ID.TYPE="INTEGER" NAME="L4-L3_ori"
NAME.TYPE="NAME" R1="0.0" R1.TYPE="REAL" R2.TYPE="REAL" R2="0.0"
R3.TYPE="REAL" R3="0.0" />
<ORIENTATION.SUCCESSIVE_ROT AXIS_1="X" AXIS_2="Y" AXIS_3="Z"
ID.RANGE="[1,)" ID="57" ID.TYPE="INTEGER" NAME="L3-L2_ori"
NAME.TYPE="NAME" R1="0.0" R1.TYPE="REAL" R2.TYPE="REAL" R2="0.0"
R3.TYPE="REAL" R3="0.0" />
<ORIENTATION.SUCCESSIVE_ROT AXIS_1="X" AXIS_2="Y" AXIS_3="Z"
ID.RANGE="[1,)" ID="58" ID.TYPE="INTEGER" NAME="L2-L1_ori"
NAME.TYPE="NAME" R1="0.0" R1.TYPE="REAL" R2.TYPE="REAL" R2="0.0"
R3.TYPE="REAL" R3="0.0" />
<ORIENTATION.SUCCESSIVE_ROT AXIS_1="X" AXIS_2="Y" AXIS_3="Z"
ID.RANGE="[1,)" ID="59" ID.TYPE="INTEGER" NAME="L1-T12_ori"
NAME.TYPE="NAME" R1="0.0" R1.TYPE="REAL" R2.TYPE="REAL" R2="0.0"
R3.TYPE="REAL" R3="0.0" />
<ORIENTATION.SUCCESSIVE_ROT AXIS_1="X" AXIS_2="Y" AXIS_3="Z"
ID.RANGE="[1,)" ID="60" ID.TYPE="INTEGER" NAME="T12-T11_ori"
NAME.TYPE="NAME" R1="0.0" R1.TYPE="REAL" R2.TYPE="REAL" R2="0.0"
R3.TYPE="REAL" R3="0.0" />
<ORIENTATION.SUCCESSIVE_ROT AXIS_1="X" AXIS_2="Y" AXIS_3="Z"
ID.RANGE="[1,)" ID="61" ID.TYPE="INTEGER" NAME="T11-T10_ori"

NAME.TYPE="NAME" R1="0.0" R1.TYPE="REAL" R2.TYPE="REAL" R2="0.0"
R3.TYPE="REAL" R3="0.0" />
<ORIENTATION.SUCCESSIVE_ROT AXIS_1="X" AXIS_2="Y" AXIS_3="Z"
ID.RANGE="[1,)" ID="62" ID.TYPE="INTEGER" NAME="T10-T9_ori"
NAME.TYPE="NAME" R1="0.0" R1.TYPE="REAL" R2.TYPE="REAL" R2="0.0"
R3.TYPE="REAL" R3="0.0" />
<ORIENTATION.SUCCESSIVE_ROT AXIS_1="X" AXIS_2="Y" AXIS_3="Z"
ID.RANGE="[1,)" ID="63" ID.TYPE="INTEGER" NAME="T9-T8_ori"
NAME.TYPE="NAME" R1="0.0" R1.TYPE="REAL" R2.TYPE="REAL" R2="0.0"
R3.TYPE="REAL" R3="0.0" />
<ORIENTATION.SUCCESSIVE_ROT AXIS_1="X" AXIS_2="Y" AXIS_3="Z"
ID.RANGE="[1,)" ID="64" ID.TYPE="INTEGER" NAME="T8-T7_ori"
NAME.TYPE="NAME" R1="0.0" R1.TYPE="REAL" R2.TYPE="REAL" R2="0.0"
R3.TYPE="REAL" R3="0.0" />
<ORIENTATION.SUCCESSIVE_ROT AXIS_1="X" AXIS_2="Y" AXIS_3="Z"
ID.RANGE="[1,)" ID="65" ID.TYPE="INTEGER" NAME="T7-T6_ori"
NAME.TYPE="NAME" R1="0.0" R1.TYPE="REAL" R2.TYPE="REAL" R2="0.0"
R3.TYPE="REAL" R3="0.0" />
<ORIENTATION.SUCCESSIVE_ROT AXIS_1="X" AXIS_2="Y" AXIS_3="Z"
ID.RANGE="[1,)" ID="66" ID.TYPE="INTEGER" NAME="T6-T5_ori"
NAME.TYPE="NAME" R1="0.0" R1.TYPE="REAL" R2.TYPE="REAL" R2="0.0"
R3.TYPE="REAL" R3="0.0" />
<ORIENTATION.SUCCESSIVE_ROT AXIS_1="X" AXIS_2="Y" AXIS_3="Z"
ID.RANGE="[1,)" ID="67" ID.TYPE="INTEGER" NAME="T5-T4_ori"
NAME.TYPE="NAME" R1="0.0" R1.TYPE="REAL" R2.TYPE="REAL" R2="0.0"
R3.TYPE="REAL" R3="0.0" />
<ORIENTATION.SUCCESSIVE_ROT AXIS_1="X" AXIS_2="Y" AXIS_3="Z"
ID.RANGE="[1,)" ID="68" ID.TYPE="INTEGER" NAME="T4-T3_ori"
NAME.TYPE="NAME" R1="0.0" R1.TYPE="REAL" R2.TYPE="REAL" R2="0.0"
R3.TYPE="REAL" R3="0.0" />
<ORIENTATION.SUCCESSIVE_ROT AXIS_1="X" AXIS_2="Y" AXIS_3="Z"
ID.RANGE="[1,)" ID="69" ID.TYPE="INTEGER" NAME="T3-T2_ori"
NAME.TYPE="NAME" R1="0.0" R1.TYPE="REAL" R2.TYPE="REAL" R2="0.0"
R3.TYPE="REAL" R3="0.0" />
<ORIENTATION.SUCCESSIVE_ROT AXIS_1="X" AXIS_2="Y" AXIS_3="Z"
ID.RANGE="[1,)" ID="70" ID.TYPE="INTEGER" NAME="T2-T1_ori"
NAME.TYPE="NAME" R1="0.0" R1.TYPE="REAL" R2.TYPE="REAL" R2="0.0"
R3.TYPE="REAL" R3="0.0" />
<ORIENTATION.SUCCESSIVE_ROT AXIS_1="X" AXIS_2="Y" AXIS_3="Z"
ID.RANGE="[1,)" ID="71" ID.TYPE="INTEGER" NAME="T1-C7_ori"
NAME.TYPE="NAME" R1="0.0" R1.TYPE="REAL" R2.TYPE="REAL" R2="0.0"
R3.TYPE="REAL" R3="0.0" />
<ORIENTATION.SUCCESSIVE_ROT AXIS_1="X" AXIS_2="Y" AXIS_3="Z"
ID.RANGE="[1,)" ID="72" ID.TYPE="INTEGER" NAME="C7-C6_ori"
NAME.TYPE="NAME" R1="0.0" R1.TYPE="REAL" R2.TYPE="REAL" R2="0.0"
R3.TYPE="REAL" R3="0.0" />

<ORIENTATION.SUCCESSIVE_ROT AXIS_1="X" AXIS_2="Y" AXIS_3="Z" ID.RANGE="[1,)" ID="73" ID.TYPE="INTEGER" NAME="C6-C5_ori" NAME.TYPE="NAME" R1="0.0" R1.TYPE="REAL" R2.TYPE="REAL" R2="0.0" R3.TYPE="REAL" R3="0.0" />
<ORIENTATION.SUCCESSIVE_ROT AXIS_1="X" AXIS_2="Y" AXIS_3="Z" ID.RANGE="[1,)" ID="74" ID.TYPE="INTEGER" NAME="C5-C4_ori" NAME.TYPE="NAME" R1="0.0" R1.TYPE="REAL" R2.TYPE="REAL" R2="0.0" R3.TYPE="REAL" R3="0.0" />
<ORIENTATION.SUCCESSIVE_ROT AXIS_1="X" AXIS_2="Y" AXIS_3="Z" ID.RANGE="[1,)" ID="75" ID.TYPE="INTEGER" NAME="C4-C3_ori" NAME.TYPE="NAME" R1="0.0" R1.TYPE="REAL" R2.TYPE="REAL" R2="0.0" R3.TYPE="REAL" R3="0.0" />
<ORIENTATION.SUCCESSIVE_ROT AXIS_1="X" AXIS_2="Y" AXIS_3="Z" ID.RANGE="[1,)" ID="76" ID.TYPE="INTEGER" NAME="C3-C2_ori" NAME.TYPE="NAME" R1="0.0" R1.TYPE="REAL" R2.TYPE="REAL" R2="0.0" R3.TYPE="REAL" R3="0.0" />
<ORIENTATION.SUCCESSIVE_ROT AXIS_1="X" AXIS_2="Y" AXIS_3="Z" ID.RANGE="[1,)" ID="77" ID.TYPE="INTEGER" NAME="C2-C1_ori" NAME.TYPE="NAME" R1="0.0" R1.TYPE="REAL" R2.TYPE="REAL" R2="0.0" R3.TYPE="REAL" R3="0.0" />
<ORIENTATION.SUCCESSIVE_ROT AXIS_1="X" AXIS_2="Y" AXIS_3="Z" ID.RANGE="[1,)" ID="78" ID.TYPE="INTEGER" NAME="C1-Head_ori" NAME.TYPE="NAME" R1="0.0" R1.TYPE="REAL" R2.TYPE="REAL" R2="0.0" R3.TYPE="REAL" R3="0.0" />
<ORIENTATION.SUCCESSIVE_ROT AXIS_1="X" AXIS_2="Z" AXIS_3="Y" ID.RANGE="[1,)" ID="82" ID.TYPE="INTEGER" NAME="ScapulaR-ArmUpR_ori" NAME.TYPE="NAME" R1="1.361357" R1.TYPE="REAL" R2.TYPE="REAL" R2="0.50" R3.TYPE="REAL" R3="0.0" />
<ORIENTATION.SUCCESSIVE_ROT AXIS_1="X" AXIS_2="Z" AXIS_3="Y" ID.RANGE="[1,)" ID="93" ID.TYPE="INTEGER" NAME="ScapulaL-ArmUpL_ori" NAME.TYPE="NAME" R1="-1.361357" R1.TYPE="REAL" R2.TYPE="REAL" R2="-0.5" R3.TYPE="REAL" R3="0.0" />
<ORIENTATION.SUCCESSIVE_ROT AXIS_1="Y" AXIS_2="X" AXIS_3="Z" ID.RANGE="[1,)" ID="102" ID.TYPE="INTEGER" NAME="HipR_ori" NAME.TYPE="NAME" R1="-1.8" R1.TYPE="REAL" R2.TYPE="REAL" R2="0.0" R3.TYPE="REAL" R3="0.0" />
<ORIENTATION.SUCCESSIVE_ROT AXIS_1="X" AXIS_2="Y" AXIS_3="Z" ID.RANGE="[1,)" ID="103" ID.TYPE="INTEGER" NAME="KneeR_ori" NAME.TYPE="NAME" R1="0.0" R1.TYPE="REAL" R2.TYPE="REAL" R2="1.0" R3.TYPE="REAL" R3="0.0" />
<ORIENTATION.SUCCESSIVE_ROT AXIS_1="Y" AXIS_2="X" AXIS_3="Z" ID.RANGE="[1,)" ID="104" ID.TYPE="INTEGER" NAME="AnkleR_ori" NAME.TYPE="NAME" R1="-1.4" R1.TYPE="REAL" R2.TYPE="REAL" R2="0.0" R3.TYPE="REAL" R3="0.0" />
<ORIENTATION.SUCCESSIVE_ROT AXIS_1="Y" AXIS_2="X" AXIS_3="Z" ID.RANGE="[1,)" ID="105" ID.TYPE="INTEGER" NAME="HipL_ori"

NAME.TYPE="NAME" R1="-1.8" R1.TYPE="REAL" R2.TYPE="REAL" R2="0.0"
R3.TYPE="REAL" R3="0.0" />
<ORIENTATION.SUCCESSIVE_ROT AXIS_1="X" AXIS_2="Y" AXIS_3="Z"
ID.RANGE="[1,)" ID="106" ID.TYPE="INTEGER" NAME="KneeL_ori"
NAME.TYPE="NAME" R1="0.0" R1.TYPE="REAL" R2.TYPE="REAL" R2="1.0"
R3.TYPE="REAL" R3="0.0" />
<ORIENTATION.SUCCESSIVE_ROT AXIS_1="Y" AXIS_2="X" AXIS_3="Z"
ID.RANGE="[1,)" ID="107" ID.TYPE="INTEGER" NAME="AnkleL_ori"
NAME.TYPE="NAME" R1="-1.40" R1.TYPE="REAL" R2.TYPE="REAL" R2="0.0"
R3.TYPE="REAL" R3="0.0" />
</SYSTEM.MODEL>
<BELT ID.RANGE="[1,)" ID.TYPE="INTEGER" ID="1" NAME="belt_1"
NAME.TYPE="NAME" >
<BELT_SEGMENT ADD_LENGTH.RANGE="[0,)"
ADD_LENGTH.TYPE="REAL" CHAR.TYPE="REF" CHAR="/2/char_319"
FORCE_CORRECTION="0.0" FORCE_CORRECTION.TYPE="REAL" ID="1"
ID.RANGE="[1,)" ID.TYPE="INTEGER" INITIAL_STRAIN.RANGE="(-1,)"
INITIAL_STRAIN.TYPE="REAL" NAME.TYPE="NAME" NAME="belt1"
POINT_REF_1="/2/belt1_1" POINT_REF_1.TYPE="REF"
POINT_REF_2="/2/belt1_2" POINT_REF_2.TYPE="REF"
RUPTURE_STRAIN.RANGE="(0,)" RUPTURE_STRAIN.TYPE="REAL" />
<BELT_SEGMENT ADD_LENGTH.RANGE="[0,)"
ADD_LENGTH.TYPE="REAL" CHAR.TYPE="REF" CHAR="/2/char_320"
FORCE_CORRECTION="0.0" FORCE_CORRECTION.TYPE="REAL" ID="2"
ID.RANGE="[1,)" ID.TYPE="INTEGER" INITIAL_STRAIN.RANGE="(-1,)"
INITIAL_STRAIN.TYPE="REAL" NAME.TYPE="NAME" NAME="belt2"
POINT_REF_1="/2/belt2_1" POINT_REF_1.TYPE="REF"
POINT_REF_2="/2/belt2_2" POINT_REF_2.TYPE="REF"
RUPTURE_STRAIN.RANGE="(0,)" RUPTURE_STRAIN.TYPE="REAL" />
<BELT_SEGMENT ADD_LENGTH.RANGE="[0,)"
ADD_LENGTH.TYPE="REAL" CHAR.TYPE="REF" CHAR="/2/char_321"
FORCE_CORRECTION="0.0" FORCE_CORRECTION.TYPE="REAL" ID="3"
ID.RANGE="[1,)" ID.TYPE="INTEGER" INITIAL_STRAIN.RANGE="(-1,)"
INITIAL_STRAIN.TYPE="REAL" NAME.TYPE="NAME" NAME="belt3"
POINT_REF_1="/2/belt3_1" POINT_REF_1.TYPE="REF"
POINT_REF_2="/2/belt3_2" POINT_REF_2.TYPE="REF"
RUPTURE_STRAIN.RANGE="(0,)" RUPTURE_STRAIN.TYPE="REAL" />
<BELT_SEGMENT ADD_LENGTH.RANGE="[0,)"
ADD_LENGTH.TYPE="REAL" CHAR.TYPE="REF" CHAR="/2/char_322"
FORCE_CORRECTION="0.0" FORCE_CORRECTION.TYPE="REAL" ID="4"
ID.RANGE="[1,)" ID.TYPE="INTEGER" INITIAL_STRAIN.RANGE="(-1,)"
INITIAL_STRAIN.TYPE="REAL" NAME.TYPE="NAME" NAME="belt4"
POINT_REF_1="/2/belt4_1" POINT_REF_1.TYPE="REF"
POINT_REF_2="/2/belt4_2" POINT_REF_2.TYPE="REF"
RUPTURE_STRAIN.RANGE="(0,)" RUPTURE_STRAIN.TYPE="REAL" />

<BELT_SEGMENT ADD_LENGTH.RANGE="[0,)"
ADD_LENGTH.TYPE="REAL" CHAR.TYPE="REF" CHAR="/2/char_323"
FORCE_CORRECTION="0.0" FORCE_CORRECTION.TYPE="REAL" ID="5"
ID.RANGE="[1,)" ID.TYPE="INTEGER" INITIAL_STRAIN.RANGE="(-1,)"
INITIAL_STRAIN.TYPE="REAL" NAME.TYPE="NAME" NAME="belt5"
POINT_REF_1="/2/belt5_1" POINT_REF_1.TYPE="REF"
POINT_REF_2="/2/belt5_2" POINT_REF_2.TYPE="REF"
RUPTURE_STRAIN.RANGE="(0,)" RUPTURE_STRAIN.TYPE="REAL" />
<BELT_SEGMENT ADD_LENGTH.RANGE="[0,)"
ADD_LENGTH.TYPE="REAL" CHAR.TYPE="REF" CHAR="/2/char_324"
FORCE_CORRECTION="0.0" FORCE_CORRECTION.TYPE="REAL" ID="6"
ID.RANGE="[1,)" ID.TYPE="INTEGER" INITIAL_STRAIN.RANGE="(-1,)"
INITIAL_STRAIN.TYPE="REAL" NAME.TYPE="NAME" NAME="belt6"
POINT_REF_1="/2/belt6_1" POINT_REF_1.TYPE="REF"
POINT_REF_2="/2/belt6_2" POINT_REF_2.TYPE="REF"
RUPTURE_STRAIN.RANGE="(0,)" RUPTURE_STRAIN.TYPE="REAL" />
<BELT_SEGMENT ADD_LENGTH.RANGE="[0,)"
ADD_LENGTH.TYPE="REAL" CHAR.TYPE="REF" CHAR="/2/char_325"
FORCE_CORRECTION="0.0" FORCE_CORRECTION.TYPE="REAL" ID="7"
ID.RANGE="[1,)" ID.TYPE="INTEGER" INITIAL_STRAIN.RANGE="(-1,)"
INITIAL_STRAIN.TYPE="REAL" NAME.TYPE="NAME" NAME="belt7"
POINT_REF_1="/2/belt7_1" POINT_REF_1.TYPE="REF"
POINT_REF_2="/2/belt7_2" POINT_REF_2.TYPE="REF"
RUPTURE_STRAIN.RANGE="(0,)" RUPTURE_STRAIN.TYPE="REAL" />
<BELT_SEGMENT ADD_LENGTH.RANGE="[0,)"
ADD_LENGTH.TYPE="REAL" CHAR.TYPE="REF" CHAR="/2/char_326"
FORCE_CORRECTION="0.0" FORCE_CORRECTION.TYPE="REAL" ID="8"
ID.RANGE="[1,)" ID.TYPE="INTEGER" INITIAL_STRAIN.RANGE="(-1,)"
INITIAL_STRAIN.TYPE="REAL" NAME.TYPE="NAME" NAME="belt8"
POINT_REF_1="/2/belt8_1" POINT_REF_1.TYPE="REF"
POINT_REF_2="/2/belt8_2" POINT_REF_2.TYPE="REF"
RUPTURE_STRAIN.RANGE="(0,)" RUPTURE_STRAIN.TYPE="REAL" />
<BELT_SEGMENT ADD_LENGTH.RANGE="[0,)"
ADD_LENGTH.TYPE="REAL" CHAR.TYPE="REF" CHAR="/2/char_327"
FORCE_CORRECTION="0.0" FORCE_CORRECTION.TYPE="REAL" ID="9"
ID.RANGE="[1,)" ID.TYPE="INTEGER" INITIAL_STRAIN.RANGE="(-1,)"
INITIAL_STRAIN.TYPE="REAL" NAME.TYPE="NAME" NAME="belt9"
POINT_REF_1="/2/belt9_1" POINT_REF_1.TYPE="REF"
POINT_REF_2="/2/belt9_2" POINT_REF_2.TYPE="REF"
RUPTURE_STRAIN.RANGE="(0,)" RUPTURE_STRAIN.TYPE="REAL" />
<BELT_TYING FRIC_COEF.RANGE="[0,)" FRIC_COEF.TYPE="REAL"
ID.RANGE="[1,)" ID="1" ID.TYPE="INTEGER" NAME="tying_1"
NAME.TYPE="NAME" POINT_REF_1="/2/belt1_2" POINT_REF_1.TYPE="REF"
POINT_REF_2.TYPE="REF" POINT_REF_2="/2/belt2_1" />
<BELT_TYING FRIC_COEF.RANGE="[0,)" FRIC_COEF.TYPE="REAL"
ID.RANGE="[1,)" ID="2" ID.TYPE="INTEGER" NAME="tying_2"

```
NAME.TYPE="NAME" POINT_REF_1="/2/belt2_2" POINT_REF_1.TYPE="REF"
POINT_REF_2.TYPE="REF" POINT_REF_2="/2/belt3_1"    />
   <BELT_TYING FRIC_COEF.RANGE="[0, )" FRIC_COEF.TYPE="REAL"
ID.RANGE="[1, )" ID="3" ID.TYPE="INTEGER" NAME="tying_3"
NAME.TYPE="NAME" POINT_REF_1="/2/belt3_2" POINT_REF_1.TYPE="REF"
POINT_REF_2.TYPE="REF" POINT_REF_2="/2/belt4_1"    />
   <BELT_TYING FRIC_COEF.RANGE="[0, )" FRIC_COEF.TYPE="REAL"
ID.RANGE="[1, )" ID="4" ID.TYPE="INTEGER" NAME="tying_4"
NAME.TYPE="NAME" POINT_REF_1="/2/belt4_2" POINT_REF_1.TYPE="REF"
POINT_REF_2.TYPE="REF" POINT_REF_2="/2/belt5_1"    />
   <BELT_TYING FRIC_COEF.RANGE="[0, )" FRIC_COEF.TYPE="REAL"
ID.RANGE="[1, )" ID="5" ID.TYPE="INTEGER" NAME="tying_5"
NAME.TYPE="NAME" POINT_REF_1="/2/belt5_2" POINT_REF_1.TYPE="REF"
POINT_REF_2.TYPE="REF" POINT_REF_2="/2/belt6_1"    />
   <BELT_TYING FRIC_COEF.RANGE="[0, )" FRIC_COEF.TYPE="REAL"
ID.RANGE="[1, )" ID="6" ID.TYPE="INTEGER" NAME="tying_6"
NAME.TYPE="NAME" POINT_REF_1="/2/belt6_2" POINT_REF_1.TYPE="REF"
POINT_REF_2.TYPE="REF" POINT_REF_2="/2/belt7_1"    />
   <BELT_TYING FRIC_COEF.RANGE="[0, )" FRIC_COEF.TYPE="REAL"
ID.RANGE="[1, )" ID="7" ID.TYPE="INTEGER" NAME="tying_7"
NAME.TYPE="NAME" POINT_REF_1="/2/belt7_2" POINT_REF_1.TYPE="REF"
POINT_REF_2.TYPE="REF" POINT_REF_2="/2/belt8_1"    />
   <BELT_TYING FRIC_COEF.RANGE="[0, )" FRIC_COEF.TYPE="REAL"
ID.RANGE="[1, )" ID="8" ID.TYPE="INTEGER" NAME="tying_8"
NAME.TYPE="NAME" POINT_REF_1="/2/belt8_2" POINT_REF_1.TYPE="REF"
POINT_REF_2.TYPE="REF" POINT_REF_2="/2/belt9_1"    />
 </BELT>
 <SYSTEM.MODEL ID.RANGE="[1, )" ID.TYPE="INTEGER" ID="3"
NAME="Uterine" NAME.TYPE="NAME"  >
   <INCLUDE FILE="uterus_7-3_inc.xml"    />
   <INITIAL.FE_MODEL BODY="/2/Pelvis_bod" BODY.TYPE="REF"
FE_MODEL.TYPE="REF" FE_MODEL="1" ORIENT.TYPE="REF" ORIENT="11"
POS.TYPE="REAL[3]" POS="0.0270 0.0 0.113" REF_NODE.RANGE="[1, )"
REF_NODE.TYPE="INTEGER" VEL.TYPE="REAL[3]" VEL="0.0 0.0 0.0"    />
   <ORIENTATION.SUCCESSIVE_ROT AXIS_1="X" AXIS_2="Z" ID.RANGE="[1,
)" ID="11" ID.TYPE="INTEGER" NAME.TYPE="NAME" R1="1.570796"
R1.TYPE="REAL" R2.TYPE="REAL" R2="-.523599" R3.TYPE="REAL"    />
   <INITIAL.FE_MODEL BODY="/2/Pelvis_bod" BODY.TYPE="REF"
FE_MODEL.TYPE="REF" FE_MODEL="2" ORIENT.TYPE="REF" ORIENT="12"
POS.TYPE="REAL[3]" POS="0.0270 0.0 0.113" REF_NODE.RANGE="[1, )"
REF_NODE.TYPE="INTEGER" VEL.TYPE="REAL[3]" VEL="0.0 0.0 0.0"    />
   <ORIENTATION.SUCCESSIVE_ROT AXIS_1="X" AXIS_2="Z" ID.RANGE="[1,
)" ID="12" ID.TYPE="INTEGER" NAME.TYPE="NAME" R1="1.570796"
R1.TYPE="REAL" R2.TYPE="REAL" R2="-.523599" R3.TYPE="REAL"    />
   <INITIAL.FE_MODEL BODY="/2/Pelvis_bod" BODY.TYPE="REF"
DESCRIPTION="fat" FE_MODEL.TYPE="REF" FE_MODEL="3"
```

ORIENT.TYPE="REF" ORIENT="13" POS.TYPE="REAL[3]" POS="0.0270 0.0 0.113" REF_NODE.RANGE="[1,)" REF_NODE.TYPE="INTEGER" VEL.TYPE="REAL[3]" VEL="0.0 0.0 0.0" />
<ORIENTATION.SUCCESSIVE_ROT AXIS_1="X" AXIS_2="Y" AXIS_3="X" ID.RANGE="[1,)" ID="13" ID.TYPE="INTEGER" NAME.TYPE="NAME" R1="1.570796" R1.TYPE="REAL" R2.TYPE="REAL" R2="1.570796" R3.TYPE="REAL" R3="0.5236" />
<SUPPORT BODY="/2/Pelvis_bod" BODY.TYPE="REF" DESCRIPTION="cervix support" DOF_ALL="ON" FE_MODEL.TYPE="REF" FE_MODEL="1" GROUP_LIST.TYPE="LIST" NODE_LIST="562 576:579 593:596 754:757 763:765 772 773 781 1550:1553 1647:1650 1656:1658 1665 1666 1674 2019:2022 2133:2136 2142:2144 2151 2152 2160 2683:2686 2692:2694 2701 2702 2710" NODE_LIST.TYPE="ILIST" />
<SUPPORT BODY="/2/Pelvis_bod" BODY.TYPE="REF" DESCRIPTION="uterosacral ligaments support" DOF_ALL="ON" FE_MODEL.TYPE="REF" FE_MODEL="1" GROUP_LIST.TYPE="LIST" NODE_LIST="15008 15009 15010 16008 16009 16010 17008 17009 17010 18008 18009 18010 19008 19009 19010 20008 20009 20010" NODE_LIST.TYPE="ILIST" />
<SUPPORT BODY="/2/Pelvis_bod" BODY.TYPE="REF" DESCRIPTION="round ligaments support" DOF_ALL="ON" FE_MODEL.TYPE="REF" FE_MODEL="1" GROUP_LIST.TYPE="LIST" NODE_LIST="21008 21009 21010 22008 22009 22010 23008 23009 23010 24008 24009 24010 25008 25009 25010 26008 26009 26010" NODE_LIST.TYPE="ILIST" />
<SUPPORT BODY="/2/Pelvis_bod" BODY.TYPE="REF" DESCRIPTION="fat support" DOF_ALL="ON" FE_MODEL.TYPE="REF" FE_MODEL="3" GROUP_LIST.TYPE="LIST" NODE_LIST="12173 12178 12183 12188 12193 12198 12203 12557:12611 12613:12622 12888 12889 12891:12893 12895:12898 12900:12904 12906:12911 12913:12919 12921:12928 12930:12938 12940:12949 12951 13030 13191 13291 13391 13491 13591 15353 15354 15357 15358 15361 15362 15365 15366 15369 15370 15373 15374 15377 15378 15381 15382 15385 15386 15389 15390 15393 15394 15397 15398 15401 15402 15405 15406 15409 15410 15413 15414 15417 15418 15421 15422 15425 15426 15553 15555 15557 15559 15561 15563 15565 15567 15569 15571 15573 15575 15577 15579 15581 15583 15585 15587 15589 15653 15655 15657 15659 15661 15663 15665 15667 15669 15671 15673 15675 15677 15679 15681 15683 15685 15687 15689 15753 15755 15757 15759 15761 15763 15765 15767 15769 15771 15773 15775 15777 15779 15781 15783 15785 15787 15789 15853 15855 15857 15859 15861 15863 15865 15867 15869 15871 15873 15875 15877 15879 15881 15883 15885 15887 15889 15953 15955 15957 15959 15961 15963 15965 15967 15969 15971 15973 15975 15977 15979 15981 15983 15985 15987 15989 16319 16320 16322:16324 16326:16329 16331:16335 16337:16342 16344:16350 16352:16359 16361:16369 16380 16649 16651 16654 16655 16657 16659 16660 16662 16663 16665 16666 16668:16670 16672 16673 16675:16678 16680 16681 16683:16687 16689 16690 16692:16697 16699 17742 17747 17752 17757 17918 17920 17922 17924 17926 17928 17930 17932 17934 17936 17938 17940 17942 17944 17946 17948 17950 17952 17954 18038:18056 18138:18156 18238:18256 18338:18356 18438:18456 19018 19020 19022 19024 19026 19028 19030

19032 19034 19036 19038 19040 19042 19044 19046 19048 19050 19052 19054 19056
19138:19257 19338:19357 19567 19572 19577 19582 19587 19592 19597 19602 19607
19612 20547 20548 20551 20552 20555 20556 20559 20560 20563 20564 20567 20568
20571 20572 20575 20576 20579 20580 20583 20584 20587 20588 20591 20592 20595
20596 20599 20600 20603 20604 20607 20608 20611 20612 20615 20616 20619 20620
20623 20624 20626 20628 20630 20632 20634 20636 20638 20640 20642 20644 20646
20648 20650 20652 20654 20656 20658 20660 20662 20664 20666 20668 20670 20672
20674 20676 20678 20680 20682 20684 20686 20688 20690 20692 20694 20696 20698
20700 20702 20704 20706 20708 20710 20712 20714 20716 20718 20720 20722 20724
20726 20728 20730 20732 20734 20736 20738 20740 20742 20744 20746 20748 20750
20752 20754 20756 20758 20760 20762 20764 20766 20768 20770 20772 20774 20776
20778 20780 20782 20784 20786 20788 20790 20792 20794 20796 20798 20800 20802
20804 20806 20808 20810 20812 20814 20816 20818 20820 20822 20824 20826 20828
20830 20832 20834 20836 20838 20840 20842 20844 20846 20848 20850 20852 20854
20856 20858 20860 20862 20864 20866 20868 20870 20872 20874 20876 20878 20880
20882 20884 20886 20888 20890 20892 20894 20896 20898 20900 20902 20904 20906
20908 20910 20912 20914 20916 20918 20920 20922 20924 20926 20928 20930 20932
20934 20936 20938 20940 20942 20944" NODE_LIST.TYPE="ILIST"   />
<GROUP_FE CONTACT_CHAR.TYPE="REF" DESCRIPTION="includes supports"
ELEMENT_LIST="1:2736" ELEMENT_LIST.TYPE="ILIST"
FE_MODEL.TYPE="REF" FE_MODEL="/3/UTERUS" ID.RANGE="[1,)" ID="6"
ID.TYPE="INTEGER" MATERIAL_LIST.TYPE="LIST" NAME="uterus_gfe"
NAME.TYPE="NAME" NODE_LIST.TYPE="ILIST" PART_LIST.TYPE="LIST"
PROPERTY_LIST.TYPE="LIST"   />
<GROUP_FE CONTACT_CHAR.TYPE="REF" DESCRIPTION="no nodes that are
supported" ELEMENT_LIST.TYPE="ILIST" FE_MODEL.TYPE="REF"
FE_MODEL="/3/UTERUS" ID.RANGE="[1,)" ID="10" ID.TYPE="INTEGER"
MATERIAL_LIST.TYPE="LIST" NAME="uterus2_gfe" NAME.TYPE="NAME"
NODE_LIST="1:561 563:575 580:592 597:753 758:762 766:771 774:780 782:1549
1554:1646 1651:1655 1659:1664 1667:1673 1675:2018 2023:2132 2137:2141 2145:2150
2153:2159 2161:2682 2687:2691 2695:2700 2703:2709 2711:5476"
NODE_LIST.TYPE="ILIST" PART_LIST.TYPE="LIST"
PROPERTY_LIST.TYPE="LIST"   />
<GROUP_FE CONTACT_CHAR.TYPE="REF" DESCRIPTION="for fluid - uterus
contact" ELEMENT_LIST="1:3136" ELEMENT_LIST.TYPE="ILIST"
FE_MODEL.TYPE="REF" FE_MODEL="/3/A_FLUID" ID.RANGE="[1,)" ID="7"
ID.TYPE="INTEGER" MATERIAL_LIST.TYPE="LIST" NAME="fluid_gfe"
NAME.TYPE="NAME" NODE_LIST.TYPE="ILIST" PART_LIST.TYPE="LIST"
PROPERTY_LIST.TYPE="LIST"   />
<GROUP_FE CONTACT_CHAR.TYPE="REF" DESCRIPTION="for fluid -
placenta contact" ELEMENT_LIST="65:80 145:160 225:240 305:320 385:400 465:480
545:560 625:640 705:720 785:800 865:880 945:960" ELEMENT_LIST.TYPE="ILIST"
FE_MODEL.TYPE="REF" FE_MODEL="/3/A_FLUID" ID.RANGE="[1,)" ID="98"
ID.TYPE="INTEGER" MATERIAL_LIST.TYPE="LIST" NAME="fluid2_gfe"
NAME.TYPE="NAME" NODE_LIST.TYPE="ILIST" PART_LIST.TYPE="LIST"
PROPERTY_LIST.TYPE="LIST"   />

<GROUP_FE CONTACT_CHAR.TYPE="REF" DESCRIPTION="placenta to uterus" ELEMENT_LIST="3001:5000" ELEMENT_LIST.TYPE="ILIST" FE_MODEL.TYPE="REF" FE_MODEL="/3/UTERUS" ID.RANGE="[1,)" ID="8" ID.TYPE="INTEGER" MATERIAL_LIST.TYPE="LIST" NAME="placenta_gfe" NAME.TYPE="NAME" NODE_LIST.TYPE="ILIST" PART_LIST.TYPE="LIST" PROPERTY_LIST.TYPE="LIST" />
<GROUP_FE CONTACT_CHAR.TYPE="REF" DESCRIPTION="placenta to fluid" ELEMENT_LIST.TYPE="ILIST" FE_MODEL.TYPE="REF" FE_MODEL="/3/UTERUS" ID.RANGE="[1,)" ID="97" ID.TYPE="INTEGER" MATERIAL_LIST.TYPE="LIST" NAME="placenta2_gfe" NAME.TYPE="NAME" NODE_LIST="10002 10011:10021 10030 10036 10060:10063 10079:10172 10190:10209 10226:10290 10308 10336:10348 10384:10403 10480:10559 10608:10696 10720:10821 10831:10888 10916:10983 11060:11139 11188:11276 " NODE_LIST.TYPE="ILIST" PART_LIST.TYPE="LIST" PROPERTY_LIST.TYPE="LIST" />
<GROUP_FE CONTACT_CHAR.TYPE="REF" ELEMENT_LIST="28:30 52:54 1008:1015 1024:1031 1040:1047 1055:1063 1072:1079 1088:1095 1104:1111 1120:1127 1136:1143 1152:1159" ELEMENT_LIST.TYPE="ILIST" FE_MODEL.TYPE="REF" FE_MODEL="/2/Skin_fem" ID.RANGE="[1,)" ID="99" ID.TYPE="INTEGER" MATERIAL_LIST.TYPE="LIST" NAME="skin_gfe" NAME.TYPE="NAME" NODE_LIST.TYPE="ILIST" PART_LIST.TYPE="LIST" PROPERTY_LIST.TYPE="LIST" />
<GROUP_FE CONTACT_CHAR.TYPE="REF" DESCRIPTION="all fat elements" ELEMENT_LIST="89:528 2289:3208 3249:3728 3889:4288 4341:5560" ELEMENT_LIST.TYPE="ILIST" FE_MODEL.TYPE="REF" FE_MODEL="/3/FAT" ID.RANGE="[1,)" ID="95" ID.TYPE="INTEGER" MATERIAL_LIST.TYPE="LIST" NAME="fat1_gfe" NAME.TYPE="NAME" NODE_LIST.TYPE="ILIST" PART_LIST.TYPE="LIST" PROPERTY_LIST.TYPE="LIST" />
<GROUP_FE CONTACT_CHAR.TYPE="REF" DESCRIPTION="fat elements in the front" ELEMENT_LIST="4209:4288 4341:4740 5341:5394 5451:5560" ELEMENT_LIST.TYPE="ILIST" FE_MODEL.TYPE="REF" FE_MODEL="/3/FAT" ID.RANGE="[1,)" ID="93" ID.TYPE="INTEGER" MATERIAL_LIST.TYPE="LIST" NAME="fat2_gfe" NAME.TYPE="NAME" NODE_LIST.TYPE="ILIST" PART_LIST.TYPE="LIST" PROPERTY_LIST.TYPE="LIST" />
<GROUP_FE CONTACT_CHAR.TYPE="REF" ELEMENT_LIST="7000:7059 8000:8059 9000:9091 10000:10091" ELEMENT_LIST.TYPE="ILIST" FE_MODEL.TYPE="REF" FE_MODEL="/3/UTERUS" ID.RANGE="[1,)" ID="94" ID.TYPE="INTEGER" MATERIAL_LIST.TYPE="LIST" NAME="lig_gfe" NAME.TYPE="NAME" NODE_LIST.TYPE="ILIST" PART_LIST.TYPE="LIST" PROPERTY_LIST.TYPE="LIST" />
<CONTACT.FE_FE FLAG.RANGE="[1,)" FLAG.TYPE="INTEGER" GAP_FUNC.TYPE="REF" ID="1" ID.RANGE="[1,)" ID.TYPE="INTEGER" INITIAL_USNORM.TYPE="REAL[3]" MASTER_SURFACE="fluid2_gfe" MASTER_SURFACE.TYPE="LIST" NAME.TYPE="NAME" NAME="fluid-to-placenta" NORMAL_USER.TYPE="REAL[3]"

SEARCH_FACTOR.TYPE="INTEGER" SLAVE_SURFACE="placenta2_gfe"
SLAVE_SURFACE.TYPE="LIST" SWITCH.TYPE="REF" >
<CONTACT_FORCE.PENALTY FRIC_FUNC.TYPE="REF"
MAX_FORCE_PAR.TYPE="REAL" MAX_FORCE_PAR="100.0" PENALTY=".1"
PENALTY.TYPE="REAL" />
</CONTACT.FE_FE>
<CONTACT.FE_FE FLAG.RANGE="[1,)" FLAG.TYPE="INTEGER"
GAP_FUNC.TYPE="REF" ID="2" ID.RANGE="[1,)" ID.TYPE="INTEGER"
INITIAL_USNORM.TYPE="REAL[3]" MASTER_SURFACE="fluid_gfe"
MASTER_SURFACE.TYPE="LIST" NAME.TYPE="NAME" NAME="fluid-to-uterus"
NORMAL_USER.TYPE="REAL[3]" SEARCH_FACTOR.TYPE="INTEGER"
SLAVE_SURFACE="uterus_gfe" SLAVE_SURFACE.TYPE="LIST"
SWITCH.TYPE="REF" >
<CONTACT_FORCE.PENALTY FRIC_FUNC.TYPE="REF"
MAX_FORCE_PAR.TYPE="REAL" MAX_FORCE_PAR="100.0" PENALTY=".1"
PENALTY.TYPE="REAL" />
</CONTACT.FE_FE>
<CONTACT.FE_FE FLAG.RANGE="[1,)" FLAG.TYPE="INTEGER"
GAP_FUNC.TYPE="REF" ID="3" ID.RANGE="[1,)" ID.TYPE="INTEGER"
INITIAL_USNORM.TYPE="REAL[3]" MASTER_SURFACE="uterus_gfe"
MASTER_SURFACE.TYPE="LIST" NAME.TYPE="NAME" NAME="uterus-to-
placenta" NORMAL_USER.TYPE="REAL[3]"
SEARCH_FACTOR.TYPE="INTEGER" SLAVE_SURFACE="placenta_gfe"
SLAVE_SURFACE.TYPE="LIST" SWITCH.TYPE="REF" >
<CONTACT_FORCE.PENALTY FRIC_FUNC.TYPE="REF"
MAX_FORCE_PAR.TYPE="REAL" MAX_FORCE_PAR="10.0" PENALTY=".1"
PENALTY.TYPE="REAL" />
</CONTACT.FE_FE>
<CONTACT.FE_FE FLAG.RANGE="[1,)" FLAG.TYPE="INTEGER"
GAP_FUNC.TYPE="REF" ID="4" ID.RANGE="[1,)" ID.TYPE="INTEGER"
INITIAL_USNORM.TYPE="REAL[3]" MASTER_SURFACE="skin_gfe"
MASTER_SURFACE.TYPE="LIST" NAME.TYPE="NAME" NAME="uterus-skin"
NORMAL_USER.TYPE="REAL[3]" SEARCH_FACTOR.TYPE="INTEGER"
SLAVE_SURFACE="uterus_gfe" SLAVE_SURFACE.TYPE="LIST"
SWITCH.TYPE="REF" >
<CONTACT_FORCE.PENALTY FRIC_FUNC.TYPE="REF"
MAX_FORCE_PAR.TYPE="REAL" MAX_FORCE_PAR="0.1" PENALTY=".1"
PENALTY.TYPE="REAL" />
</CONTACT.FE_FE>
<CONTACT.FE_FE FLAG.RANGE="[1,)" FLAG.TYPE="INTEGER"
GAP_FUNC.TYPE="REF" ID="22" ID.RANGE="[1,)" ID.TYPE="INTEGER"
INITIAL_USNORM.TYPE="REAL[3]" MASTER_SURFACE="skin_gfe"
MASTER_SURFACE.TYPE="LIST" NAME.TYPE="NAME" NAME="fluid-skin"
NORMAL_USER.TYPE="REAL[3]" SEARCH_FACTOR.TYPE="INTEGER"
SLAVE_SURFACE="fluid_gfe" SLAVE_SURFACE.TYPE="LIST"
SWITCH.TYPE="REF" >

```
    <CONTACT_FORCE.PENALTY FRIC_FUNC.TYPE="REF"
MAX_FORCE_PAR.TYPE="REAL" MAX_FORCE_PAR="0.1" PENALTY=".1"
PENALTY.TYPE="REAL"     />
   </CONTACT.FE_FE>
   <CONTACT.FE_FE FLAG.RANGE="[1, )" FLAG.TYPE="INTEGER"
GAP_FUNC.TYPE="REF" ID="23" ID.RANGE="[1, )" ID.TYPE="INTEGER"
INITIAL_USNORM.TYPE="REAL[3]" MASTER_SURFACE="fat1_gfe"
MASTER_SURFACE.TYPE="LIST" NAME.TYPE="NAME" NAME="uterus-fat"
NORMAL_USER.TYPE="REAL[3]" SEARCH_FACTOR.TYPE="INTEGER"
SLAVE_SURFACE="uterus_gfe" SLAVE_SURFACE.TYPE="LIST"
SWITCH.TYPE="REF"   >
    <CONTACT_FORCE.PENALTY FRIC_FUNC.TYPE="REF"
MAX_FORCE_PAR.TYPE="REAL" MAX_FORCE_PAR="10.0" PENALTY=".1"
PENALTY.TYPE="REAL"     />
   </CONTACT.FE_FE>
   <CONTACT.FE_FE FLAG.RANGE="[1, )" FLAG.TYPE="INTEGER"
GAP_FUNC.TYPE="REF" ID="26" ID.RANGE="[1, )" ID.TYPE="INTEGER"
INITIAL_USNORM.TYPE="REAL[3]" MASTER_SURFACE="fat1_gfe"
MASTER_SURFACE.TYPE="LIST" NAME.TYPE="NAME" NAME="fluid-fat"
NORMAL_USER.TYPE="REAL[3]" SEARCH_FACTOR.TYPE="INTEGER"
SLAVE_SURFACE="fluid_gfe" SLAVE_SURFACE.TYPE="LIST"
SWITCH.TYPE="REF"   >
    <CONTACT_FORCE.PENALTY FRIC_FUNC.TYPE="REF"
MAX_FORCE_PAR.TYPE="REAL" MAX_FORCE_PAR="10.0" PENALTY=".1"
PENALTY.TYPE="REAL"     />
   </CONTACT.FE_FE>
   <CONTACT.FE_FE FLAG.RANGE="[1, )" FLAG.TYPE="INTEGER"
GAP_FUNC.TYPE="REF" ID="25" ID.RANGE="[1, )" ID.TYPE="INTEGER"
INITIAL_USNORM.TYPE="REAL[3]" MASTER_SURFACE="skin_gfe"
MASTER_SURFACE.TYPE="LIST" NAME.TYPE="NAME" NAME="skin-fat"
NORMAL_USER.TYPE="REAL[3]" SEARCH_FACTOR.TYPE="INTEGER"
SLAVE_SURFACE="fat2_gfe" SLAVE_SURFACE.TYPE="LIST"
SWITCH.TYPE="REF"   >
    <CONTACT_FORCE.PENALTY FRIC_FUNC.TYPE="REF"
MAX_FORCE_PAR.TYPE="REAL" MAX_FORCE_PAR="10.0" PENALTY=".1"
PENALTY.TYPE="REAL"     />
   </CONTACT.FE_FE>
   <CONTACT.FE_FE FLAG.RANGE="[1, )" FLAG.TYPE="INTEGER"
GAP_FUNC.TYPE="REF" ID="24" ID.RANGE="[1, )" ID.TYPE="INTEGER"
INITIAL_USNORM.TYPE="REAL[3]" MASTER_SURFACE="lig_gfe"
MASTER_SURFACE.TYPE="LIST" NAME.TYPE="NAME" NAME="uterus-lig"
NORMAL_USER.TYPE="REAL[3]" SEARCH_FACTOR.TYPE="INTEGER"
SLAVE_SURFACE="uterus_gfe" SLAVE_SURFACE.TYPE="LIST"
SWITCH.TYPE="REF"   >
```

```
    <CONTACT_FORCE.PENALTY FRIC_FUNC.TYPE="REF"
MAX_FORCE_PAR.TYPE="REAL" MAX_FORCE_PAR="0.1" PENALTY=".1"
PENALTY.TYPE="REAL"     />
   </CONTACT.FE_FE>
  </SYSTEM.MODEL>
  <LOAD.SYSTEM_ACC AX_FUNC.TYPE="REF" AX_FUNC="SledPulse_fcn"
AY_FUNC.TYPE="REF" AZ_FUNC="Gravity_fcn" AZ_FUNC.TYPE="REF"
SYSTEM.TYPE="REF" SYSTEM="PregHumanFemale05%"  >
   <FUNC_USAGE FUNC.TYPE="REF" FUNC="SledPulse_fcn"
INTERPOLATION="SPLINE"    />
  </LOAD.SYSTEM_ACC>
  <LOAD.SYSTEM_ACC AX_FUNC.TYPE="REF" AX_FUNC="SledPulse_fcn"
AY_FUNC.TYPE="REF" AZ_FUNC="Gravity_fcn" AZ_FUNC.TYPE="REF"
SYSTEM.TYPE="REF" SYSTEM="Uterine"  >
   <FUNC_USAGE FUNC.TYPE="REF" FUNC="SledPulse_fcn"
INTERPOLATION="SPLINE"    />
  </LOAD.SYSTEM_ACC>
  <FUNCTION.XY ID.RANGE="[1, )" ID.TYPE="INTEGER" ID="1000"
NAME="SledPulse_fcn" NAME.TYPE="NAME"  >
   <TABLE DESCRIPTION="35 kph pulse" TYPE="XY_PAIR"    >
     |      XI              YI      |
0.00E+00       0.00E+00
5.00E-04       2.40E+00
1.00E-03       4.80E+00
1.50E-03       7.19E+00
2.00E-03       9.59E+00
2.50E-03       1.20E+01
3.00E-03       1.44E+01
3.50E-03       1.68E+01
4.00E-03       1.91E+01
4.50E-03       2.15E+01
5.00E-03       2.39E+01
5.50E-03       2.63E+01
6.00E-03       2.86E+01
6.50E-03       3.10E+01
7.00E-03       3.33E+01
7.50E-03       3.57E+01
8.00E-03       3.80E+01
8.50E-03       4.03E+01
9.00E-03       4.26E+01
9.50E-03       4.49E+01
1.00E-02       4.72E+01
1.05E-02       4.95E+01
1.10E-02       5.17E+01
1.15E-02       5.40E+01
1.20E-02       5.62E+01
```

1.25E-02	5.84E+01
1.30E-02	6.07E+01
1.35E-02	6.28E+01
1.40E-02	6.50E+01
1.45E-02	6.72E+01
1.50E-02	6.93E+01
1.55E-02	7.15E+01
1.60E-02	7.36E+01
1.65E-02	7.57E+01
1.70E-02	7.77E+01
1.75E-02	7.98E+01
1.80E-02	8.18E+01
1.85E-02	8.38E+01
1.90E-02	8.58E+01
1.95E-02	8.78E+01
2.00E-02	8.98E+01
2.05E-02	9.17E+01
2.10E-02	9.36E+01
2.15E-02	9.55E+01
2.20E-02	9.73E+01
2.25E-02	9.92E+01
2.30E-02	1.01E+02
2.35E-02	1.03E+02
2.40E-02	1.05E+02
2.45E-02	1.06E+02
2.50E-02	1.08E+02
2.55E-02	1.10E+02
2.60E-02	1.11E+02
2.65E-02	1.13E+02
2.70E-02	1.15E+02
2.75E-02	1.16E+02
2.80E-02	1.18E+02
2.85E-02	1.19E+02
2.90E-02	1.21E+02
2.95E-02	1.22E+02
3.00E-02	1.24E+02
3.05E-02	1.25E+02
3.10E-02	1.26E+02
3.15E-02	1.28E+02
3.20E-02	1.29E+02
3.25E-02	1.30E+02
3.30E-02	1.31E+02
3.35E-02	1.33E+02
3.40E-02	1.34E+02
3.45E-02	1.35E+02
3.50E-02	1.36E+02

3.55E-02	1.37E+02
3.60E-02	1.38E+02
3.65E-02	1.39E+02
3.70E-02	1.40E+02
3.75E-02	1.41E+02
3.80E-02	1.42E+02
3.85E-02	1.43E+02
3.90E-02	1.44E+02
3.95E-02	1.44E+02
4.00E-02	1.45E+02
4.05E-02	1.46E+02
4.10E-02	1.47E+02
4.15E-02	1.47E+02
4.20E-02	1.48E+02
4.25E-02	1.48E+02
4.30E-02	1.49E+02
4.35E-02	1.50E+02
4.40E-02	1.50E+02
4.45E-02	1.50E+02
4.50E-02	1.51E+02
4.55E-02	1.51E+02
4.60E-02	1.52E+02
4.65E-02	1.52E+02
4.70E-02	1.52E+02
4.75E-02	1.52E+02
4.80E-02	1.52E+02
4.85E-02	1.53E+02
4.90E-02	1.53E+02
4.95E-02	1.53E+02
5.00E-02	1.53E+02
5.05E-02	1.53E+02
5.10E-02	1.53E+02
5.15E-02	1.53E+02
5.20E-02	1.52E+02
5.25E-02	1.52E+02
5.30E-02	1.52E+02
5.35E-02	1.52E+02
5.40E-02	1.52E+02
5.45E-02	1.51E+02
5.50E-02	1.51E+02
5.55E-02	1.50E+02
5.60E-02	1.50E+02
5.65E-02	1.50E+02
5.70E-02	1.49E+02
5.75E-02	1.48E+02
5.80E-02	1.48E+02

5.85E-02	1.47E+02
5.90E-02	1.47E+02
5.95E-02	1.46E+02
6.00E-02	1.45E+02
6.05E-02	1.44E+02
6.10E-02	1.44E+02
6.15E-02	1.43E+02
6.20E-02	1.42E+02
6.25E-02	1.41E+02
6.30E-02	1.40E+02
6.35E-02	1.39E+02
6.40E-02	1.38E+02
6.45E-02	1.37E+02
6.50E-02	1.36E+02
6.55E-02	1.35E+02
6.60E-02	1.34E+02
6.65E-02	1.33E+02
6.70E-02	1.31E+02
6.75E-02	1.30E+02
6.80E-02	1.29E+02
6.85E-02	1.28E+02
6.90E-02	1.26E+02
6.95E-02	1.25E+02
7.00E-02	1.24E+02
7.05E-02	1.22E+02
7.10E-02	1.21E+02
7.15E-02	1.19E+02
7.20E-02	1.18E+02
7.25E-02	1.16E+02
7.30E-02	1.15E+02
7.35E-02	1.13E+02
7.40E-02	1.11E+02
7.45E-02	1.10E+02
7.50E-02	1.08E+02
7.55E-02	1.06E+02
7.60E-02	1.05E+02
7.65E-02	1.03E+02
7.70E-02	1.01E+02
7.75E-02	9.92E+01
7.80E-02	9.73E+01
7.85E-02	9.55E+01
7.90E-02	9.36E+01
7.95E-02	9.17E+01
8.00E-02	8.98E+01
8.05E-02	8.78E+01
8.10E-02	8.58E+01

```
8.15E-02        8.38E+01
8.20E-02        8.18E+01
8.25E-02        7.98E+01
8.30E-02        7.77E+01
8.35E-02        7.57E+01
8.40E-02        7.36E+01
8.45E-02        7.15E+01
8.50E-02        6.93E+01
8.55E-02        6.72E+01
8.60E-02        6.50E+01
8.65E-02        6.28E+01
8.70E-02        6.07E+01
8.75E-02        5.84E+01
8.80E-02        5.62E+01
8.85E-02        5.40E+01
8.90E-02        5.17E+01
8.95E-02        4.95E+01
9.00E-02        4.72E+01
9.05E-02        4.49E+01
9.10E-02        4.26E+01
9.15E-02        4.03E+01
9.20E-02        3.80E+01
9.25E-02        3.57E+01
9.30E-02        3.33E+01
9.35E-02        3.10E+01
9.40E-02        2.86E+01
9.45E-02        2.63E+01
9.50E-02        2.39E+01
9.55E-02        2.15E+01
9.60E-02        1.91E+01
9.65E-02        1.68E+01
9.70E-02        1.44E+01
9.75E-02        1.20E+01
9.80E-02        9.59E+00
9.85E-02        7.19E+00
9.90E-02        4.80E+00
9.95E-02        2.40E+00
1.00E-01        -4.91E-14
0.5     0
</TABLE>
 </FUNCTION.XY>
 <FUNCTION.XY ID.RANGE="[1, )" ID.TYPE="INTEGER" ID="1001"
NAME="Gravity_fcn" NAME.TYPE="NAME"  >
   <TABLE TYPE="XY_PAIR"    >
     |      XI              YI      |
      -1.00000000E+00    -9.81000000E+00
```

```
      1.00000000E+02     -9.81000000E+00
    </TABLE>
  </FUNCTION.XY>
  <CONTACT.MB_FE ID.RANGE="[1, )" ID="5" ID.TYPE="INTEGER"
MASTER_SURFACE="/1/Seat_cushion" MASTER_SURFACE.TYPE="LIST"
NAME="Seat_Cush-Pelvis" NAME.TYPE="NAME"
SLAVE_SURFACE.TYPE="LIST" SLAVE_SURFACE="/2/BodyNoArms_gfe"
SURFACE_THICK.TYPE="REAL"  >
    <CONTACT_FORCE.CHAR CONTACT_AREA.TYPE="REAL"
CONTACT_TYPE="SLAVE" FRIC_FUNC.TYPE="REF" USER_CHAR.TYPE="REF"
/>
  </CONTACT.MB_FE>
  <CONTACT.MB_FE ID.RANGE="[1, )" ID="6" ID.TYPE="INTEGER"
MASTER_SURFACE="/1/Seat_Back" MASTER_SURFACE.TYPE="LIST"
NAME="Seat_Back-Pelvis" NAME.TYPE="NAME"
SLAVE_SURFACE.TYPE="LIST" SLAVE_SURFACE="/2/BodyNoArms_gfe"
SURFACE_THICK.TYPE="REAL"  >
    <CONTACT_FORCE.CHAR CONTACT_AREA.TYPE="REAL"
CONTACT_TYPE="SLAVE" FRIC_FUNC.TYPE="REF" USER_CHAR.TYPE="REF"
/>
  </CONTACT.MB_FE>
  <CONTACT.MB_FE ID.RANGE="[1, )" ID="7" ID.TYPE="INTEGER"
MASTER_SURFACE="/1/Seat_Back" MASTER_SURFACE.TYPE="LIST"
NAME="Seat_Back-LumbarSpineLow" NAME.TYPE="NAME"
SLAVE_SURFACE.TYPE="LIST" SLAVE_SURFACE="/2/Thorax_gfe"
SURFACE_THICK.TYPE="REAL"  >
    <CONTACT_FORCE.CHAR CONTACT_AREA.TYPE="REAL"
CONTACT_TYPE="SLAVE" FRIC_FUNC.TYPE="REF" USER_CHAR.TYPE="REF"
/>
  </CONTACT.MB_FE>
  <CONTACT.MB_FE ID.RANGE="[1, )" ID="8" ID.TYPE="INTEGER"
MASTER_SURFACE="/1/Sled_Floor" MASTER_SURFACE.TYPE="LIST"
NAME="Sled_Floor-ShoeL" NAME.TYPE="NAME"
SLAVE_SURFACE.TYPE="LIST" SLAVE_SURFACE="/2/LegL_gfe"
SURFACE_THICK.TYPE="REAL"  >
    <CONTACT_FORCE.CHAR CONTACT_AREA.TYPE="REAL"
CONTACT_TYPE="SLAVE" FRIC_FUNC.TYPE="REF" USER_CHAR.TYPE="REF"
/>
  </CONTACT.MB_FE>
  <CONTACT.MB_FE ID.RANGE="[1, )" ID="9" ID.TYPE="INTEGER"
MASTER_SURFACE="/1/Sled_Floor" MASTER_SURFACE.TYPE="LIST"
NAME="Sled_Floor-ShoeR" NAME.TYPE="NAME"
SLAVE_SURFACE.TYPE="LIST" SLAVE_SURFACE="/2/LegR_gfe"
SURFACE_THICK.TYPE="REAL"  >
```

```
   <CONTACT_FORCE.CHAR CONTACT_AREA.TYPE="REAL"
CONTACT_TYPE="SLAVE" FRIC_FUNC.TYPE="REF" USER_CHAR.TYPE="REF"
/>
  </CONTACT.MB_FE>
  <CONTACT.MB_FE ID.RANGE="[1, )" ID="10" ID.TYPE="INTEGER"
MASTER_SURFACE="/1/Knee" MASTER_SURFACE.TYPE="LIST"
NAME="Knee1" NAME.TYPE="NAME" SLAVE_SURFACE.TYPE="LIST"
SLAVE_SURFACE="/2/LegL_gfe" SURFACE_THICK.TYPE="REAL"  >
   <CONTACT_FORCE.CHAR CONTACT_AREA.TYPE="REAL"
CONTACT_TYPE="SLAVE" FRIC_FUNC.TYPE="REF" USER_CHAR.TYPE="REF"
/>
  </CONTACT.MB_FE>
  <CONTACT.MB_FE ID.RANGE="[1, )" ID="11" ID.TYPE="INTEGER"
MASTER_SURFACE="/1/Knee" MASTER_SURFACE.TYPE="LIST"
NAME="Knee2" NAME.TYPE="NAME" SLAVE_SURFACE.TYPE="LIST"
SLAVE_SURFACE="/2/LegR_gfe" SURFACE_THICK.TYPE="REAL"  >
   <CONTACT_FORCE.CHAR CONTACT_AREA.TYPE="REAL"
CONTACT_TYPE="SLAVE" FRIC_FUNC.TYPE="REF" USER_CHAR.TYPE="REF"
/>
  </CONTACT.MB_FE>
  <CONTACT.MB_FE ID.RANGE="[1, )" ID="12" ID.TYPE="INTEGER"
MASTER_SURFACE="/1/Steering_wheel" MASTER_SURFACE.TYPE="LIST"
NAME="steering-body" NAME.TYPE="NAME" SLAVE_SURFACE.TYPE="LIST"
SLAVE_SURFACE="/2/BodyNoArms_gfe" SURFACE_THICK.TYPE="REAL"  >
   <CONTACT_FORCE.CHAR CONTACT_AREA.TYPE="REAL"
CONTACT_TYPE="SLAVE" FRIC_FUNC.TYPE="REF" USER_CHAR.TYPE="REF"
/>
  </CONTACT.MB_FE>
  <CONTACT.MB_FE ID.RANGE="[1, )" ID="15" ID.TYPE="INTEGER"
MASTER_SURFACE="/1/Steering_wheel" MASTER_SURFACE.TYPE="LIST"
NAME="steeringwheel-uterus" NAME.TYPE="NAME"
SLAVE_SURFACE.TYPE="LIST" SLAVE_SURFACE="/3/uterus2_gfe"
SURFACE_THICK.TYPE="REAL"  >
   <CONTACT_FORCE.KINEMATIC FRIC_COEF.RANGE="[0, )"
FRIC_COEF.TYPE="REAL" FRIC_COEF="0.2"    />
  </CONTACT.MB_FE>
  <CONTACT.MB_FE ID.RANGE="[1, )" ID="16" ID.TYPE="INTEGER"
MASTER_SURFACE="/1/Steering_wheel" MASTER_SURFACE.TYPE="LIST"
NAME="steeringwheel-fluid" NAME.TYPE="NAME"
SLAVE_SURFACE.TYPE="LIST" SLAVE_SURFACE="/3/fluid_gfe"
SURFACE_THICK.TYPE="REAL"  >
   <CONTACT_FORCE.KINEMATIC FRIC_COEF.RANGE="[0, )"
FRIC_COEF="0.2" FRIC_COEF.TYPE="REAL"    />
  </CONTACT.MB_FE>
  <CONTACT.MB_FE ID.RANGE="[1, )" ID="17" ID.TYPE="INTEGER"
MASTER_SURFACE="/1/Steering_wheel" MASTER_SURFACE.TYPE="LIST"
```

NAME="steeringwheel-fat" NAME.TYPE="NAME"
SLAVE_SURFACE.TYPE="LIST" SLAVE_SURFACE="/3/fat2_gfe"
SURFACE_THICK.TYPE="REAL" >
<CONTACT_FORCE.KINEMATIC FRIC_COEF.RANGE="[0,)"
FRIC_COEF="0.2" FRIC_COEF.TYPE="REAL" />
</CONTACT.MB_FE>
<CONTACT.FE_FE FLAG.RANGE="[1,)" FLAG.TYPE="INTEGER"
GAP_FUNC="fid_108" GAP_FUNC.TYPE="REF" GAP_TYPE="FUNC" ID="13"
ID.RANGE="[1,)" ID.TYPE="INTEGER" INITIAL_USNORM.TYPE="REAL[3]"
MASTER_SURFACE="/2/HumanBody_gfe" MASTER_SURFACE.TYPE="LIST"
NAME.TYPE="NAME" NAME="Thorax-ShoulderBelt"
NORMAL_USER.TYPE="REAL[3]" SEARCH_FACTOR.TYPE="INTEGER"
SLAVE_SURFACE="/VEHICLE/ShoulderBelt_gfe"
SLAVE_SURFACE.TYPE="LIST" SWITCH.TYPE="REF" TORQUE_FRIC="ON" >
<CONTACT_FORCE.CHAR CONTACT_AREA.TYPE="REAL"
CONTACT_TYPE="MASTER" FRIC_FUNC.TYPE="REF" FRIC_FUNC="fid_107"
USER_CHAR.TYPE="REF" />
</CONTACT.FE_FE>
<CONTACT.FE_FE FLAG.RANGE="[1,)" FLAG.TYPE="INTEGER"
GAP_FUNC="fid_108" GAP_FUNC.TYPE="REF" GAP_TYPE="FUNC" ID="14"
ID.RANGE="[1,)" ID.TYPE="INTEGER" INITIAL_USNORM.TYPE="REAL[3]"
MASTER_SURFACE="/2/BodyNoArms_gfe" MASTER_SURFACE.TYPE="LIST"
NAME.TYPE="NAME" NAME="Pelvis-LapBelt"
NORMAL_USER.TYPE="REAL[3]" SEARCH_FACTOR.TYPE="INTEGER"
SLAVE_SURFACE="/VEHICLE/LapBelt_gfe" SLAVE_SURFACE.TYPE="LIST"
SWITCH.TYPE="REF" TORQUE_FRIC="ON" >
<CONTACT_FORCE.CHAR CONTACT_AREA.TYPE="REAL"
CONTACT_TYPE="MASTER" FRIC_FUNC.TYPE="REF" FRIC_FUNC="fid_107"
USER_CHAR.TYPE="REF" />
</CONTACT.FE_FE>
<CONTACT.FE_FE FLAG.RANGE="[1,)" FLAG.TYPE="INTEGER"
GAP_FUNC.TYPE="REF" ID="808" ID.RANGE="[1,)" ID.TYPE="INTEGER"
INITIAL_USNORM.TYPE="REAL[3]"
MASTER_SURFACE="/VEHICLE/LapBelt_gfe" MASTER_SURFACE.TYPE="LIST"
NAME.TYPE="NAME" NAME="lapbelt-uterus" NORMAL_USER.TYPE="REAL[3]"
SEARCH_FACTOR.TYPE="INTEGER" SLAVE_SURFACE="/3/uterus_gfe"
SLAVE_SURFACE.TYPE="LIST" SWITCH.TYPE="REF" TORQUE_FRIC="ON" >
<CONTACT_FORCE.PENALTY FRIC_FUNC.TYPE="REF"
MAX_FORCE_PAR.TYPE="REAL" MAX_FORCE_PAR="1.0"
PENALTY.TYPE="REAL" />
</CONTACT.FE_FE>
<CONTACT.FE_FE FLAG.RANGE="[1,)" FLAG.TYPE="INTEGER"
GAP_FUNC.TYPE="REF" ID="809" ID.RANGE="[1,)" ID.TYPE="INTEGER"
INITIAL_USNORM.TYPE="REAL[3]"
MASTER_SURFACE="/VEHICLE/LapBelt_gfe" MASTER_SURFACE.TYPE="LIST"
NAME.TYPE="NAME" NAME="lapbelt-fluid" NORMAL_USER.TYPE="REAL[3]"

```
SEARCH_FACTOR.TYPE="INTEGER" SLAVE_SURFACE="/3/fluid_gfe"
SLAVE_SURFACE.TYPE="LIST" SWITCH.TYPE="REF" TORQUE_FRIC="ON"  >
      <CONTACT_FORCE.PENALTY FRIC_FUNC.TYPE="REF"
MAX_FORCE_PAR.TYPE="REAL" MAX_FORCE_PAR="0.1"
PENALTY.TYPE="REAL"    />
 </CONTACT.FE_FE>
    <CONTACT.FE_FE FLAG.RANGE="[1, )" FLAG.TYPE="INTEGER"
GAP_FUNC.TYPE="REF" ID="810" ID.RANGE="[1, )" ID.TYPE="INTEGER"
INITIAL_USNORM.TYPE="REAL[3]"
MASTER_SURFACE="/VEHICLE/LapBelt_gfe" MASTER_SURFACE.TYPE="LIST"
NAME.TYPE="NAME" NAME="lapbelt-fat" NORMAL_USER.TYPE="REAL[3]"
SEARCH_FACTOR.TYPE="INTEGER" SLAVE_SURFACE="/3/fat2_gfe"
SLAVE_SURFACE.TYPE="LIST" SWITCH.TYPE="REF" TORQUE_FRIC="ON"  >
       <CONTACT_FORCE.PENALTY FRIC_FUNC.TYPE="REF"
MAX_FORCE_PAR.TYPE="REAL" MAX_FORCE_PAR="0.1"
PENALTY.TYPE="REAL"    />
 </CONTACT.FE_FE>
    <FUNCTION.XY ID.RANGE="[1, )" ID.TYPE="INTEGER" ID="107"
NAME="fid_107" NAME.TYPE="NAME"  >
     <TABLE TYPE="XY_PAIR"    >
  |      XI               YI      |
    0.00000000E+00      0.00000000E+00
    5.00000000E-02      2.50000000E-01
    1.00000000E+00      2.50000000E-01
      </TABLE>
   </FUNCTION.XY>
   <FUNCTION.XY ID.RANGE="[1, )" ID.TYPE="INTEGER" ID="108"
NAME="fid_108" NAME.TYPE="NAME"  >
     <TABLE TYPE="XY_PAIR"    >
  |      XI               YI      |
    0.00000000E+00      2.00000000E-03
    1.00000000E+00      2.00000000E-03
      </TABLE>
   </FUNCTION.XY>
   <BELT ID.RANGE="[1, )" ID.TYPE="INTEGER" ID="2" NAME="Segment2"
NAME.TYPE="NAME"  >
     <BELT_SEGMENT ADD_LENGTH.RANGE="[0, )"
ADD_LENGTH.TYPE="REAL" CHAR.TYPE="REF" CHAR="/Beltprop"
FORCE_CORRECTION.TYPE="REAL" ID="2" ID.RANGE="[1, )"
ID.TYPE="INTEGER" INITIAL_STRAIN.RANGE="(-1, )"
INITIAL_STRAIN.TYPE="REAL" NAME.TYPE="NAME" NAME="seg1"
POINT_REF_1="/Buckle" POINT_REF_1.TYPE="REF" POINT_REF_2="/Node3"
POINT_REF_2.TYPE="REF" RUPTURE_STRAIN.RANGE="(0, )"
RUPTURE_STRAIN.TYPE="REAL"    />
   </BELT>
```

```
   <BELT ID.RANGE="[1, )" ID.TYPE="INTEGER" ID="3" NAME="Segment3"
NAME.TYPE="NAME"  >
     <BELT_SEGMENT ADD_LENGTH.RANGE="[0, )"
ADD_LENGTH.TYPE="REAL" CHAR.TYPE="REF" CHAR="/Beltprop"
FORCE_CORRECTION.TYPE="REAL" ID="1" ID.RANGE="[1, )"
ID.TYPE="INTEGER" INITIAL_STRAIN.RANGE="(-1, )"
INITIAL_STRAIN.TYPE="REAL" NAME.TYPE="NAME" NAME="seg1"
POINT_REF_1="/Node4" POINT_REF_1.TYPE="REF" POINT_REF_2="/Floor"
POINT_REF_2.TYPE="REF" RUPTURE_STRAIN.RANGE="(0, )"
RUPTURE_STRAIN.TYPE="REAL"    />
   </BELT>
   <POINT_OBJECT BODY.TYPE="REF" CRDSYS="REF_SPACE"
FE_MODEL.TYPE="REF" ID.RANGE="[1, )" ID="4" ID.TYPE="INTEGER"
NAME="Buckle" NAME.TYPE="NAME" NODE.TYPE="INTEGER"
POS.TYPE="REAL[3]" POS="-0.220  0.314  0.0"  />
   <POINT_OBJECT BODY.TYPE="REF" FE_MODEL.TYPE="REF"
FE_MODEL="/VEHICLE/FE2_LAPBELT" ID.RANGE="[1, )" ID="5"
ID.TYPE="INTEGER" NAME="Node3" NAME.TYPE="NAME" NODE="133"
NODE.TYPE="INTEGER" POS.TYPE="REAL[3]"  />
   <POINT_OBJECT BODY.TYPE="REF" FE_MODEL.TYPE="REF"
FE_MODEL="/VEHICLE/FE2_LAPBELT" ID.RANGE="[1, )" ID="6"
ID.TYPE="INTEGER" NAME="Node4" NAME.TYPE="NAME" NODE="134"
NODE.TYPE="INTEGER" POS.TYPE="REAL[3]"  />
   <POINT_OBJECT BODY.TYPE="REF" FE_MODEL.TYPE="REF"
ID.RANGE="[1, )" ID="7" ID.TYPE="INTEGER" NAME="Floor"
NAME.TYPE="NAME" NODE.TYPE="INTEGER" POS.TYPE="REAL[3]" POS="-
0.215  -0.318  0.0"  />
   <CHARACTERISTIC.LOAD AMPLIFICATION.TYPE="REF"
DAMP_COEF.RANGE="[0, )" DAMP_COEF.TYPE="REAL"
DAMP_STRESS_FUNC.TYPE="REF" DAMP_VEL_FUNC.TYPE="REF"
ELAS_LIMIT="0.0" ELAS_LIMIT.RANGE="[0, )" ELAS_LIMIT.TYPE="REAL"
HYS_MODEL="1" HYS_SLOPE="3.0E5" HYS_SLOPE.RANGE="[0, )"
HYS_SLOPE.TYPE="REAL" ID="1" ID.RANGE="[1, )" ID.TYPE="INTEGER"
LOAD_FUNC="beltloading" LOAD_FUNC.TYPE="REF" NAME.TYPE="NAME"
NAME="Beltprop" UNLOAD_FUNC.TYPE="REF" UNLOAD_FUNC="beltunloading"
/>
   <FUNCTION.XY ID.RANGE="[1, )" ID.TYPE="INTEGER" ID="3"
NAME="beltloading" NAME.TYPE="NAME"  >
     <TABLE TYPE="XY_PAIR"    >|          XI        YI        |
     0.0        0.0
     0.021   1000.0
     0.030   2950.0
     0.040   4000.0
     0.050   4700.0
     0.060   5320.0
     0.070   6000.0
```

```
    0.080   6600.0
    0.090   7250.0
    0.100   8000.0
    0.110   8680.0
    0.120   9500.0
    0.126  10000.0
 </TABLE>
  </FUNCTION.XY>
  <FUNCTION.XY ID.RANGE="[1, )" ID.TYPE="INTEGER" ID="4"
NAME="beltunloading" NAME.TYPE="NAME"  >
    <TABLE TYPE="XY_PAIR"    >|          XI        YI        |
 0.0     0.0
 0.1  1000.0

 </TABLE>
  </FUNCTION.XY>
  <OUTPUT_BELT ID.RANGE="[1, )" ID="101" ID.TYPE="INTEGER"
INPUT_REF="/2/seg1" INPUT_REF.TYPE="REF"
INPUT_TYPE="BELT_SEGMENT" NAME="belt_out_01" NAME.TYPE="NAME"
/>
  <OUTPUT_BELT ID.RANGE="[1, )" ID="102" ID.TYPE="INTEGER"
INPUT_REF="/3/seg1" INPUT_REF.TYPE="REF"
INPUT_TYPE="BELT_SEGMENT" NAME="belt_out_02" NAME.TYPE="NAME"
/>
  <BELT ID.RANGE="[1, )" ID.TYPE="INTEGER" ID="4" NAME="Segment4"
NAME.TYPE="NAME"  >
    <BELT_SEGMENT ADD_LENGTH.RANGE="[0, )"
ADD_LENGTH.TYPE="REAL" CHAR.TYPE="REF" CHAR="/Beltprop"
FORCE_CORRECTION.TYPE="REAL" ID="4" ID.RANGE="[1, )"
ID.TYPE="INTEGER" INITIAL_STRAIN.RANGE="(-1, )"
INITIAL_STRAIN.TYPE="REAL" NAME.TYPE="NAME" NAME="seg4"
POINT_REF_1="/Retractor" POINT_REF_1.TYPE="REF" POINT_REF_2="/Node6"
POINT_REF_2.TYPE="REF" RUPTURE_STRAIN.RANGE="(0, )"
RUPTURE_STRAIN.TYPE="REAL"    />
  </BELT>
  <BELT ID.RANGE="[1, )" ID.TYPE="INTEGER" ID="5" NAME="Segment5"
NAME.TYPE="NAME"  >
    <BELT_SEGMENT ADD_LENGTH.RANGE="[0, )"
ADD_LENGTH.TYPE="REAL" CHAR.TYPE="REF" CHAR="/Beltprop"
FORCE_CORRECTION.TYPE="REAL" ID="5" ID.RANGE="[1, )"
ID.TYPE="INTEGER" INITIAL_STRAIN.RANGE="(-1, )"
INITIAL_STRAIN.TYPE="REAL" NAME.TYPE="NAME" NAME="seg5"
POINT_REF_1="/Node5" POINT_REF_1.TYPE="REF" POINT_REF_2="/Floor"
POINT_REF_2.TYPE="REF" RUPTURE_STRAIN.RANGE="(0, )"
RUPTURE_STRAIN.TYPE="REAL"    />
  </BELT>
```

```
   <POINT_OBJECT BODY.TYPE="REF" CRDSYS="REF_SPACE"
DESCRIPTION="does not rectract - just a name" FE_MODEL.TYPE="REF"
ID.RANGE="[1, )" ID="8" ID.TYPE="INTEGER" NAME="Retractor"
NAME.TYPE="NAME" NODE.TYPE="INTEGER" POS.TYPE="REAL[3]" POS="-
0.220  0.114  0.6"  />
   <POINT_OBJECT BODY.TYPE="REF" FE_MODEL.TYPE="REF"
FE_MODEL="/VEHICLE/FE1_Shoulder_belt" ID.RANGE="[1, )" ID="9"
ID.TYPE="INTEGER" NAME="Node5" NAME.TYPE="NAME" NODE="190"
NODE.TYPE="INTEGER" POS.TYPE="REAL[3]"  />
   <POINT_OBJECT BODY.TYPE="REF" FE_MODEL.TYPE="REF"
FE_MODEL="/VEHICLE/FE1_Shoulder_belt" ID.RANGE="[1, )" ID="10"
ID.TYPE="INTEGER" NAME="Node6" NAME.TYPE="NAME" NODE="84"
NODE.TYPE="INTEGER" POS.TYPE="REAL[3]"  />
   <OUTPUT_BELT ID.RANGE="[1, )" ID="103" ID.TYPE="INTEGER"
INPUT_REF="/5/seg5" INPUT_REF.TYPE="REF"
INPUT_TYPE="BELT_SEGMENT" NAME="belt_out_03" NAME.TYPE="NAME"
/>
   <OUTPUT_BELT ID.RANGE="[1, )" ID="104" ID.TYPE="INTEGER"
INPUT_REF="/4/seg4" INPUT_REF.TYPE="REF"
INPUT_TYPE="BELT_SEGMENT" NAME="belt_out_04" NAME.TYPE="NAME"
/>
 <SYSTEM.MODEL ID.RANGE="[1, )" ID.TYPE="INTEGER" ID="9"
NAME="Airbag" NAME.TYPE="NAME"  >
   <FE_MODEL ID.RANGE="[1, )" ID.TYPE="INTEGER" ID="3"
NAME="Driver_Airbag_600mm_diameter" NAME.TYPE="NAME"    >
     <CONTROL_FE_MODEL ALPHA_COEF="50.0" ALPHA_COEF.RANGE="[0, )"
ALPHA_COEF.TYPE="REAL" ALPHA_FUNC.TYPE="REF"
IMM_STRETCH_PRINT.RANGE="[0, 100]"
IMM_STRETCH_PRINT.TYPE="INTEGER"      />
     <CONTROL_FE_TIME_STEP CRITICAL_ELEMENTS.RANGE="[1, 100]"
CRITICAL_ELEMENTS.TYPE="INTEGER" MAX_STEP.RANGE="(0, )"
MAX_STEP.TYPE="REAL" MIN_STEP.RANGE="[0, )" MIN_STEP.TYPE="REAL"
NR_OF_CYCLES.TYPE="INTEGER" REDUCTION_FACTOR.TYPE="REAL"     />
     <CONTROL_AIRBAG BLOCK_FLOW="0.0" BLOCK_FLOW.RANGE="[0, 1]"
BLOCK_FLOW.TYPE="REAL" PRESSURE.TYPE="REAL"
PRESSURE="1.013250E+05" TEMPERATURE="288.1499938965"
TEMPERATURE.TYPE="REAL" THERMC.TYPE="INTEGER"     >
       <GAS_MIXTURE>
         <GAS_FRACTION GAS_NAME="N2" MOL_FRACTION="0.78084"
MOL_FRACTION.RANGE="[0, 1]" MOL_FRACTION.TYPE="REAL"         />
         <GAS_FRACTION GAS_NAME="O2" MOL_FRACTION="0.20946"
MOL_FRACTION.RANGE="[0, 1]" MOL_FRACTION.TYPE="REAL"         />
         <GAS_FRACTION GAS_NAME="CO2" MOL_FRACTION="3.300000E-04"
MOL_FRACTION.RANGE="[0, 1]" MOL_FRACTION.TYPE="REAL"         />
         <GAS_FRACTION GAS_NAME="AR" MOL_FRACTION="0.00937"
MOL_FRACTION.RANGE="[0, 1]" MOL_FRACTION.TYPE="REAL"         />
```

```
  </GAS_MIXTURE>
 </CONTROL_AIRBAG>
 <TABLE TYPE="COORDINATE.CARTESIAN"     >
      |   ID          X               Y               Z       |
</TABLE>
 <TABLE TYPE="COORDINATE_REF.CARTESIAN"     >
      |   ID          X               Y               Z       |
</TABLE>
 <MATERIAL.ORTHOLIN DAMP_COEF.RANGE="[0, )"
DAMP_COEF.TYPE="REAL" DAMP_COEF="0.1" DENSITY.RANGE="(0, )"
DENSITY.TYPE="REAL" DENSITY="750.0" E11="2.500000E+08" E11.RANGE="(0,
)" E11.TYPE="REAL" E22.RANGE="(0, )" E22.TYPE="REAL" E22="2.500000E+08"
G12="2.500000E+07" G12.RANGE="(0, )" G12.TYPE="REAL" ID="1"
ID.RANGE="[1, )" ID.TYPE="INTEGER" KAPPA.TYPE="REAL"
KAPPA.RANGE="[0, )" MAT_DIR.TYPE="REAL[3]" MAT_DIR="1.0 0.0 0.0"
MU.TYPE="INTEGER" NAME.TYPE="NAME" NAME="mat_1" NU12.RANGE="(-
1, 0.5)" NU12.TYPE="REAL" TENSION_ONLY="ON"     />
 <MATERIAL.ORTHOLIN DAMP_COEF.RANGE="[0, )"
DAMP_COEF.TYPE="REAL" DAMP_COEF="0.1" DENSITY.RANGE="(0, )"
DENSITY.TYPE="REAL" DENSITY="750.0" E11="2.500000E+08" E11.RANGE="(0,
)" E11.TYPE="REAL" E22.RANGE="(0, )" E22.TYPE="REAL" E22="2.500000E+08"
G12="2.500000E+07" G12.RANGE="(0, )" G12.TYPE="REAL" ID="2"
ID.RANGE="[1, )" ID.TYPE="INTEGER" KAPPA.TYPE="REAL"
KAPPA.RANGE="[0, )" MAT_DIR.TYPE="REAL[3]" MAT_DIR="1.0 0.0 0.0"
MU.TYPE="INTEGER" NAME.TYPE="NAME" NAME="mat_2" NU12.RANGE="(-
1, 0.5)" NU12.TYPE="REAL" TENSION_ONLY="ON"     />
 <MATERIAL.ORTHOLIN DAMP_COEF.RANGE="[0, )"
DAMP_COEF.TYPE="REAL" DAMP_COEF="0.1" DENSITY.RANGE="(0, )"
DENSITY.TYPE="REAL" DENSITY="750.0" E11="2.500000E+08" E11.RANGE="(0,
)" E11.TYPE="REAL" E22.RANGE="(0, )" E22.TYPE="REAL" E22="2.500000E+08"
G12="2.500000E+07" G12.RANGE="(0, )" G12.TYPE="REAL" ID="3"
ID.RANGE="[1, )" ID.TYPE="INTEGER" KAPPA.TYPE="REAL"
KAPPA.RANGE="[0, )" MAT_DIR.TYPE="REAL[3]" MAT_DIR="1.0 0.0 0.0"
MU.TYPE="INTEGER" NAME.TYPE="NAME" NAME="mat_3" NU12.RANGE="(-
1, 0.5)" NU12.TYPE="REAL" TENSION_ONLY="ON"     />
 <MATERIAL.ORTHOLIN DAMP_COEF.RANGE="[0, )"
DAMP_COEF.TYPE="REAL" DAMP_COEF="0.1" DENSITY.RANGE="(0, )"
DENSITY.TYPE="REAL" DENSITY="750.0" E11="2.500000E+08" E11.RANGE="(0,
)" E11.TYPE="REAL" E22.RANGE="(0, )" E22.TYPE="REAL" E22="2.500000E+08"
G12="2.500000E+07" G12.RANGE="(0, )" G12.TYPE="REAL" ID="4"
ID.RANGE="[1, )" ID.TYPE="INTEGER" KAPPA.TYPE="REAL"
KAPPA.RANGE="[0, )" MAT_DIR.TYPE="REAL[3]" MAT_DIR="0.7071067812
0.7071067812 0.0" MU.TYPE="INTEGER" NAME.TYPE="NAME" NAME="mat_4"
NU12.RANGE="(-1, 0.5)" NU12.TYPE="REAL" TENSION_ONLY="ON"     />
 <MATERIAL.ORTHOLIN DAMP_COEF.RANGE="[0, )"
DAMP_COEF.TYPE="REAL" DAMP_COEF="0.1" DENSITY.RANGE="(0, )"
```

DENSITY.TYPE="REAL" DENSITY="750.0" E11="2.500000E+08" E11.RANGE="(0,
)" E11.TYPE="REAL" E22.RANGE="(0,)" E22.TYPE="REAL" E22="2.500000E+08"
G12="2.500000E+07" G12.RANGE="(0,)" G12.TYPE="REAL" ID="5"
ID.RANGE="[1,)" ID.TYPE="INTEGER" KAPPA.TYPE="REAL"
KAPPA.RANGE="[0,)" MAT_DIR.TYPE="REAL[3]" MAT_DIR="0.7071067812
0.7071067812 0.0" MU.TYPE="INTEGER" NAME.TYPE="NAME" NAME="mat_5"
NU12.RANGE="(-1, 0.5)" NU12.TYPE="REAL" TENSION_ONLY="ON" />
<MATERIAL.HOLE ID.RANGE="[1,)" ID.TYPE="INTEGER" ID="6"
NAME="mat_6" NAME.TYPE="NAME" >
<HOLE.MODEL1 CDEX.RANGE="[0,)" CDEX.TYPE="REAL"
CDEX="2.09467" CDP_FUNC.TYPE="REF" CDT_FUNC.TYPE="REF"
DELTEX="0.0" DELTEX.RANGE="[0,)" DELTEX.TYPE="REAL" DPEX="0.0"
DPEX.TYPE="REAL" DTEX="0.0" DTEX.TYPE="REAL" />
</MATERIAL.HOLE>
<PROPERTY.MEM3 ID.RANGE="[1,)" ID="1" ID.TYPE="INTEGER"
IMM_DAMP.RANGE="[0,)" IMM_DAMP.TYPE="REAL"
IMM_STRAIN.TYPE="REAL" IMM_TRANS.TYPE="REAL" NAME="prp_1"
NAME.TYPE="NAME" THICK.RANGE="(0,)" THICK.TYPE="REAL"
THICK="5.000000E-04" />
<PROPERTY.MEM3 ID.RANGE="[1,)" ID="2" ID.TYPE="INTEGER"
IMM_DAMP.RANGE="[0,)" IMM_DAMP.TYPE="REAL"
IMM_STRAIN.TYPE="REAL" IMM_TRANS.TYPE="REAL" NAME="prp_2"
NAME.TYPE="NAME" THICK.RANGE="(0,)" THICK.TYPE="REAL" />
<PART ID.RANGE="[1,)" ID.TYPE="INTEGER" ID="1"
MATERIAL.TYPE="REF" MATERIAL="6" NAME.TYPE="NAME"
PROPERTY.TYPE="REF" PROPERTY="2" />
<PART ID.RANGE="[1,)" ID.TYPE="INTEGER" ID="2"
MATERIAL.TYPE="REF" MATERIAL="1" NAME.TYPE="NAME"
PROPERTY.TYPE="REF" PROPERTY="1" />
<PART ID.RANGE="[1,)" ID.TYPE="INTEGER" ID="3"
MATERIAL.TYPE="REF" MATERIAL="2" NAME.TYPE="NAME"
PROPERTY.TYPE="REF" PROPERTY="1" />
<PART ID.RANGE="[1,)" ID.TYPE="INTEGER" ID="4"
MATERIAL.TYPE="REF" MATERIAL="3" NAME.TYPE="NAME"
PROPERTY.TYPE="REF" PROPERTY="1" />
<PART ID.RANGE="[1,)" ID.TYPE="INTEGER" ID="5"
MATERIAL.TYPE="REF" MATERIAL="4" NAME.TYPE="NAME"
PROPERTY.TYPE="REF" PROPERTY="1" />
<PART ID.RANGE="[1,)" ID.TYPE="INTEGER" ID="6"
MATERIAL.TYPE="REF" MATERIAL="5" NAME.TYPE="NAME"
PROPERTY.TYPE="REF" PROPERTY="1" />
<TABLE TYPE="ELEMENT.TRIAD3" >
| ID PART N1 N2 N3 |
</TABLE>
<TABLE TYPE="STRAP" >

```
        | ID       N1       N2       STIF         LENGTH       RUPTURE
RUPTURE_DURATION RUPTURE_WINDOW |
           1      521      976   2.000000E+04    2.500000E-01  1.000000E+00
0.000000E+00    0.000000E+00
           2      327      782   2.000000E+04    2.500000E-01  1.000000E+00
0.000000E+00    0.000000E+00
           3      439      894   2.000000E+04    2.500000E-01  1.000000E+00
0.000000E+00    0.000000E+00
           4      205      660   2.000000E+04    2.500000E-01  1.000000E+00
0.000000E+00    0.000000E+00
       </TABLE>
    <AIRBAG_CHAMBER CHAMBER_V0="1.000000E-04"
CHAMBER_V0.RANGE="[0, )" CHAMBER_V0.TYPE="REAL"
ELEMENT_LIST="ALL" ELEMENT_LIST.TYPE="ILIST"
GROUP_LIST.TYPE="LIST" ID.RANGE="[1, )" ID="1" ID.TYPE="INTEGER"
INV_ELEMENT_LIST.TYPE="ILIST" INV_GROUP_LIST.TYPE="LIST"
NAME.TYPE="NAME" PF_FUNC.TYPE="REF" TF_FUNC.TYPE="REF"     >
      <INFLATOR EXIT_PRES_FUNC.TYPE="REF" ID.RANGE="[1, )" ID="1"
ID.TYPE="INTEGER" MASS_FLOW_RATE_FUNC="fid_87"
MASS_FLOW_RATE_FUNC.TYPE="REF" NAME.TYPE="NAME"
POLYTROPIC_CONSTANT.TYPE="REAL" SWITCH="/5" SWITCH.TYPE="REF"
TEMP_FUNC.TYPE="REF" TEMP_FUNC="fid_88"       >
        <GAS_MIXTURE>
         <GAS_FRACTION GAS_NAME="N2" MOL_FRACTION="1.0"
MOL_FRACTION.RANGE="[0, 1]" MOL_FRACTION.TYPE="REAL"          />
        </GAS_MIXTURE>
        <JET.IDELCHIK BODY.TYPE="REF" CENTRE="0.0 0.0 0.0"
CENTRE.TYPE="REAL[3]" EFAC.RANGE="(0, 2]" EFAC.TYPE="REAL"
ELEMENT_LIST="ALL" ELEMENT_LIST.TYPE="ILIST"
GROUP_LIST.TYPE="LIST" ID.RANGE="[1, )" ID="1" ID.TYPE="INTEGER"
NAME.TYPE="NAME" OUTFLOW_DIR.TYPE="REAL[3]" OUTFLOW_DIR="0.0
0.0 1.0"        >
         <JET_SHAPE.CIRCULAR RADIUS="0.025" RADIUS.RANGE="(0, )"
RADIUS.TYPE="REAL"          />
        </JET.IDELCHIK>
      </INFLATOR>
    </AIRBAG_CHAMBER>
    <OUTPUT_AIRBAG_CHAMBER AIRBAG_CHAMBER_LIST.TYPE="LIST"
AIRBAG_CHAMBER_LIST="1" ID.RANGE="[1, )" ID.TYPE="INTEGER" ID="1"
NAME="v_N_m_2_airbag_cham_1_FE_model_3" NAME.TYPE="NAME"     >
      <SELECT.PRES WRITE_REL="ON"       />
    </OUTPUT_AIRBAG_CHAMBER>
    <OUTPUT_AIRBAG_CHAMBER AIRBAG_CHAMBER_LIST.TYPE="LIST"
AIRBAG_CHAMBER_LIST="1" ID.RANGE="[1, )" ID.TYPE="INTEGER" ID="2"
NAME="temp_K_airbag_cham_1_FE_model_3" NAME.TYPE="NAME"     >
      <SELECT.TEMP WRITE_ABS="ON"       />
```

```
    </OUTPUT_AIRBAG_CHAMBER>
    <OUTPUT_AIRBAG_CHAMBER AIRBAG_CHAMBER_LIST.TYPE="LIST"
AIRBAG_CHAMBER_LIST="1" ID.RANGE="[1, )" ID.TYPE="INTEGER" ID="3"
NAME="BAG_VOLUME_m3" NAME.TYPE="NAME"     >
      <SELECT.VOLUME WRITE_TOTAL="ON"       />
    </OUTPUT_AIRBAG_CHAMBER>
    <OUTPUT_AIRBAG_CHAMBER AIRBAG_CHAMBER_LIST.TYPE="LIST"
AIRBAG_CHAMBER_LIST="1" ID.RANGE="[1, )" ID.TYPE="INTEGER" ID="4"
NAME="MASS_OF_GAS_IN_BAG_kg" NAME.TYPE="NAME"     >
      <SELECT.MASS       />
    </OUTPUT_AIRBAG_CHAMBER>
    <OUTPUT_AIRBAG_CHAMBER AIRBAG_CHAMBER_LIST.TYPE="LIST"
AIRBAG_CHAMBER_LIST="1" ID.RANGE="[1, )" ID.TYPE="INTEGER" ID="5"
NAME="MASS_OF_GAS_SUPPLIED_kg" NAME.TYPE="NAME"     >
      <SELECT.INFLOW WRITE_TOTAL="ON"       />
    </OUTPUT_AIRBAG_CHAMBER>
    <OUTPUT_AIRBAG_CHAMBER AIRBAG_CHAMBER_LIST.TYPE="LIST"
AIRBAG_CHAMBER_LIST="1" ID.RANGE="[1, )" ID.TYPE="INTEGER" ID="6"
NAME="MASS_OF_GAS_EXHAUSTED_kg" NAME.TYPE="NAME"     >
      <SELECT.OUTFLOW AIRBAG_CHAMBER.TYPE="REF"
WRITE_TOTAL="ON"       />
    </OUTPUT_AIRBAG_CHAMBER>
    <SUPPORT BODY.TYPE="REF" DOF_ALL="ON" FE_MODEL.TYPE="REF"
GROUP_LIST.TYPE="LIST" NODE_LIST="97:112 1019:1026"
NODE_LIST.TYPE="ILIST"     />
    <FUNCTION.XY ID.RANGE="[1, )" ID.TYPE="INTEGER" ID="87"
NAME="fid_87" NAME.TYPE="NAME"     >
      <TABLE TYPE="XY_PAIR"       >
            |      XI                YI      |
              0.00000000E+00     0.00000000E+00
              2.00000000E-03     1.44400000E+00
              4.00000000E-03     1.97500000E+00
              6.00000000E-03     2.07800000E+00
              8.00000000E-03     2.04000000E+00
              1.00000000E-02     1.97000000E+00
              1.20000000E-02     1.91600000E+00
              1.40000000E-02     1.82900000E+00
              1.60000000E-02     1.63700000E+00
              1.80000000E-02     1.35100000E+00
              2.00000000E-02     1.06400000E+00
              2.20000000E-02     8.47000000E-01
              2.40000000E-02     6.78000000E-01
              2.60000000E-02     5.08000000E-01
              2.80000000E-02     3.32000000E-01
              3.00000000E-02     1.81000000E-01
              3.20000000E-02     8.30000000E-02
```

```
            3.40000000E-02      3.10000000E-02
            3.60000000E-02      1.30000000E-02
            3.80000000E-02      1.40000000E-02
            4.00000000E-02      2.00000000E-02
          </TABLE>
    </FUNCTION.XY>
    <FUNCTION.XY ID.RANGE="[1, )" ID.TYPE="INTEGER" ID="88"
NAME="fid_88" NAME.TYPE="NAME"     >
      <TABLE TYPE="XY_PAIR"       >
            |      XI                YI      |
            0.00000000E+00      5.00000000E+02
            4.00000000E-02      5.00000000E+02
          </TABLE>
    </FUNCTION.XY>
   </FE_MODEL>
   <ORIENTATION.SUCCESSIVE_ROT AXIS_1="Y" ID.RANGE="[1, )" ID="1"
ID.TYPE="INTEGER" NAME="Orientation" NAME.TYPE="NAME" R1="-1.22"
R1.TYPE="REAL" R2.TYPE="REAL" R3.TYPE="REAL"    />
   <INITIAL.FE_MODEL BODY.TYPE="REF" FE_MODEL.TYPE="REF"
FE_MODEL="3" ORIENT.TYPE="REF" ORIENT="Orientation"
POS.TYPE="REAL[3]" POS="0.365 0.00 0.51" REF_NODE.RANGE="[1, )"
REF_NODE.TYPE="INTEGER" VEL.TYPE="REAL[3]" VEL="0.0 0.0 0.0"    />
  </SYSTEM.MODEL>
  <SWITCH.LOGIC ID.RANGE="[1, )" ID.TYPE="INTEGER" ID="5"
LOGIC_EXPRESSION="/trgcon_4" NAME.TYPE="NAME"  />
  <SWITCH.TIME ELAPSED_TIME="1.000000E-03"
ELAPSED_TIME.TYPE="REAL" ID.RANGE="[1, )" ID.TYPE="INTEGER" ID="7"
NAME="trig_retr_1" NAME.TYPE="NAME"  />
  <SWITCH.TIME ELAPSED_TIME="0.015" ELAPSED_TIME.TYPE="REAL"
ID.RANGE="[1, )" ID.TYPE="INTEGER" ID="4" NAME="trgcon_4"
NAME.TYPE="NAME"  />
  <GROUP_FE CONTACT_CHAR.TYPE="REF" ELEMENT_LIST.TYPE="ILIST"
FE_MODEL.TYPE="REF" FE_MODEL="/Airbag/Driver_Airbag_600mm_diameter"
ID.RANGE="[1, )" ID="15" ID.TYPE="INTEGER" MATERIAL_LIST.TYPE="LIST"
NAME="AirbagPart1_gfe" NAME.TYPE="NAME" NODE_LIST="113:116 572:1018"
NODE_LIST.TYPE="ILIST" PART_LIST.TYPE="LIST"
PROPERTY_LIST.TYPE="LIST"  />
  <GROUP_FE CONTACT_CHAR.TYPE="REF" ELEMENT_LIST.TYPE="ILIST"
FE_MODEL.TYPE="REF" FE_MODEL="/Airbag/Driver_Airbag_600mm_diameter"
ID.RANGE="[1, )" ID="16" ID.TYPE="INTEGER" MATERIAL_LIST.TYPE="LIST"
NAME="AirbagPart2_gfe" NAME.TYPE="NAME" NODE_LIST="1:96 113:1018"
NODE_LIST.TYPE="ILIST" PART_LIST.TYPE="LIST"
PROPERTY_LIST.TYPE="LIST"  />
  <GROUP_FE CONTACT_CHAR.TYPE="REF" ELEMENT_LIST.TYPE="ILIST"
FE_MODEL.TYPE="REF" FE_MODEL="/Airbag/Driver_Airbag_600mm_diameter"
ID.RANGE="[1, )" ID="17" ID.TYPE="INTEGER" MATERIAL_LIST.TYPE="LIST"
```

NAME="AirbagPart3_gfe" NAME.TYPE="NAME" NODE_LIST="1:96 117:571"
NODE_LIST.TYPE="ILIST" PART_LIST.TYPE="LIST"
PROPERTY_LIST.TYPE="LIST" />
<GROUP_FE CONTACT_CHAR.TYPE="REF" ELEMENT_LIST.TYPE="ILIST"
FE_MODEL.TYPE="REF" FE_MODEL="/Airbag/Driver_Airbag_600mm_diameter"
ID.RANGE="[1,)" ID="18" ID.TYPE="INTEGER" MATERIAL_LIST.TYPE="LIST"
NAME="AirbagPart4_gfe" NAME.TYPE="NAME" NODE_LIST="1:1027"
NODE_LIST.TYPE="ILIST" PART_LIST.TYPE="LIST"
PROPERTY_LIST.TYPE="LIST" />
<CONTACT.FE_FE FLAG.RANGE="[1,)" FLAG.TYPE="INTEGER"
GAP_FUNC.TYPE="REF" ID="18" ID.RANGE="[1,)" ID.TYPE="INTEGER"
INITIAL_USNORM.TYPE="REAL[3]" MASTER_SURFACE="AirbagPart3_gfe"
MASTER_SURFACE.TYPE="LIST" NAME.TYPE="NAME"
NAME="airbag_contact1" NORMAL_USER.TYPE="REAL[3]"
SEARCH_FACTOR.TYPE="INTEGER" SLAVE_SURFACE="/2/HumanBody_gfe"
SLAVE_SURFACE.TYPE="LIST" SWITCH.TYPE="REF" >
<CONTACT_FORCE.PENALTY FRIC_FUNC.TYPE="REF"
MAX_FORCE_PAR.TYPE="REAL" MAX_FORCE_PAR="1.0" PENALTY=".1"
PENALTY.TYPE="REAL" />
</CONTACT.FE_FE>
<CONTACT.FE_FE FLAG.RANGE="[1,)" FLAG.TYPE="INTEGER"
GAP_FUNC.TYPE="REF" ID="19" ID.RANGE="[1,)" ID.TYPE="INTEGER"
INITIAL_USNORM.TYPE="REAL[3]" MASTER_SURFACE="AirbagPart4_gfe"
MASTER_SURFACE.TYPE="LIST" NAME.TYPE="NAME"
NAME="airbag_contact3" NORMAL_USER.TYPE="REAL[3]"
SEARCH_FACTOR.TYPE="INTEGER" SLAVE_SURFACE="/3/uterus_gfe"
SLAVE_SURFACE.TYPE="LIST" SWITCH.TYPE="REF" >
<CONTACT_FORCE.PENALTY FRIC_FUNC.TYPE="REF"
MAX_FORCE_PAR.TYPE="REAL" MAX_FORCE_PAR="1.0" PENALTY=".1"
PENALTY.TYPE="REAL" />
</CONTACT.FE_FE>
<CONTACT.FE_FE FLAG.RANGE="[1,)" FLAG.TYPE="INTEGER"
GAP_FUNC.TYPE="REF" ID="20" ID.RANGE="[1,)" ID.TYPE="INTEGER"
INITIAL_USNORM.TYPE="REAL[3]" MASTER_SURFACE="AirbagPart4_gfe"
MASTER_SURFACE.TYPE="LIST" NAME.TYPE="NAME"
NAME="airbag_contact4" NORMAL_USER.TYPE="REAL[3]"
SEARCH_FACTOR.TYPE="INTEGER" SLAVE_SURFACE="/3/fat2_gfe"
SLAVE_SURFACE.TYPE="LIST" SWITCH.TYPE="REF" >
<CONTACT_FORCE.PENALTY FRIC_FUNC.TYPE="REF"
MAX_FORCE_PAR.TYPE="REAL" MAX_FORCE_PAR="1.0" PENALTY=".1"
PENALTY.TYPE="REAL" />
</CONTACT.FE_FE>
<CONTACT.FE_FE FLAG.RANGE="[1,)" FLAG.TYPE="INTEGER"
GAP_FUNC.TYPE="REF" ID="21" ID.RANGE="[1,)" ID.TYPE="INTEGER"
INITIAL_USNORM.TYPE="REAL[3]" MASTER_SURFACE="AirbagPart4_gfe"
MASTER_SURFACE.TYPE="LIST" NAME.TYPE="NAME"

```
NAME="airbag_contact5" NORMAL_USER.TYPE="REAL[3]"
SEARCH_FACTOR.TYPE="INTEGER" SLAVE_SURFACE="/3/fluid_gfe"
SLAVE_SURFACE.TYPE="LIST" SWITCH.TYPE="REF"  >
   <CONTACT_FORCE.PENALTY FRIC_FUNC.TYPE="REF"
MAX_FORCE_PAR.TYPE="REAL" MAX_FORCE_PAR="0.1" PENALTY=".1"
PENALTY.TYPE="REAL"    />
  </CONTACT.FE_FE>
</MADYMO>
```

Uterus_inc

```
<?xml version="1.0" encoding="UTF-8"?>
<!DOCTYPE MADYMO_INCLUDE SYSTEM "mtd_3d.dtd">
<MADYMO_INCLUDE>
        <PRODUCT_INFORMATION DATE="$Date: 2001/05/09 08:48:32 $"
DESCRIPTION="MADYMO 5th percentile human female model" FILE="$RCSfile:
h_occ05f_inc.xml,v $ (model file)" STATE="$State: Exp $" VERSION="$Revision: 1.1
$">
   <COPYRIGHT>
(c) 2001 TNO Automotive
   P.O. Box 6033, 2600 JA Delft, The Netherlands

 All rights reserved

 MADYMO software programs and MADYMO databases are confidential
 information and proprietary products of TNO, Delft, The Netherlands.
 The terms and conditions governing the licensing of MADYMO software
 consist solely of those set forth in the written contracts between
 TNO and its customers. The software may only be used or copied in
 accordance with the terms of these contracts.
</COPYRIGHT>
 </PRODUCT_INFORMATION>
   <FE_MODEL ID.RANGE="[1, )" ID.TYPE="INTEGER" ID="1"
NAME="UTERUS" NAME.TYPE="NAME">
   <CONTROL_FE_MODEL ALPHA_COEF="50.0" ALPHA_COEF.RANGE="[0, )"
ALPHA_COEF.TYPE="REAL" ALPHA_FUNC.TYPE="REF"
IMM_STRETCH_PRINT.RANGE="[0, 100]"
IMM_STRETCH_PRINT.TYPE="INTEGER"    />
   <CONTROL_FE_TIME_STEP CRITICAL_ELEMENTS.RANGE="[1, 100]"
CRITICAL_ELEMENTS.TYPE="INTEGER" MAX_STEP.RANGE="(0, )"
MAX_STEP.TYPE="REAL" MIN_STEP.RANGE="[0, )" MIN_STEP.TYPE="REAL"
NR_OF_CYCLES.TYPE="INTEGER" REDUCTION_FACTOR.TYPE="REAL"    />
   <TABLE TYPE="COORDINATE.CARTESIAN"    >           |    ID          X
Y               Z       |
</TABLE>
   <MATERIAL.ISOLIN DAMP_COEF.RANGE="[0, )"
DAMP_COEF.TYPE="REAL" DAMP_COEF="0.20" DENSITY.RANGE="(0, )"
DENSITY.TYPE="REAL" DENSITY="1052" DESCRIPTION="uterus"
E.TYPE="REAL" E="566000" E.RANGE="(0, )" ID="2" ID.RANGE="[1, )"
ID.TYPE="INTEGER" KAPPA.TYPE="REAL" KAPPA.RANGE="[0, )"
MU.TYPE="INTEGER" NAME.TYPE="NAME" NU.RANGE="(-1, 0.5)" NU="0.40"
NU.TYPE="REAL"    />
   <MATERIAL.ISOLIN DAMP_COEF.RANGE="[0, )"
DAMP_COEF.TYPE="REAL" DAMP_COEF="0.20" DENSITY.RANGE="(0, )"
DENSITY.TYPE="REAL" DENSITY="995" DESCRIPTION="placenta"
```

E.TYPE="REAL" E="63000" E.RANGE="(0,)" ID="3" ID.RANGE="[1,)"
ID.TYPE="INTEGER" KAPPA.TYPE="REAL" KAPPA.RANGE="[0,)"
MU.TYPE="INTEGER" NAME.TYPE="NAME" NU.RANGE="(-1, 0.5)" NU="0.45"
NU.TYPE="REAL" />
<MATERIAL.ISOLIN DAMP_COEF.RANGE="[0,)"
DAMP_COEF.TYPE="REAL" DAMP_COEF="0.20" DENSITY.RANGE="(0,)"
DENSITY.TYPE="REAL" DENSITY="1000" DESCRIPTION="ligaments"
E.TYPE="REAL" E="56600000" E.RANGE="(0,)" ID="5" ID.RANGE="[1,)"
ID.TYPE="INTEGER" KAPPA.TYPE="REAL" KAPPA.RANGE="[0,)"
MU.TYPE="INTEGER" NAME.TYPE="NAME" NU.RANGE="(-1, 0.5)" NU="0.40"
NU.TYPE="REAL" />
<PROPERTY.SOLID8 HOURGLASS_PAR.RANGE="[0,)"
HOURGLASS_PAR.TYPE="REAL" ID.RANGE="[1,)" ID="1"
ID.TYPE="INTEGER" NAME="PROP1" NAME.TYPE="NAME" />
<PROPERTY.MEM3 ID.RANGE="[1,)" ID="4" ID.TYPE="INTEGER"
IMM_DAMP.RANGE="[0,)" IMM_DAMP.TYPE="REAL"
IMM_STRAIN.TYPE="REAL" IMM_TRANS.TYPE="REAL"
NAME.TYPE="NAME" THICK.RANGE="(0,)" THICK.TYPE="REAL"
THICK=".01" />
<PROPERTY.TRUSS2 AREA.RANGE="(0,)" AREA.TYPE="REAL"
AREA="0.000001" ID.RANGE="[1,)" ID.TYPE="INTEGER" ID="5"
NAME="PROP5" NAME.TYPE="NAME" />
<PART DESCRIPTION="uterus" ID.RANGE="[1,)" ID="1" ID.TYPE="INTEGER"
MATERIAL="2" MATERIAL.TYPE="REF" NAME="UT_prt"
NAME.TYPE="NAME" PROPERTY="1" PROPERTY.TYPE="REF" />
<PART DESCRIPTION="uterus" ID.RANGE="[1,)" ID="11"
ID.TYPE="INTEGER" MATERIAL="2" MATERIAL.TYPE="REF"
NAME="UT_prt2" NAME.TYPE="NAME" PROPERTY="1"
PROPERTY.TYPE="REF" />
<PART DESCRIPTION="placenta" ID.RANGE="[1,)" ID="3"
ID.TYPE="INTEGER" MATERIAL="3" MATERIAL.TYPE="REF"
NAME="PLA_prt" NAME.TYPE="NAME" PROPERTY="1"
PROPERTY.TYPE="REF" />
<PART DESCRIPTION="placenta" ID.RANGE="[1,)" ID="13"
ID.TYPE="INTEGER" MATERIAL="3" MATERIAL.TYPE="REF"
NAME="PLA_prt2" NAME.TYPE="NAME" PROPERTY="1"
PROPERTY.TYPE="REF" />
<PART DESCRIPTION="uterosacral ligament - left" ID.RANGE="[1,)" ID="4"
ID.TYPE="INTEGER" MATERIAL="5" MATERIAL.TYPE="REF" NAME="UT-
L_prt" NAME.TYPE="NAME" PROPERTY="4" PROPERTY.TYPE="REF" />
<PART DESCRIPTION="uterosacral ligament - right" ID.RANGE="[1,)" ID="5"
ID.TYPE="INTEGER" MATERIAL="5" MATERIAL.TYPE="REF" NAME="UT-
R_prt" NAME.TYPE="NAME" PROPERTY="4" PROPERTY.TYPE="REF" />
<PART DESCRIPTION="round ligament - left" ID.RANGE="[1,)" ID="6"
ID.TYPE="INTEGER" MATERIAL="5" MATERIAL.TYPE="REF" NAME="R-L_prt"
NAME.TYPE="NAME" PROPERTY="4" PROPERTY.TYPE="REF" />

<PART DESCRIPTION="round ligament - right" ID.RANGE="[1,)" ID="7"
ID.TYPE="INTEGER" MATERIAL="5" MATERIAL.TYPE="REF" NAME="R-R_prt"
NAME.TYPE="NAME" PROPERTY="4" PROPERTY.TYPE="REF" />
<PART DESCRIPTION="UPI" ID.RANGE="[1,)" ID="8" ID.TYPE="INTEGER"
MATERIAL="3" MATERIAL.TYPE="REF" NAME="UPI_prt"
NAME.TYPE="NAME" PROPERTY="5" PROPERTY.TYPE="REF" />
<TABLE TYPE="ELEMENT.HEXA8" > | ID PART N1 N2
N3 N4 N5 N6 N7 N8 |
</TABLE>
<TABLE TYPE="ELEMENT.TRIAD3" > | ID PART N1 N2
N3 |
</TABLE>
<TABLE TYPE="ELEMENT.LINE2" > | ID PART N1 N2 |
</TABLE>
<SCALING NODE_LIST="ALL" NODE_LIST.TYPE="ILIST"
REF_NODE.RANGE="[1,)" REF_NODE.TYPE="INTEGER" SCALE_TYPE="SIZE"
SEQ_NR.RANGE="[1,)" SEQ_NR.TYPE="INTEGER" X_SCALE="0.01"
X_SCALE.TYPE="REAL" Y_SCALE="0.01" Y_SCALE.TYPE="REAL"
Z_SCALE="0.01" Z_SCALE.TYPE="REAL" />
<OUTPUT_ANIMATION ID.RANGE="[1,)" ID.TYPE="INTEGER" ID="90"
NAME="uterus_out" NAME.TYPE="NAME" SELECT_ELEMENT="ON" />
<OUTPUT_ELEMENT ELEMENT_LIST="163:243 1495:1575 2332:2412
2656:2736" ELEMENT_LIST.TYPE="ILIST" GROUP_LIST.TYPE="LIST"
ID.RANGE="[1,)" ID="44" ID.TYPE="INTEGER" INT_POINT_LIST="1"
INT_POINT_LIST.TYPE="ILIST" NAME="ut_out" NAME.TYPE="NAME" >
<SELECT.STRAIN WRITE_PRINC_1="ON" WRITE_PRINC_2="OFF"
WRITE_PRINC_3="OFF" WRITE_VON_MISES="ON" WRITE_ZZ.RANGE="" />
</OUTPUT_ELEMENT>
<OUTPUT_ELEMENT ELEMENT_LIST="3022:3025 3046:3050 3071:3075
3096:3100 3121:3125 3146:3150 3171:3175 3196:3200 3221:3225 3246:3250 3271:3275
3296:3300 3321:3325 3346:3350 3371:3375 3521:3525 3546:3550 3571:3575 3596:3600
3621:3625 3646:3650 3671:3675 3696:3700 3721:3725 3746:3750 3771:3775 3796:3800
3821:3825 3846:3850 3871:3875 4021:4025 4046:4050 4071:4075 4096:4100 4121:4125
4146:4150 4171:4175 4196:4200 4221:4225 4246:4250 4271:4275 4296:4300 4321:4325
4346:4350 4371:4375 4521:4525 4546:4550 4571:4575 4596:4600 4621:4625 4646:4650
4671:4675 4696:4700 4721:4725 4746:4750 4771:4775 4796:4800 4821:4825 4846:4850
4871:4875" ELEMENT_LIST.TYPE="ILIST" GROUP_LIST.TYPE="LIST"
ID.RANGE="[1,)" ID="45" ID.TYPE="INTEGER" INT_POINT_LIST="1"
INT_POINT_LIST.TYPE="ILIST" NAME="pla_out" NAME.TYPE="NAME" >
<SELECT.STRAIN WRITE_PRINC_1="ON" WRITE_PRINC_2="OFF"
WRITE_PRINC_3="OFF" WRITE_VON_MISES="ON" WRITE_ZZ.RANGE="" />
</OUTPUT_ELEMENT>
<OUTPUT_ELEMENT ELEMENT_LIST="6002:6146"
ELEMENT_LIST.TYPE="ILIST" GROUP_LIST.TYPE="LIST" ID.RANGE="[1,)"
ID="46" ID.TYPE="INTEGER" INT_POINT_LIST="1"
INT_POINT_LIST.TYPE="ILIST" NAME="UPI_eout" NAME.TYPE="NAME" >

```
    <SELECT.STRESS_TRUSS2     />
    <SELECT.STRAIN_TRUSS2 WRITE_ELONG_REL="ON"     />
   </OUTPUT_ELEMENT>
   <OUTPUT_NODE GROUP_LIST.TYPE="LIST" ID.RANGE="[1, )"
ID.TYPE="INTEGER" ID="47" NAME="UPI_nout" NAME.TYPE="NAME"
NODE_LIST="15000:15010 16000:16010 17000:17010 18000:18010 19000:19010
20000:20010 21000:21010 22000:22010 23000:23010 24000:24010 25000:25010
26000:26010" NODE_LIST.TYPE="ILIST"    >
    <SELECT.FORCE WRITE_R="ON"     />
   </OUTPUT_NODE>
  </FE_MODEL>
  <FE_MODEL ID.RANGE="[1, )" ID.TYPE="INTEGER" ID="2" NAME="A_FLUID"
NAME.TYPE="NAME">
   <CONTROL_FE_MODEL ALPHA_COEF="50.0" ALPHA_COEF.RANGE="[0, )"
ALPHA_COEF.TYPE="REAL" ALPHA_FUNC.TYPE="REF"
IMM_STRETCH_PRINT.RANGE="[0, 100]"
IMM_STRETCH_PRINT.TYPE="INTEGER"    />
   <CONTROL_FE_TIME_STEP CRITICAL_ELEMENTS.RANGE="[1, 100]"
CRITICAL_ELEMENTS.TYPE="INTEGER" MAX_STEP.RANGE="(0, )"
MAX_STEP.TYPE="REAL" MIN_STEP.RANGE="[0, )" MIN_STEP.TYPE="REAL"
NR_OF_CYCLES.TYPE="INTEGER" REDUCTION_FACTOR.TYPE="REAL"    />
   <TABLE TYPE="COORDINATE.CARTESIAN"    >           |    ID          X
Y              Z       |
</TABLE>
   <MATERIAL.ISOLIN DAMP_COEF.RANGE="[0, )"
DAMP_COEF.TYPE="REAL" DAMP_COEF="0.20" DENSITY.RANGE="(0, )"
DENSITY.TYPE="REAL" DENSITY="993" DESCRIPTION="fluid"
E.TYPE="REAL" E="20000" E.RANGE="(0, )" ID="7" ID.RANGE="[1, )"
ID.TYPE="INTEGER" KAPPA.TYPE="REAL" KAPPA.RANGE="[0, )"
MU.TYPE="INTEGER" NAME.TYPE="NAME" NU.RANGE="(-1, 0.5)" NU="0.49"
NU.TYPE="REAL"    />
   <PROPERTY.SOLID8 HOURGLASS_PAR.RANGE="[0, )"
HOURGLASS_PAR.TYPE="REAL" ID.RANGE="[1, )" ID="2"
ID.TYPE="INTEGER" NAME="PROP2" NAME.TYPE="NAME"    />
   <PART ID.RANGE="[1, )" ID.TYPE="INTEGER" ID="2"
MATERIAL.TYPE="REF" MATERIAL="7" NAME.TYPE="NAME"
PROPERTY.TYPE="REF" PROPERTY="2"    />
   <PART ID.RANGE="[1, )" ID.TYPE="INTEGER" ID="12"
MATERIAL.TYPE="REF" MATERIAL="7" NAME.TYPE="NAME"
PROPERTY.TYPE="REF" PROPERTY="2"    />
   <TABLE TYPE="ELEMENT.HEXA8"    > |       ID       PART        N1        N2
N3       N4       N5       N6       N7       N8 |
</TABLE>
   <SCALING NODE_LIST="ALL" NODE_LIST.TYPE="ILIST"
REF_NODE.RANGE="[1, )" REF_NODE.TYPE="INTEGER" SCALE_TYPE="SIZE"
SEQ_NR.RANGE="[1, )" SEQ_NR.TYPE="INTEGER" X_SCALE="0.0099"
```

```
X_SCALE.TYPE="REAL" Y_SCALE="0.0099" Y_SCALE.TYPE="REAL"
Z_SCALE="0.0099" Z_SCALE.TYPE="REAL"    />
   <OUTPUT_ANIMATION ID.RANGE="[1, )" ID.TYPE="INTEGER" ID="91"
NAME="placenta_out" NAME.TYPE="NAME" SELECT_ELEMENT="ON"    />
  </FE_MODEL><FE_MODEL ID.RANGE="[1, )" ID.TYPE="INTEGER" ID="3"
NAME="FAT" NAME.TYPE="NAME">
   <CONTROL_FE_MODEL ALPHA_COEF="50.0" ALPHA_COEF.RANGE="[0, )"
ALPHA_COEF.TYPE="REAL" ALPHA_FUNC.TYPE="REF"
IMM_STRETCH_PRINT.RANGE="[0, 100]"
IMM_STRETCH_PRINT.TYPE="INTEGER"    />
   <CONTROL_FE_TIME_STEP CRITICAL_ELEMENTS.RANGE="[1, 100]"
CRITICAL_ELEMENTS.TYPE="INTEGER" MAX_STEP.RANGE="(0, )"
MAX_STEP.TYPE="REAL" MIN_STEP.RANGE="[0, )" MIN_STEP.TYPE="REAL"
NR_OF_CYCLES.TYPE="INTEGER" REDUCTION_FACTOR.TYPE="REAL"    />
   <TABLE TYPE="COORDINATE.CARTESIAN"    >
         |    ID          X               Y               Z       |
</TABLE>
   <MATERIAL.ISOLIN DAMP_COEF.RANGE="[0, )"
DAMP_COEF.TYPE="REAL" DAMP_COEF="0.30" DENSITY.RANGE="(0, )"
DENSITY.TYPE="REAL" DENSITY="993" DESCRIPTION="fat" E.TYPE="REAL"
E="47000" E.RANGE="(0, )" ID="9" ID.RANGE="[1, )" ID.TYPE="INTEGER"
KAPPA.TYPE="REAL" KAPPA.RANGE="[0, )" MU.TYPE="INTEGER"
NAME.TYPE="NAME" NU.RANGE="(-1, 0.5)" NU=".49" NU.TYPE="REAL"    />
   <PROPERTY.SOLID8 HOURGLASS_PAR.RANGE="[0, )"
HOURGLASS_PAR.TYPE="REAL" ID.RANGE="[1, )" ID="1"
ID.TYPE="INTEGER" NAME="hi" NAME.TYPE="NAME"    />
   <PART ID.RANGE="[1, )" ID.TYPE="INTEGER" ID="3"
MATERIAL.TYPE="REF" MATERIAL="9" NAME.TYPE="NAME"
PROPERTY.TYPE="REF" PROPERTY="1"    />
   <PART ID.RANGE="[1, )" ID.TYPE="INTEGER" ID="6"
MATERIAL.TYPE="REF" MATERIAL="9" NAME.TYPE="NAME"
PROPERTY.TYPE="REF" PROPERTY="1"    />
   <PART ID.RANGE="[1, )" ID.TYPE="INTEGER" ID="7"
MATERIAL.TYPE="REF" MATERIAL="9" NAME.TYPE="NAME"
PROPERTY.TYPE="REF" PROPERTY="1"    />
   <PART ID.RANGE="[1, )" ID.TYPE="INTEGER" ID="9"
MATERIAL.TYPE="REF" MATERIAL="9" NAME.TYPE="NAME"
PROPERTY.TYPE="REF" PROPERTY="1"    />
   <PART ID.RANGE="[1, )" ID.TYPE="INTEGER" ID="10"
MATERIAL.TYPE="REF" MATERIAL="9" NAME.TYPE="NAME"
PROPERTY.TYPE="REF" PROPERTY="1"    />
   <PART ID.RANGE="[1, )" ID.TYPE="INTEGER" ID="11"
MATERIAL.TYPE="REF" MATERIAL="9" NAME.TYPE="NAME"
PROPERTY.TYPE="REF" PROPERTY="1"    />
```

<PART ID.RANGE="[1,)" ID.TYPE="INTEGER" ID="13"
MATERIAL.TYPE="REF" MATERIAL="9" NAME.TYPE="NAME"
PROPERTY.TYPE="REF" PROPERTY="1" />
<PART ID.RANGE="[1,)" ID.TYPE="INTEGER" ID="14"
MATERIAL.TYPE="REF" MATERIAL="9" NAME.TYPE="NAME"
PROPERTY.TYPE="REF" PROPERTY="1" />
<PART ID.RANGE="[1,)" ID.TYPE="INTEGER" ID="15"
MATERIAL.TYPE="REF" MATERIAL="9" NAME.TYPE="NAME"
PROPERTY.TYPE="REF" PROPERTY="1" />
<PART ID.RANGE="[1,)" ID.TYPE="INTEGER" ID="16"
MATERIAL.TYPE="REF" MATERIAL="9" NAME.TYPE="NAME"
PROPERTY.TYPE="REF" PROPERTY="1" />
<PART ID.RANGE="[1,)" ID.TYPE="INTEGER" ID="17"
MATERIAL.TYPE="REF" MATERIAL="9" NAME.TYPE="NAME"
PROPERTY.TYPE="REF" PROPERTY="1" />
<TABLE TYPE="ELEMENT.HEXA8" >
| ID PART N1 N2 N3 N4 N5 N6 N7 N8 |
</TABLE>
<SCALING NODE_LIST="ALL" NODE_LIST.TYPE="ILIST"
REF_NODE.RANGE="[1,)" REF_NODE.TYPE="INTEGER" SCALE_TYPE="SIZE"
SEQ_NR.RANGE="[1,)" SEQ_NR.TYPE="INTEGER" X_SCALE="0.0101"
X_SCALE.TYPE="REAL" Y_SCALE="0.0101" Y_SCALE.TYPE="REAL"
Z_SCALE="0.0101" Z_SCALE.TYPE="REAL" />
<OUTPUT_ANIMATION ID.RANGE="[1,)" ID.TYPE="INTEGER" ID="92"
NAME="fat_out" NAME.TYPE="NAME" SELECT_ELEMENT="ON" />
</FE_MODEL>
</MADYMO_INCLUDE>

Vita

David M. Moorcroft

David Moorcroft was born in Trenton, New Jersey on March 30, 1978. He attended Notre Dame High School in Lawrence, NJ. He then attended Virginia Tech and received a Bachelors of Science degree in Engineering Science and Mechanics in May of 2000 with a focus on Biomechanics and a minor in Mathematics. Remaining at Virginia Tech for his Masters of Science in Engineering Mechanics with a biomedical option, he completed his thesis studying restraint effectiveness in pregnant occupants. He has published articles in the engineering and medical journals and conferences and was given an Outstanding Research Award, in the MS student competition for the Virginia Tech Center for Biomedical Engineering and the Wake Forest School of Medicine 1st Student Research Symposium. In the fall of 2002, he will enter industry. He has plans to pursue a Professional Engineering License shortly thereafter and become an expert witness in the area of accident reconstruction. Dave enjoys playing hockey and volleyball and one day hopes to open up a Microbrewery.

Further information can be obtained by writing to his permanent address:

1302 Oporto Drive
The Villages, FL 32162-0162

David M. Moorcroft